

## CHAPTER 2

# *Sediment Transport and Morphodynamics*

*Marcelo H. García*

ASCE Manual 54, *Sedimentation Engineering*, prepared under the leadership of Professor Vito A. Vanoni, has provided guidance to theoreticians and practitioners' world wide on the primary topic of sediment problems involved in the development, use, and conservation of water and land resources. First published in 1975, Manual 54 gives an understanding of the nature and scope of sedimentation problems, of the methods for their investigation, and of practical approaches to their solution. It is essentially a textbook on sedimentation engineering, as its title accurately reflects. Manual 54 was the first and most comprehensive text of its kind and has been circulated throughout the world for the past 30 years as the most complete reference on sedimentation engineering in the world. It has recently been published again as the *Classic Edition* (Vanoni 2006). In the spirit of its predecessor, this chapter of Manual of Practice 110, *Sedimentation Engineering*, aims at presenting the state of the art concerning the hydraulics of sediment transport in fluvial systems based on the knowledge gained in the last three decades. A concerted effort is made to relate the mechanics of sediment transport in rivers and by turbidity currents to the morphodynamics of lake and reservoir sedimentation, including the formation of fluvial deltas.

### 2.1 SEDIMENT TRANSPORT MECHANICS AND RELATED PHENOMENA

The field of sediment transport might just as well be called "transport of granular particles by fluids." As such, it embodies a type of two-phase flow, in which one phase is fluid and the other phase is solid. The prototype for the field is the river. Here, the fluid phase is river water, and the solid phase is sediment grains, e.g., quartz sand. The most common modes of sediment transport in rivers are those of bed load and suspended load. In bed load, particles roll, slide, or saltate over each other, never rising too far above the bed. In

suspended load, fluid turbulence comes into play, carrying the particles well up into the water column. In both cases, the driving force for sediment transport is the action of gravity on the fluid phase; this force is transmitted to the particles via drag. Whether the mode of transport is saltation or suspension, the volume concentration of solids anywhere in the water column tends to be rather dilute in rivers. As a result, it is generally possible to treat the two phases separately.

In the geophysical domain, the field is much broader than rivers alone. The same phenomena of bed load and suspended load transport occur in a variety of other geophysical contexts. Sediment transport is accomplished in the near-shore of lakes and oceans by wave action. Turbidity currents act to carry suspended sediment into lakes, reservoirs, and the deep sea. Landslides, debris flows and mud flows provide mass transport mechanisms for the delivery of sediment from highlands to lowlands.

The solid phase can vary greatly in size, ranging from clay particles to silt, sand, gravel, cobbles, and boulders. Rock types can include quartz, feldspar, limestone, granite, basalt, and other less common types such as magnetite. The fluid phase can, in principle, be almost anything that constitutes a fluid. In the geophysical sense, however, the two fluids of major importance are water and air.

The phenomenon of sediment transport can sometimes be disguised as rather esoteric phenomena. When water is supercooled, large quantities of particulate frazil ice can form. As the water moves under a frozen ice cover, one has the phenomenon of sediment transport in rivers stood on its head. The frazil ice particles float rather than sink, and thus tend to accumulate on the bottom side of the ice cover rather than on the riverbed. Turbulence tends to suspend the particles downward rather than upward.

In the case of a powder snow avalanche, the fluid phase is air and the solid phase consists of snow particles. The dominant mode of transport is suspension. These flows are close analogues of turbidity currents, insofar as the driving

force for the flow is the action of gravity on the solid phase rather than the fluid phase. That is, if all the particles drop out of suspension, the flow ceases. In the case of sediment transport in rivers, it is accurate to say that the fluid phase drags the solid phase along. In the cases of turbidity currents and powder snow avalanches, the solid phase drags the fluid phase along.

Desert sand dunes provide an example for which the fluid phase is air, but the dominant mode of transport is saltation rather than suspension. Because air is so much lighter than water, quartz sand particles saltate in long, high trajectories, relatively unaffected by the direct action of turbulent fluctuations. The dunes themselves are created by the effect of the fluid phase acting on the solid phase. They, in turn, affect the fluid phase by changing the resistance.

In the limiting case of vanishing solids, the field reduces to pure fluid mechanics. As a result, sediment transport must be considered to be a subfield of fluid mechanics. In the limiting case of vanishing fluid, the problem reduces to that of the flow of a granular substance in a vacuum. The driving force now typically, but not always, becomes gravity. This problem, as well, can be treated with the techniques of fluid mechanics, as long as one is willing to move far afield of traditional Newtonian fluid mechanics. Martian rock avalanches constitute a geophysical realization of grain flows in a near vacuum, and it is likely that the fluid phase plays only a subsidiary role in many terrestrial rock avalanches. Another example of grain flow is a slab avalanche of snow. If they attain sufficient speed, slab avalanches tend to devolve into more dilute powder snow avalanches in which the fluid phase plays a greater role.

Among the more interesting intermediate cases are debris flows, mud flows, and hyperconcentrated flows. In all of these cases, the solid and fluid phases are present in similar quantities. A debris flow typically carries a heterogeneous mixture of grain sizes ranging from boulders to clay. Mud flows and hyperconcentrated flows are generally restricted to finer grain sizes. In most cases, it proves useful to think of such flows as consisting of a single phase, the mechanics of which is highly non-Newtonian.

The study of the movement of grains under the influence of fluid drag and gravity constitutes a fascinating field in its own right. The subject becomes even more interesting when one considers the link between sediment transport and morphology. In the laboratory, the phenomenon can be studied in the context of a variety of containers, such as flumes and wave tanks, specified by the experimentalist. In the field, however, the fluid-sediment mixture constructs its own container: the river. This new degree of freedom opens up a variety of intriguing possibilities for river and coastal morphodynamics (Parker and Garcia 2006).

Consider a river. Depending on the existence or lack thereof of a viscous sublayer and the relative importance of bed load and suspended load, a variety of rhythmic structures can form on the riverbed. These include ripples, dunes,

antidunes, and alternate bars. The first three of these can have a profound effect on the resistance to flow offered by the riverbed. Thus, they act to control river depth. Riverbanks themselves can also be considered to be a self-formed morphological feature, thus specifying the entire container.

The container itself can deform in plan. Alternate bars cause rivers to erode their banks in a rhythmic pattern, thus allowing the onset of meandering. Fully developed river meandering implies an intricate balance between sediment erosion and deposition. If a stream is sufficiently wide, it will braid rather than meander, dividing into several intertwining channels. Braided rivers are an important component of the Earth's surface. The deposits of ancient braided rivers may contain significant reserves of water and hydrocarbon.

Rivers create morphological structures on much larger scales as well. These include canyons, alluvial fans, and deltas. Turbidity currents act to create similar structures in the oceanic environment. In the coastal environment, the beach profile itself is created by the interaction of water and sediment. On a larger scale, offshore bars, spits, and capes constitute rhythmic features created by wave-current-sediment interaction. The boulder levees often created by debris flows provide another example of a morphological structure created by a sediment-bearing flow.

This chapter is an introduction to the mechanics of sediment transport and river morphodynamics. Rivers evolve over time in accordance with the interaction between the flow and sediment-transport fields over an erodible bed (which changes the bed) and the changing morphology of the bed (which changes the flow and sediment-transport fields). This co-evolution is termed morphodynamics. Sediment transport by turbidity currents and the mechanics of lake and reservoir sedimentation are also considered in this chapter. The approach is intended to be as mechanistic and deductive as possible so that readers will be able to gain a firm foundation in the mechanics of sediment transport. This should be beneficial both for understanding the rest of the material presented in the manual as well as for sedimentation engineering and teaching purposes.

### 2.1.1 The Sediment Cycle in the Environment

The sediment cycle starts with the process of erosion, whereby particles or fragments are weathered from rock material. Action by water, wind, and glaciers as well as plant and animal activities, contributes to the erosion of the earth's surface. Fluvial sediment is the term used to describe the case where water is the key agent for erosion. Natural, or geological, erosion takes place slowly, over centuries or millennia. Erosion that occurs as a result of human activity may take place much faster. It is important to understand the role of each when studying sediment transport.

The dynamics of sediment in the environment and its morphological consequences are schematized in Fig. 2-1. Any material that can be dislodged is ready to be transported. The

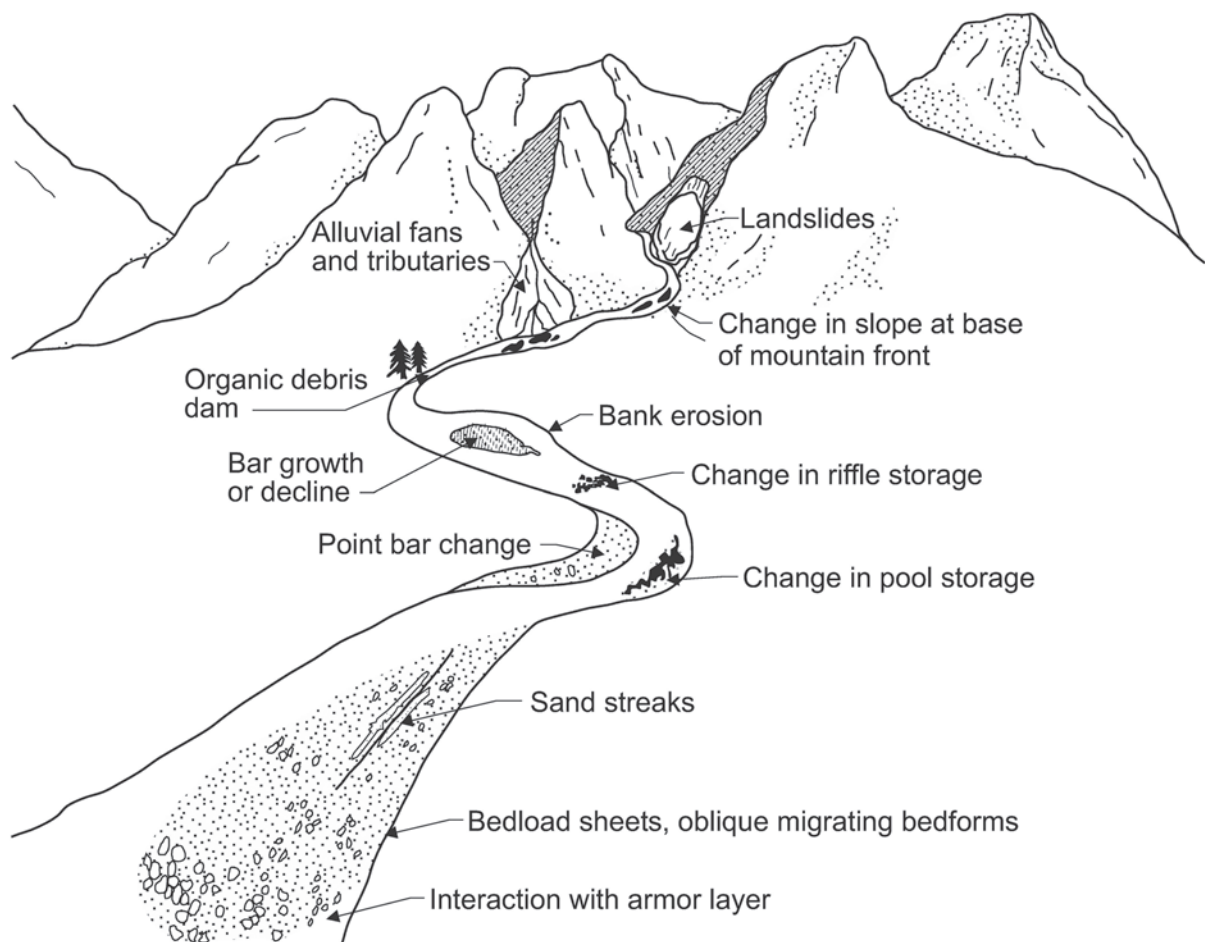


**Fig. 2-1.** Sedimentation processes and associated morphological changes in a Watershed (adapted from Dietrich and Gallinatti 1991).

transportation process is initiated on the land surface when raindrops result in sheet erosion. Rills, gullies, streams, and rivers then act as conduits for sediment movement. The greater the discharge, or rate of flow, the higher the capacity for sediment transport. Mass sediment transport can also occur through landslides, debris flows, and mudflows. Hyperconcentrated flows have also a tremendous capacity to transport vast amounts of sediment as observed after the release of large amounts of sediment following the eruption of Mt. St. Helens in Washington State, USA (Chapter 19).

The final process in the sediment transport cycle is deposition. When there is not enough energy to transport the sediment, it comes to rest. Sinks, or depositional areas, can be visible as newly deposited material on a floodplain, bars and islands in a channel, and deltas. Considerable deposition occurs that may not be apparent, as on lake and river beds. Alluvial fans are depositional environments typically encountered at the base of a mountain front. Flooding processes occurring on alluvial fans are considerably different from those occurring along single-thread rivers with well-defined floodplains (French 1987; Bridge 2003). Active

erosion, rapid deposition, and uncertainty in flow path make the prediction of flood evolution and extent rather difficult (NRC 1996).

### 2.1.2 Scope of this Chapter

This chapter presents fundamental aspects of the erosion, entrainment into suspension, transport, and deposition of sediment in fluvial systems. The emphasis is on providing an introduction to the fluid mechanics of sediment transport in rivers and the morphodynamics of lake and reservoir sedimentation by turbidity currents, with the objective of establishing the background needed for sedimentation engineering and management. Emphasis is placed on the transport of noncohesive sediment, where the material involved is in granular form and ranges in size from fine silt to coarse sand. The transport of gravel and sediment mixtures is treated in Chapter 3, whereas the transport of fine-grained, cohesive sediment is considered in Chapter 4. Fluvial processes are addressed in Chapter 6 while engineering aspects of geomorphology are covered in Chapter 16. Sediment

transport in ice-covered rivers is the subject of Chapter 13. Hyperconcentrated flows, including mud flows and debris flows as well as sediment hazards related to flows in alluvial fans, are treated in Chapter 19. This chapter is intended to provide the foundation for the rest of the manual.

## 2.2 FLUID MECHANICS AND HYDRAULICS FOR SEDIMENT TRANSPORT

In this section, basic fluid mechanics and hydraulics concepts needed for the analysis of sedimentation processes are presented.

### 2.2.1 Flow Velocity Distribution: Law of the Wall

Consider a steady, turbulent, uniform, open-channel flow having a mean depth  $H$  and a mean flow velocity  $U$  (Fig. 2-2). The channel has a mean width  $B$  that is much greater than the mean flow depth  $H$ , and its bottom has a mean slope  $S$  and a surface roughness that can be characterized by the effective height  $k_s$  (Brownlie 1981). For very wide channels (i.e.  $B/H \gg 1$ ), the hydraulic radius of the channel,  $R_h$  (cross-sectional area over wetted perimeter), can be approximated by the mean flow depth  $H$ . When the bottom of the channel is covered with sediment having a mean size or diameter  $D$ , the roughness height  $k_s$  will be proportional to this diameter. Due to the weight of the water, the flow exerts on the bottom a tangential force per unit bed area known as the bed shear stress  $\tau_b$ , which in the case of steady, uniform flow can be expressed as:

$$\tau_b = \rho g H S \quad (2-1)$$

where

$\rho$  = water density and

$g$  = gravitational acceleration.

This equation is simply the one-dimensional momentum conservation equation for the channel reach under

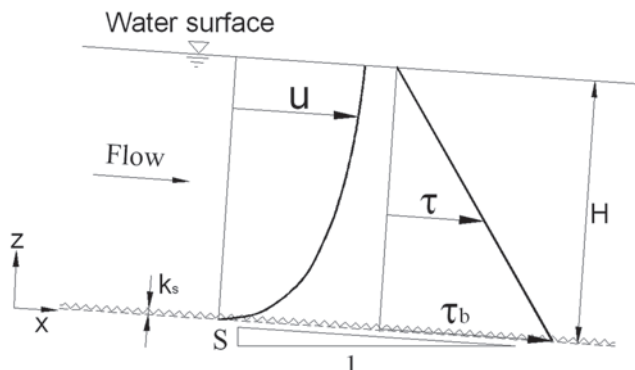


Fig. 2-2. Definition diagram for open-channel flow over a sediment bed.

consideration. With the help of the boundary shear stress, it is possible to define the shear velocity  $u_*$  as

$$u_* = \sqrt{\tau_b / \rho} \quad (2-2)$$

The shear velocity, and thus the boundary shear stress, provides a direct measure of the flow intensity and its ability to entrain and transport sediment particles. The size of the sediment particles on the bottom determines the surface roughness, which in turn affects the flow velocity distribution and its sediment transport capacity. Because flow resistance and sediment transport rates are interrelated, it is important to be able to determine the role played by the bottom roughness.

In the case of steady, uniform flow the shear stress varies linearly in the vertical direction as shown in Fig. 2-2 and is given by the following expression:

$$\tau = \tau_b \left( 1 - \frac{z}{H} \right) \quad (2-3)$$

It is well established, both experimentally and from dimensional arguments (Schlichting 1979; Nezu and Rodi 1986) that the flow velocity distribution is well represented by:

$$\frac{u}{u_*} = \frac{1}{\kappa} \ln \left( \frac{z}{z_0} \right) \quad (2-4)$$

Here

$u$  = time-averaged flow velocity at a distance  $z$  above the bed;

$z_0$  = bed roughness length (i.e., distance above the bed where the flow velocity goes to zero); and

$\kappa$  is known as von Karman's constant and has a value of approximately 0.41 (Nezu and Rodi 1986; Long et al. 1993). The above law is known as the "law of the wall." It strictly applies only in a relatively thin layer ( $z/H < 0.2$ ) near the bed (Nezu and Nakagawa 1993). It is commonly used as a reasonable approximation throughout most of the flow in many streams and rivers.

If the bottom boundary is sufficiently smooth, a condition rarely satisfied in rivers, turbulence will be drastically suppressed in an extremely thin layer near the bed, known as the viscous sublayer. In this region, a linear velocity profile holds (O'Connor 1995):

$$\frac{u}{u_*} = \frac{u_* z}{v} \quad (2-5)$$

where  $v$  is the kinematic viscosity of water. This law merges with the logarithmic law near  $z = \delta_v$ , where

$$\delta_v = 11.6 \frac{v}{u_*} \quad (2-6)$$

denotes the height of the viscous sublayer. In the logarithmic region, the constant of integration introduced above has been evaluated from data to yield

$$\frac{u}{u_*} = \frac{1}{\kappa} \ln \left( \frac{u_* z}{v} \right) + 5.5 \quad (2-7)$$

Comparing Eqs. (2-7) and (2-4), it follows that  $z_o = v/u_*$  for a hydraulically smooth flow.

Understanding the physics of the flow in the viscous sublayer is of relevance in benthic boundary layer flows (e.g., Boudreau and Jorgensen 2001). For example, sediment oxygen demand is affected by viscous effects as well as near-bed turbulence levels, as is shown in Chapter 22 of this manual. Also, the existence of a viscous sublayer seems to be a necessary condition for the development of ripples in unidirectional flows (e.g., Raudkivi 1997; Coleman and Melville 1994, 1996).

Most boundaries in alluvial rivers are hydraulically rough. Let  $k_s$  denote an effective roughness height. If  $k_s/\delta_v > 1$ , then no viscous sublayer will exist, because the roughness elements will protrude through such layer. In this case the corresponding logarithmic velocity profile is given by

$$\frac{u}{u_*} = \frac{1}{\kappa} \ln \left( \frac{z}{k_s} \right) + 8.5 = \frac{1}{\kappa} \ln \left( 30 \frac{z}{k_s} \right) \quad (2-8)$$

It follows that  $z_o = k_s/30$  for a hydraulically rough flow. As noted above, the logarithmic velocity distribution often holds as a first approximation throughout the flow depth in a river. It is by no means exact since wake effects near the free surface can be important (Coleman 1981; Lyn 1991). Sediment-induced stratification as well as the presence of bed forms can also influence the flow velocity distribution. For many years, the effect of suspended sediment was understood to be in a change of von Karman's constant  $k$  (Einstein and Chien 1955; Vanoni 1975). However, there is now conclusive evidence that von Karman's constant is not affected by the presence of suspended sediment as previously believed, and its clear-water value ( $k \approx 0.41$ ) can be considered to be a universal one (Smith and McLean 1977; Coleman 1981, 1986; Lyn 1991; Soulsby and Wainright 1987; Wright and Parker 2004a).

As is to be shown, it is not uncommon under field conditions to find that the flow regime is neither hydraulically smooth nor hydraulically rough. The conditions  $k_s/\delta_v \gg 1$  for hydraulically rough flow and  $k_s/\delta_v \ll 1$  for hydraulically smooth flow can be rewritten to indicate that the roughness Reynolds number, given by  $u_* k_s/v$ , should be much larger than 11.6 for turbulent rough flow, and much smaller than 11.6 for turbulent smooth flow. A composite form that

represents both ranges, as well as the transitional range between them, can be written as (Yalin 1992)

$$\frac{u}{u_*} = \frac{1}{\kappa} \ln \left( \frac{z}{k_s} \right) + B_s \quad (2-9a)$$

with  $B_s$  as a function of  $Re_* = u_* k_s/v$  which can be estimated with the following empirical fit

$$B_s = 8.5 + [2.5 \ln(Re_*) - 3] e^{-0.121[\ln(Re_*)]}^{2.42} \quad (2-9b)$$

A plot of this function can be seen in Fig. 2-3.

An alternative way of writing Eq. (2-9a) is

$$\frac{u}{u_*} = \frac{1}{\kappa} \ln \left( A_s \frac{z}{k_s} \right) \quad (2-9c)$$

It follows then that  $A_s$  and  $B_s$  are related by

$$A_s = e^{\kappa B_s} \quad (2-9d)$$

Another useful fit to the vertical velocity distribution in open-channel flows, which also covers the entire range from hydraulically smooth to hydraulically rough as well as the transition, was proposed by Swamee (1993),

$$\frac{u}{u_*} = \left\{ \left( \frac{v}{u_* z} \right)^{10/3} + \left[ \kappa^{-1} \ln \left( 1 + \frac{9(u_* z/v)}{1 + 0.3(u_* k_s/v)} \right) \right]^{-10/3} \right\}^{-0.3} \quad (2-10)$$

Typically, muddy bottoms as well as beds covered with silt and fine sand are hydraulically smooth, whereas the presence of coarse sands and gravel leads, in general, to hydraulically rough conditions.

## 2.2.2 Flow Velocity Distribution: Velocity-Defect and Log-Wake Laws

The flow velocity distribution given by the law of the wall, Eq. (2-4), requires some knowledge of the bed roughness characteristics. An alternative formulation can be obtained if the flow depth  $H$  is introduced as the relevant length scale. Assuming that the maximum flow velocity  $u_{\max}$  takes place at the water surface,  $z = H$ , Eq. (2-4) can be manipulated to obtain the so-called velocity-defect law, also known as the outer form of the law of the wall (Schlichting 1979)

$$\frac{u_{\max} - u}{u_*} = -\frac{1}{\kappa} \ln \frac{z}{H} \quad (2-11)$$

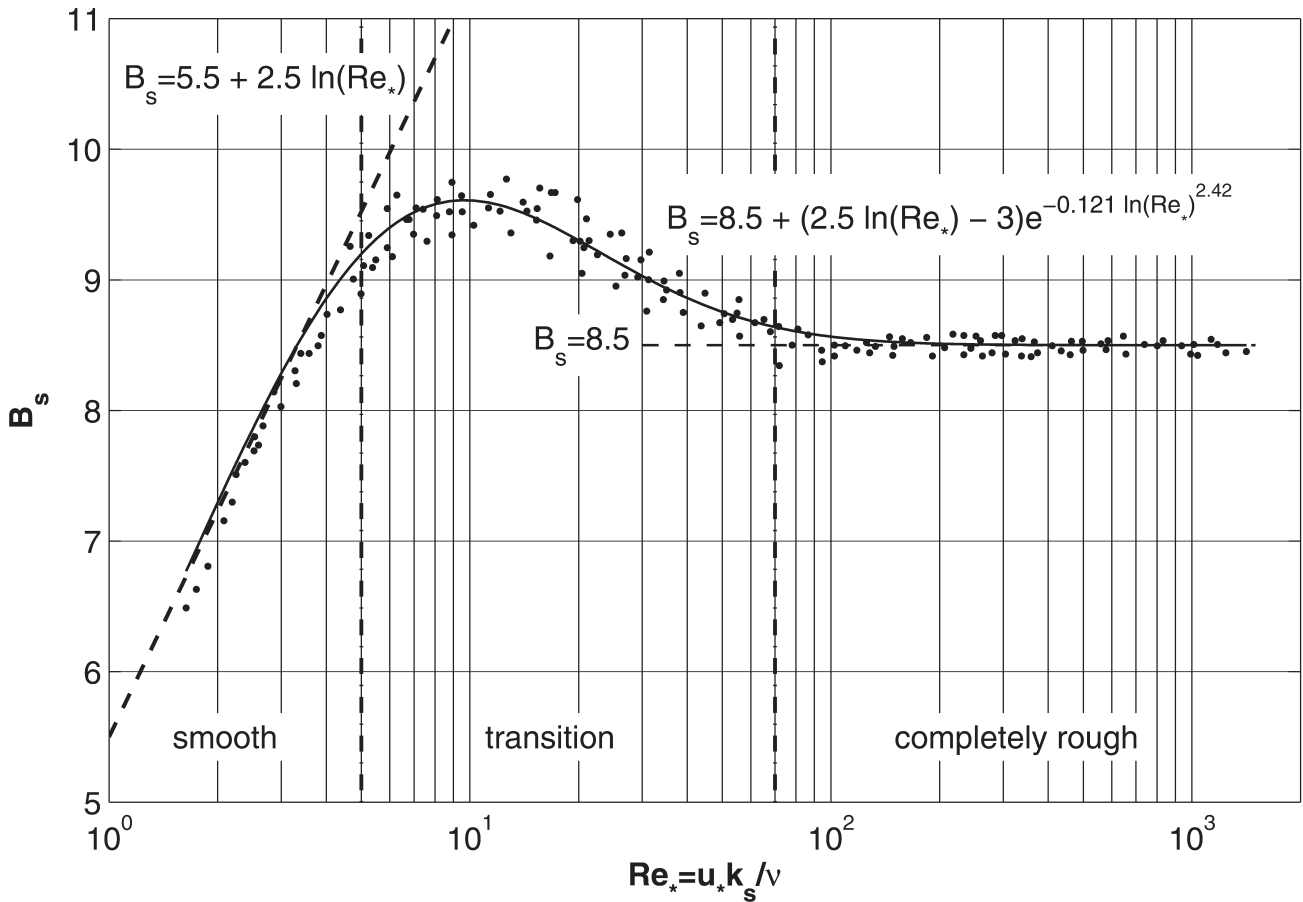


**Fig. 2-3.** Plot of  $B_s$  function in log-law velocity distribution.

A number of researchers have argued that the logarithmic behavior of the velocity distribution, either in the inner form given by Eq. (2-4) or in the outer form given by Eq. (2-11), can be justified only for a restricted region near the bed ( $z/H < 0.2$ ), and that, for  $z/H > 0.2$ , a correction of the logarithmic function is necessary (Coleman and Alonso 1983; Sarma et al. 1983).

Nezu and Nakagawa (1993) added a wake function to the standard log law given by Eq. (2-7), calling it the “log-wake law,” as follows,

$$\frac{u}{u_*} = \frac{1}{\kappa} \ln\left(\frac{u_* z}{v}\right) + 5.5 + w\left(\frac{z}{H}\right) \quad (2-12a)$$

where  $w(z/H)$  is the wake function first proposed by Coles (1956) for turbulent boundary-layer flows, which takes the form

$$w\left(\frac{z}{H}\right) = \frac{2W_0}{\kappa} \sin^2\left(\frac{\pi}{2} \frac{z}{H}\right) \quad (2-12b)$$

In this relation  $W_0$  is known as the Coles wake parameter, expressing the strength of the wake function. Through trigonometric substitution, Eq. (2-11) can also be written in log-wake form (Coleman 1981; Coleman and Alonso 1983).

$$\frac{u_{max} - u}{u_*} = -\frac{1}{\kappa} \ln\left(\frac{z}{H}\right) + \frac{2W_0}{\kappa} \cos^2\left(\frac{\pi z}{2H}\right) \quad (2-13)$$

A procedure to estimate the Coles wake parameter from flow velocity measurements, originally proposed by Coleman (1981), can be found in Julien (1995 p. 103). Nezu and Rodi (1986), in experiments on flat-bed, smooth-bed, turbulent flows, found  $W_0$  to vary from 0 to 0.253, with a mean value of  $W_0 \approx 0.2$ . This result was confirmed independently by Lyn (1991). Coleman (1981) and Parker and Coleman (1986) demonstrated that for the case of sediment-laden flows over flat beds,  $W_0$  increases with increasing sediment concentration, ranging from 0.191 to 0.861. Lyn (1993) found that for flow over artificial bed forms,  $W_0$  ranged from -0.05 to 0.1, and suggested that negative values of  $W_0$  are the result of

strong, favorable pressure gradients. Lyn (1993) also found good results in replicating measured velocity profiles over bed forms with the log-wake law.

Most knowledge of flow velocity distribution in turbulent, free-surface flows stems from laboratory studies (e.g., Nezu and Rodi 1986; Nelson et al. 1993; Song et al. 1994; Bennett and Best 1995; 1996; Best et al. 2001; Lemmin and Rolland 1997; Muste and Patel 1997; Graf and Cellino 2002). In the past few years, however, new acoustic technology for flow measurement has made possible the observation of velocity profiles in streams and rivers as well (Kostaschuk et al. 2004; Dinehart and Burau 2005). With the help of observations made in the Missouri river, Holmes (2003) has found that the velocity-defect law, Eq. (2-13), works well for field conditions and the Coles wake parameter takes values ranging from  $-0.035$  to  $0.36$ . In all cases, dune-like bed forms were present, suggesting that such features might be responsible for the deviations from the logarithmic velocity distribution, observed away from the bottom. More field observations need to be made to quantify the effect of bed forms on the velocity distribution in alluvial rivers as well as the role played by stratification induced by suspended sediments. A recent review of mean flow, turbulence and bed form dynamics in alluvial rivers can be found in Best (2005).

### 2.2.3 Relations for Channel Flow Resistance

Most river flows are commonly considered to be hydraulically rough. Neglecting wake effects, Eq. (2-8) can be used to obtain an approximate expression for depth-averaged velocity  $U$  that is reasonably accurate for most flows. Integrating the mean flow velocity distribution given by Eq. (2-8) and dividing by the mean flow depth yields

$$U = \frac{1}{H} \int_0^H u dz \quad (2-14)$$

Now by slightly changing the lower limit of integration to avoid the fact that the logarithmic law is singular at  $z = 0$ , the following result is obtained:

$$\frac{U}{u_*} = \frac{1}{H} \int_{k_s}^H \left[ \frac{1}{\kappa} \ln \left( \frac{z}{k_s} \right) + 8.5 \right] dz \quad (2-15)$$

or after the integration is performed

$$\frac{U}{u_*} = \frac{1}{\kappa} \ln \left( \frac{H}{k_s} \right) + 6 = \frac{1}{\kappa} \ln \left( 11 \frac{H}{k_s} \right) \quad (2-16)$$

This relation is known as Keulegan's resistance law for rough flow (Keulegan 1938) and it has been extensively used

to estimate grain-induced resistance in gravel-bed streams (e.g. Bray 1979; Parker 1990).

It can be shown that the logarithmic form of Eqs. (2-8) and (2-16) can be approximated by power laws of the Manning-Strickler form, as follows:

$$\frac{u}{u_*} = \frac{1}{\kappa} \ln \left( 30 \frac{z}{k_s} \right) \cong 9.34 \left( \frac{z}{k_s} \right)^{1/6} \quad (2-17a)$$

$$\frac{U}{u_*} = \frac{1}{\kappa} \ln \left( 11 \frac{H}{k_s} \right) \cong 8.1 \left( \frac{H}{k_s} \right)^{1/6} \quad (2-17b)$$

To facilitate their comparison, a plot of Eqs. (2-17a) and (2-17b) is shown in Fig. 2-4. It is similar to the one presented by Brownlie (1983). The relative error between the log law and the power law is less than 4.2% in Eq. (2-17a) and less than 3% in the case of Eq. (2-17b). Keulegan (1938) was the first to point out the equivalence between the log-law and the power-law, given by Eq. (2-17b), in the context of open-channel flows. Chen (1991) provides a rigorous discussion of logarithmic and power-law velocity distributions, including a comparison of the associated flow resistance relations for both hydraulically smooth flows and fully rough flows.

Now, between Eqs. (2-2) and (2-16), a resistance relation can be found for the bed shear stress:

$$\tau_b = \rho C_f U^2 \quad (2-18)$$

where the friction coefficient  $C_f$  is given by

$$C_f = \left[ \frac{1}{\kappa} \ln \left( 11 \frac{H}{k_s} \right) \right]^{-2} \quad (2-19)$$

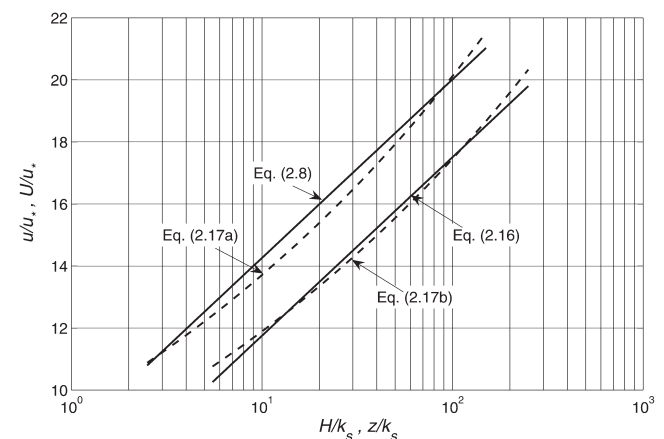


**Fig. 2-4.** Comparison of logarithmic laws versus power laws for velocity distribution and flow resistance.

If Eq. (2-17b) is used instead of Eq. (2-16), the friction coefficient takes the form:

$$C_f = \left[ 8.1 \left( \frac{H}{k_s} \right)^{1/6} \right]^{-2} \quad (2-20)$$

It is important to emphasize that Eq. (2-18) provides a local point estimate of bed shear stress, while Eq. (2-1) gives a reach-averaged value of the bed shear stress (Yen 2002).

It is useful to show the relationship between the friction coefficient  $C_f$  and the roughness parameters in open-channel flow relations commonly used in practice. Between Eqs. (2-1) and (2-18), a form of Chezy's law can be derived (Chow 1959):

$$U = C_z H^{1/2} S^{1/2} \quad (2-21)$$

where the Chezy coefficient  $C_z$  is given by the relation

$$C_z = \left( \frac{g}{C_f} \right)^{1/2} \quad (2-22)$$

A specific evaluation of Chezy's coefficient can be obtained by substituting Eq. (2-19) into Eq. (2-22). It is seen that the coefficient is not constant, but varies as the logarithm of the relative roughness  $H/k_s$ . A logarithmic dependence is typically a weak one, partially justifying the common assumption that Chezy's coefficient in Eq. (2-21) is roughly a constant. By substituting Eq. (2-20) into Eq. (2-21) and Eq. (2-22), Manning's equation in metric units is obtained

$$U = \frac{1}{n} H^{2/3} S^{1/2} \quad (2-23a)$$

Here Manning's  $n$  is given by

$$n = \frac{k_s^{1/6}}{8.1 g^{1/2}} \quad (2-23b)$$

This relation is often called the *Manning-Strickler* form of Manning's  $n$  (Brownlie 1983). It is deceptively simple but it also contains important information. Even for large increases in roughness height  $k_s$ , Manning's  $n$  does not change much. The opposite behavior is seen if large values of Manning's  $n$  are considered, and the corresponding value of  $k_s$  is estimated with the help of Eq. (2-23b). Often the back-calculated values of  $k_s$  turn out to be larger than the mean flow depth  $H$ , suggesting that the value of Manning's  $n$  being used is not a realistic one. From the analysis above, it should also be apparent that Manning's equation can only be applied to uniform,

hydraulically rough, fully turbulent flows. Extensive tables of Manning's  $n$  values for different channel characteristics are given in Chow (1959) and Yen (1991).

It is also important to notice that according to Eq. (2-23b), Manning's  $n$  is not a dimensionless parameter. Yen (1992, 2002) and Dooge (1991), as well as Mostafa and McDermid (1971), have proposed dimensionally homogeneous forms of Manning's equation. Such dimensionless equation can be readily obtained from Eqs. (2-23a) and (2-23b) as follows:

$$U = M \left( \frac{H}{k_s} \right)^{1/6} \sqrt{g H S} \quad (2-24a)$$

Where the dimensionless constant  $M = 8.1$  in this case and is valid for very wide channels. Different values for  $M$  can be found in the literature depending on the Strickler (1923) coefficient used in Eq. (2-23b). Yen (1993) reports values of  $M$  between 6.71 and 12.82, while Julien (2002) fits a value of  $M = 5$  to field observations. With the help of Eq. (2-23b), it is possible to define a dimensionless Strickler number

$$St = \frac{n \sqrt{g}}{k_s^{1/6}} = \frac{1}{8.1} = 0.12 \quad (2-24b)$$

It follows that the constant  $M$  in Eq. (2-24a) is the inverse of the Strickler number  $St$ . An alternative way to express the Strickler number is with Keulegan's equation and power-law equivalent. Assuming that  $k_s = D$ , the identity given in Eq. (2-17b) can also be used to estimate the Strickler number

$$St = \frac{(H/D)^{1/6}}{(1/\kappa) \ln(11H/D)} \quad (2-24c)$$

This relation gives values of  $St$  close to 0.12, as obtained from Eq. (2-24b) in the range of relative flow depth  $H/D$  from 10 to 1,000 (Niño 2002). For values  $H/D$  lower than about 10, a sharp increase of  $St$  has been reported (e.g., Limerinos 1970), due to form resistance added to the grain (skin) friction, associated with flow separation in the wake of large bed elements relative to the flow depth. For instance, Ayala and Oyarce (1993) calibrated the following relation from field data obtained in the Mapocho River in the Chilean side of the Andean mountains, for values of  $H/D$  lower than 10 and taking  $D = D_{90}$ ,

$$St = 0.30 \left( \frac{H}{D_{90}} \right)^{-0.40} \quad (2-24d)$$

This implies that  $M$  in the relation to estimate the mean flow velocity (Eq. 2-24a) would no longer be constant but would change as a function of flow depth for  $H/D < 10$ .

There is no accepted standard equation for predicting flow velocities in channels with large relative roughness, i.e. where channel bed material is large relative to water depth. This is typical of mountain streams (Jarrett 1984; Aguirre-Pérez and Fuentes 1990). Smart et al. (2002) conducted an analysis of existing flow resistance equations which points to the difficulties associated with the definition of depth and hydraulic radius when the bed roughness is large relative to the flow depth. They found that the log law, or the equivalent power law, is only applicable when the roughness is of sufficiently small scale, and recommended the use of a square-root power law to estimate flow velocity in the presence of large-scale roughness.

In the case of sand-bed streams, flow resistance is influenced by both grain or skin friction as well as form drag induced by the development of bed forms such as ripples, dunes and bars, so any estimate of Manning's  $n$ , or any other roughness coefficient, has to account for the possibility of different flow regimes (i.e., lower and upper regimes). Bruschin (1985), Camacho and Yen (1991), Wu and Wang (1999), and Hager and Del Giudice (2001) have proposed equations to estimate Manning's  $n$  for the case of sand-bed rivers. A modified Manning-Strickler formula for flow in alluvial channels with sand beds has also been advanced by Yu and Lim (2003). Flow resistance predictors for sand-bed streams are discussed later in the chapter.

#### 2.2.4 Fixed-Bed (Skin or Grain) Roughness

It is clear that to use these relations for channel flow resistance, a criterion for evaluating the equivalent roughness height  $k_s$  is necessary. Friction factors for turbulent flow in pipes and in fixed-bed channels have their roots in the classic sand-roughened pipe experiments conducted by Nikuradse (1933). He conducted a set of pioneer experiments and proposed the following criterion. Suppose a rough surface is subjected to a flow. Then the equivalent roughness height  $k_s$  of the surface would be equal to the diameter of sand grains that, when glued uniformly to a completely smooth wall, and then subjected to the same external conditions, yields the same velocity profile. Nikuradse used sand glued to the inside of pipes to conduct this evaluation.

To analyze the work of Nikuradse, it is convenient to introduce another relation that can be used to estimate mean flow velocity in open-channel flows, known as the Darcy-Weisbach equation

$$U = \sqrt{\frac{8}{f}} \sqrt{gR_h S} = \sqrt{\frac{8}{f}} u_* \quad (2-26)$$

In this equation

$g$  = gravitational acceleration;

$u_*$  = shear velocity;

$R_h$  is the hydraulic radius (approximately equal to the flow depth  $H$  for very wide channels); and  $f$  is the

dimensionless Darcy-Weisbach friction coefficient, which, for a pipe with diameter  $D$  is known to be a function of the flow Reynolds number  $R_e = UD/v$  and the relative roughness  $D/k_s$ .

Brownlie (1981) re-examined Nikuradse's data and proposed the friction factor diagram shown in Fig. 2-5. The diagram provides the values of the friction factor  $f$ , introduced in Eq. (2-26), as a function of the Reynolds number  $R_e = UD/v$  and the relative roughness  $D/k_s$ . This diagram is equivalent to the well known Moody diagram shown in Fig. C-2 of Appendix C, and can be used for sidewall corrections in laboratory experiments (Vanoni and Brooks 1957) as well as for separating total resistance into grain resistance and form resistance in alluvial streams with dunes (Brownlie 1981; Fedele and García 2001). For open-channel flow calculations, the pipe diameter  $D$  should be replaced by  $4R_h$ , in which  $R_h$  is the hydraulic radius. Again, for a very wide channel, the hydraulic radius can be replaced by the mean flow depth. The sidewall correction procedure is explained in detail both in Brownlie (1981) as well as in ASCE Manual 54 (Vanoni 2006) and therefore is not repeated here.

In the late 1930s, Zegzhda conducted a set of experiments in straight rectangular flumes of varying roughness, using an experimental method (gluing sand to the walls) similar to the one used by Nikuradse for flow in pipes (see Novak and Cabelka 1981, p. 124). Because this work was not published in English, it is not as well known as Nikuradse's work on pipes. However, this experimental study was conducted for a set of relative-roughness ( $R_h/k_s$ ) values more representative of the conditions observed in the field for the case of sand-bed streams with plane beds. In fact, the relation obtained by Zegzhda for fully-rough hydraulic conditions is very similar to the expression advanced independently at about the same time by Keulegan (Eq. 2-16).

A fit to the experimental results of Nikuradse that can be used to estimate the roughness length parameter  $z_0$  in Eq. (2-4) as a function of  $k_s$  was proposed by Christofferson and Jonsson (1985)

$$z_0 = \frac{k_s}{30} \left[ 1 - \exp\left(\frac{-u_* k_s}{27v}\right) \right] + \frac{v}{9u_*} \quad (2-27)$$

Smith (1977) seems to have been the first to plot Nikuradse's data in a way useful to estimate the roughness length. Similar empirical relations have been proposed by Fuentes and Carrasquel (1981) and Dade et al. (2001). For  $u_* k_s / v < 3$ , the flow is hydraulically smooth and  $z_0 = 0.11v/u_*$ ; whereas for  $u_* k_s / v > 100$  the flow is hydraulically rough and  $z_0 = 0.033k_s$ . In many interesting sediment transport situations the flow is hydraulically transitional and an equation such as Eq. (2-27) has to be used to estimate the roughness length in Eq. (2-4) associated with grain-induced roughness (Kamphuis 1974). Typically, muds and flat fine sands are

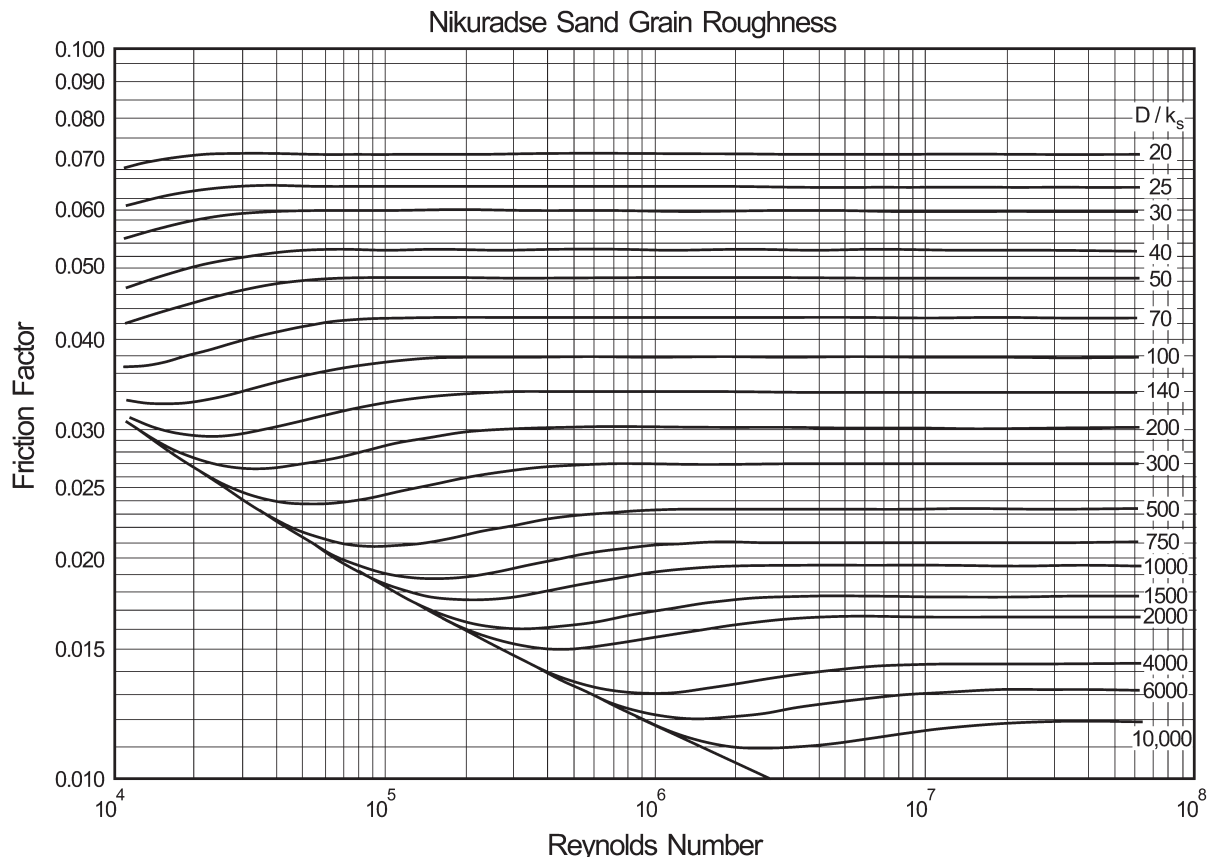


**Fig. 2-5.** Revised Nikuradse friction factor diagram for flow in pipes of diameter D or open-channel flows with hydraulic radius  $R_h = D/4$  (after Brownlie, 1981).

hydraulically smooth or transitional, and coarse sands and gravels are hydraulically rough (Soulsby, 1997). It is common practice to treat all flows over sands as being hydrodynamically rough since this simplifies the analysis. This simplifying approximation makes less than 10% error in the estimation of the shear velocity  $u_*$ , for all values  $u_*$  above the threshold of motion (see Section 2.4.2) of grains larger than  $60 \mu\text{m}$ .

Although it is clear that the sediment size distribution in most rivers is not as uniform as the material used in his experiments, Nikuradse's concept of grain-induced roughness for pipe flows has been extended to estimate friction factors in streams and rivers as well (Yen 1992). Nikuradse's equivalent sand-grain roughness,  $k_s$ , is commonly taken to be proportional to a representative sediment size  $D_x$ ,

$$k_s = \alpha_s D_x \quad (2-28)$$

Suggested values of  $\alpha_s$  which have appeared in the literature are listed in Table 2-1, originally compiled by Yen (1992; 2002) and updated for this manual. Different sediment sizes have been suggested for  $D_x$  in Eq. (2-28). Statistically,  $D_{50}$  (the grain size for which 50% of the bed material is finer) is most readily available. Physically, a representative

size larger than  $D_{50}$  is more meaningful to estimate flow resistance because of the dominant effect of large sediment particles. The range of  $\alpha_s$  values and the diverse representative sediment size used for  $D_x$  indicate that further research on this concept is necessary.

In a study of flow resistance associated with rip-rapped surfaces, Maynard (1991) reviewed a number of formulations commonly used to estimate the Darcy-Weisbach friction coefficient and found that a power-law equation can be used for most riprap (i.e., fixed-bed) problems in very wide open-channel flows, as follows:

$$\left(\frac{8}{f}\right)^{1/2} = 6.89 \left(\frac{H}{D_{50}}\right)^{1/6} \quad (2-29)$$

Notice the similarity with the power-law equations for flow resistance presented earlier. Maynard (1991) also found a logarithmic expression for flow resistance, based on his own experiments as well as on data from other sources, given by

$$\left(\frac{8}{f}\right)^{1/2} = 3.92 \log\left(\frac{H}{D_{50}}\right) + 6.86 \quad (2-30)$$

**Table 2-1 Ratio of Nikuradse Equivalent Roughness Size and Sediment Size for Rivers**

Investigator	Measure of sediment size, $D_x$	$\alpha_s = k_s/D_x$
Ackers and White (1973)	$D_{35}$	1.23
Aguirre-Pe and Fuentes (1990)	$D_{84}$	1.6
Strickler (1923)	$D_{50}$	3.3
Katul et al (2002)	$D_{84}$	3.5
Keulegan (1938)	$D_{50}$	1
Meyer-Peter and Muller (1948)	$D_{50}$	1
Thompson and Campbell (1979)	$D_{50}$	2.0
Hammond et al. (1984)	$D_{50}$	6.6
Einstein and Barbarossa (1952)	$D_{65}$	1
Irmay (1949)	$D_{65}$	1.5
Engelund and Hansen (1967)	$D_{65}$	2.0
Lane and Carlson (1953)	$D_{75}$	3.2
Gladki (1979)	$D_{80}$	2.5
Leopold et al. (1964)	$D_{84}$	3.9
Limerinos (1970)	$D_{84}$	2.8
Mahmood (1971)	$D_{84}$	5.1
Hey (1979), Bray (1979)	$D_{84}$	3.5
Ikeda (1983)	$D_{84}$	1.5
Colosimo et al. (1986)	$D_{84}$	3.6
Whiting and Dietrich (1990)	$D_{84}$	2.95
Simons and Richardson (1966)	$D_{85}$	1
Kamphuis (1974)	$D_{90}$	2.0
Van Rijn (1982)	$D_{90}$	3.0

which applies in the range  $2.2 < H/D_{50} < 23$ . Similar empirical relations have been advanced by Hey (1979), Thompson and Campbell (1979), Griffiths (1981), Pyle and Novak (1981), and Bathurst (1985).

From these equations, it follows that for wide, open channel flows the Darcy-Weisbach friction coefficient and Manning's roughness coefficient are related by

$$\left(\frac{8}{f}\right)^{1/2} = \frac{K_n H^{1/6}}{ng^{1/2}} = \frac{U}{\sqrt{gHS}} \quad (2-31)$$

in which  $K_n$  is a constant equal to 1 in metric units and equal to 1.486 in English units (Yen 2002). The velocity distribution in high-gradient streams with relatively low values of relative submergence  $H/D_{50}$  is no longer logarithmic near the bed due to the wake effect produced by large roughness elements. Wiberg and Smith (1991) have developed a model for the velocity field in steep streams with coarse gravel beds that is capable of reproducing the field observations made by

Marchand et al. (1984). At about the same time, Aguirre-Pe and Fuentes (1990) proposed a theory for flow resistance in steep, rough streams that takes into account the existence of the highly turbulent wake zone near a very rough bed. Their model predictions compare favorably against field observations by several authors. As shown by Smart (1999; 2002), most of the uncertainty when dealing with coarse gravel and cobbles in shallow channels is in the determination of the mean bed location so that the origin of the flow velocity profile can be ascertained. In relation to the difficulties associated with defining the mean bed elevation, Nikora et al. (2001) show the importance of spatial averaging when dealing with shallow flows over gravel bed streams. In the absence of a logarithmic velocity distribution, Katul et al. (2002) developed a velocity distribution equation based on mixing-length theory capable of reproducing flow resistance characteristics observed in shallow streams with large relative roughness. More recently, Buffington et al. (2004) studied the effects of channel type and associated hydraulic roughness on salmonid spawning-gravel availability in mountain catchments.

## 2.2.5 Movable Flat-Bed Roughness

In flows over geometrically smooth, fixed boundaries, the apparent roughness of the bed  $k_s$  can be computed using Nikuradse's approach, as shown above. However, once the transport of bed material has been instigated, the characteristic grain diameter and the viscous sublayer thickness no longer provide the relevant length scales. The characteristic length scale in this situation is the thickness of the layer where the sediment particles are being transported by the flow, usually referred to as the bed-load layer height (Wiberg and Rubin 1989). As the grains start to roll and saltate along the bed, they take momentum away from the mean flow via drag, resulting in an increase in flow resistance that translates into an increase in bed roughness.

Once the bed shear stress  $\tau_b$  exceeds the critical shear stress for particle motion  $\tau_c$ , the roughness length can be estimated with an expression inspired by the work of Owen (1964) for wind-induced sediment transport, and first proposed by Smith (1977) for sediment transport by water currents,

$$z_0 = \alpha_0 \frac{(\tau_b - \tau_c)}{(\rho_s - \rho)g} + z_{0N} \quad (2-32a)$$

where

$$\begin{aligned} \alpha_0 &= 26.3; \\ z_{0N} &= 0.033k_s \text{ and } k_s = \text{Nikuradse roughness length; and} \\ \rho_s &= \text{bed sediment density.} \end{aligned}$$

This approach is particularly suitable for sand-bed rivers and has been widely used in coastal sedimentation (e.g., Smith and McLean 1977).

The roughness parameter also can be estimated with a scheme proposed by Dietrich and Whiting (1989),

$$z_0 = \alpha_1 \delta_b + z_{0N} \quad (2-32b)$$

where

$$\begin{aligned} \alpha_1 &= \text{empirical constant equal to 0.077;} \\ z_{0N} &= 0.033k_s \text{ and } k_s = \text{Nikuradse roughness length; and} \\ \delta_b &= \text{bedload-layer height,} \end{aligned}$$

which is computed as

$$\delta_b = \frac{1.2 D (1 - \cos\phi) \left[ \frac{\tau_b}{\tau_c} \right]}{1 + 0.2 \left[ \frac{\tau_b}{\tau_c} \right]} \quad (2-32c)$$

where

$$\begin{aligned} \phi &= \text{angle of friction, and} \\ D &= \text{mean diameter of the bed material.} \end{aligned}$$

Since both estimators depend on the flow intensity as given by the bed shear stress, Eqs. (2-32a) and (2-32b) provide an estimate of a variable roughness appropriate for movable beds without the presence of bed forms.

Wiberg and Rubin (1989) evaluated several expressions for characterizing bed roughness produced by a layer of saltating sediment grains; they proposed with the help of a formulation for the vertical eddy diffusivity coefficient (Gelfenbaum and Smith 1986; Long et al. 1993) a formulation which makes use of a vertical flow velocity distribution given by the following expression

$$u(z) = \frac{u_*}{\kappa} \int_{z_0}^z \frac{1 - (z/H)}{z \exp[-(z/H) - 3.3(z/H)^2 + 2.2(z/H)^3]} dz \quad (2-33)$$

where

$$\begin{aligned} z &= \text{distance from the bed;} \\ H &= \text{flow depth; and} \\ \kappa &= 0.41 = \text{von Karman's constant.} \end{aligned}$$

Seven upper plane-bed experiments of Guy et al. (1966) were used to obtain best fit values for the shear velocity  $u_*$  and bed roughness length  $z_0$  with the help of Eq. (2-33). The analysis of Wiberg and Rubin (1989) shows that the bed roughness associated with sediment transport can reach values about an order of magnitude larger than the Nikuradse grain roughness in plane-bed flows, but this roughness will in general be significantly smaller than the roughness associated with ripples and dunes when they are present on the bed surface.

At high bed shear stresses and sediment transport intensities in sand-bed streams, dunes are washed out and the bed becomes plane. In this regime, sediment is transported near the bed in a layer with a thickness that is much larger than the grain size. Collisions between grains are intense in this layer, resulting in a grain flow or granular fluid flow. This regime is known as sheet flow and measurements taken by researchers (Wilson 1987, 1989; Nnadi and Wilson 1992) have shown that flow resistance increases drastically with flow intensity in this regime. Sumer et al (1996) found that flow resistance induced by the sheet-flow layer can be expressed in terms of the ratio of Nikuradse's equivalent sand roughness to the grain diameter ( $k_s/D$ ). This ratio was found to behave differently whether or not the grains became suspended near the bed. In the absence of suspension mode,  $k_s/D$  depends only on the Shields parameter ( $\tau^*$ ) defined by Eq. (2-56). In the suspension mode,  $k_s/D$  depends not only on  $\tau^*$  but also on a dimensionless sediment fall velocity parameter  $R_f$  defined by Eq. (2-46b). There is also evidence that sediment transport in the sheet-flow layer is influenced by the turbulent bursting process (e.g., Sumer et al. 2003).

## 2.2.6 Equivalent Roughness of Bed Forms

As the flow intensity increases, bed forms such as ripples and dunes can develop (e.g., Raudkivi 1997). In this situation, the bed roughness also will be influenced by form drag due to the presence of bed forms. The fundamental problem is that the bed form characteristics and, hence, the bed roughness depend on the main flow characteristics (e.g., mean velocity, depth) and sediment characteristics (e.g., grain size, density). Thus, the hydraulic roughness in the presence of bed forms is a dynamic parameter that depends strongly on flow conditions as well as on the bed sediment properties. The equivalent roughness of alluvial beds in the presence of ripples and dunes was addressed with the Nikuradse hydraulic roughness approach by Brownlie (1981) and van Rijn (1982, 1984c). In van Rijn's approach, the height due to grain-induced roughness (Eq. 2-28) was added to an estimate of the equivalent roughness height produced by ripples and dunes obtained from field and laboratory observations, to obtain a measure of the total (grain plus form resistance) effective roughness,

$$k_s = \alpha_s D_{90} + \gamma_{sf} 1.1 \Delta (1 - e^{-25\Delta/\lambda}) \quad (2-34a)$$

where

- $\alpha_s$  = 3 (see Eq. 2-28);
- $D_{90}$  = grain size for which 90% of the bed material is finer;
- $\gamma_{sf}$  = dune shape factor = 1.
- $\Delta$  and  $\lambda$  = bed form height and length, respectively; and
- $\Delta / \lambda$  = bedform steepness.

The effective roughness height was then used to estimate the Chezy friction coefficient (Eq. 2-22),

$$C_Z = \left( \frac{g}{C_f} \right)^{1/2} = 18 \log \left( \frac{12 R_{hb}}{k_s} \right) \quad (2-34b)$$

In this equation,  $R_{hb}$  = hydraulic radius of the river bed (i.e., subtracting streambank effects on flow resistance) according to Vanoni-Brooks (1957) (see Vanoni 2006, p. 91). Notice that the Chezy coefficient is not dimensionless. A dimensionless expression of the Chezy coefficient applicable to bank-full sand bed and gravel bed streams can be found in Chapter 3.

Application of Eq. (2-34a) to field conditions resulted in considerable overestimation of the hydraulic roughness (van Rijn 1996). Further analysis showed that the lee-side slopes of natural sand dunes in rivers were less steep than those of dunes in the laboratory and a shape factor  $\gamma_{sf} = 0.7$  was recommended for application to natural river dunes.

A different approach based on boundary-layer theory and measured velocity profiles was proposed by Fedele and García (2001). When spatially-averaged velocity profiles

of flow (Nikora et al. 2001) over dunes are available, this method can be used to estimate a spatially-averaged composite roughness  $k_c$  due to the combined effect of both grain friction and form drag due to bed forms in large sand-bed rivers. Boundary layer studies have shown that an alternative to Eq. (2-9a) for describing the vertical flow velocity distribution in flows where the geometry and size of the roughness elements is such that skin friction and form drag are present, is given by the following equation

$$\frac{u}{u_*} = \frac{1}{\kappa} \ln \left( \frac{z u_*}{v} \right) + A - \frac{\Delta u}{u_*} \left[ \frac{u_* k_c}{v} \right] \quad (2-35a)$$

In Eq. (2-35a),  $\kappa = 0.41$  and  $A = 5.5$  are universal constants previously introduced, and  $\Delta u/u_*$  is a roughness function which is equal to zero for smooth walls (square brackets indicate functional relationship). When plotting  $u/u_*$  versus  $\ln(u_* z/v)$ , this equation represents a family of parallel lines, each being displaced downwards from the smooth-wall velocity profile by an amount  $\Delta u/u_*$  (Schlichting 1979).

The roughness function for alluvial streams with dunes is shown in Fig. 2-6. It shows  $\Delta u/u_*$  as a function of the parameter  $k_c u_*/v$  for laboratory and field streams with fully-developed dunes (Fedele and García 2001). It is observed that for values of the roughness Reynolds number  $k_c u_*/v$  larger than 100–200, most of the data collapse along a straight line, along the fully-rough hydraulic regime, which is well represented by the following fit,

$$\frac{\Delta u}{u_*} = 2.43 \ln \left( \frac{u_* k_c}{v} \right) - 3.24 \quad (2-35b)$$

An application of the alluvial roughness function is its potential use to assess the effect of temperature changes on flow structure and bed morphology. It is observed in Fig. 2-6 that even though the flows are under fully-rough hydraulic conditions, temperature variations will affect the viscosity of the water and this in turn will cause variations in the roughness Reynolds number and the flow structure.

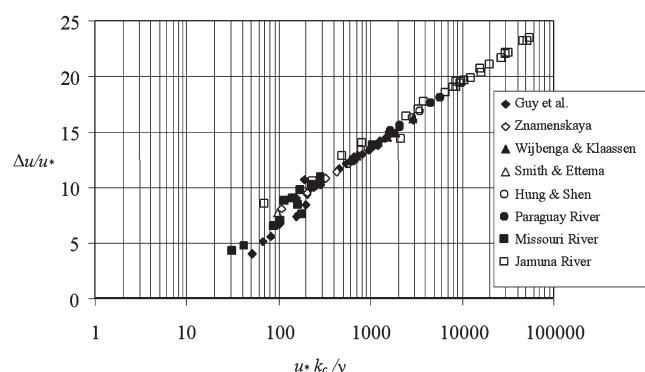


Fig. 2-6. Roughness function for alluvial streams with dunes (after Fedele and García 2001).

Fedele and García (2001) also found that the composite roughness  $k_c$  could be approximated with

$$\frac{k_c}{D} = 1.45 \times \tau^{*3/2} R_{ep} \left( \frac{H}{D} \right)^{1/3} \quad (2-35c)$$

which is valid for  $(H/D) > 10^3$  and  $R_{ep} < 30$ , which are commonly found conditions for large alluvial rivers with sand dunes.

Here,

- $\tau^*$  = dimensionless bed shear stress (i.e., Shields parameter) for uniform flow =  $(HS)/(RD)$ ;
- $H$  = flow depth;
- $S$  = channel slope;
- $R$  =  $\rho_s/\rho - 1$  = submerged specific gravity of sediment;
- $D$  = sediment size;
- $R_{ep}$  =  $\sqrt{gRDD/v}$  = particle Reynolds number; and
- $H/D$  = relative flow depth.

A simple method to estimate the composite roughness  $k_c$  has been proposed by Wright and Parker (2004b) and can be found in Section 2.8.3.3 below.

The total friction coefficient for flow in an alluvial channel in the presence of dunes can be estimated with the help of Keulegan's Eq. (2-16), Eq. (2-19), and Eq. (2-35c),

$$C_f^{-1/2} = \frac{U}{u_*} = \frac{1}{\kappa} \ln \left[ \frac{(H/D)^{3/2}}{\tau^{*3/2} R_{ep}} \right] + 5.1 \quad (2-35d)$$

The data used to by Fedele and García (2001) to obtain this fit are shown in Fig. 2-7. This expression provides only a crude approximation for the friction factor, but clearly indicates that the roughness in alluvial streams with dunes is a dynamic parameter that depends nonlinearly on the flow intensity given by the Shields stress parameter ( $\tau^*$ ), the relative flow depth ( $H/D$ ), and the particle Reynolds number ( $R_{ep}$ ).

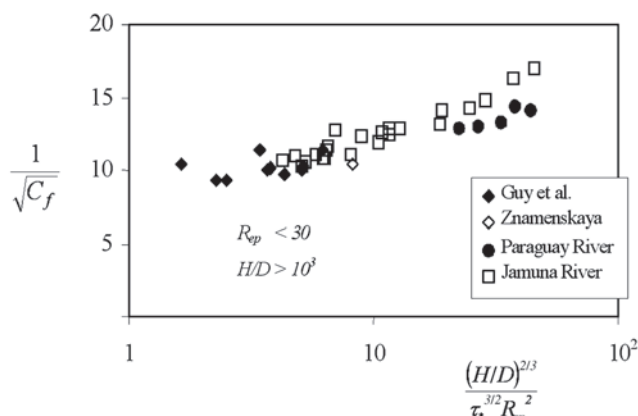


Fig. 2-7. Total friction coefficient for alluvial flows with sand dunes (after Fedele and García 2001).

## 2.3 SEDIMENT PROPERTIES

In this section, rock types, as well as fundamental characteristics of sediment particles such as size, size distribution, density, and fall velocity are considered. The role of sediment size on stream morphology is analyzed also, with the goal of understanding the behavior of sand-bed and gravel-bed streams.

### 2.3.1 Rock Types

The solid phase in sediment transport can be any granular substance. In terms of engineering applications, however, the granular substance in question typically consists of fragments ultimately derived from rocks—hence the name “sediment” transport. The properties of these rock-derived fragments, taken singly or in groups of many particles, all play a role in determining the transportability of the grains under fluid action. The important properties of groups of particles include porosity and size distribution. The most common rock type one is likely to encounter in the river or coastal environment is quartz. Quartz is a highly resistant rock and can travel long distances or remain in place for long periods of time without losing its integrity. Another highly resistant rock type that is often found together with quartz is feldspar. Other common rock types include limestone, basalt, granite, and more esoteric types such as magnetite. Limestone is not a resistant rock; it tends to abrade to silt rather easily. Silt-sized limestone particles are susceptible to solution unless the water is sufficiently buffered. As a result, limestone is not typically found to be a major component of sediments at locations distant from its source. On the other hand, it can often be the dominant rock type in mountain environments.

Basaltic rocks tend to be heavier than most rocks composing the crust of the earth. They are typically brought to the surface by volcanic activity. Basaltic gravels are relatively common in rivers that derive their sediment supply from areas subjected to volcanism in recent geologic history. Basaltic sands are much less common. Regions of weathered granite often provide copious supplies of sediment. The particles produced by weathering are often in the granule size but often quickly break down to sand sizes.

Sediments in the fluvial or coastal environment in the size range of silt, or coarser, are generally produced by mechanical means, including fracture or abrasion. The clay minerals, on the other hand, are produced by chemical action. As a result, they are fundamentally different from other sediments in many ways. Their ability to absorb water means that the porosity of clay deposits can vary greatly over time. Clays also display cohesiveness, which renders them more resistant to erosion.

### 2.3.2 Specific Gravity

Sediment specific gravity is defined as the ratio between the sediment density  $\rho_s$  and the density of water  $\rho$ . Some typical

specific gravities for various natural and artificial sediments are listed in Table 2-2.

### 2.3.3 Model Laboratory Sediments

In the laboratory, it is often of value to employ light weight model sediment (Shen 1990). To see the utility of this, it is useful to consider a movable-bed scale model of an actual river. Consider a reach of the Minnesota River, Minnesota, with a bank-full width of 90 m, a bank-full depth of 4 m, a streamwise slope of 0.0002, and a median sediment size  $D_{50}$  of 0.5 mm. The reach is scaled down by a factor of 100 to fit into a typical laboratory model basin, resulting in a bank-full width of 90 cm and a bank-full depth of 4 cm. In an undistorted model, slope remains constant at 0.0002.

If the sediment employed in the model were to be the same as in the field, it would most likely not move at all in the scale model. Carrying the analogy to its logical conclusion, it would be as if the sediment in the field Minnesota River had a median size of  $0.5 \text{ mm} \times 100 = 0.5 \text{ m}$ , i.e., boulders. It should be clear that, in this case, the field sediment cannot be employed directly in the model. The obvious alternative is to scale down sediment size by the same factor as all other lengths, i.e., by a factor of 100. This would yield a size of 5  $\mu\text{m}$ , which is so close to the clay range that it can be expected to display some kind of pseudocohesiveness. In addition, viscous effects are expected to be greatly exaggerated due to the small size. The net result is model sediment that is much less mobile than it ought to be and, in addition, behaves in ways radically different from the prototype sediment.

There are several ways out of this dilemma. One of them involves using artificial sediment with a low specific gravity. Let  $\rho$  denote the density of water, and  $\rho_s$  denote the specific gravity of the material in question. The weight  $W$  of a particle of volume  $V_p$  is given by

$$W = \rho_s g V_p \quad (2-36a)$$

**Table 2-2 Specific Gravity of Rock Types and Artificial Materials**

Rock type or material	Specific gravity $\rho_s/\rho$
Quartz	2.60–2.70
Limestone	2.60–2.80
Basalt	2.70–2.90
Magnetite	3.20–3.50
Bakelite	1.30–1.45
Coal	1.30–1.50
Ground walnut shells	1.30–1.40
PVC	1.14–1.25

where

$$g = \text{acceleration of gravity.}$$

Quartz, for example, is a mineral with a specific gravity  $\rho_s/\rho$  near 2.65. If a grain of the same volume were modeled in the laboratory using crushed coal with a specific gravity of 1.3, it would follow from Eq. (2-36a) that the coal grain would be only  $1.3/2.65$  or 0.49 times the weight of the quartz grain. Rephrasing, the coal grain is 2.04 times lighter than the quartz grain, and thus, in some sense, twice as mobile.

In fact, the benefit of using lightweight material is much greater than this, because the effective weight determining the mobility of a grain is the submerged weight  $W_s$ , i.e., the actual weight minus the buoyancy force associated with the hydrostatic pressure distribution about the particle. That is,

$$W_s = (\rho_s - \rho)gV_p = \rho R g V_p \quad (2-36b)$$

where

$$R = \left( \frac{\rho_s}{\rho} - 1 \right) \quad (2-36c)$$

denotes the submerged specific gravity of the sediment. Comparing coal and quartz again in terms of submerged weight, it is seen that

$$\frac{(W_s)_{\text{coal}}}{(W_s)_{\text{quartz}}} = \frac{(R)_{\text{coal}}}{(R)_{\text{quartz}}} = \frac{0.30}{1.65} = 0.18 \quad (2-36d)$$

It follows that under water, the coal grain is  $1/0.18 = 5.5$  times lighter than a quartz grain of the same size. Lightweight model sediments are thus a very effective way of increasing mobility in laboratory experiments (Zwamborn 1981; ASCE 2000, p. 105). More material on physical modeling of sedimentation processes can be found in Appendix C.

### 2.3.4 Size

The notation  $D$  will be used to denote sediment size, the typical units of which are millimeters (mm—sand and coarser material) or micrometers ( $\mu\text{m}$ —clay and silt). Another standard way of classifying grain sizes is the sedimentological  $\Phi$  scale, according to which

$$D = 2^{-\Phi} \quad (2-37a)$$

Taking the logarithm of both sides, it is seen that

$$\Phi = -\log_2(D) = -\frac{\ln(D)}{\ln(2)} \quad (2-37b)$$

Note that the size  $\Phi = 0$  corresponds to  $D = 1 \text{ mm}$ . The utility of the  $\Phi$  scale will become apparent upon a consideration of grain size distributions. The minus sign has been

inserted into Eq. (2-37b) simply as a matter of convenience to sedimentologists, who are more accustomed to working with material finer than 1 mm rather than coarser material. The reader should always recall that larger  $\Phi$  implies finer material.

The  $\Phi$  scale provides a very simple way of classifying grain sizes into the following size ranges in descending order: boulders, cobbles, gravel, sand, silt, and clay. This is illustrated in Table 2-3.

It should be noted that the definition of clay according to size ( $D < 2 \mu\text{m}$ ) does not always correspond to the definition of clay according to mineral. That is, some clay mineral particles can be coarser than this limit, and some silt particles produced by grinding can be finer than this. In general, however, the effect of viscosity makes it quite difficult to grind up particles in water to sizes finer than  $2 \mu\text{m}$ .

In practical terms, there are several ways to determine grain size. The most popular way for grains ranging from  $\Phi = 4$  to  $\Phi = -4$  (0.0625 to 16 mm) is with sieves. Each sieve has a square mesh, the gap size of which corresponds to the diameter of the largest sphere that would fit through. The grain size  $D$  thus measured exactly corresponds to diameter only in the case of a sphere. In general, the sieve size  $D$  corresponds to the smallest sieve gap size through which a given grain can be fitted.

For coarser grain sizes, it is customary to approximate the grain as an ellipsoid. Three lengths can be defined. The length along the major (longest) axis is denoted as  $a$ , that along the intermediate axis is denoted as  $b$ , and that along the minor (smallest) axis is denoted as  $c$ . These lengths are typically measured with a caliper. The value  $b$  is then equated to grain size  $D$ .

**Table 2-3 Sediment Grade Scale**

Class Name	Millimeters	Size range		Inches	Approximate sieve mesh openings per inch	
		F	Microns		Tyler	U.S. standard
Very large boulders	4096 ~ 2048			160 ~ 80		
Large boulders	2048 ~ 1024			80 ~ 40		
Medium boulders	1024 ~ 512			40 ~ 20		
Small boulders	512 ~ 256	-9 ~ -8		20 ~ 10		
Large cobbles	256 ~ 128	-8 ~ -7		10 ~ 5		
Small cobbles	128 ~ 64	-7 ~ -6		5 ~ 2.5		
Very coarse gravel	64 ~ 32	-6 ~ -5		2.5 ~ 1.3		
Coarse gravel	32 ~ 16	-5 ~ -4		1.3 ~ 0.6	2 ~ 1/2	
Medium gravel	16 ~ 8	-4 ~ -3		0.6 ~ 0.3	5	5
Fine gravel	8 ~ 4	-3 ~ -2		0.3 ~ 0.16	9	10
Very fine gravel	4 ~ 2	-2 ~ -1		0.16 ~ 0.08	16	18
Very coarse sand	2.000 ~ 1.000	-1 ~ 0	2000 ~ 1000		32	35
Coarse sand	1.000 ~ 0.500	0 ~ 1	1000 ~ 500		60	60
Medium sand	0.500 ~ 0.250	1 ~ 2	500 ~ 250		115	120
Fine sand	0.250 ~ 0.125	2 ~ 3	250 ~ 125		250	230
Very fine sand	0.125 ~ 0.062	3 ~ 4	125 ~ 62			
Coarse silt	0.062 ~ 0.031	4 ~ 5	62 ~ 31			
Medium silt	0.031 ~ 0.016	5 ~ 6	31 ~ 16			
Fine silt	0.016 ~ 0.008	6 ~ 7	16 ~ 8			
Very fine silt	0.008 ~ 0.004	7 ~ 8	8 ~ 4			
Coarse clay	0.004 ~ 0.002	8 ~ 9	4 ~ 2			
Medium clay	0.002 ~ 0.001		2 ~ 1			
Fine clay	0.001 ~ 0.0005		1 ~ 0.5			
Very fine clay	0.0005 ~ 0.00024		0.5 ~ 0.24			

For grains in the silt and clay sizes, many methods (hydrometer, sedigraph, etc.) are based on the concept of equivalent fall diameter. That is, the terminal fall velocity  $v_s$  of a grain in water at a standard temperature is measured. The equivalent fall diameter  $D$  is the diameter of the sphere having exactly the same fall velocity under the same conditions. Sediment fall velocity is discussed in more detail below.

A variety of other more recent methods for sizing fine particles rely on blockage of light beams. The area blocked can be used to determine the diameter of the equivalent circle, i.e., the projection of the equivalent sphere. It can be seen that all of these methods can be expected to operate consistently as long as grain shape does not deviate too greatly from that of a sphere. In general, this turns out to be the case. There are some important exceptions, however. At the fine end of the spectrum, mica particles tend to be platelike; the same is true of shale grains at the coarser end. Comparison with a sphere is not necessarily a particularly useful way to characterize grain size for such materials. More recently, techniques employing light-scattering are becoming more popular for both particle-size analysis and settling velocity measurements (e.g., Pedocchi and García 2006). More material can be found in Chapter 5.

### 2.3.5 Size Distribution

Any sediment sample normally contains a range of sizes. An appropriate way to characterize these samples is in terms of a grain size distribution. Consider a large bulk sample of sediment of given weight. Let  $p_f(D)$ —or  $p_f(\Phi)$ —denote the fraction by weight of material in the sample of material finer than size  $D(\Phi)$ . The customary engineering representation of the grain size distribution consists of a plot of  $p_f \times 100$

(percent finer) versus  $\log_{10}(D)$ —that is, a semilogarithmic plot is employed. The plot, then, would look like the one in Fig. 2-8(a).

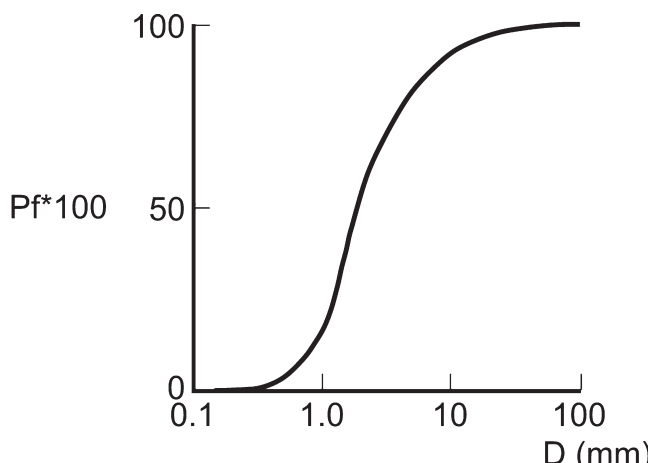
The same size distribution plotted in sedimentological form would involve plotting  $p_f \times 100$  versus  $\Phi$  on a linear plot, like shown in Fig. 2-8(b).

Note that  $\Phi$  on a linear axis is completely equivalent to  $D$  on a logarithmic axis because  $\Phi$  is related linearly to  $\log_{10}(D)$ :

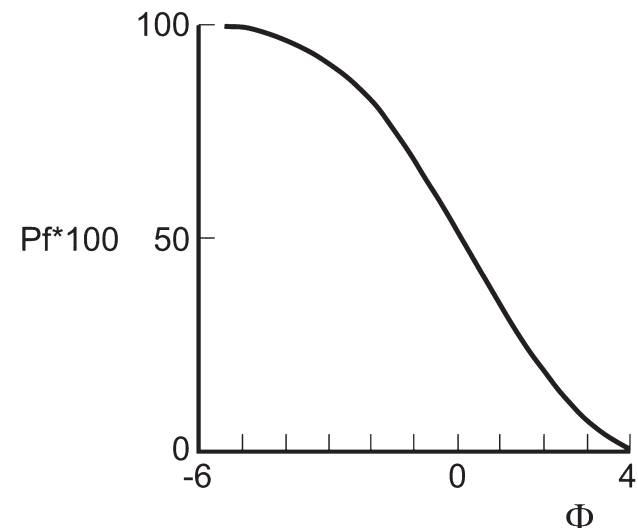
$$\Phi = -\frac{1}{\log_{10}(2)} \log_{10}(D) \quad (2-38)$$

The utility of a logarithmic scale for grain size now becomes apparent. Consider a sediment sample in which one-third of the material lies in the range 0.1–1.0 mm, one-third lies in the range 1.0–10 mm, and one-third lies in the range 10–100 mm. In Fig. 2-8(c)  $p_f \times 100$  is plotted versus  $D$  on a linear scale, and in Fig. 2-8(d)  $p_f \times 100$  is plotted versus  $D$  on a logarithmic scale— $p_f \times 100$  is plotted against  $\log_{10}(D)$ . Plot (c) is virtually unreadable, as the finest two ranges are crowded off the scale. Plot (d) provides a useful and consistent characterization of the distribution. It can be concluded that for the purposes of statistics, the relevant grain size should be on a logarithmic scale, e.g.,  $\Phi$  rather than  $D$  itself.

The size distribution  $p_f(\Phi)$  and size density  $p(\Phi)$  by weight (Fig. 2-8(e)) can be used to extract useful statistics concerning the sediment in question. Let  $x$  denote some percentage, say 50%; the grain size  $\Phi_x$  denotes the size such that  $x\%$  of the weight of the sample is composed of finer grains. That is,  $\Phi_x$  is defined such that



(a)



(b)

**Fig. 2-8.** Sediment grain size distribution in (a) semilog scale, (b) sedimentological scale  $\Phi$ , (c) linear scale, (d) log scale, (e) size distribution and size density, and (f) discretization of grain size distribution.

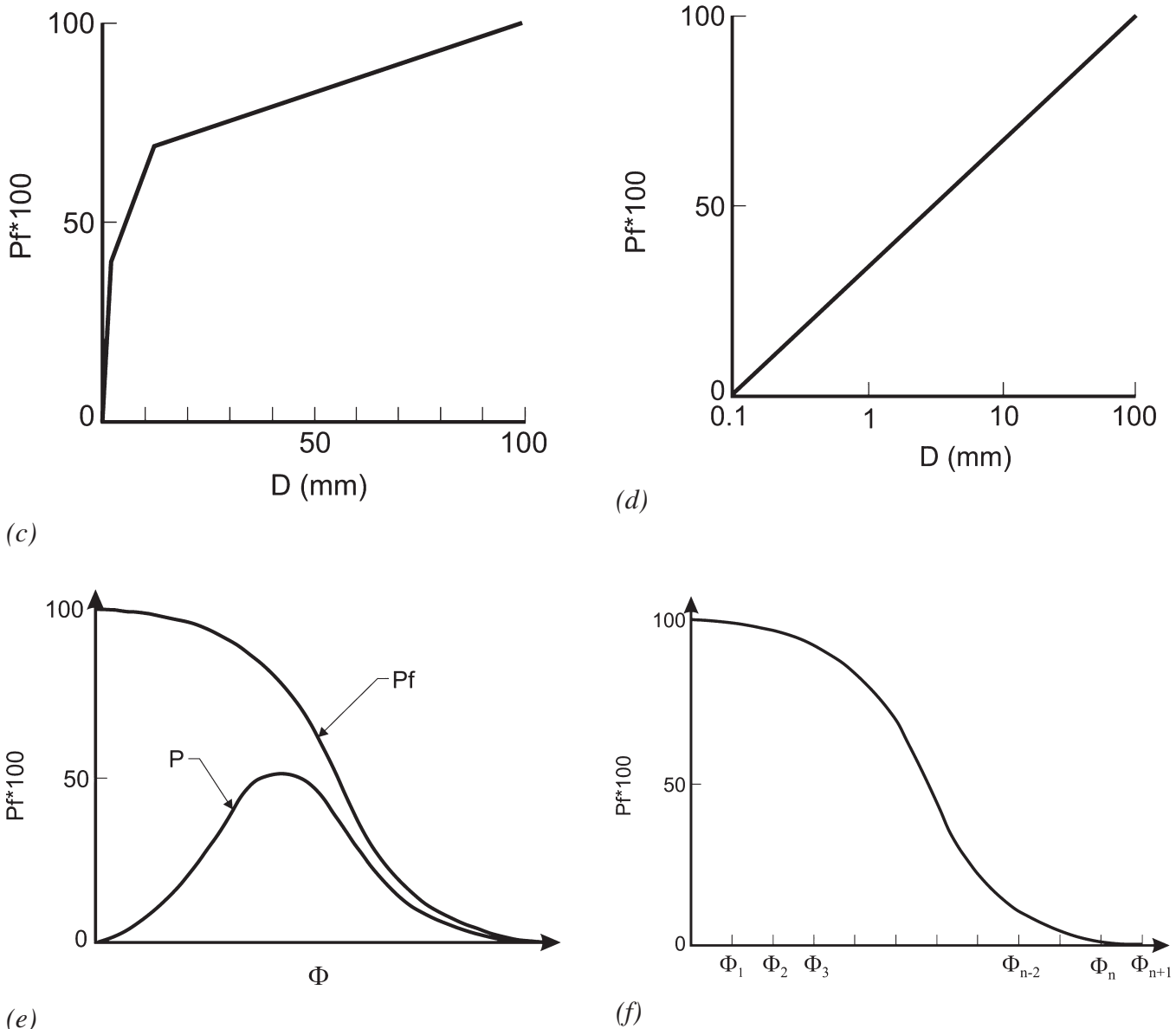


**Fig. 2-8.** Sediment grain size distribution in (a) semilog scale, (b) sedimentological scale  $\Phi$ , (c) linear scale, (d) log scale, (e) size distribution and size density, and (f) discretization of grain size distribution. (Continued)

$$p_f(\Phi_x) = \frac{x}{100} \quad (2-39a)$$

It follows that the corresponding grain size in terms of equivalent diameter is given by  $D_x$ , where

$$D_x = 2^{-\Phi_x} \quad (2-39b)$$

The most commonly used grain sizes of this type are the median size  $D_{50}$  and the size  $D_{90}$  such that 90% of the sample by weight consists of finer grains. The latter size is

particularly useful for characterizing bed roughness, as discussed previously.

The density  $p(\Phi)$  can be used to extract statistical moments. Of these, the most useful are the mean size  $\Phi_m$  and the standard deviation  $\sigma$ . These are given by the relations

$$\Phi_m = \int \Phi p(\Phi) d\Phi \quad (2-40a)$$

$$\sigma^2 = \int (\Phi - \Phi_m)^2 p(\Phi) d\Phi \quad (2-40b)$$

The corresponding geometric mean diameter  $D_g$  and geometric standard deviation  $\sigma_g$  are given as

$$D_g = 2^{\Phi_m} \quad (2-41a)$$

$$\sigma_g = 2^\sigma \quad (2-41b)$$

Note that for a perfectly uniform material,  $\sigma = 0$  and  $\sigma_g = 1$ . As a practical matter, a sediment mixture with a value of  $\sigma_g$  of less than 1.3 is often termed well-sorted and can be treated as a uniform material. When the geometric standard deviation exceeds 1.6, the material can be said to be poorly-sorted.

In point of fact, one never has the continuous function  $p(\Phi)$  with which to compute the moments of Eqs. (2-40a) and (2-40b). One must rather rely on a discretization. To this end, the size range covered by a given sediment sample is discretized in terms of  $n$  intervals bounded by  $n + 1$  grain sizes  $\Phi_1, \Phi_2, \dots, \Phi_{n+1}$  in ascending order of  $\Phi$ , as illustrated in Fig. 2-8(f). The following definitions are made from  $i = 1$  to  $n$ :

$$\bar{\Phi}_i = \frac{1}{2} (\Phi_i + \Phi_{i+1}) \quad (2-42a)$$

$$p_i = p_f(\Phi_i) - p_f(\Phi_{i+1}) \quad (2-42b)$$

Relations (2-40a) and (2-40b) now discretize to

$$\Phi_m = \sum_{i=1}^n \bar{\Phi}_i p_i \quad (2-43a)$$

$$\sigma^2 = \sum_{i=1}^n (\bar{\Phi}_i - \Phi_m)^2 p_i \quad (2-43b)$$

In some cases, especially when the material in question is sand, the size distribution can be approximated as Gaussian on the  $\Phi$  scale (i.e., log-normal in  $D$ ). For a perfectly Gaussian distribution, the mean and median sizes coincide:

$$\Phi_m = \Phi_{50} = \frac{1}{2} (\Phi_{84} + \Phi_{16}) \quad (2-43c)$$

Furthermore, it can be demonstrated from a standard table that in the case of the Gauss distribution the size  $\Phi$  displaced one standard deviation larger than  $\Phi_m$  is accurately given by  $\Phi_{84}$ ; by symmetry, the corresponding size one standard deviation smaller than  $\Phi_{84}$  is  $\Phi_{16}$ . The following relations thus hold:

$$\sigma = \frac{1}{2} (\Phi_{84} + \Phi_{16}) \quad (2-44a)$$

$$\Phi_m = \frac{1}{2} (\Phi_{84} + \Phi_{16}) \quad (2-44b)$$

Rearranging the relations with the aid of Eqs. (2-40a), (2-40b) and (2-43) and (2-44a), it is found that

$$\sigma_g = \left( \frac{D_{84}}{D_{16}} \right)^{1/2} \quad (2-45a)$$

$$D_g = (D_{84} D_{16})^{1/2} \quad (2-45b)$$

It must be emphasized that the relations are exact only for a Gaussian distribution in  $\Phi$ . This is often not the case in nature. As a result, it is strongly recommended that  $D_g$  and  $\sigma_g$  be computed from the full size distribution via Eqs. (2-43a), (2-43b), (2-41a), and (2-41b) rather than the approximate form embodied in the above relations.

### 2.3.6 Porosity

The porosity  $\lambda_p$  quantifies the fraction of a given volume of sediment that is composed of void space. That is,

$$\lambda_p = \frac{\text{volume of voids}}{\text{volume of total space}}$$

If a given mass of sediment of known density is deposited, the volume of the deposit must be computed assuming that at least part of it will consist of voids. In the case of well-sorted sand, the porosity can often take values between 0.3 and 0.4. Gravels tend to be more poorly-sorted. In this case, finer particles can occupy the spaces between coarser particles, reducing the void ratio to as low as 0.2. So-called open work gravels are essentially devoid of sand and finer material in their interstices; these may have porosities similar to that of sand. Freshly deposited clays are notorious for having high porosities. As time passes, clay deposits tend to consolidate under its own weight so that porosity slowly decreases. Wu and Wang (2006) proposed an empirical relation to estimate the initial porosity of sediments, which have been deposited within a year or less, as a function of the median diameter  $D_{50}$  of the sediment mixture. In situ measurements of porosity indicate that biological activity can have an important effect on the porosity of sediments (Wheatcroft 2002).

The issue of porosity becomes of practical importance as regards, for example, salmon spawning grounds in gravel-bed rivers (Alonso and Mendoza 1992; Huang and García 2000). The percentage of sand and silt contained in the

sediment is often referred to as the percentage of “fines” in the gravel deposit. When this fraction rises above 20–26 % by weight, the deposit is often rendered unsuitable for spawning. Salmon bury their eggs within the gravel, and high fines content implies low porosity and thus reduced permeability. The flow of groundwater necessary to carry oxygen to the eggs and remove metabolic waste products is impeded. In addition, newly hatched fry may encounter difficulty in finding pore space through which to emerge to the surface. All of the above factors dictate lowered survival rates. An empirical relationship between percent embryo survival and the geometric mean diameter of the substrate in

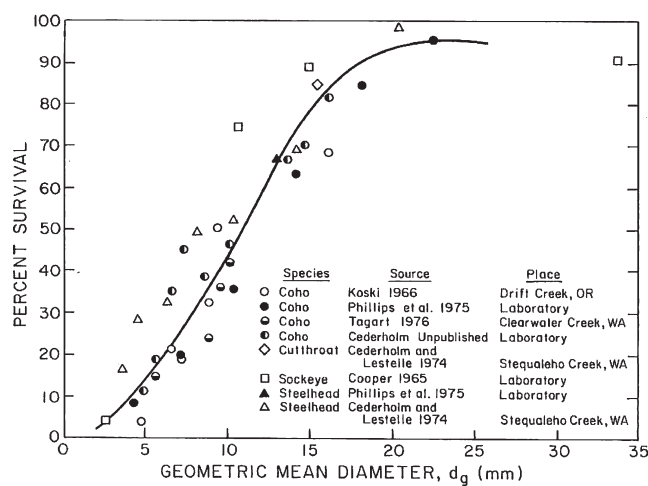


**Fig. 2-9.** Relationship between percent embryo survival and the geometric mean diameter of the substrate (after Shirazi and Seim, 1981).

gravel-bed rivers is shown in Fig. 2-9 (Shirazi and Seim 1981). It is clear that as the material becomes coarser, the substrate porosity can be expected to increase accordingly, augmenting the embryo survival rates. Chief causes of elevated fines in gravel-bed rivers include road building and clear-cutting of timber in the watershed.

### 2.3.7 Shape

There are a number of ways in which to classify grain shape (Vanoni 2006). One of these, the Zingg classification scheme, is illustrated here. According to the definitions introduced earlier, a simple way to characterize the shape of an irregular clast (stone) is in terms of the lengths  $a$ ,  $b$ , and  $c$  of the major, intermediate, and minor axes, respectively. If these three are all equal, the grain can be said to be close to a sphere in shape. If  $a$  and  $b$  are equal but  $c$  is much smaller, the grain is rodlike. Finally, if  $c$  is much smaller than  $b$ , which is, in turn, much smaller than  $a$ , the resulting shape should be bladelike. This is illustrated in terms of the Zingg diagram in Fig. 2-10.

In studies of the fall velocity of geometric shapes and sand grains by McNamee, Albertson and others, the shape of the particles has been expressed by the Corey shape factor  $SF$ , which makes use of the characteristic lengths, defined above, and is given by (Vanoni 2006, p. 14)

$$SF = \frac{c}{\sqrt{ab}}$$

It follows that a spherical particle will have a  $SF = 1$ . For natural sands  $SF = 0.7$ . The shape factor has been used in

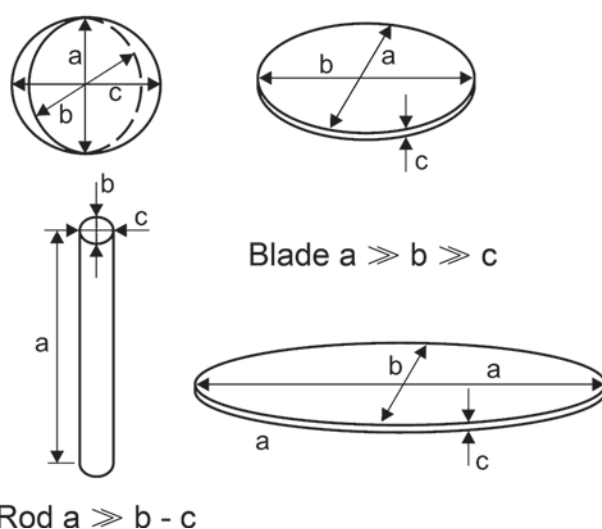
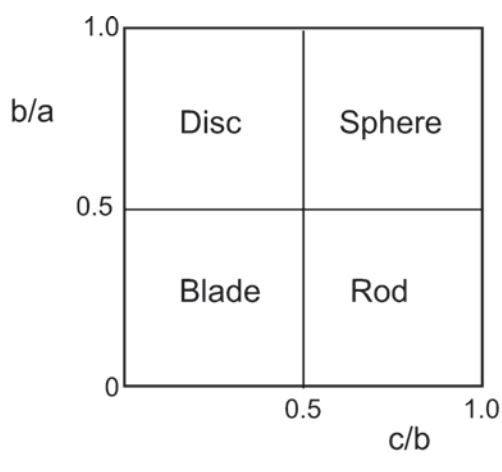


**Fig. 2-10.** Definition of Zingg diagram.

studies of particle fall velocity (Dietrich 1982; Jimenez and Madsen 2003; Wu and Wang 2006). More material on sediment particle shape and its effect on particle fall velocity can be found in Vanoni (2006, p. 14).

### 2.3.8 Fall Velocity

A fundamental property of sediment particles is their fall or settling velocity. The fall velocity of sediment grains in water is determined by their diameter and density and by the viscosity of the water. Falling under the action of gravity, a particle will reach a constant, terminal velocity once the drag equals the submerged weight of the particle. The relation for terminal fall velocity for a spherical particle in quiescent fluid  $v_s$  can be presented as

$$R_f = \left[ \frac{4}{3} \frac{1}{C_D (R_p)} \right]^{1/2} \quad (2-46a)$$

where

$$R_f = \frac{v_s}{\sqrt{gRD}} \quad (2-46b)$$

$$R_p = \frac{v_s D}{v} \quad (2-46c)$$

and the functional relation  $C_D = f(R_p)$  denotes the drag coefficient for spheres (García 1999). Here  $g$  is the acceleration of gravity,  $R = (\rho_s - \rho)/\rho$  is the submerged specific gravity of the sediment, and  $v$  is the kinematic viscosity of water. This relation is not very useful because it is not explicit in  $v_s$ ; one must compute fall velocity by trial and error. One can use the following equation for the drag coefficient  $C_D$

$$C_D = \frac{24}{R_p} \left( 1 + 0.152 R_p^{1/2} + 0.0151 R_p \right) \quad (2-46d)$$

and the definition

$$R_{ep} = \frac{\sqrt{gRD} D}{v} \quad (2-46e)$$

to obtain an explicit relation for fall velocity in the form of  $R_f$  versus  $R_{ep}$ . Such a diagram is presented in Fig. 2-11, where

the ranges for silt, sand, and gravel are plotted for a kinematic viscosity  $v = 0.01 \text{ cm}^2/\text{s}$  (clear water at 20°C) and a submerged specific gravity  $R = 1.65$  (quartz). An equivalent diagram to estimate fall velocity of particles was proposed earlier by Parker (1978).

Notice that for fine silts,  $R_p$  is smaller than one and the drag coefficient given by Eq. (2-46d) reduces to

$$C_D = \frac{24}{R_p} \quad (2-46f)$$

Substitution of (2-46f) into (2-46a) yields the well-known Stokes law for settling velocity of fine particles,

$$v_s = \frac{gRD^2}{18v} \quad (2-46g)$$

A useful empirical relation to estimate the kinematic viscosity of clear water is:

$$v = \frac{1.79 \cdot 10^{-6}}{1 + 0.03368T + 0.00021T^2} (\text{m}^2/\text{s}) \quad (2-46h)$$

where

$T$  = temperature of the water in degrees centigrade (°C).

A number of relations for terminal fall velocity for the case of nonspherical (natural) particles can be found in the literature. Dietrich (1982) analyzed fall velocity data for natural particles and used dimensional analysis to obtain the useful fit

$$R_f = \exp \left\{ -b_1 + b_2 \ln(R_{ep}) - b_3 [\ln(R_{ep})]^2 - b_4 [\ln(R_{ep})]^3 + b_5 [\ln(R_{ep})]^4 \right\} \quad (2-47a)$$

where

$$\begin{aligned} b_1 &= 2.891394, b_2 = 0.95296, b_3 = 0.056835, \\ b_4 &= 0.002892, b_5 = 0.000245 \end{aligned} \quad (2-47b)$$

In an attempt to obtain a more practical relation, Jimenez and Madsen (2003) fitted the formula of Dietrich (1982) to the expression

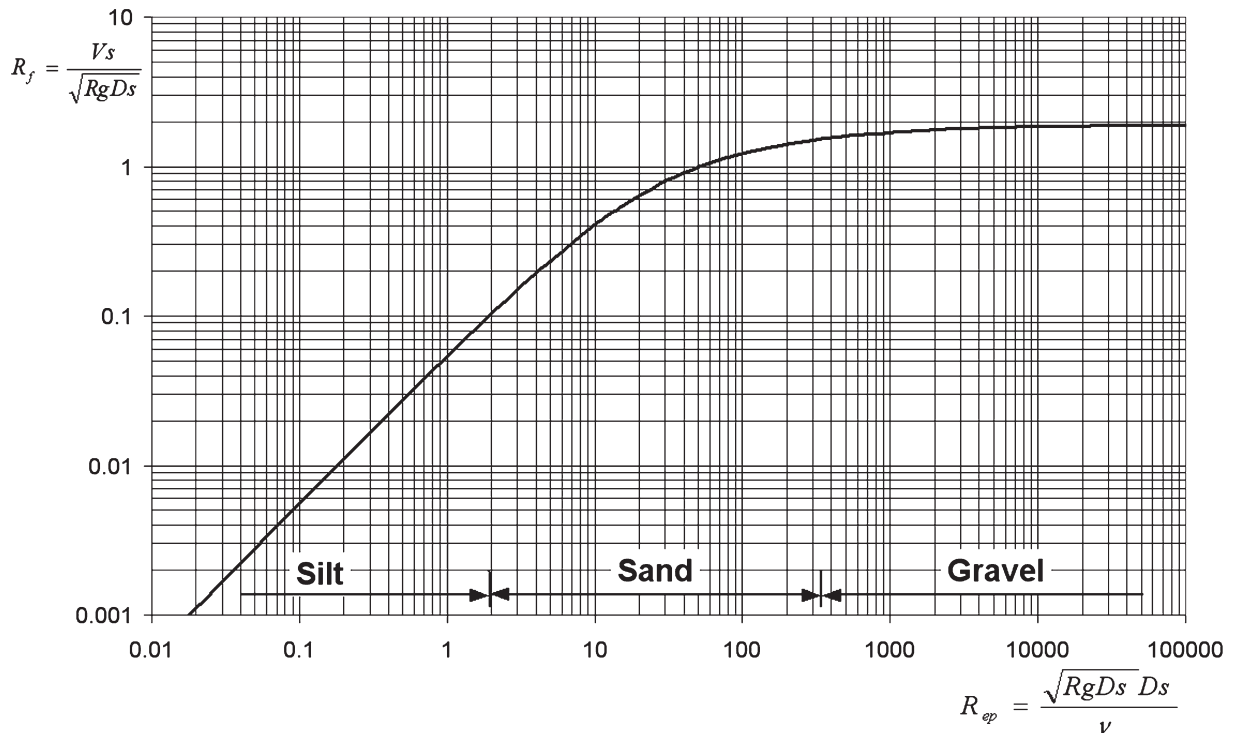


**Fig. 2-11.** Diagram of  $R_f$  versus  $R_{ep}$  calculated from the drag coefficient for spheres.

$$W_* = \frac{v_s}{\sqrt{g R D_N}} = \left( A + \frac{B}{S_*} \right)^{-1} \quad (2-48a)$$

$$v_s = \frac{v}{D} \left[ (10.36^2 + 1.049 D_*^3)^{1/2} - 10.36 \right] \quad (2-49a)$$

in which

$$S_* = \frac{D_N}{4v} \sqrt{g R D_N} \quad (2-48b)$$

Here,  $D_N$  = nominal particle diameter. The coefficients  $A$  and  $B$  in Eq. (2-48a) are functions of Corey shape factor and particle roundness and are expressed graphically by Jimenez and Madsen (2003). In many practical applications, the sediment is naturally worn quartz sands characterized by their sieve diameter  $D_s$ . For this typical application,  $D_N = D_s/0.9$ ,  $A = 0.954$  and  $B = 5.12$ , are recommended. With these values incorporated in to it, Eq. (2-48a) was found to provide reliable predictions of fall velocity for natural quartz sediment with sieving diameters ranging from 0.063 mm up to 2 mm (Jimenez and Madsen 2003).

Another simple relation to estimate the fall velocity of natural sand particles has been proposed by Soulsby (1997) for use in the marine environment,

where

$$D_* = \left[ \frac{g R}{v^2} \right]^{1/3} D \quad (2-49b)$$

Here

$g$  = acceleration of gravity;

$v$  = kinematic viscosity of water;

$D$  = mean sieve diameter of grains; and

$R = (\rho_s - \rho)/\rho$  is the submerged specific gravity of the grains.

Equations very similar to (2-49a) have been proposed independently by Zanke (1977) and van Rijn (1984).

At high concentrations the flows around adjacent settling grains interact resulting in a larger drag than for the same grain in isolation. This phenomenon is known as hindered settling and results in the hindered settling velocity  $v_{sc}$  for high sediment concentrations to be smaller than the fall velocity  $v_s$  at low sediment concentrations (less than 0.05). Applying reasoning similar to the one that led to Eq. (2-49a),

Soulsby (1997) proposed the following relation for the hindered fall velocity  $v_{sc}$  of grains in a dense suspension having a volumetric sediment concentration  $C$ :

$$v_{sc} = \frac{v}{D} \left[ (10.36^2 + 1.049(1-C)^{4.7} D_*^3)^{1/2} - 10.36 \right] \quad (2-49c)$$

which is valid for all values of  $D_*$  and  $C$ . When  $C = 0$ , Eq. (2-49c) reduces to Eq. (2-49a).

The subject of sediment fall velocity is far from being resolved. However, the empirical fits presented here should suffice for engineering purposes. Other useful relations to estimate sediment fall velocity can be found in Swamee and Ojha (1991), Cheng (1997), Ahrens (2000), and Ahrens (2003). Recently, Wu and Wang (2006) compared different formulations and developed another empirical fit to estimate fall velocity which accounts for the effect of particle shape through the Corey shape factor ( $SF = c/\sqrt{ab}$ ).

Material on particle settling for the case of fine-grained cohesive sediment is presented in Chapter 4.

### 2.3.9 Relation between Size Distribution and Stream Morphology

The study of sediment properties, and in particular size distribution, is most relevant in the context of stream morphology. The material that follows is intended to point out some of the more interesting issues, and in particular, morphological differences between sand-bed and gravel-bed streams. More discussion on the subject can be found in Chapters 3 and 6.

In Fig. 2-12, several size distributions from the sand-bed Kankakee River, Illinois, are shown (Bhowmik et al. 1980). The characteristic S-shape suggests that these distributions might be approximated by a Gaussian curve. The median size  $D_{50}$  falls near 0.3–0.4 mm. The distributions are very tight with a near-absence of either gravel or silt. For practical purposes, the material can be approximated as uniform.

In Fig. 2-13, several size distributions pertaining to the gravel-bed Oak Creek, Oregon, are shown (Milhous 1973). In gravel-bed streams, the surface layer ("armor" or "pavement") tends to be coarser than the substrate (identified as "subpavement" in the figure). Whether the surface or substrate is

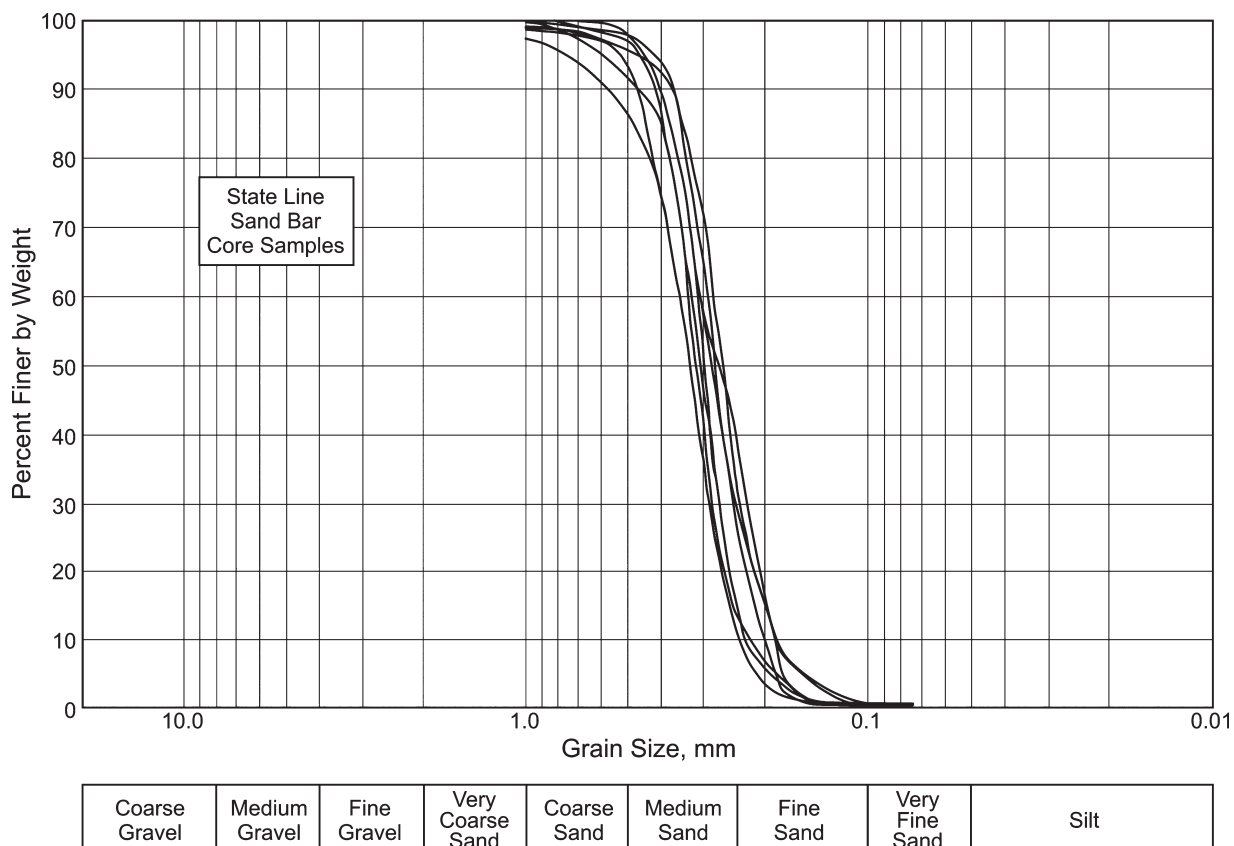


**Fig. 2-12.** Particle size distributions of bed materials in Kankakee River, Illinois (after Bhowmik et al. 1980).

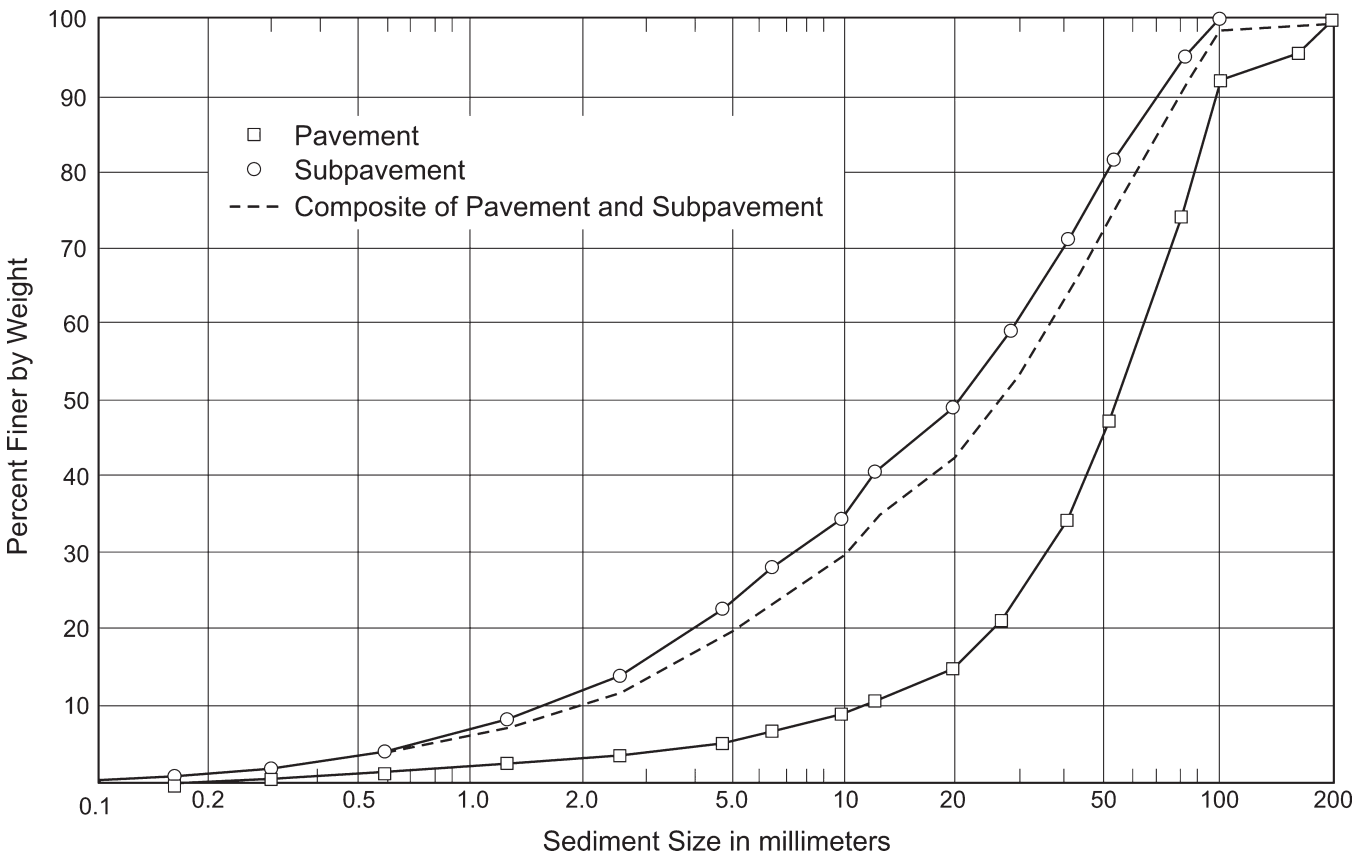


Fig. 2-13. Size distribution of bed material samples in Oak Creek, Oregon (after Milhous 1973).

considered, it is apparent that the distribution ranges over a much wider range of grain sizes than in the case of Fig. 2-12. More specifically, in the distributions of the sand-bed Kankakee River,  $\Phi$  varies from about 0 to about 3, whereas in Oak Creek,  $\Phi$  varies from about -8 to about 3. In addition, the distribution of Fig. 2-13 is upward concave almost everywhere, and thus deviates strongly from the Gaussian distribution.

These two examples provide a window toward generalization. A river may loosely be classified as sand-bed or gravel-bed according to whether the median size  $D_{50}$  of the surface material or substrate is less or greater than 2 mm. The size distributions of sand-bed streams tend to be relatively narrow and also tend to be S-shaped. The size distributions of gravel-bed streams tend to be much broader and to display an upward-concave shape. There are, of course, many exceptions to this behavior, but it is sufficiently general to warrant emphasis.

More evidence for this behavior is provided in Fig. 2.14. Here, the grain size distributions for a variety of stream reaches have been normalized using the median sediment size  $D_{50}$ . Four sand-bed reaches are included with three

gravel-bed reaches. All of the sand-bed distributions are S-shaped, and all have a lower spread than the gravel-bed distributions. The figure indicates that the standard deviation of the grain size distribution can be expected to increase systematically with increasing sediment size (White et al. 1973). The three gravel-bed size distributions differ systematically from the sand-bed distributions in a fashion that accurately reflects Oak Creek (Fig. 2-13). The standard deviation is, in all cases, markedly larger than for any of the sand-bed distributions, and the distributions are upward concave except perhaps near the coarsest sizes.

## 2.4 THRESHOLD CONDITION FOR SEDIMENT MOVEMENT

In this section the threshold conditions for initiation of motion are analyzed. A mechanistic model for initiation of motion is presented. The Shields diagram and other methods for assessing initiation of motion are introduced. The analysis is limited to noncohesive granular sediments such as silt, sand and gravel.

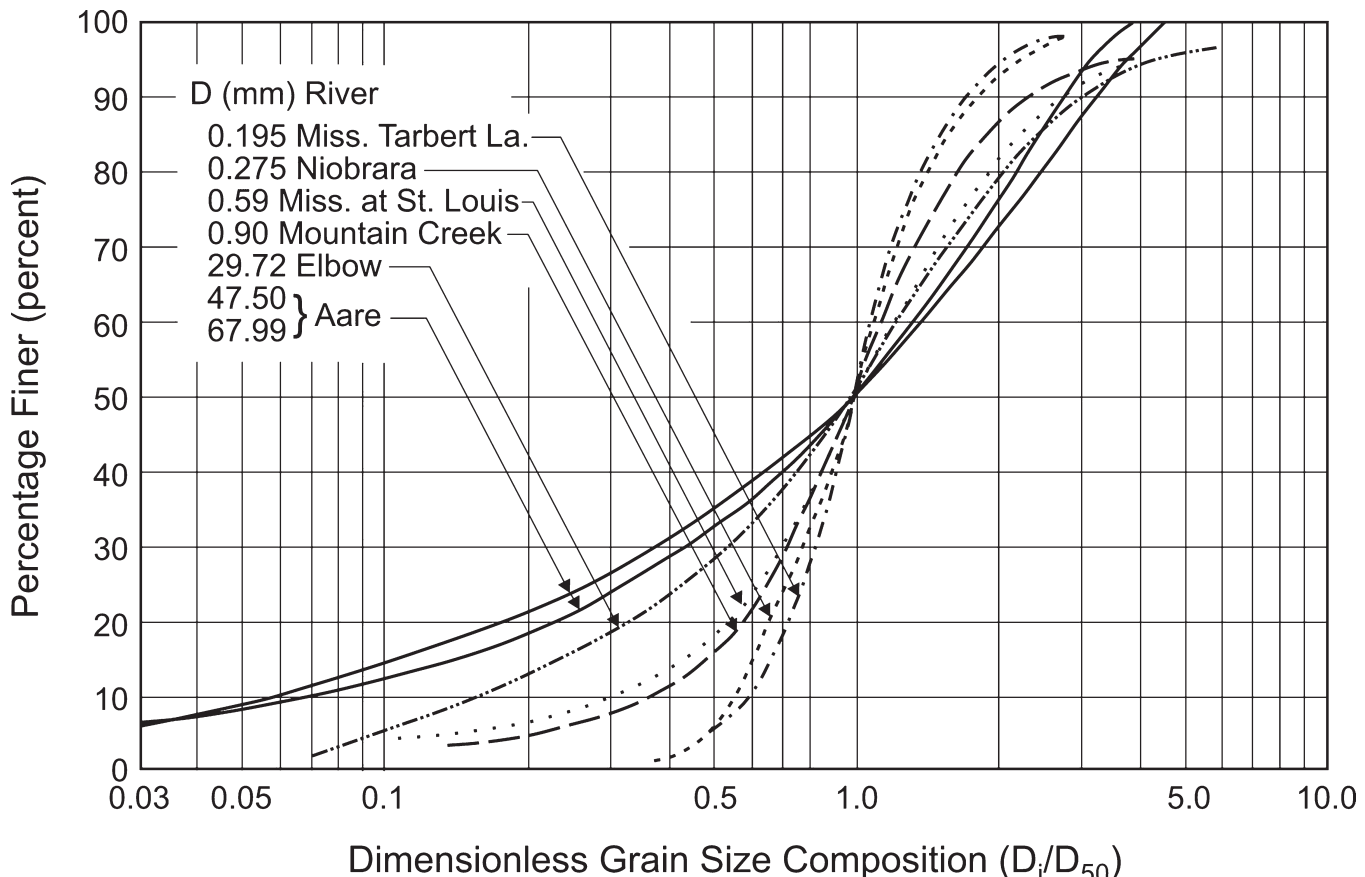


**Fig. 2-14.** Dimensionless grain-size distribution for different rivers (after White et al. 1973).

#### 2.4.1 Submerged Angle of Repose

If granular particles are allowed to pile up while submerged in a fluid, there is a specific slope angle  $\phi$  beyond which spontaneous failure of the slope occurs. This angle is termed the angle of repose, or alternatively, the friction angle. To study this in more detail, consider a typical grain resting on the surface of such a slope as shown in Fig. 2-15.

The coefficient of Coulomb friction is defined to be  $\mu$ , where

$$\mu = \frac{\text{tangential resistive force}}{\text{downward normal force}} \quad (2-50a)$$

The forces acting on the particle along the slope are the submerged force of gravity (gravitational force minus buoyancy force), which has a downslope component  $F_{gt}$  and a normal component  $F_{gn}$ , and a tangential resistive force  $F_r$  due to Coulomb friction. These are given by

$$F_{gt} = (\rho_s - \rho)gV_p \sin\phi \quad (2-50b)$$

$$F_{gn} = (\rho_s - \rho)gV_p \cos\phi \quad (2-50c)$$

$$F_r = \mu F_{gn} \quad (2-50d)$$

The condition for incipient motion is given by

$$F_{gt} = F_r \quad (2-50e)$$

That is, the downslope impelling force of gravity should just balance with the Coulomb resistive force. From the above four relations, it is found that

$$\mu = \tan\phi \quad (2-50f)$$

The angle of repose is an empirical quantity. Tests with well-sorted material indicate that  $\phi$  is near  $30^\circ$  for sand, gradually increasing to  $40^\circ$  for gravel. Poorly sorted, angular material tends to interlock, giving greater resistance to failure, and as a result, a higher friction angle  $\phi$ . Such material is thus often chosen for riprap (see Appendix B).

Friction angle measurements obtained in gravel-bed streams, including implications for critical shear stress estimations, can be found in Kirchner et al. (1990) and Buffington et al. (1992).

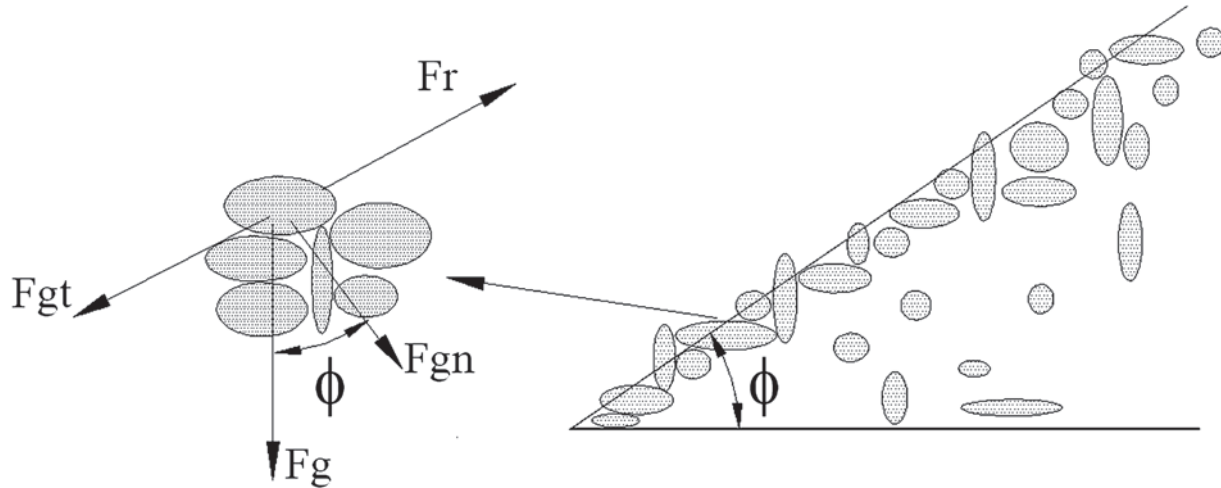
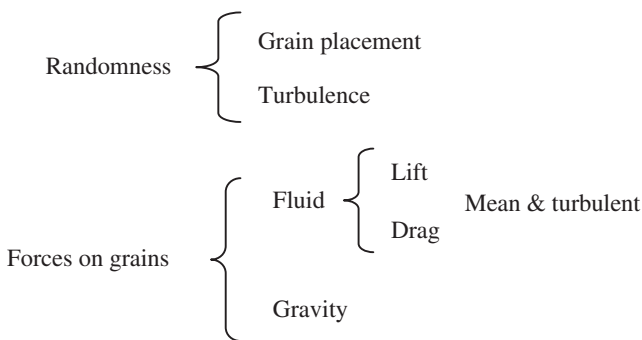


**Fig. 2-15.** Definition diagram for angle of repose.

#### 2.4.2 Critical Stress for Flow over a Granular Bed

When a granular bed is subjected to a turbulent flow, it is found that virtually no motion of the grains is observed at some flows, but that the bed is noticeably mobilized at other flows (Cheng and Chiew 1998; Papanicolaou et al. 2002; Niño et al. 2003). Literature reviews on incipient motion can be found in Miller et al. (1977); Lavelle and Mofjeld (1987); and Buffington and Montgomery (1997).

Factors that affect the mobility of grains subjected to a flow are summarized as follows,



In the presence of turbulent flow, random fluctuations typically prevent the clear definition of a critical or threshold condition for motion: the probability of grain movement is never precisely zero (Paintal 1971; Graf and Paziz 1977; Lopez and García 2001; Zanke 2003). It is, nevertheless, possible to define a condition below which movement can be neglected for many practical purposes.

The following analysis is a slightly generalized version of the derivation of the full Shields curve for the threshold

of motion presented by Ikeda (1982), which is based on the work of Iwagaki (1956) and Coleman (1967). A similar analysis was presented by Wiberg and Smith (1987) for the case of nonuniform sediment size. Consider the granular bed of Fig. 2-16. The flow forces on a dangerously placed spherical sediment particle protruding upward from the mean bed are considered in order to analyze the threshold of motion.

Certain assumptions enter into the Ikeda-Coleman-Iwagaki analysis. The flow is taken to follow the logarithmic law near the boundary (Eq. 2-4). The origin of the  $z$ -coordinate for evaluating the logarithmic law is taken to be the base of the dangerously exposed particle. Turbulent forces on the particle are neglected. Drag and lift forces act through the particle center (in general, they do not, giving rise to torque as well as forces). The value of the drag coefficient  $c_D$  can be approximated by the free-stream value (Coleman 1967). The coordinate  $z$  is taken to be vertically upward, corresponding to very low streamwise slopes  $S$ . The roughness height  $k_s$  is equated to the particle diameter  $D$ .

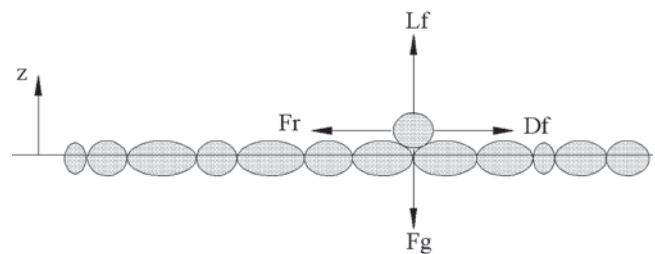


**Fig. 2-16.** Forces acting on a “dangerously” placed particle.

It is seen from the above assumptions that the particle center is located at  $z = D/2$ . It is necessary to use some information about turbulent boundary layers to define the effective fluid velocity  $u_f$  acting on the particle in order to facilitate computation of the fluid forces. A viscous sublayer exists (see Eq. 2-6) when  $D/\delta_v$  is less than about 0.5, or  $(u_*D/v) < 5$ . In this case, the effective fluid velocity  $u_f$  acting on the particle is estimated with Eq. (2-5) as

$$\frac{u_f}{u_*} = \frac{1}{2} \frac{u_* D}{v} \quad (2-51a)$$

On the other hand, if  $D/\delta_v > 2$ , no viscous sublayer exists, and the logarithmic law applies near (but not at) the bed. So the flow velocity acting on the particle can be estimated by

$$\frac{u_f}{u_*} = 2.5 \ln \left( 30 \frac{z}{D} \right) \Big|_{z=\frac{1}{2}D} = 6.77 \quad (2-51b)$$

It follows then that Eqs. (2-51a) and (2-51b) can be written in the more general form

$$\frac{u_f}{u_*} = F \left( \frac{u_* D}{v} \right) \quad (2-51c)$$

where

$$F = \frac{1}{2} \frac{u_* D}{v} \text{ for } \frac{u_* D}{v} < 13.5 \quad (2-51d)$$

and

$$F = 6.77 \text{ for } \frac{u_* D}{v} > 13.5 \quad (2-51e)$$

However, it would be more convenient to have a continuous function  $F$ , so that the transition between hydraulically smooth and fully rough condition, is smooth. The fit proposed by Swamee (1993) can be used to evaluate  $F$  in Eq. (2-51c) by setting  $z=D/2$  and  $k_s = D$  in Eq. (2-10),

$$F = \left\{ \left( \frac{2v}{u_* D} \right)^{10/3} + \left[ \kappa^{-1} \ln \left( 1 + \frac{\frac{9}{2} \frac{u_* D}{v}}{1 + 0.3 \frac{u_* D}{v}} \right) \right]^{-10/3} \right\}^{-0.3} \quad (2-51f)$$

Now the forces acting on the particle can be considered. The streamwise fluid drag force  $D_f$ , upward normal (vertical in this case) fluid lift force  $L_f$ , and downward vertical submerged gravitational force  $F_g$  acting on the particle of the previous figure are thus

$$D_f = \rho \frac{1}{2} \pi \left( \frac{D}{2} \right)^2 c_D u_f^2 \quad (2-52a)$$

$$L_f = \rho \frac{1}{2} \pi \left( \frac{D}{2} \right)^2 c_L u_f^2 \quad (2-52b)$$

$$F_g = \rho Rg \frac{4}{3} \pi \left( \frac{D}{2} \right)^3 \quad (2-52c)$$

From Eq. (2-50d), it is seen that the Coulomb resistive force  $F_r$  is given by

$$F_r = \mu (F_g - L_f) \quad (2-52d)$$

The critical condition for incipient motion of the particle is that the impelling drag force is just balanced by the resisting Coulomb frictional force:

$$D_f = F_r \quad (2-53)$$

That is, if  $D_f < F_r$ , the particle will not move, and if  $D_f > F_r$ , it will move. Between Eqs. (2-52a), (2-52b), (2-52c), (2-52d), and (2-53), the following relation is obtained for critical fluid velocity  $u_f$  at  $z = D/2$ :

$$\frac{u_f^2}{RgD} = \frac{4}{3} \frac{\mu}{c_D + \mu c_L} \quad (2-54)$$

This relation is now converted to a relation in terms of boundary shear stress. It may be recalled that by definition  $\rho u_*^2 = \tau_b$ , where  $\tau_b$  denotes the boundary shear stress. In this case, the shear stress in question is the critical one for the onset of motion and is denoted by  $\tau_{bc}$ . Between Eqs. (2-51c) and (2-54), the Ikeda-Coleman-Iwagaki relation is obtained for the critical shear stress:

$$\tau_c^* = \frac{4}{3} \frac{\mu}{(c_D + \mu c_L)} \frac{1}{F^2 (u_{*c} D/v)} \quad (2-55a)$$

The equation is valid for nearly horizontal beds but the effect of channel slope can be readily incorporated. For a channel with a downstream slope angle  $\alpha$ , the downslope

effect of gravity has to be included in the force balance presented earlier, resulting in the following expression for the critical shear stress

$$\tau_c^* = \frac{4(\mu \cos \alpha - \sin \alpha)}{3(c_D + \mu c_L)} \frac{1}{F^2(u_{*c} D/v)} \quad (2-55b)$$

Notice that for  $\alpha = 0$ , Eq. (2-55b) reduces to Eq. (2-55a).

A predecessor of all these equations was advanced by Egiazarovoff (1965). It can be found in Vanoni (2006, p. 58) and is used for sediment mixtures in Chapter 3. Similar relations were also obtained by Fredsøe and Deigaard (1992, p. 203) and can also be found, albeit without derivation, in Chien and Wan (1999, p. 319).

In the above relation,  $\tau_c^*$  is a dimensionless measure of boundary shear stress known as the Shields parameter and given by the definition

$$\tau_c^* = \frac{\tau_{bc}}{\rho g R D} \quad (2-56)$$

where

$\tau_{bc} = \rho u_{*c}^2$  = critical bed shear stress for initiation of motion;  
 $u_{*c}$  = critical shear velocity;  
 $\rho$  = water density;  
 $R = (\rho_s - \rho)/\rho$  is the submerged specific gravity of the sediment;  
 $g$  = acceleration of gravity; and  
 $D$  = sediment particle diameter.

The most relevant fact about the mechanistic approach to this problem of initiation of motion relates to the possibility of obtaining an explicit formulation of the relation explored by Shields with dimensional analysis and experiments. Eq. (2-55a) can be evaluated with the aid of Eq. (2-51f) and certain realistic assumptions about the internal angle of friction  $\phi$ , and the drag  $c_D$  and lift  $c_L$  coefficients. As an example, two internal friction angles are considered,  $\phi = 40^\circ$  ( $\mu = 0.84$ ) and  $\phi = 60^\circ$  ( $\mu = 1.73$ ), and the following assumptions are made:  $k_s = 2D$ , and  $c_L = 0.85 c_D$ . It is furthermore assumed that  $c_D$  is given as a function of  $u_* D/v$  according to the standard drag curve for spheres (i.e., Eq. 2-46d). A plot of Eq. (2-55a) is shown in Fig. 2-17, together with the data of Shields (1936). Considering all the assumptions made for developing the theoretical model, the agreement is quite reasonable. The best agreement between the Ikeda-Coleman-Iwagaki model and Shields observations is found for  $\phi = 60^\circ$  ( $\mu = 1.73$ ). Such friction angle is rather high but is not possible to know the exact value of this parameter for the sediment used by Shields in his experiments, and whether or not incipient transport conditions were present

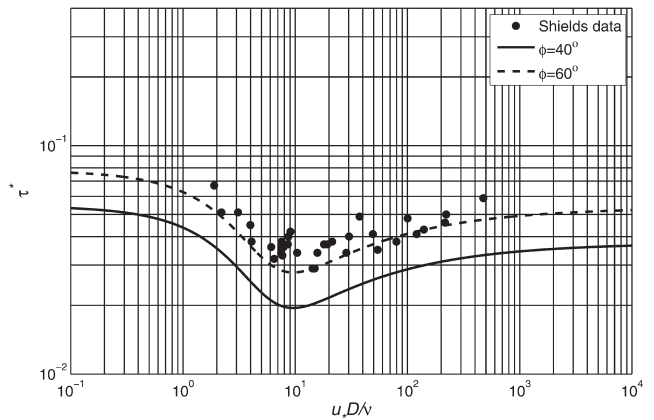


Fig. 2-17. Comparison of Ikeda-Coleman-Iwagaki model for initiation of motion with Shields data.

(Buffington 1999). The theoretical model developed here is for idealized spherical particles for which the friction angle can be expected to be lower than for natural sediments. For the case of  $\phi = 40^\circ$  ( $\mu = 0.84$ ), the curve predicted with Eq. (2-55a), follows the trend of Shields data but predicts values of critical shear stress that are smaller by a factor of about 1.6. It is interesting that several researchers have found that Shields critical shear stress values are indeed higher than those observed. More discussion on the internal friction angle is given below when the model of Wiberg and Smith (1987) is presented.

Although there are a number of assumptions made in its derivation, the mechanistic Ikeda-Coleman-Iwagaki model (Eq. 2.55a) makes it possible to visualize the sources of uncertainty (i.e., angle of repose, drag and lift coefficients, particle location, etc.) and helps to understand why it is so difficult to characterize the threshold condition with a deterministic model (e.g., Bettess 1984; Lavelle and Mojfeld 1987; Komar 1996; Papanicolaou et al. 2001; Shvidchenko and Pender 2001; Niño et al. 2001; Dancey et al. 2002). Recently the role played by turbulence on initiation of motion has been examined by Zanke (2003), who found that turbulence-induced fluctuations in the lift force make particles “lighter” and easier to move.

### 2.4.3 Shields Diagram

Shields (1936) conducted his set of pioneering experiments to elucidate the conditions for which sediment grains would be at the verge of moving. While doing this, Shields introduced the fundamental concepts of similarity and dimensional analysis and made a set of observations that have become legendary in the field of sediment transport (Kennedy 1995). Shields deduced from dimensional analysis and fluid mechanics considerations that  $\tau_c^*$  should be a function of shear Reynolds number  $u_{*c} D/v$ , as implied by Eq. (2-55a). The Shields diagram is expressed by dimensionless

combinations of critical shear stress  $\tau_{bc}$ , sediment and water specific weights  $\gamma_s$  and  $\gamma$ , respectively, sediment size  $D$ , critical shear velocity  $u_{*c} = \sqrt{\tau_{bc}/\rho}$ , and kinematic viscosity of water  $\nu$ . These quantities can be expressed in any consistent set of units. The Shields dimensionless parameters are related by a simple expression,

$$\tau_c^* = \frac{\tau_{bc}}{\rho g R D} = F_* \left( \frac{u_{*c} D}{\nu} \right) \quad (2-57)$$

The Shields diagram shown in Fig. 2-18 was originally prepared by Vanoni (1964). This diagram is the predecessor of the one that finally appeared when Manual 54 was first published in 1975 (Vanoni 2006, p. 57). A modern account of the Shields diagram and its history can be found in Kennedy (1995). Critical Shields values  $\tau_c^*$  are commonly used to denote conditions under which bed sediment particles are stable but on the verge of being entrained. The curve in the Shields diagram was originally introduced by Rouse (1939), whereas the auxiliary scale was proposed by Vanoni (1964) to facilitate the determination of the critical shear stress  $\tau_{bc}$  once the submerged specific gravity, the particle diameter  $D$  and the kinematic viscosity of water  $\nu$  are specified. It is known that the values obtained from the Shields diagram (Fig. 2-18) for initiation of motion are indeed larger than those observed by other researchers, in particular for coarse material. For example, Neill (1968) gives  $\tau_c^* = 0.03$  instead of 0.06 for the dimension-

less critical shear stress for values of  $Re_* = u_* D / \nu$  in excess of 500, while Gessler (1971) suggests using a value of  $\tau_c^* = 0.046$  for such condition.

The value of  $\tau_c^*$  to be used in design depends on the particular case at hand. If the situation is such that grains that are moved can be replaced by others moving from upstream, some motion can be tolerated, and the values from the Shields curve may be used. On the other hand, if grains removed cannot be replaced as on a stream bank, the Shields value of  $\tau_c^*$  are too large and should be reduced. As already mentioned it is well known from observations by Neill and Yalin (1969) and Gessler (1970) that Shields original values for initiation of motion of coarse material are too high and should be divided by a factor of 2 for engineering purposes.

As first noticed by Vanoni (1964), the Shields diagram is not practical in the form of Fig. 2-18, because in order to find the critical shear stress for incipient motion  $\tau_{bc}$ , one must know the critical shear velocity  $u_{*c} = \sqrt{\tau_{bc}/\rho}$ . The relation can be cast in explicit form by plotting  $\tau_c^*$  versus  $R_{ep}$ , noting the internal relation

$$\frac{u_* D}{\nu} = \frac{u_*}{\sqrt{g R D}} \frac{\sqrt{g R D} D}{\nu} = (\tau_c^*)^{1/2} R_{ep} \quad (2-58)$$

where  $R = \frac{\rho_s - \rho}{\rho}$  is the submerged specific gravity of the sediment.

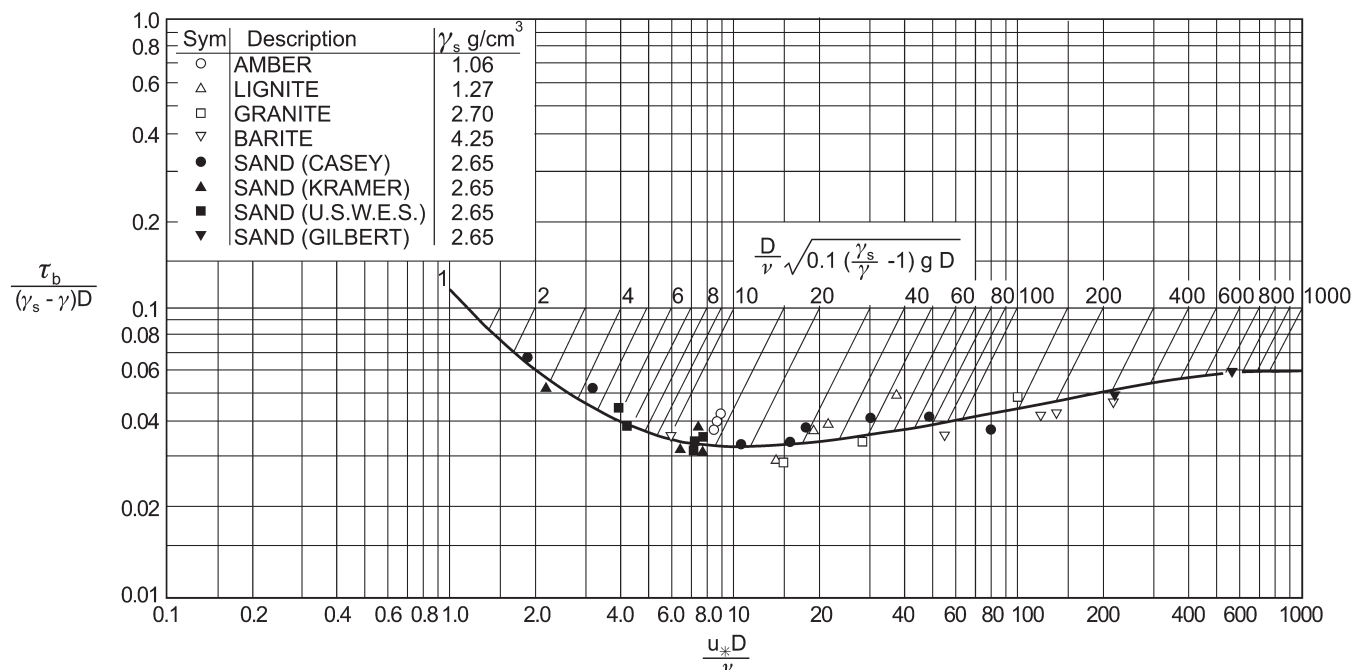


**Fig. 2.18.** Shields diagram for initiation of motion (source Vanoni, 1964).

Brownlie (1981) used this relation to convert the original Shields diagram into one with  $\tau_c^*$  versus  $R_{ep}$ . Similar diagrams using  $D^*$  (see Eq. 2-49b) instead of  $R_{ep}$  have been advanced among others by Bonnefile (1963), Smith (1977), van Rijn (1984a), García and Maza (1997), and Soulsby and Whitehouse (1997). A useful fit to the Shields data was proposed by Brownlie (1981, p.161):

$$\tau_c^* = 0.22 R_{ep}^{-0.6} + 0.06 \exp(-17.77 R_{ep}^{-0.6}) \quad (2-59a)$$

With this relation, the value of  $\tau_c^*$  can be readily computed when the properties of the water and the sediment are given. As already mentioned, to be on the safe side the values given by Eq. (2-59a) should be divided by 2 for engineering purposes, resulting in the following expression

$$\tau_c^* = \frac{1}{2} [0.22 R_{ep}^{-0.6} + 0.06 \exp(-17.77 R_{ep}^{-0.6})] \quad (2-59b)$$

This equation is plotted in the modified Shields diagram shown in Fig. 2-19, where the size ranges for silt, sand and gravel are also shown.

For fine-grained sediments (silt and finer), the Shields diagram does not provide realistic results. Mantz (1977)

conducted a series of experiments and observed that for fine-grained, noncohesive sediments the critical shear stresses can be estimated with the following relation

$$\tau_c^* = 0.135 R_{ep}^{-0.261} \quad (2-59c)$$

which is valid for the range  $0.056 < R_{ep} < 3.16$ . Equations (2-59a) and (2-59c) merge for  $R_{ep} = 4.22$ .

Lavelle and Mofjeld (1987) used the pioneering bed-stability observations made by Grass (1970) to question the existence of a deterministic value of critical stress for incipient motion as foreseen by Shieds and to promote a probabilistic approach to address threshold conditions for initiation of motion and entrainment into suspension. Along the same line of thought, Lopez and García (2001) have proposed a risk-based approach showing that the Shields diagram can be interpreted in a probabilistic way. At the same time, there is also evidence that the Shields diagram is quite useful for field application. For instance, Fisher et al. (1983) experimentally investigated incipient motion of organic detritus and inorganic sediment particles on sand and gravel beds and found that their observations followed the characteristics of the Shields diagram. Recently, Marsh et al (2004) tested the Shields approach together with three other methods available in the literature and showed that it is still one of the best methods available for sand-bed streams. More

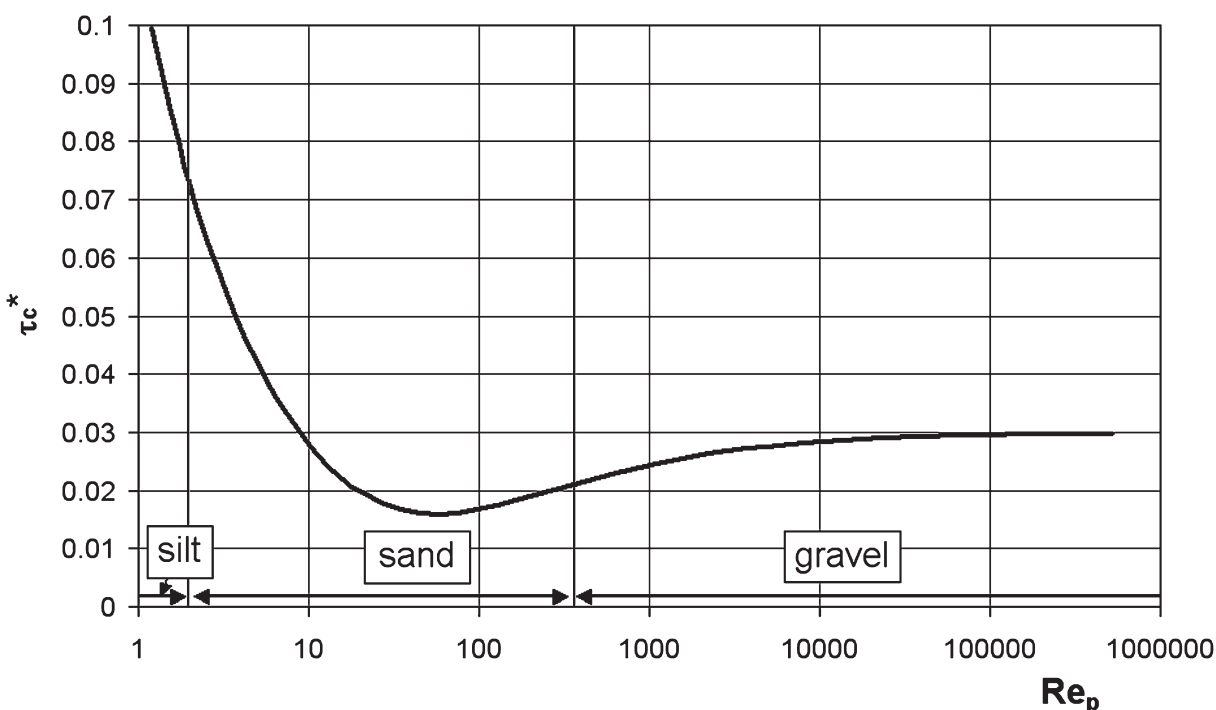


Fig. 2-19. Modified Shields diagram (after Parker 2005).

recently, Sarmiento and Falcon (2006) introduced the novel idea of using spatially-averaged (over many particles) shear stresses to define incipient conditions for particle motion at low transport rates.

Buffington (1999) thoroughly reanalyzed Shields' work, pointing out some inconsistencies in the way Shields observations had been interpreted and used by others. This motivated a discussion that analyzed the universality of the Shields diagram in the context of sand- and gravel-bed rivers (García 2000), resulting in the river sedimentation diagram presented below (Fig. 2-29).

**2.4.3.1 Application to Riprap Sizing and Flow Competence** It is worthwhile to show how knowledge about velocity distribution and initiation of motion can be used for a practical problem. Consider the design of a riprap cap to protect contaminated river-bed sediment against erosion. A geotextile or a filter layer can be used to cover the contaminated river-bed portion and then this layer can be protected with riprap material having a size  $D_{RR}$ . The riprap size has to be determined to ensure the stability of the cap design.

As introduced earlier, the Manning-Strickler relation for flow resistance is

$$(i) \quad \frac{U}{u_*} = 8.1 \left( \frac{H}{k_s} \right)^{1/6}$$

Here

$$(ii) \quad k_s = \alpha_s D_{RR}$$

Typical values for the coefficient  $\alpha_s$  can be found in Table 2-1.

The critical condition for motion of the coarse material making up the riprap can be written as

$$(iii) \quad \tau_c^* = \frac{u_{*c}^2}{R g D_{RR}}$$

Where  $\tau_c^*$  should be between 0.02 and 0.03 depending upon how broadly the bed is covered with riprap (see Fig. 2-19). Combining the above relations yields

$$(iv) \quad \frac{U}{\sqrt{R g D_{RR}}} = 8.1 \left( \tau_c^* \right)^{1/2} \alpha_s^{-1/6} \left( \frac{H}{D_{RR}} \right)^{1/6}$$

For example, if  $\tau_c^* = 0.03$  and  $\alpha_s = 2.5$ , this relation reduces to:

$$(v) \quad \frac{U}{\sqrt{R g D_{RR}}} = 1.204 \left( \frac{H}{D_{RR}} \right)^{1/6}$$

This equation is very similar to the many empirical equations that have been determined for riprap design (see

Eq. B.5 in Appendix B). In particular, this relation is very similar to the one proposed by Neill (1968) for initiation of motion of coarse material

$$(vi) \quad \frac{U}{\sqrt{R g D_{RR}}} = 1.204 \left( \frac{H}{D_{RR}} \right)^{1/6}$$

Suppose that the riprap is to be designed to be able to withstand a 10-year flood, at which the mean flow velocity  $U$  is estimated to be 3 m/s and the flow depth  $H$  is estimated to be 2.5 m. Using a submerged specific gravity  $R = 1.65$ , Eq. (v) gives a riprap size  $D_{RR} = 15.2$  cm (6 inches), and Neill's relation yields  $D_{RR} = 9.3$  cm (3.65 inches). A safety factor should be built into the design and if the material is poorly-sorted, the riprap size should be selected so that  $D_{RR} = D_{90}$ . The reader is referred to Appendix B for a full treatment of this topic.

A similar analysis can be used to estimate the flow competence to move coarse river-bed material of a given size. In this case, the question would be what mean flow velocity and depth are needed to move coarse material of a certain size? This is a typical problem when analyzing salmonid spawning gravel streams (e.g., Buffington et al. 2004).

#### 2.4.4 Yalin and Karahan Diagram

In a study of temperature effects on initiation of motion, Taylor and Vanoni (1972) reported that small but finite amounts of fine-grained sediment were transported in flows with values of  $\tau_c^*$  well below those given by the Shields curve. They found that as the size of sediment grains decreases, the dimensionless critical shear stress increases more slowly than one would infer by extrapolating the Shields curve. Similar observations were made by Mantz (1977; 1980) but the most conclusive evidence for such behavior was provided by Yalin and Karahan (1979) through carefully conducted experiments.

Yalin and Karahan (1979) compiled a substantial number of data while conducting their own set of experiments with sand sizes ranging from 0.10 to 2.86 mm for both laminar and turbulent flow conditions. In this diagram,  $Y_{cr} = \tau_c^*$  and  $X_{cr} = Re_*$ . They used glycerine in some of the experiments to increase the thickness of the viscous sublayer, thus making it possible to observe initiation of motion under laminar and turbulent flow conditions. As shown in Fig. 2-20, Yalin and Karahan were able to elucidate the nature of transport inception conditions for a wide range of grain Reynolds number  $Re_* = u_{*c} D/v$ . For  $Re_* > 70$ , hydraulically rough conditions,  $\tau_c^*$  takes a value of about 0.045. For values of  $Re_* < 10$ , the relation between  $\tau_c^*$  and  $Re_*$  depends on the flow regime, i.e., whether the flow is laminar or turbulent.

Like the original Shields diagram, the Yalin-Karahan diagram can only be used in an iterative way since  $\tau_c^*$  appears

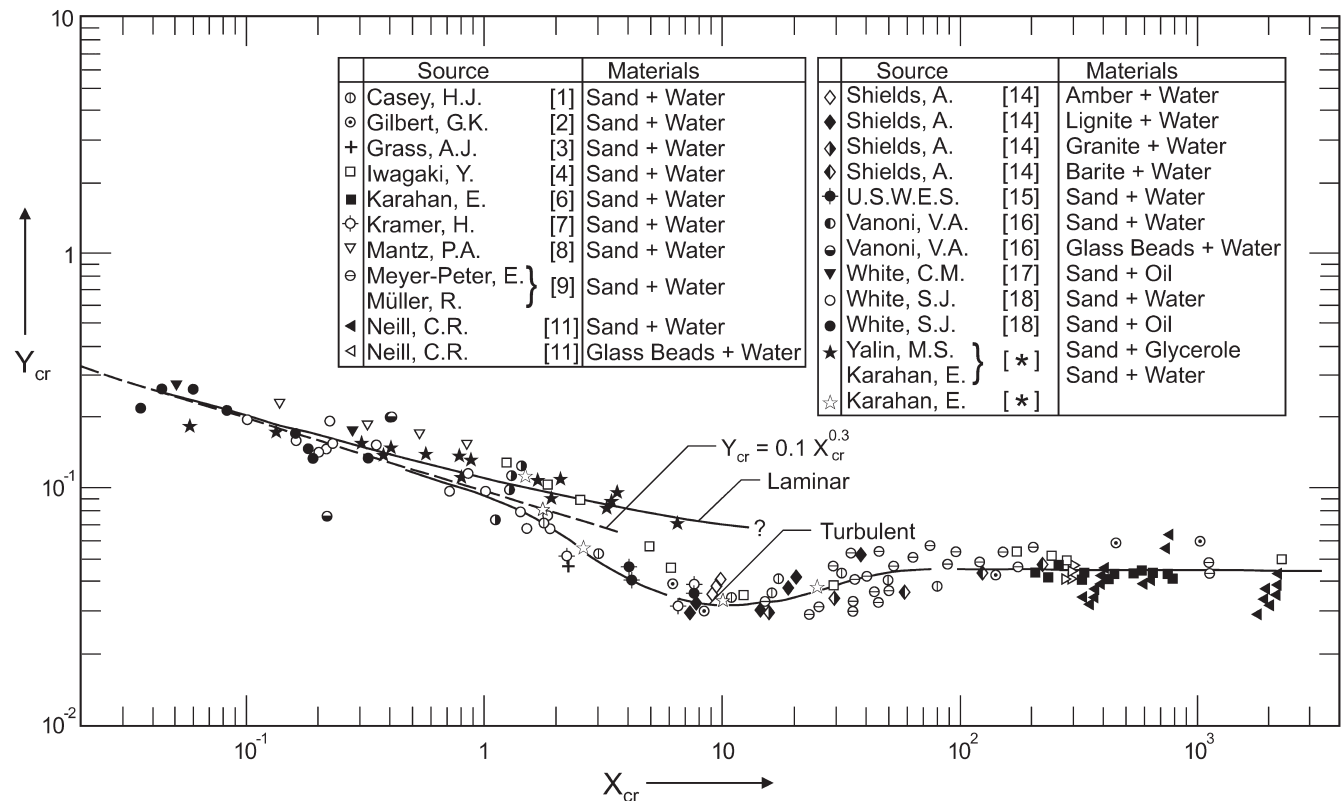


Fig. 2-20. Diagram for Initiation of Motion, Yalin and Karahan (1979).

both in the abscissas and in the ordinates. To obtain an explicit set of curves, a transformation similar to Eq. (2-58) can be introduced, as follows

$$D_{*c} = \left( \frac{Re_{*c}^2}{\tau_c^*} \right)^{1/3} = D \left( \frac{(\gamma_s - \gamma)}{\gamma} \frac{g}{v^2} \right)^{1/3} \quad (2-60)$$

Here  $\gamma$  and  $\gamma_s$  = specific weight of water and sediment, respectively. García and Maza (1997) have proposed the following useful fit to the Yalin-Karahan data:

For turbulent flow conditions,

$$\tau_c^* = 0.137 D_{*c}^{-0.377}; \quad 0.1074 < D_{*c} < 2.084 \quad (2-61a)$$

For laminar flow conditions,

$$\tau_{*c} = \frac{0.1439}{D_{*c}^{0.352}} + 0.0084 \exp - \left[ \frac{5.6243}{D_{*c}} \right]^{9.21}; \quad 0.2164 < D_{*c} < 11.252 \quad (2-61d)$$

These relations can be used to estimate critical shear stress for a wide range of sediment sizes and flow conditions. Dey (1999) has also proposed a rather simple model for threshold conditions that captures the behavior displayed by the Yalin and Karahan (1979) laboratory observations.

#### 2.4.5 Wiberg and Smith Diagram for Heterogeneous Sediments

Most of the work on initiation of motion has been done for uniform size sediment. One exception is the model advanced by Wiberg and Smith (1987). They derived an expression for the critical shear stress of noncohesive sediment using a balance of forces on individual particles very similar to the one shown previously. For a given grain size and density, the resulting equation depends on the near-bed drag force, lift force to drag force ratio, and particle angle

$$\tau_c^* = \frac{0.178}{D_{*c}^{0.7303}} + 0.0437 \exp - \left[ \frac{31.954}{D_{*c} + 10} \right]^{2.453} \quad (2-61b)$$

$$2.084 < D_{*c} < 47.75$$

$$\tau_c^* = 0.045; \quad D_{*c} > 47.75 \quad (2-61c)$$

of repose. They were able to reproduce the observations of Shields for uniform size sediments as well as initiation of motion in the case of sediment mixtures. They found that for mixed grain sizes the initiation of motion also depends on the relative protrusion of the grains into the flows and the particle angle of repose. The relation obtained by Wiberg and Smith (1987) for natural sediment is practically identical to the Ikeda-Coleman-Iwagaki relation (Eq. 2-55b) presented earlier for nearly spherical particles, and can be written as

$$\tau_c^* = \frac{4}{3} \frac{(\tan \phi_0 \cos \alpha - \sin \alpha)}{(c_D + \tan \phi_0 c_L)} \frac{1}{F^2(z/z_o)} \quad (2-62a)$$

where

$\alpha$  = bed slope angle;

$\phi_0$  = angle of repose of the grains;  $c_D$  and  $c_L$  drag and lift coefficients, respectively;

and the function  $F = u(z)/u_*$  is the logarithmic function (i.e. Eq. 2-4) that relates the effective fluid velocity acting on the particle to the shear velocity. Wiberg and Smith (1987) evaluate the logarithmic function with an equation for the velocity distribution first proposed by Reichardt in the early 1950s, which provides a smooth transition between the viscous sublayer and the outer portion of the velocity profile (Schlichting 1979, p. 601). Critical shear velocities computed with Eq. (2-62a) as a function of nominal grain diameter for quartz density sediment are shown in

Fig. 2-21. The agreement with observations made by a number of authors is excellent.

To evaluate the angle of repose  $\phi_0$  of natural particles in mixed-size beds, the observations made by Miller and Byrne (1966) with naturally sorted sediments were used. The following geometric relationship was found to represent the data well,

$$\phi_0 = \cos^{-1} \left[ \frac{D/k_s + z_*}{D/k_s + 1} \right] \quad (2-62b)$$

where  $z_* = -0.02$  is the average level of the bottom of an “almost moving” grain and depends on particle sphericity and roundness. Here  $k_s$  is the equivalent Nikuradse roughness length. Equation (2-62b) was found to represent the data of Miller and Byrne (1966) well for  $D/k_s > 0.5$ . Computed curves for nondimensional critical shear stress for a range of ratios of particle diameter to bed roughness,  $D/k_s = 0.5 - 5.0$ , are shown in Fig. 2-22a. A large ratio of  $D/k_s$  indicates a larger particle on a smaller bed, and vice versa. In this plot, the critical roughness Reynolds number  $(R_*)_{cr} = (u_*)_{cr} k_s / v$  is a characteristic of the bed. Thus, for any bed roughness, the intersections of a vertical line through some  $(R_*)_{cr}$  and the  $(\tau_*)_{cr}$  curves for the appropriate  $D/k_s$  values determine the critical shear stress for the sizes of material present in the bed.

Wiberg and Smith (1987) found that their model (i.e., Eqs. (2-62a) and (2-62b)) reproduced such observations. As in the case of the original Shields diagram, Wiberg and

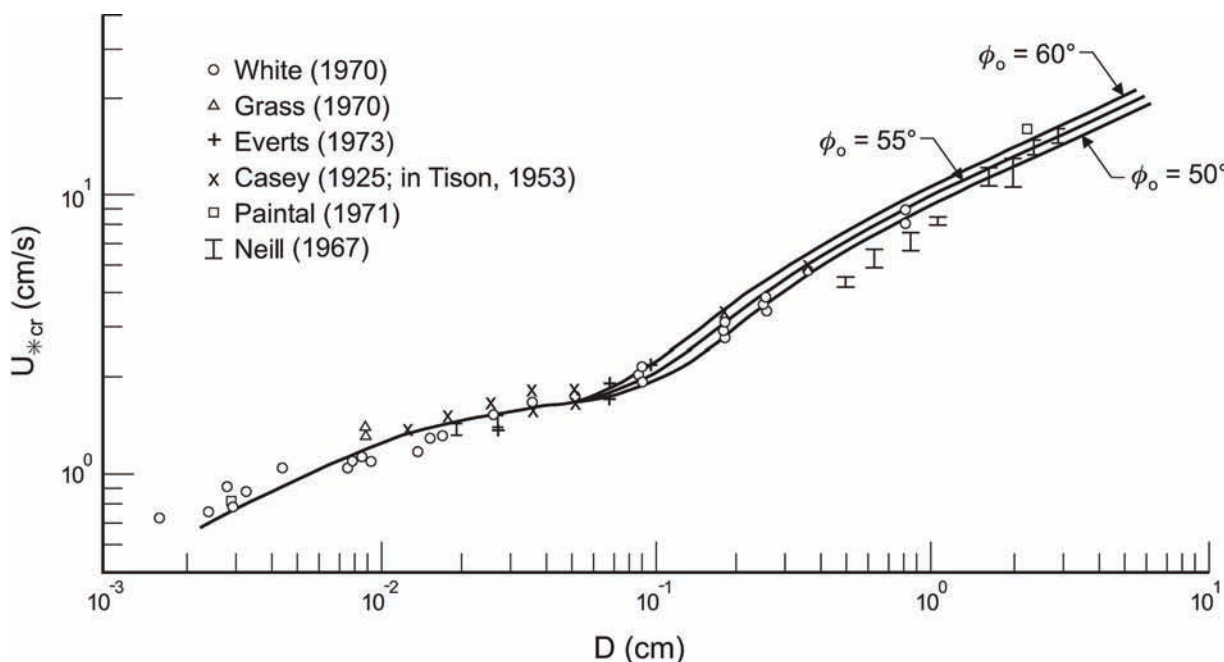
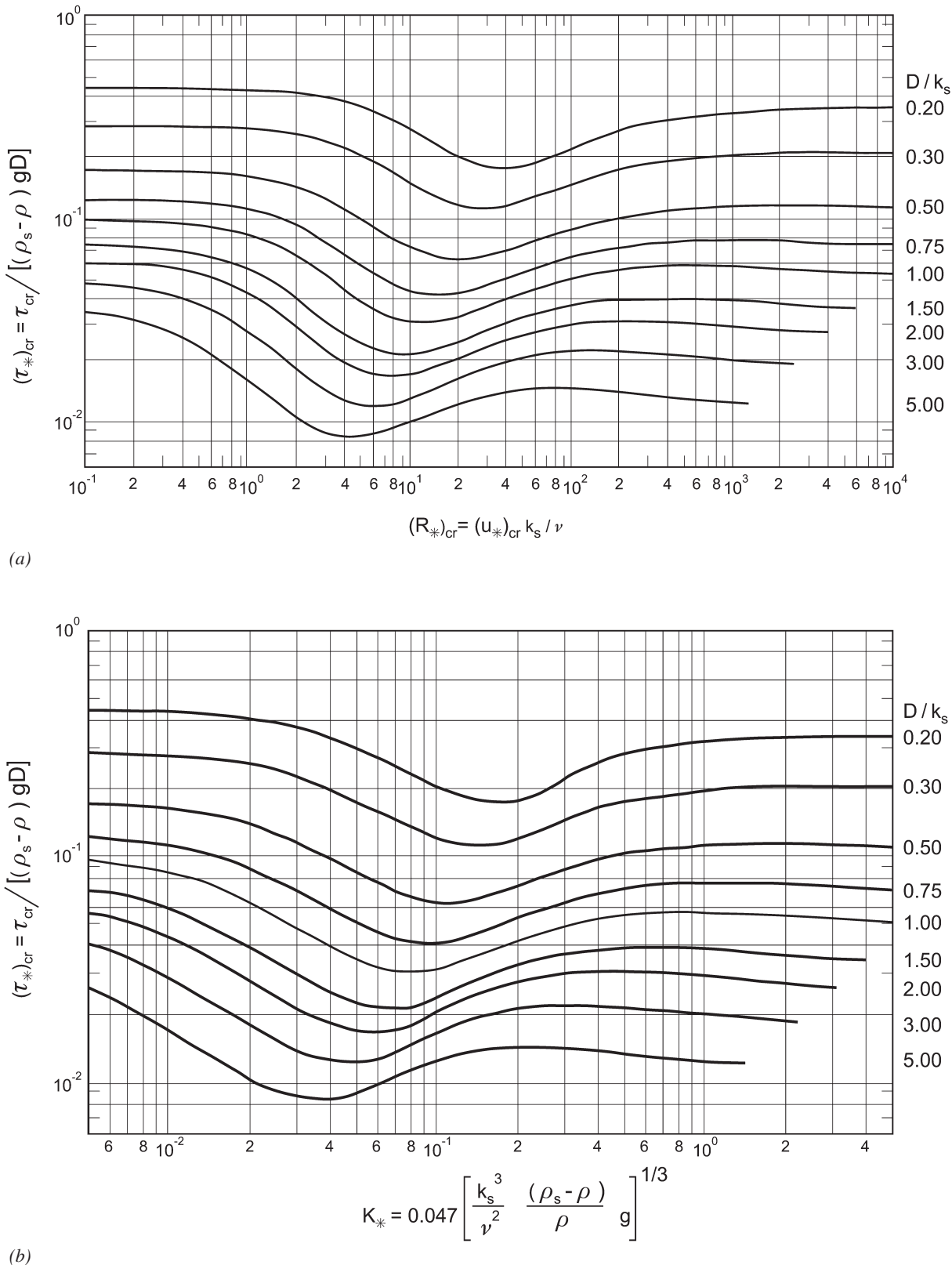


Fig. 2-21. Calculated critical shear velocity as a function of grain diameter (after Wiberg and Smith 1987).



**Fig. 2-22.** (a) Calculated nondimensional critical shear stress as a function of critical roughness Reynolds number for values of particle diameter to bed roughness scale. (b) Calculated nondimensional critical shear stress as a function of nondimensional particle diameter for values of particle diameter to bed roughness scale ratio (after Wiberg and Smith, 1987).

Smith found it more useful to express the critical shear stress in terms of a parameter that depends only on grain size and density and on fluid density and viscosity. As shown in Fig. 2-22b, the abscissa in the critical shear stress diagram is given by a variable  $K_* = 0.0047(\zeta_*)^{1/3}$  where

$$\zeta_* = \frac{D^3}{v^2} \frac{\rho_s - \rho}{\rho} g = \frac{[(R_*)_{cr} D/k_s]^2}{(\tau_*)_{cr}} \quad (2-62c)$$

In this fashion, iteration is not needed to find the critical shear stress for a particle of diameter  $D$  in a bed with characteristic roughness length  $k_s$ .

A systematic analysis of eight decades of incipient motion studies, with special reference to gravel-bed rivers was conducted by Buffington and Montgomery (1997). Different models available in the literature to estimate entrainment into motion of sediments having mixed grain sizes and densities are reviewed by Komar (1996). The work of James (1990) with spheres and Carling et al (1992) employing regularly shaped particles (rods, cylinders, discs and cubes) illustrates that grain-shape variability and grain orientation are important to entrainment, resulting in a range of stresses for particles that have otherwise the same weight. Bridge and Bennett (1992) have developed a mathematical model for entrainment and transport, which accounts for different grain sizes, shapes and densities. Niño et al (2003) were able to measure the effect of grain-size variability on sediment entrainment into suspension with the help of laboratory experiments. More information about initiation of motion and transport of gravel and sediment mixtures can be found in Chapter 3.

#### 2.4.6 Lischvan-Lebediev Diagram for Maximum Permissible Flow Velocity

In practice, it is often convenient to estimate the flow velocity necessary for initiation of motion and sediment erosion. A number of researchers have conducted flume experiments to collect data relating grain sizes and densities to flow velocities, discharges and mean stresses needed to initiate particle movement (e.g. Miller et al. 1977). In the early 1920s, Fortier and Scobey first introduced the concept of maximum permissible flow velocity (Chow 1959, p. 165). The maximum permissible flow velocity, or the nonerosible flow, is the greatest mean velocity that will not cause erosion of the channel bed. Lischvan and Lebediev used observations made in Russian channels (Lebediev 1959) for wide ranges of quartz sediment sizes ( $0.005 \text{ mm} < D < 500 \text{ mm}$ ) and flow depths ( $0.40 \text{ m} < H < 10 \text{ m}$ ) to obtain values of the maximum permissible flow velocity  $U_c^*$  as a function of the relative flow depth  $H/D$  (Garcia and Maza 1997). The Lischvan-Lebediev data are plotted in dimensionless form in Fig. 2-23. Two curves have been found to fit the data by García and Maza (1997).

For  $H/D \leq 744.2$

$$\frac{U_c}{\sqrt{RgD}} = 1.630 \left( \frac{H}{D} \right)^{0.1283} \quad (2-63a)$$

For  $H/D > 744.2$

$$\frac{U_c}{\sqrt{RgD}} = 1.453 \left( \frac{H}{D} \right)^{0.3221} \quad (2-63b)$$

An inspection of Fig. 2-23 suggests that Eq. (2-63a) corresponds to flow conditions representative of gravel-bed and cobble-bed streams (i.e., low relative flow depth), while Eq. (2.63b) corresponds conditions commonly found in sand-bed streams (i.e., large relative flow depth). Notice that the general form of these relations is very similar to the one obtained in Section 2.4.3.1. The Lischvan-Lebediev relations are widely used in Latin America for the design of stable channels and to estimate potential sediment erosion conditions in sand-bed rivers (e.g. Schreider et al. 2001).

#### 2.4.7 Effect of Bed Slope on Incipient Motion

**2.4.7.1 Granular Sediment on a Sloping Bed** The work of Shields and others on initiation of motion applies only to the case of nearly horizontal slopes. Most streams, particularly in mountain areas, have steep gradients, creating a need to account for the effect of the downslope component of gravity on the initiation of motion. In fact, the model of Wiberg and Smith (1987) as given by Eq. (2-62a) does account for the effect of streamwise channel slope.

As shown for the case of negligible longitudinal slope, the effect of the streamwise bed slope on incipient sediment motion can be illustrated by considering the forces (lift, drag, buoyancy, and gravity) acting on a particle lying in a bed consisting of similar particles over which water flows. Such analysis yields the equation (Chiew and Parker 1994)

$$\frac{\tau_{c\alpha}^*}{\tau_{co}^*} = \cos \alpha \left( 1 - \frac{\tan \alpha}{\tan \phi} \right) \quad (2-65a)$$

where

$\phi$  = angle of repose;

$\tau_{c\alpha}^*$  = critical shear stress for sediment on a bed with a longitudinal slope angle  $\alpha$ ; and

$\tau_{co}^*$  = critical shear stress for a bed with very small slope.

The value of  $\tau_{co}^*$  can be found from the Shields diagram with Eq. (2-59), or with Eq. (2-61). Eq. (2-65a) is for positive  $\alpha$ , which applies for downward sloping beds. For beds with adverse slope,  $\alpha$  is negative and the term  $\tan \alpha / \tan \phi$  in

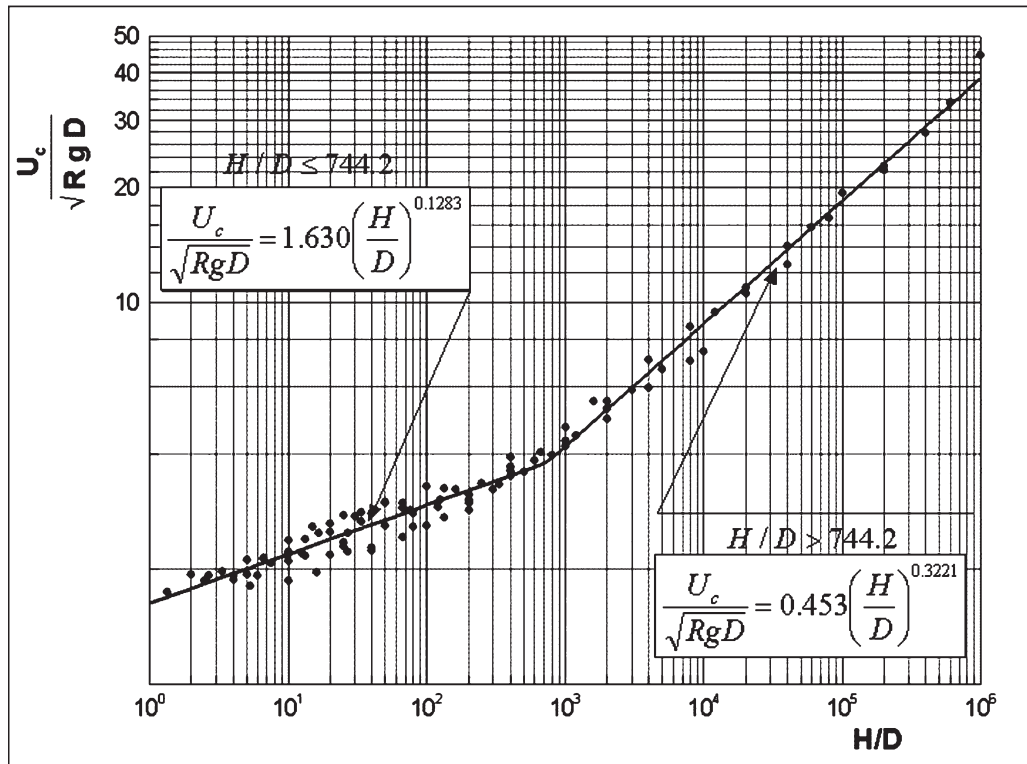


**Fig. 2-23.** Lischitzvan-Lebedev diagram for maximum permissible flow velocity.

Eq. (2-65a) is positive. In terms of shear velocities the relation takes the form

$$\frac{u_{*c}}{u_{*o}} = \sqrt{\cos\alpha \left(1 - \frac{\tan\alpha}{\tan\phi}\right)} \quad (2-65b)$$

An expression similar to Eq. (2-65a) was derived by Lysne (1969), who also performed a set of experiments on the effect of the bed slope on the incipient motion of sand in a closed channel. Lysne's results agree very well with the curve given by equation (2-65a) for a value of  $\phi = 47^\circ$ . A similar result was found by Fernandez-Luque and Van Beek (1976), who also fitted a relationship similar to Eq. (2-65a) to their results for the incipient motion of sand, gravel, and magnetite in open channel flow on sloping beds.

Chiew and Parker (1994) conducted a set of laboratory experiments with a closed duct, to test the validity of Eq. (2-65b) for both positive and adverse slopes. The results are plotted in Fig. 2-24. In general, good agreement is observed between the experimental observations and the values predicted with Eq. (2-65b).

Lau and Engel (1999) used dimensional analysis coupled with the observations made by Fernandez-Luque and Van Beek (1976) and Chiew and Parker (1994) to obtain an

equation mathematically equivalent to Eq. (2-65a) of the form

$$\frac{\tau_{ca}^*}{\tau_{co}^*} = \frac{\sin(\phi - \alpha)}{\sin\phi} \quad (2-65c)$$

They found that the condition for inception of motion depends on the slope angle as well as on the Reynolds number of the flow. Their recommendation is that Eq. (2-65c) can be used for slope angles all the way up to the angle of repose together with Shields criteria to estimate  $\tau_{co}^*$ . Whitehouse et al. (2000) tested Eq. (2-65c), finding good agreement with experimental observations. This relation has been rediscovered many times since Armin Schoklitsch introduced it for the first time in the early 1900s.

Several investigators, such as Stevens et al. (1976), Fernandez Luque and van Beek (1976), Howard (1977), Allen (1982), Smart (1984), Dyer (1986), Whitehouse and Hardisty (1988); Chiew and Parker (1994), Iversen and Rasmussen (1994), Dey (1999), and Dey and Debnath (2000), have used relationships similar to either Eq. (2-65a), Eq. (2-65b), Eq. (2-65c) to determine the critical shear stress for sediment lying on a nonhorizontal slopes. Stevens et al. (1976) used such relationship to investigate the factor of safety

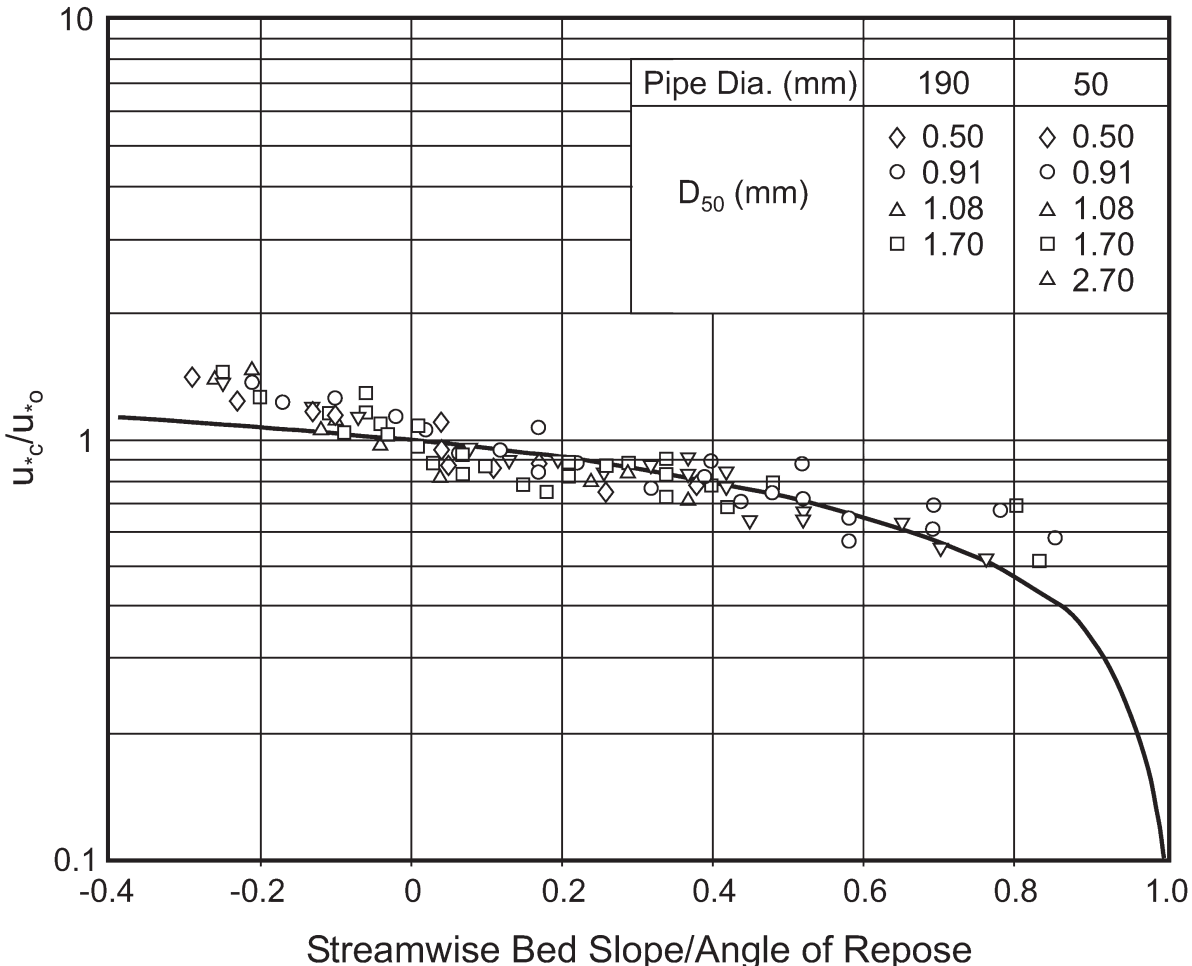


**Fig. 2-24.** Effect of streamwise bedslope on critical shear velocity. Curve correspond to Eq. 2.65b (modified from Chiew and Parker 1994).

for riprap protection, whereas Smart (1984) used them to evaluate sediment transport rates in a steep channel. Kostic et al. (2002) used Eq. (2-65a) to study the foreset slope of prograding deltas in lakes and reservoirs. Whitehouse and Hardisty (1988), Graf et al. (2000), and Damgaard et al. (2003) used similar concepts to study the inception of bed load transport on steep slopes. The effect of seepage on initiation of motion has been analyzed by Oldenziel and Brink (1974), Cheng and Chiew (1999), and Dey and Zanke (2004).

**2.4.7.2 Threshold Condition on Side Slopes** The analyses presented above apply strictly to the case of flow on a nearly horizontal or sloping bed in the streamwise direction that is horizontal in the transverse direction (i.e., negligible transverse bed slope). An important problem in engineering applications is the case of sediment particles on a side slope (Simons and Senturk 1992). This problem is of particular relevance to the design of riprap protection and

stable channels in coarse material (see Appendix B). Thus it is worthwhile to present a more detailed analysis.

In the present simplified analysis, the flow velocity profile is again taken to be logarithmic upward normal from the bed. A force balance is done for a particle located on a side slope, as shown in Fig. 2-25. The flow is taken to be in the streamwise direction, parallel to the side slope. The vectorial fluid drag force  $D_f$  acting on a particle is thus given as

$$D_f = \rho \frac{1}{2} \pi \left( \frac{D}{2} \right)^2 c_D u_f^2 \vec{e}_1 \quad (2-66a)$$

The gravitational force  $F_g$  has a transverse as well as a downward normal component:

$$F_g = F_{g2} \vec{e}_2 + F_{g3} \vec{e}_3 \quad (2-66b)$$

where  $\vec{e}_1$ ,  $\vec{e}_2$ , and  $\vec{e}_3$  are unit vectors in the streamwise, transverse, and downward normal to the side directions, respectively.

$$(F_{g2}, F_{g3}) = -\rho R g \frac{4}{3} \pi \left(\frac{D}{2}\right)^3 (\sin\theta, \cos\theta) \quad (2-66c)$$

and  $\theta$  denotes the local transverse angle of the side slope, as illustrated in Fig. 2-25.

The lift force is given as

$$L_f = \rho \frac{1}{2} \pi \left(\frac{D}{2}\right)^2 c_L u_f^2 \vec{e}_3 \quad (2-67)$$

The Coulomb resistive force acting on a grain has a magnitude given by  $\mu |F_{g3} \vec{e}_3| + L_f$ . As shown in the diagram, under critical conditions, it must precisely balance the vectorial sum of the impelling forces due to flow ( $D_f$ ) and due to the transverse downslope pull of gravity ( $F_{g2} \vec{e}_2$ ).

These conditions on magnitude and direction lead to the following result for threshold conditions:

$$\mu^2 |F_{g3} \vec{e}_3 + L_f|^2 = |D_f|^2 + |F_{g2} \vec{e}_2|^2 \quad (2-68)$$

Substituting Eqs. (2-66a), (2-66b), (2-66c) and (2-67) into Eq. (2-68) and reducing, the following relation is obtained:

$$\begin{aligned} & \left[ \left( \frac{u_f^2}{R g D} \right)^2 + \left( \frac{4}{3 c_D} \sin\theta \right)^2 \right]^{1/2} \\ &= \mu \left( \frac{4}{3 c_D} \cos\theta - \frac{c_L}{c_D} \frac{u_f^2}{R g D} \right) \end{aligned} \quad (2-69a)$$

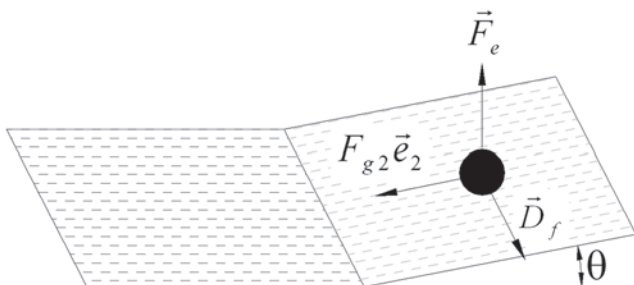


Fig. 2-25. Definition diagram for particle located on a side slope.

Further reducing with the aid of Eqs. (2-54) and (2-55), it is found that

$$\begin{aligned} & \left[ \left( \frac{\tau_c^*}{\tau_{co}^*} \right)^2 + \left( \frac{4}{3 c_D F^2} \sin\theta \right)^2 \right]^{1/2} \\ &= \frac{4\mu}{3 c_D F^2} \cos\theta - \mu \frac{c_L}{c_D} \frac{\tau_c^*}{\tau_{co}^*} \end{aligned} \quad (2-69b)$$

The case of a transversely horizontal bed is recovered by setting  $\theta = 0$ . The critical Shields stress is found to be given by Eq. (2-55a) for this case. This value is denoted as  $\tau_{co}^*$ , the subscript  $o$  denoting that the bed is horizontal in the transverse direction. Using this value to normalize the value  $\tau_c^*$  obtained on a side slope of angle  $\theta$ , Eq. (2-69b) reduces to

$$\begin{aligned} & \left\{ \left( \frac{\tau_c^*}{\tau_{co}^*} \right)^2 + \left[ \frac{(1 + \mu c_L/c_D)}{\mu} \sin\theta \right]^2 \right\}^{1/2} \\ &= (1 + \mu c_L/c_D) \cos\theta - \mu \frac{c_L}{c_D} \left( \frac{\tau_c^*}{\tau_{co}^*} \right) \end{aligned} \quad (2-69c)$$

Equation (2-69c) is a quadratic polynomial in  $\tau_c^*/\tau_{co}^*$ , and as such is easily solved. A solution is shown in Fig. 2-26, which has been evaluated for the case  $\mu = 0.84$  ( $\phi = 40^\circ$ ) and  $c_L = 0.85 c_D$ . It is also assumed that  $c_D$  is given as a function of  $u_f D/v$  according to the standard drag curve for spheres (i.e. Eq. 2-46d). As can be seen there, the Shields stress takes the value  $\tau_{co}^*$  on a horizontal bed ( $\theta = 0$ ). It progressively decreases as the side slope angle  $\theta$  increases, reaching a value of 0 at the angle of repose.

Many methods for stable channel design, starting with the classic work of Glover and Florey in the early 1950s, make use of Eq. (2-69c) to design a channel in coarse alluvium that is at the threshold for sediment motion but is stable (e.g., Li et al. 1976; Diplas and Vigilar 1992). Parker (1978) also used this approach to analyze flow in self-formed straight rivers with mobile beds and stable banks. More material on stable movable-bed channels can be found in Chapter 7.

If the lift force is neglected (i.e.,  $c_L = 0$ ), Eq. (2-69c) reduces to the well-known Lane (1955) relation,

$$\frac{\tau_c^*}{\tau_{co}^*} = \cos\theta \sqrt{1 - \left( \frac{\tan\theta}{\tan\phi} \right)^2} \quad (2-70)$$

Equation (2-70) has also been derived for application to coastal sediment transport problems by Fredsøe and Deigaard (1992, p. 204). Whitehouse et al (2000) tested

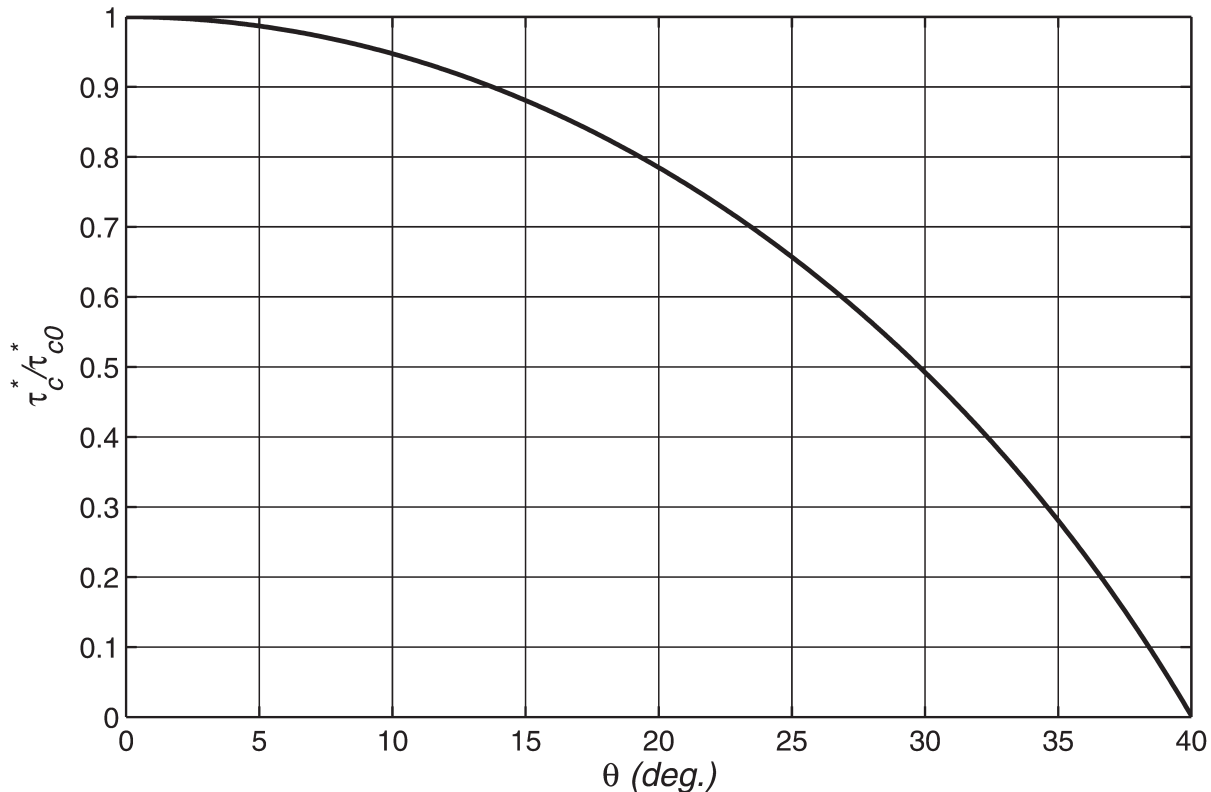


**Fig. 2-26.** Variation of normalized critical Shields stress for initiation of motion as a function of side slope angle as predicted by Eq. 2.69c.

the values predicted by Eq. (2-70) with the observations made by Ikeda (1982) and found reasonable agreement. Christensen (1972) found out that the critical shear stresses estimated with Eq. (2-70) have a tendency to be too conservative and proposed an alternative method that takes into account the ratio between the bed roughness and the grain size. As this ratio increases, Lane's Eq. (2-70) and Christensen's method give identical results. The method of Wiberg and Smith (1987) presented above also takes into account the effect of the relative roughness  $D/k_s$  on the evaluation of critical shear stress condition for motion. James (1990) has also provided useful information on the effect of such parameter on initiation of motion. Similar approaches, which follow the so-called grain pivoting model, have been suggested by Slingerland (1977) and Komar and Li (1988) among others (Komar, 1996). Bridge and Bennett (1992) have also advanced a model that accounts for bedslope effects on initiation of motion.

**2.4.7.3 Threshold Condition for Motion on an Arbitrarily Sloping Bed** The general case of an arbitrarily sloping bed was first treated analytically by Kovacs and Parker (1994), who developed a vectorial equation for sediment threshold on a combined transverse and longitudinal

sloping bed. Their analysis was extended by Seminara et al. (2002) to include the effect of lift force. While studying coastal sediment transport, Calantoni (2002, p. 77) generalized the analysis of Fredsøe and Deigaard (1992) and obtained a quadratic equation for the threshold condition for motion, similar to Eq. (2-69c), which shows promise for practical use. The positive root of the equation gives an equation that can be used to estimate the critical shear stress for motion of a particle located on a bed surface having a longitudinal (parallel the flow direction) slope angle  $\alpha$  and a transverse (perpendicular to flow direction) slope angle  $\theta$ ,

$$\frac{\tau_c^*}{\tau_{co}^*} = \cos \alpha \left( \cos \theta \sqrt{1 - \left( \frac{\tan \theta}{\tan \phi} \right)^2} - \frac{\tan \alpha}{\tan \phi} \right) \quad (2-71a)$$

Notice that when  $\alpha = 0$ , Eq. (2-71a) reduces to Eq. (2-70) and when  $\theta = 0$ , Eq. (2-71a) reduces to Eq. (2-65a). Calantoni and Drake (1999) used Eq. (2-71) to develop a discrete-particle model for bed load transport in the surf zone that accounts for variations in bottom slope.

Duan et al. (2001) and Duan and Julien (2005) have used the following formulation for sediment transport modeling in meandering channels,

$$\frac{\tau_c^*}{\tau_{co}^*} = \cos \theta \left[ 1 - \left( \frac{\tan \theta}{\tan \phi} \right)^2 \right]^{1/2} \left( \frac{\sin(\phi - \alpha)}{\sin \phi} \right) \quad (2-71b)$$

Notice that when  $\theta = 0$ , Eq. (2-71b) reduces Eq. (2-65c) which is also equivalent to Eq. (2-65a). When  $\alpha = 0$ , Eq. (2-71b) reduces to Eq. (2-65a). It should be clear that Eqs. (2-71a) and (2-71b) are mathematically equivalent. In the early 1960s, Norman Brooks provided an excellent theoretical analysis of this problem in the context of river bends. It can be found in Vanoni (2006, p.64).

Other efforts to estimate critical shear stress values for sediments on arbitrarily sloping beds include the work of Dey (1999, 2003). More research, including experiments over a wide range of conditions that can be used to test and improve different formulations, is needed on this important topic. Stream channel stability, bank erosion, and meandering channels are topics where the material covered previously plays a crucial role. This will become apparent in Chapter 7, Chapter 8, and in Appendix B “RipRap design.”

## 2.5 SEDIMENT TRANSPORT

Sediment load in this manual refers to the sediment that is in motion in a river. There are two common ways of classifying the sediment load as shown in Table 2-4. The first divides the sediment load according to the mechanism for transport into bed load and suspended load. The second classifies the load based on particle size into wash load and bed sediment load. The suspended load, as the term denotes, moves in suspension and is that part of the load which is not bed load. Wash load is fine sediment moving in suspension which makes up a very small part, usually a few percent, of the sediment on the bed. Wash load is commonly taken as the silt and clay fraction of the bed sediment, i.e., that fraction with grain sizes finer than 0.062 mm. The bed sediment load consists of particles that are coarser than the wash load. The transport rate or discharge of wash load tends not to be correlated with water discharge while discharge of bed sediment, both in suspension and as bed load, is usually correlated with water discharge. The total sediment load is made up of wash load, suspended (bed-material) load and bed load. Methods and technologies for measuring sediment transport are covered in Chapter 5.

In some rivers the different components of the sediment load can be clearly differentiated. This is the case of the Niger River, Nigeria, depicted in Fig. 2-27, where the different components of the sediment load were measured in cubic meters per year by NEDECO (1959). In this particular

**Table 2-4 Sediment Load Classification**

	Classification system	
	Based on mechanism of transport	Based on particle size
Total sediment load		
Wash load	Suspended load	Wash load
Suspended bed-material load	Suspended load	Bed-material load
Bed load	Bed load	Bed-material load

example the wash load is many times larger than the load of bed material transported as suspended and bed load. Notice also that there are two peaks for the wash load associated with sediment grain sizes of about 0.001 mm and 0.025 mm. These might be related to the watershed activities taking place at the time the observations were made.

### 2.5.1 Sediment Transport Modes: Bed-Material Load and Wash Load

The sediment transport processes that can be characterized with fluid and sediment dynamics principles are those of bed load and suspended load. In the former case, the particles roll, slide, or saltate along the bed, never deviating too far above the bed. In the latter case, the fluid turbulence comes into play carrying the particles well up into the water column. In both cases, the driving force for sediment transport is the action of gravity on the fluid phase; this force is transmitted to the particles via drag. While it is possible to quantify the mechanics of bed-material transport as suspended load and bed load, a similar analysis to assess the wash load has proved rather elusive. Before considering bed-material transport in more detail, the wash load will be considered next. Important questions are what is role of sediment in the flow energy balance and how the division between wash load and bed-material load in sand-bed streams can be made?

The floodplains of most sand-bed rivers often contain copious amounts of silt and clay finer than about 0.062 mm. This material is known as wash load because it often moves through the river system in suspension without being present in the bed in significant quantities (Colby 1957). Increased wash load does not cause deposition on the bed, and decreased wash load does not cause erosion, because it is transported at well below capacity. This is not meant to imply that the wash load does not interact with the river system. Wash load in the water column exchanges with the banks and the floodplain rather than the bed. Greatly increased washload, for example, can lead to thickened floodplain deposits with a consequent increase in bank-full channel depth. Soil fertility depends

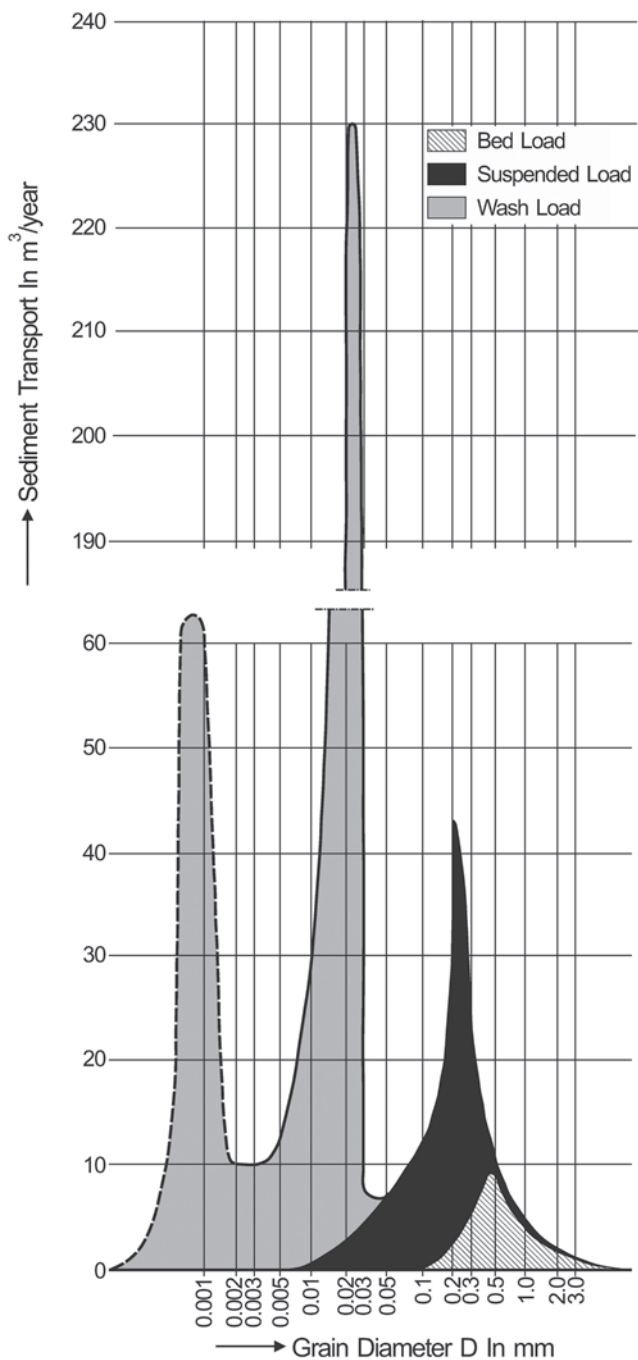


**Fig. 2-27.** Total Sediment Load in the upper Niger River, Nigeria (adapted from Jansen et al. 1979). Ordinates are in hundreds of thousands of cubic meters per year for each sediment size fraction.

largely on the amount of wash load deposited by floods on a given floodplain over the years. This fact was well known by the Egyptians, who practice agriculture in the floodplains of the Nile River. Also of relevance, is the fact that contaminants such as PCBs and heavy metals are often attached to the fine-grained sediments that constitute the wash load. The wash load is controlled by land surface erosion (rainfall, vegetation, land use) and not by channel-bed erosion. However,

cohesive stream banks can contribute to the wash load during bank full flow events. Mining activities can also contribute substantially to the wash load of river systems, with potential environmental effects on estuarine and coastal areas (e.g., coral reefs). Despite its importance, a physical characterization of the wash load is not an easy task.

By definition, the wash load is not determined by the hydraulic characteristics of a given river reach; hence it can not be computed (Einstein and Chien 1953). At the same time, sediment transport formulae apply only to bed-material transport and do not account for wash load. De Vries (1993) argues that there are at least two reasons why a quantitative distinction between bed-material load and wash load is necessary.

- (i) For comparison of sediment transport predictions with values measured in the field it is necessary to subtract the wash load component.
- (ii) A reduction of the flow velocity in the direction of the current will make a fraction of the wash load become bed-material load (e.g., reservoir sedimentation).

Vlugter (1962) discriminated between *sinking* material and *floating* material. He argued that fine sediment particles (i.e., floating material) being moved downstream in a river add part of their potential energy to the flow and can be transported in suspension indefinitely as long as the flow conditions do not change. On the other hand, coarse grains (i.e., sinking material) require kinetic energy from the mean flow to remain in suspension. Bagnold (1962) arrived to a similar conclusion while studying turbidity currents, and called this condition "autosuspension." Interestingly, both Vlugter and Bagnold ideas were very similar to those articulated a few years earlier by Knapp (1938) while looking at the energy balance in streams carrying suspended sediment. As pointed out by Jansen et al (1979) in their river engineering book, the energy balance concept underlying the Vlugter and Bagnold arguments has not yet been accepted by everyone (e.g., Parker 1982). In order to better understand some of these ideas it is useful to consider the energy balance in sediment-laden flows.

Consider a steady, uniform sediment-laden open-channel flow in a channel with a bed slope  $S$ , as described in Fig. 2-31. The role of fine sediment in the energy balance can be observed by considering the average rate of work  $P_g$  (i.e., dot product of momentum and velocity) done by gravity on the flow which can be approximated as follows,

$$P_g \equiv \rho g S U H + \rho R g S C U H - \rho R g H C v_s \quad (2-72a)$$

$$(1) \qquad (2) \qquad (3)$$

In this simplified energy balance relation,  $U$  = mean flow velocity,  $H$  = flow depth,  $C$  = mean volumetric concentration of suspended sediment,  $R = (\rho_s/\rho - 1)$  = submerged

specific gravity of the sediment,  $\rho_s$  = sediment density,  $\rho$  = water density,  $v_s$  = sediment fall velocity, and  $g$  = gravitational acceleration.

The physical significance of the terms in Eq. (2-72a) can be identified as follows:

- (1) Mean rate of energy input to the fluid phase (i.e., water).
- (2) Mean rate of energy input to the mean flow through the solid phase (i.e. sediment).
- (3) Mean rate of energy loss by mean flow through turbulent mixing required for maintaining sediment in suspension.

The main input of energy to the mean flow through the sediment phase can thus be positive or negative, depending on whether or not term (2) is greater than term (3). If term (2) is larger than (3), it means that the suspended sediment contributes energy to the flow. On the other hand, if (3) is larger than (2) it means that the flow is expending energy to keep the sediment in suspension. However for a dilute open-channel suspension ( $C \ll 1$ ), terms (2) and (3) are very small compared to term (1). Thus the flow energetics is to a first approximation independent of sediment concentration. It follows that whether or not term (2) is greater than term (3) has essentially nothing to do with whether the flow has enough energy to sustain itself, since almost all the energy enters through the water via term (1).

In the case of a turbid underflow or turbidity current overlain by clear, still, nonstratified water and flowing down a submarine channel with a slope  $S$  (Fig. 2-59), the situation is drastically changed. Clear water will not flow down a submarine channel or canyon due to gravity in the absence of suspended sediment. An analysis of the equations of motion (see Section 2.11.3) shows that the work done by the hydrostatic pressure gradient of the fluid phase just cancels term (1), so that in fact there is no positive energy input to the fluid phase. In the case of turbidity currents, gravity acts on the solid phase which in turn drags the fluid phase downslope forming an underflow. The net mean energy input through the solid phase  $P_{gs}$  is simply

$$P_{gs} = \rho R g S C U H - \rho R g H C v_s \quad (2-72b)$$

$$(2) \quad (3)$$

Thus the only positive energy input into the turbidity current is via term (2). It follows that term (2) must exceed term (3) for a self-sustaining turbidity current,

$$\rho R g S C U H > \rho R g H C v_s \quad (2-72c)$$

This relation can be reduced to

$$\frac{U S}{v_s} > 1 \quad (2-72d)$$

This is the classical Bagnold criterion for turbidity currents (Bagnold 1962). It ensures that the sediment supplies more energy than it consumes. The Bagnold criterion must be satisfied if a self-sustaining turbidity current is to occur. This is a necessary condition but is not sufficient as described by Parker et al (1986) since the flow has to be capable of entraining sediment into suspension to sustain itself.

The analogous energy constraint for a self-sustaining, dilute ( $RC \leq 0.1$ ), open-channel suspension is found to be from Eq. (2-72a),

$$\frac{U S}{v_s} > \frac{R C}{I + R C} \cong R C \quad (2-72e)$$

This condition was first articulated by Knapp (1938) and expressed mathematically by Vlugter (1942, 1962). An open-channel suspension can guarantee that the Knapp-Vlugter criterion is satisfied, by lowering the suspended sediment concentration  $C$ , and thus its excess fractional density  $RC$ , via sediment deposition. Vlugter (1962) used the above criterion to design stable irrigation channels in Indonesia. According to Vlugter, sediment with a fall velocity  $v_s$  that satisfies the above condition constitutes the *floating* material that does not require energy from the flow to be transported. The *floating* material is equivalent to the wash load. On the other hand, sediment with fall velocities that do not satisfy the Knapp-Vlugter condition and that take energy away from the flow to be transported is dubbed the *sinking* material. The *sinking* material can be regarded as the bed-material load. Vlugter states that in practice, when the mean flow velocity  $U > 0.5$  m/s, all silt particles smaller than 0.07 mm appear to behave as *floating material* (i.e., wash load). This is close to the grain diameter of 0.062 mm commonly used to define the wash load (e.g., Colby 1957).

De Vries (1993) has suggested that the Knapp-Vlugter criterion (Eq. 2-72e) could be used to find a tentative division between wash load and bed-material load in sand-bed streams. There have also been attempts to use Bagnold's ideas, which are applicable only to turbidity currents as previously shown, for the analysis of self-sustaining suspensions in open-channels flows (e.g., Southard and Mackintosh 1981; Wang 1984). As could be expected, this has generated a substantial amount of discussion in the literature (e.g., Parker 1982; Paola and Southard 1983; Nordin 1985a; Brush 1989). It should be clear that Bagnold's criterion does not correspond to an energy constraint on open-channel suspensions. The fundamental differences and similarities between sediment transport by rivers and turbidity currents are addressed in Section 2.11.

While conducting sedimentation studies in the Orinoco River in Venezuela, Nordin and Perez-Hernandez (1985) defined the wash load as the material that can be suspended (i.e.,  $u_*/v_s \geq 1.25$ ) as soon as its motion at the bed is initiated

(i.e.,  $\tau_b = \tau_{bc}$ ). Mathematically, this condition can be defined in dimensionless form by the relations

$$\tau^* \geq 1.11 R_f^2 \text{ when } \tau^* = \tau_c^* \quad (2-72f)$$

where

$\tau^*$  = dimensionless Shields stress parameter defined by Eq. (2-73a);

$\tau_c^*$  = dimensionless critical Shields stress for incipient motion (Fig. 2-19);

$R_f = \frac{v_s}{\sqrt{gRD}}$  = dimensionless fall velocity (Eq. 2-46b)

which is a function of

$R_{ep} = \frac{\sqrt{gRDD}}{v}$  and can be evaluated, for example, with

Dietrich's relation (Eq. 2-47).

Nordin (1985b) suggests that the most practical way to apply this criterion in the field is to plot the largest particle size that can be suspended and the largest particle size that can be moved at the bed, as functions of the shear velocity ( $u_*$ ). The sediment diameter at which the two curves intersect defines the upper limiting size of the wash load, and particles finer than this would not be found in appreciable quantities in the bed because they would go into suspension as soon as their motion is initiated. In the case of the Orinoco River, Nordin (1985b) found that the upper limiting size for the wash load is 0.095 mm for a water temperature of 25°C. A limiting size for the wash load in dimensionless form which implicitly includes the effect of temperature, can be found from the dimensionless particle Reynolds number ( $R_{ep}$ ) where the curves for initiation of motion and suspension intersect, as shown in Fig. 2-28 below. However, the relations proposed by Mantz (Eq. 2-59c) or Yalin and Karahan (Eq. 2-61a) for incipient motion of fine-grained sediment should be used instead of the Shields criterion (Eq. 2-59b) which does not work for the grain sizes found in the wash-load.

While Nordin's approach can provide an idea of the size of the particles making up the wash load, because this fine-grained material is transported well below capacity what ultimately determines how much sediment is transported as wash load is the supply of fine sediment to a given river from its watershed and not the transport capacity of the river itself. Watershed sediment yield is addressed in Chapter 17.

In what follows, the emphasis is placed on understanding the mechanics of bed load and suspended load transport in open-channel flows, including morphological changes in rivers, lakes and reservoirs, with the goal of providing the knowledge needed for sedimentation engineering. The mechanics of transport by turbidity currents is also considered, and used to analyze delta formation and reservoir sedimentation.

## 2.5.2 Shields-Parker River Sedimentation Diagram

Alluvial rivers that are free to scour and fill during floods can broadly be divided into two types: sand bed streams and

gravel bed streams. Sand bed streams typically have values of median bed sediment size between 0.1 mm and 1 mm (Fig. 2-12). The sediment tends to be relatively well sorted, with values of geometric standard deviation of the bed sediment size varying from 1.1 to 1.5. Gravel bed streams typically have values of median size of the bed sediment exposed on the surface of 15 mm to 200 mm or larger; the substrate is usually finer by a factor of 1.5 to 3 (Fig. 2-13). The geometric standard deviation of the substrate sediment size is typically quite large, with values in excess 3 being quite common. Although gravel and coarser material constitute the dominant sizes, there is usually a substantial amount of sand stored in the interstices of the gravel substrate (Chapter 3).

Two dimensionless parameters provide an effective delineator of rivers into the above two types (García 2000). The first of these parameters is the dimensionless Shields stress for uniform flow conditions, defined as:

$$\tau^* = \frac{\tau_b}{\rho g RD} = \frac{HS}{RD} \quad (2-73a)$$

where

$\tau_b$  = bed shear stress;

$g$  = gravitational acceleration

$\rho$  and  $\rho_s$  water and sediment density, respectively;

$R = (\rho_s - \rho)/\rho$  = submerged specific gravity of the sediment;

$D$  = mean sediment diameter;

$H$  is the flow depth; and

$S$  is the stream slope which for steady, uniform flow is the same as the energy gradient.

The second of these parameters is the particle Reynolds number  $R_{ep}$  defined as:

$$R_{ep} = \frac{\sqrt{gRDD}}{v} \quad (2-73b)$$

where  $v$  is the kinematic viscosity of water. This second parameter can be considered as a dimensionless surrogate for grain size.

Rivers were first introduced into the Shields diagram by Gary Parker in the early-1980s. Parker used these two parameters but his diagram, shown in Fig. 2-28, did not include field data (García 1999). Parker's diagram, however, gave an indication of the areas in the modified Shields diagram corresponding to sand-bed and gravel-bed streams.

Motivated by a thorough review of the Shields diagram done by Buffington (1999), García (2000) used field and laboratory data to confirm the early ideas of Parker, resulting in Fig. 2-29. This figure shows a plot of the values of the Shields stress (Eq. 2-73a) evaluated at bankfull flow versus particle Reynolds number (Eq. 2-73b) for six sets of field

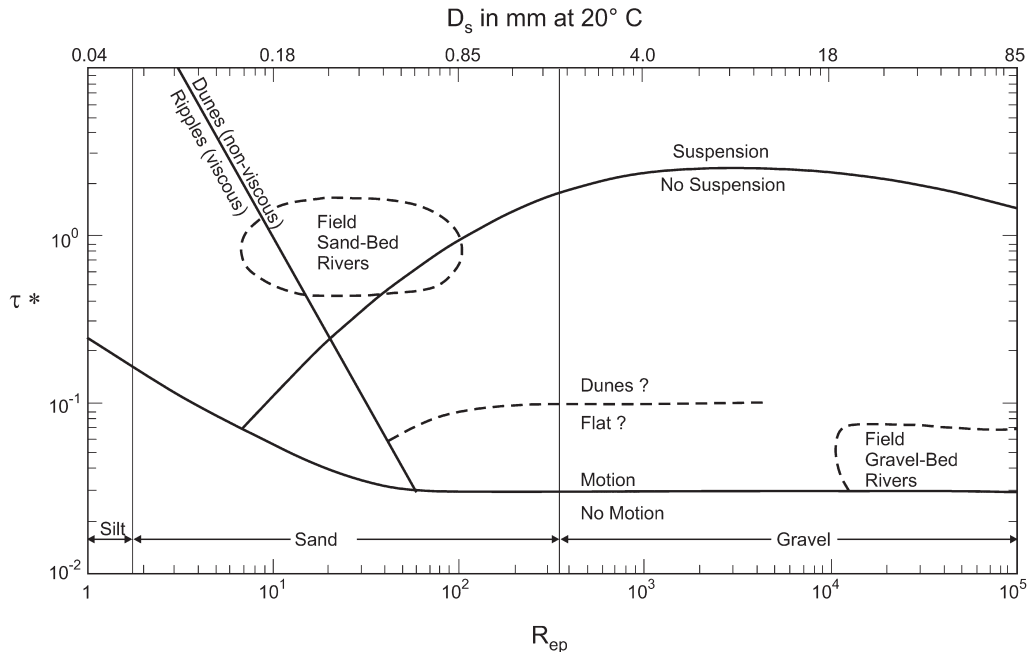


**Fig. 2-28.** Parker's River Sedimentation Diagram (García 1999).

data: a) gravel bed rivers in Wales, UK (Wales); b) gravel bed rivers in Alberta, Canada (Canada); c) gravel bed rivers in the Pacific Northwest, USA (Pacific); d) single-thread sand streams (Sand sing); e) multiple-thread sand streams (Sand mult); f) large sand-bed rivers (Parana, Missouri, etc.); and g) large-scale laboratory experiments on bridge-pier scour conducted at St Anthony Falls Laboratory (SAFL), University of Minnesota.

There are three curves in the Shields-Parker river sedimentation diagram of Fig. 2-29 that make it possible to know, for different values of ( $\tau^*, R_{ep}$ ), if a given bed sediment grain will go into motion, and if this is the case, whether or not the prevailing mode of transport will be suspended load or bed load. The diagram can also be used to estimate what kind of bed forms can be expected for different flow conditions and sediment characteristics. For example, ripples will develop in the presence of a viscous sublayer and fine-grained sediment. If the viscous sublayer is disrupted by coarse sediment particles, then dunes will be the most common type of bed form.

As could be expected, the Shields-Parker diagram (Fig. 2-29) also shows that in gravel-bed rivers, bed material is transported mainly as bed load. On the other hand, in sand-bed rivers, suspension and bed load transport of bed material coexist, particularly at high flows. The diagram is valid for steady, uniform flow conditions, where the bed shear stress can be estimated with  $\tau_b = \rho g H S$  (Eq. 2-1). The ranges for silt, sand, and gravel are also included. In this diagram, the critical Shields stress for motion was plotted with Eq. (2-59a).

The critical condition for suspension is given by the ratio (Niño and García 1998; Lopez and García 2001)

$$\frac{u_*}{v_s} = 1 \quad (2-74)$$

where  $u_*$  is the shear velocity; and  $v_s$  is the sediment fall velocity. Eq. (2-74) can be transformed into:

$$\tau_s^* = R_f^2 \quad (2-75)$$

where:

$$\tau_s^* = \frac{u_*^2}{gRD} \quad (2-76)$$

denotes a threshold Shields number for suspension and  $R_f$  is given to be Eq. (2-46b), and can be computed for different values of  $R_{ep}$  with the help of Dietrich's fall velocity relation given by Eq. (2-47a).

Finally, the critical condition for viscous effects (ripples) was obtained with the help of the definition for the viscous sublayer thickness (Eq. 2-6) as follows,

$$11.6 \frac{v}{u_* D} = 1 \quad (2-77)$$

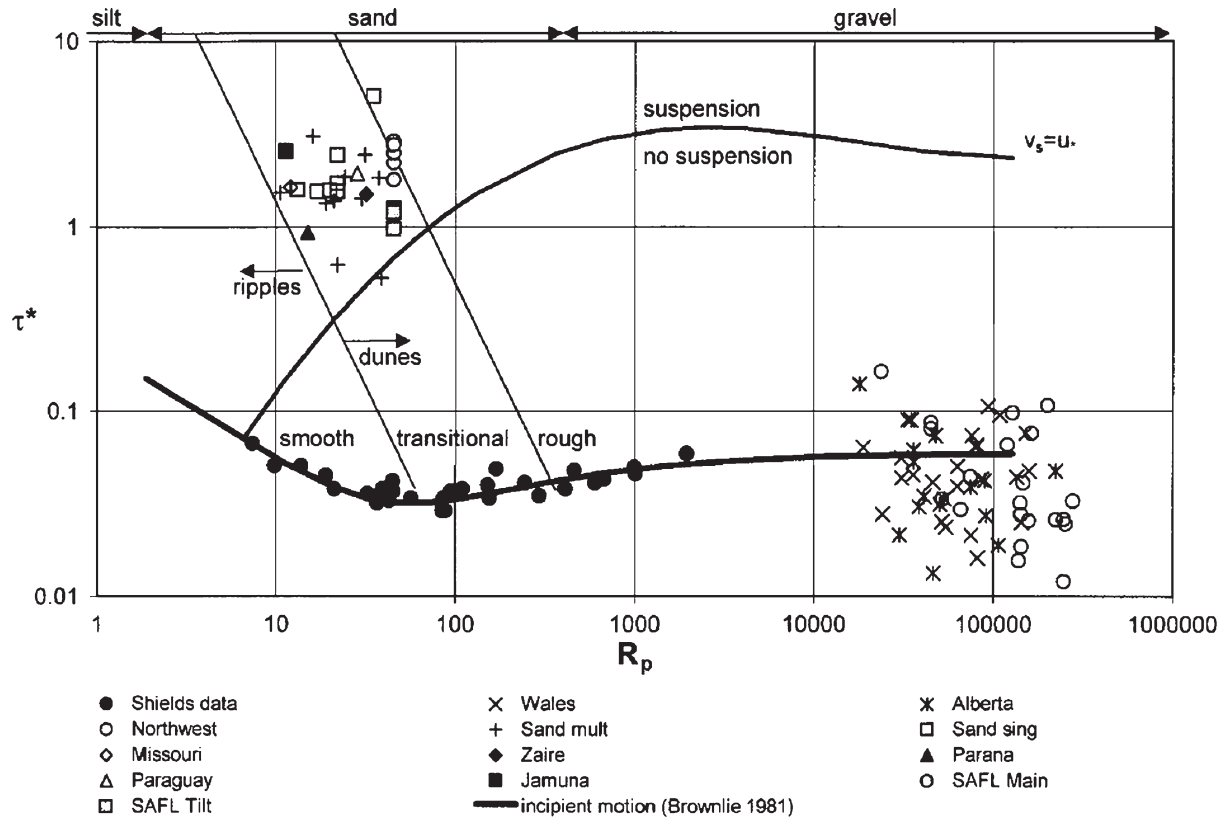


**Fig. 2-29.** Shields-Parker River Sedimentation Diagram (after García 2000).

which in dimensionless form can be written as

$$\tau_v^* = \left( \frac{11.6}{R_{ep}} \right)^2 \quad (2-78)$$

In this equation,  $\tau_v^*$  denotes the threshold Shields number below which ripples can be expected.

Relations (2-59a), (2-75), and (2-78) are the ones plotted in Fig. 2-29. The Shields-Parker diagram should be useful for studies concerning stream restoration and naturalization (Chapter 9), for it provides the range of dimensionless shear stresses corresponding to bankfull flow conditions for gravel-bed streams ( $0.01 < \tau_v^* < 0.2$ ) and for sand-bed streams ( $0.6 < \tau_v^* < 6$ ). Notice that the bank-full dimensionless Shields shear stress is in general, an order of magnitude larger for sand-bed streams than for gravel-bed streams.

An interesting observation is that sand-bed streams are in the transition between smooth and hydraulically rough conditions, while gravel-bed streams are always hydraulically rough. This has implications, for instance, for the use of Manning's relation (Eq. 2-23a) which applies only to fully rough and turbulent hydraulic conditions (Yen 2002).

The Shields-Parker diagram also shows a very clear distinction between the conditions observed in sand-bed and

gravel-bed rivers at bank-full stage, which has implications for movable-bed physical modeling. If one wanted to model in the laboratory sediment transport in rivers, the experimental conditions would be quite different depending on the river type in question. In order to satisfy similarity in a small-scale, river model, it would be necessary to satisfy the identities (García 2000)

$$\tau^*|_{model} = \tau^*|_{prototype} \quad (2-79a)$$

$$R_{ep}|_{model} = R_{ep}|_{prototype} \quad (2-79b)$$

for bank-full flow conditions. In most movable-bed models, Froude similarity is enforced and Eq. (2-79a) is used to achieve sediment transport similarity. However, sediment transport conditions and the associated bed morphology in a model, seldom precisely reproduce prototype conditions because the second condition given by Eq. (2-79b) is rarely satisfied. This leads to the common practice of using lightweight material (Table 2-2) to reproduce prototype conditions in small-scale models (e.g., Shen 1990). However, this does not imply that the bedforms observed in the model will be the same as those in the prototype. The river sedimentation

diagram provides a tool to quickly determine potential scale effects in movable-bed model studies by simply plotting the values of  $(\tau^*; R_{ep})$  for model and prototype conditions in Fig. 2-29. As discussed in Henderson (1966, p. 504), the condition given by Eq. (2-79b) can be relaxed for sufficiently large values of  $R_{ep}$  (i.e. hydraulically rough flow) in both model and prototype. It is clear from Fig. 2-29, that this would be possible only for the case of gravel-bed streams. More information on movable-bed physical models can be found in Appendix C.

## 2.6 BED LOAD TRANSPORT

Since the publication of ASCE Manual 54 (Vanoni 1975), a significant amount of work has been done to understand the mechanics of bed load transport. Two schools of thought can be clearly identified and they bear the name of two giants in the field of sedimentation, Brigadier Ralph Alger Bagnold and Professor Hans Albert Einstein.

Bagnold (1956) defined the bed load transport as that in which the successive contacts of the particles with the bed are strictly limited by the effect of gravity, whereas the suspended load transport is defined as that in which the excess weight of the particles is supported by random successions of upward impulses imported by turbulent eddies. Einstein (1942, 1950), however, presented a somewhat different view of the phenomenon. Einstein defined bed load transport as the transport of sediment particles in a thin layer about two particle diameters thick just above the bed by sliding, rolling, and making jumps with a longitudinal distance of a few particle diameters. The bed load layer is considered to be a layer in which mixing due to turbulence is so small that it cannot directly influence the sediment particles, and therefore suspension of particles is impossible in the bed load layer. Further, Einstein assumed that the average distance traveled by any bed load particle (as a series of successive movements) is a constant distance of about 100 particle diameters, independent of the flow condition, transport rate, and bed composition. In Einstein's view, saltating particles belong to the suspension mode of transport, because the jump heights and lengths of saltating particles are greater than a few grain diameters. On the other hand, Bagnold (1956, 1973) regards saltation as the main mechanism responsible for bed load transport.

Most research works that provide a mechanistic description of bed load transport under uniform equilibrium conditions have fallen into one or the other school of thought. The centerpiece of the Einsteinian formulation is the specification of an entrainment rate of particles into bed load transport (pick-up function) as a function of boundary shear stress and other parameters. The work of Nakagawa and Tsujimoto (1980), van Rijn (1984a) and Tsujimoto (1991), for example, represent formulations of this type.

In the Bagnoldean formulation, however, a relation for the areal concentration of bedload particles as a function of boundary shear stress derives automatically from the imposition of a dynamic condition at the bed, according to which the fluid shear stress drops to the critical value for the onset of sediment motion. The physical implication is that moving grains will extract enough momentum from the fluid in the bed load layer, such that the fluid stress at the bed remains at the critical shear stress for motion. This dynamic condition is referred to as the Bagnold hypothesis or Bagnold constraint. The hypothesis was used by Owen (1964) to calculate sediment transport by saltation for the case of wind-blown sand. It is implicit in the bedload formulations of Ashida and Michie (1972) and Engelund and Fredsøe (1976) for nearly horizontal beds. Wiberg and Smith (1989), Sekine and Kikkawa (1992) and Niño and García (1994; 1998), for example, have used the hypothesis to derive models of bed load transport on nearly horizontal beds based on an explicit calculation of grain saltation. Sekine and Parker (1992) used the Bagnold hypothesis to develop a saltation model for bed load on a surface with a mild transverse slope, and Kovacs and Parker (1994) extended the analysis of Ashida and Michie (1972) to the case of arbitrarily sloping beds. Bridge and Bennett (1992) have employed the Bagnold hypothesis to study the bed-load transport of sediment mixtures.

Based on the most recently published formulations of bed load transport, then, it is possible to say that the field as a whole has tended away from the Einsteinian and toward the Bagnoldean formulation. This notwithstanding, doubts have been expressed from time to time concerning the Bagnold hypothesis. For example, the experimental work of Fernandez-Luque and van Beek (1976) does not support the Bagnold hypothesis. A re-analysis of the data and formulation presented in Niño et al. (1994) and Niño and García (1994) caused Niño and García (1998) to cast further doubts on the hypothesis. Kovacs and Parker (1994) were forced to modify the hypothesis in order to obtain a well-behaved theory of bed load transport on arbitrarily sloping beds. With the help of numerical experiments, McEwan et al. (1999) have found that only in the case of high sediment availability does the fluid shear stress at the bed equal the critical stress for initiation of motion. Seminara et al. (2002) and Parker et al. (2003) have shown that Bagnold's hypothesis breaks down when applied to equilibrium bedload transport on beds with transverse slopes above a relatively modest value that is well below the angle of repose. All of the above suggests that formulae that make use of Bagnold's hypothesis might only be able to predict bed load transport for certain conditions (Niño and García 1998). This notwithstanding the ideas of Bagnold have nevertheless contributed substantially to the understanding the physics of the sediment transport problem. A collection of hallmark papers by R.A. Bagnold has been published by ASCE (Thorne et al 1988).

### 2.6.1 Bed Load Transport Analysis

Sediment can be transported in several ways. A grain will begin to move when the boundary shear stress just exceeds a critical value. At the lowest transport stages, particles move by sliding and rolling over the surface of the bed, but with a small increase in boundary shear stress these grains will hop up from the bed and follow ballistic-type trajectories. This latter mode of bed load transport is known as saltation. Gilbert (1914) seems to have been the first to use the term saltation, derived from the Latin verb *saltare*, which means to leap or dance, to describe the motion of sand particles in water.

Saltation is described as the unsuspended transport of particles over a granular bed by a fluid flow, in the form of consecutive hops within the near-bed region. It is governed mainly by the action of hydrodynamic forces that carry the particles through the flow, the downward pull of gravity and the collision of the particles with the bed, which transfers their streamwise momentum into upward momentum, thus sustaining the saltation motion (Niño and García 1998). This differs from an earlier definition given by Bagnold (1973) who assumed that the only upward impulses exerted on the saltating particles were those resulting from the impact of particles with the bed. Thus, Bagnold neglected the effect of hydrodynamic lift and vertical impulses owing to flow turbulence, which have been shown to play an essential role in the saltation phenomenon (e.g. Leeder 1979a; Bridge and Dominic 1984; Bridge and Bennett 1992; Niño et al., 1994; Niño and García 1994). Experimental studies on saltation of gravel and sand by Niño et al. (1994) and Niño and García (1998b) have given detailed information on the physics of particle saltation. In particular, they have provided a description of the particle collision with the bed, allowing calibration of a stochastic model for this phenomenon, and have also provided statistics for the geometric and kinematic properties of the saltation trajectories.

In addition to its significance for the flux of sediment moving as bed load, the bed load layer serves as an exchange zone between the bed and sediment transported in suspension; the upward flux of sediment at the top of the bed load layer provides the boundary condition for suspended sediment transport calculations. Once sediment starts moving and sliding along the bed, the prevalent mode for bed load transport will most likely be saltation for a range of bed shear stresses. At higher values of boundary shear stress, the surface layer of the bed may deform and move as a grain flow or granular fluid flow (Wilson 1987, 1989). Grain flow is also known as sheet flow (Fredsøe and Deigaard 1992; Sumer et al 1996). Collision of the moving particles with the bed exerts both a tangential and a normal stress on the bed surface. The work of Bagnold (1954), Hanes and Inman (1985), and Jenkins and Hanes (1998) on high-concentration, granular shear flows have shown that if the ratio of the applied tangential to normal shear stresses exceeds the critical yield criterion, the frictional resistance of the bed

will be overcome, and a grain flow will be initiated in the surface layer of the bed (Fredsøe and Deigaard 1992). So it is important to be able to discriminate between different modes of sediment transport so that the domain of applicability of bed load transport models can be determined (Sumer et al 1996).

In an attempt to interpret different transport modes following initiation of motion, Wiberg (1987) used a mechanistic model of bed load transport (Wiberg and Smith 1985) to produce a diagram (Fig. 2-30) of transport stage ( $T_* = \tau_b / \tau_{bc}$ ) or bed shear stress ( $\tau_b$ ) versus quartz grain diameter ( $D$ ), depicting the range of conditions over which sediment moves strictly as bed load and a saltation-based model can be used to describe the phenomenon. Conditions for the initiation of motion, the transition to suspension and the transition to grain flow, are also included.

As shown in Fig. 2-30(a), at transport stages  $T_* < 1$  no sediment moves in a uniform bed of a given grain size. For grain sizes  $D < 0.08$  cm (coarse sand and finer), the conditions for incipient motion occur at transport stages lower than those at which the applied stresses at the bed are sufficient to overcome the bed's frictional resistance. For sizes  $D > 0.08$  cm, this situation is reversed, and the conditions for potential grain flow (sheet flow) at the bed surface are reached before the particles are significantly affected by the vertical turbulent velocity fluctuations that could entrain the grains into suspension (Niño and García 1996). Wiberg (1987, p. 94) indicates that the advent of either of these processes does not preclude the possibility of the other, but changes in the bed load dynamics produced by these processes are certain to influence the transport stage at which the other could occur. This is supported by the observations made by Wilson (2005), which show that when the ratio between the shear velocity ( $u_*$ ) and the sediment fall velocity ( $v_s$ ) increases over a critical value ( $u_* / v_s > 6.5$ ), a rapid increase in both flow resistance and sediment entrainment into suspension is observed.

For all sediment sizes, Fig. 2-30(a) suggests that a transport stage of about 20 is an upper limit for saltation-based bed load transport. A saltation model might still provide reasonable transport predictions for incipient grain-flow conditions beyond this limit, but the physics of the phenomenon becomes more complicated as grain-grain interaction becomes more intense (e.g., Kobayashi and Seung 1985).

Fig. 2-30(b) presents the same results as shown in Fig. 2-30(a), but in terms of dimensional boundary shear stress,  $\tau_b$  (dy/cm<sup>2</sup>), to give a better sense of when the transition to these transport modes are actually likely to occur. For sediment sizes  $D < 0.018$  cm (fine sand and finer) at initial motion, the moving particles go directly into suspension following initiation of motion. The corresponding critical shear stress  $\tau_b < 2$  dy/cm<sup>2</sup>, is quite low, and material of these sizes is frequently mobilized, provided cohesive effects are not large (see Chapter 4). Fine to coarse sand ( $D = 0.018\text{--}0.08$  cm) moves initially as bed load, with particles starting to go into suspension at higher shear stresses. For example, medium

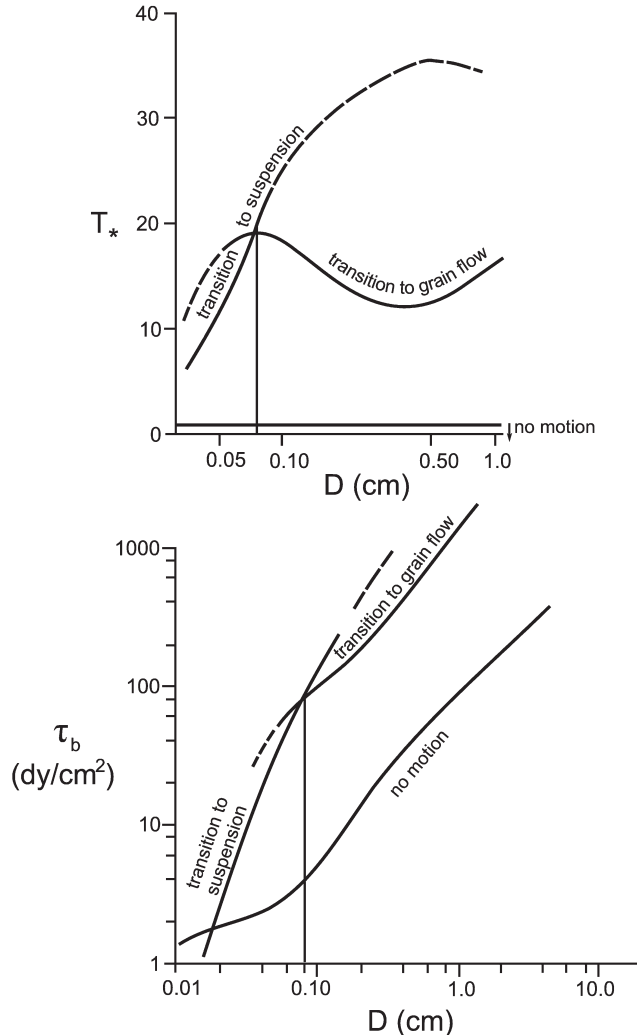


**Fig. 2-30.** Tentative ranges of conditions over which sediment moves strictly as bed load. (a) Initiation of motion, the transition to suspension and the transition to grain flow plotted in terms of transport stage versus grain size. (b) The same curves plotted in terms of dimensional boundary shear stress (in dy/cm<sup>2</sup>), versus gran size. The vertical line marks the particle size at the intersection of the incipient suspension and incipient grain flow curves,  $D \cong 0.08$  cm (adapted from Wiberg 1987).

sand begins to move at  $\tau_b = 2$  to  $3$  dy/cm<sup>2</sup> and incipient suspension begins at  $\tau_b = 10$  to  $30$  dy/cm<sup>2</sup>. Shear stresses of such magnitude can be reached during moderate river flows and during storms on continental shelves.

In very energetic environments, such as the surf zone in coastal areas or during large river floods, it may also be possible for a grain flow (sheet flow) to develop (Wilson 1987, 1989; Sumer et al 1996). For coarse sand and gravel ( $D = 0.08$ – $6$  cm), a relatively large boundary shear stress is required just to initiate the motion of the sediment. For example, for  $D = 0.5$  cm (fine gravel), the critical shear stress is  $\tau_{bc} = 45$  dy/cm<sup>2</sup>) and a grain flow is possible at a shear stress  $\tau_b > 550$  dy/cm<sup>2</sup>; these conditions are only likely to occur in very

large sand-bed rivers or in high-gradient mountain streams. Thus for the grain sizes commonly encountered, suspended-load transport is an important mode of transport for fine sediment, whereas high-concentration grain flows are probably relatively uncommon except in a few specific environments. For a large range of sediment sizes in the medium to coarse sand range and above, if the sediment is moving at all, it is certainly moving as bed load.

### 2.6.2 Bed Load Transport Definition

Bed load particles roll, slide, or saltate along the bed. The transport thus is tangential to the bed. When all of the transport is directed in the streamwise, or  $s$  direction, the volume bed load transport rate per unit width ( $n$ -direction) is given by  $q_b$ ; the units are length<sup>3</sup>/length/time, or length<sup>2</sup>/time. In general,  $q_b$  is a function of boundary shear stress  $\tau_b$  and other sediment parameters; that is,

$$q_b = q_b(\tau_b, \text{other parameters}) \quad (2-80)$$

In general, bed load transport is vectorial, with components  $q_{bs}$  and  $q_{bn}$  in the  $s$  (streamwise) and  $n$  (lateral) directions, respectively. Basically the bed load transport rate can be defined as the product of particle concentration, particle velocity, and bed load layer thickness,

$$q_b = u_b c_b \delta_b \quad (2-81)$$

in which  $q_b$  is the volumetric bed load transport rate (m<sup>2</sup>/s),  $c_b$  is the volumetric sediment concentration (i.e. volume of sediment/volume of water-sediment mixture),  $u_b$  is particle velocity (m/s), and  $\delta_b$  is the thickness of the bed load layer (m). Bagnoldian bed load transport models use this definition of the bedload transport rate (Ashida and Michiue 1972; Engelund and Fredsøe 1976; Van Rijn 1984a; Wiberg and Smith 1987; Sekine and Kikkawa 1992; Niño and García 1994; Lee and Hsu 1994; Niño and García 1998; Lee et al., 2000).

The bed load transport rate can also be defined as the product of the number of moving particles per unit area, the particle volume and the particle velocity (García 2000),

$$q_b = N_b V_b u_b \quad (2-82)$$

in which  $N_b$  is the number of particles per unit bed area (m<sup>-2</sup>),  $V_b$  is the particle volume (m<sup>3</sup>), and  $u_b$  is the particle velocity (m/s). If the particle velocity is defined as the ratio of the saltation or step length  $\lambda$  and the saltation or movement period  $T$  (i.e.  $u_b = \lambda / T$ ), then

$$q_b = N_b V_b \lambda / T = E_p \lambda = D_p \lambda \quad (2-83)$$

Here,  $E_p$  and  $D_p$  = eroded and deposited volume of particles per unit bed area per unit time (m/s), respectively. Equilibrium bed load transport conditions imply that  $E_p = D_p$ .

The idea of a pick-up rate and a step length was first proposed by Einstein (1942; 1950) and constitutes the basis of Einsteinian bedload transport models (Nakagawa and Tsujimoto, 1980; Tsujimoto, 1992). A comparison of several pick-up rate functions and their applications can be found in Van Rijn (1984b; 1986). Einstein defined the particle step length as the particle travel distance from entrainment to deposition (i.e., when the particle stops moving and comes to rest) and estimated it to be equal to about 100 times the particle diameter. Einstein's particle length can be expected to be several times the saltation length  $\lambda$  previously defined. This assumption will be considered below in light of the experimental observations made by Wong and Parker (2006a).

### 2.6.3 Conservation of Sediment Mass: The Exner Equation and Morphodynamics

Before considering bed load transport relations in more detail, it is useful to formulate the interaction between bed sediment and the water column through erosion and deposition, so that the sediment mass conservation can be formulated. Consider the definition diagram for a sediment-laden, uniform, open-channel flow shown in Fig. 2-31. The volume rate of erosion of bed material into suspension per unit time per unit bed area is denoted as  $E_r$ . The units of  $E_r$  are length<sup>3</sup>/length<sup>2</sup>/time, or velocity. A dimensionless sediment entrainment rate  $E_s$  can thus be defined in terms of the sediment fall velocity  $v_s$ :

$$E_r = v_s E_s \quad (2-84)$$

In general,  $E_s$  can be expected to be a function of boundary shear stress  $\tau_b$  and sediment related parameters (García

and Parker 1991; Niño et al. 2003). Erosion into suspension can be taken to be directed upward normal, i.e., in the positive  $z$  direction.

Let  $\bar{u}$  denote the mean flow velocity (m/s) at a point located at a distance  $z$  normal to the bed, and  $\bar{c}$  denote the mean volumetric concentration of suspended sediment (m<sup>3</sup> of sediment/m<sup>3</sup> of sediment-water mixture), averaged over turbulence. The streamwise volume transport rate of suspended sediment per unit width is given by

$$q_s = \int_0^H \bar{u} \bar{c} dz \quad (2-85)$$

Let  $s$  denote the streamwise direction and  $n$  denote the lateral direction in a two-dimensional case; then two components,  $q_{Ss}$  and  $q_{Sn}$  result, where

$$q_{Ss} = \int_0^H \bar{u} \bar{c} dz \quad (2-86a)$$

$$q_{Sn} = \int_0^H \bar{v} \bar{c} dz \quad (2-86b)$$

where  $\bar{v}$  is the mean lateral ( $n$ -direction) velocity at a distance  $z$  above the bed.

Deposition onto the bed is by means of settling. The rate at which material is fluxed vertically downward onto the bed (volume/area/time) is given by  $v_s \bar{c}_b$ , where  $\bar{c}_b$  is a near-bed value of the volumetric sediment concentration  $\bar{c}$ . Some authors assume that the value of the near-bed concentration is the same as the sediment concentration in the bed load layer defined previously (Einstein 1950; Engelund and Fredsøe 1976; Zyberman and Fredsøe 1994). The deposition rate  $D_r$  realized at the bed is obtained by computing the component of this flux that is actually directed normal to the bed as

$$D_r = v_s \bar{c}_b \quad (2-87)$$

which gives the volume of sediment deposited per unit bed area per unit time (García 2001).

Now it is possible to formulate the sediment mass conservation for bed material taking into account both bed load transport and sediment erosion into and from suspension. Consider a portion of river bottom (Fig. 2-32), where the bed material is taken to have a constant porosity  $\lambda_p$ . Mass balance of sediment requires that the following equation be satisfied:

$$\frac{\partial}{\partial t} [\text{mass of bed material}] = \text{net mass bedload inflow rate} + \text{net mass rate of deposition from suspension}$$

A datum of constant elevation is located well below the bed level, and the elevation of the bed with respect to

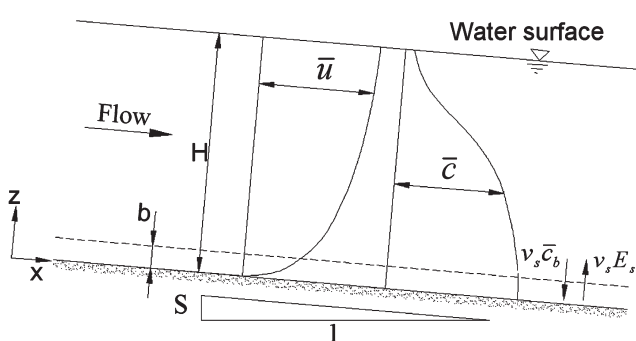
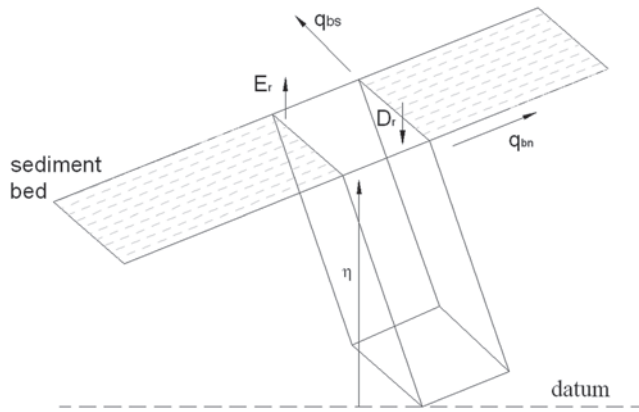


Fig. 2-31. Definition diagram for sediment-laden open channel flow.



**Fig. 2-32.** Definition diagram for sediment mass conservation.

the datum is given by  $\eta$ . The mass balance equation translates to

$$\rho_s (1 - \lambda_p) \frac{\partial}{\partial t} (\eta ds dn) = \rho_s (q_{bs}|_s - q_{bs}|_{s+ds}) dn + \rho_s (q_{bn}|_n - q_{bn}|_{n+dn}) ds + \rho_s (D_r - E_r) ds dn \quad (2-88a)$$

Or upon reduction with Eqs. (2-84) and (2-87), Eq. (2-88a) takes the final form

$$(1 - \lambda_p) \frac{\partial \eta}{\partial t} = - \frac{\partial q_{bs}}{\partial s} - \frac{\partial q_{bn}}{\partial n} + v_s (\bar{c}_b - E_s) \quad (2-88b)$$

Bed level changes with time  $t$  due to bed load transport, sediment entrainment into suspension, and sediment deposition onto the bed can be predicted with this partial differential equation. To solve this equation, it is necessary to have relations to compute bed load transport (i.e.,  $q_{bs}$  and  $q_{bn}$ ), near-bed suspended sediment concentration  $\bar{c}_b$ , and sediment entrainment into suspension  $E_s$  (García and Parker 1991; García 2001). The basic form of Eq. (2-88b), without the suspended sediment component, was first proposed for the case of a one-dimensional flow interacting with a sediment-covered bed by Felix Exner (1925).

Felix Maria Exner was an Austrian researcher who was active in the early part of the 20th Century. His main area of interest was meteorology. At some point he became interested in the formation of dunes in rivers (see Leliavsky 1966). In the course of his research on the subject, he derived and employed one version of the various statements of conservation of bed sediment that are now referred to as “Exner equations.” In addition, he made an important early contribution to one-dimensional nonlinear wave dynamics (Exner 1920). Felix Exner was the first researcher to state a morphodynamic problem in quantitative terms. The term “morphodynamics”

itself evolved many decades afterward and is now used for river, coastal, and estuarine problems (e.g., Parker and García 2006). This notwithstanding, Exner deserves recognition as the founder of morphodynamics (Parker 2005).

The field of morphodynamics consists of the class of problems for which the flow over a bed interacts strongly with the shape of the bed, both of which evolve in time. An introduction to morphodynamics of rivers and turbidity currents is given in Section 2.11 of this chapter. The Exner equation is generalized to the case of sediment mixtures in Chapter 3.

#### 2.6.4 Bed Load Transport Relations

A large number of bed load relations can be expressed in the general dimensionless form

$$q^* = q^* (\tau^*, R_{ep}, R) \quad (2-89)$$

Here,  $q^*$  is a dimensionless bed load transport rate known as the Einstein bed load number, first introduced by Hans Albert Einstein in 1950, and given by

$$q^* = \frac{q_b}{D \sqrt{gRD}} \quad (2-90a)$$

where  $q_b$  is the volumetric bedload transport rate,  $g$  is the acceleration of gravity,  $R = (\rho_s - \rho) / \rho$  is the submerged specific gravity of the sediment,  $D$  is the particle diameter, and  $R_{ep} = \sqrt{gRDD}/v$  is the particle Reynolds number. Einstein's bed load transport model can be expressed in dimensionless form as follows,

$$q^* = E_p^* L_s^* \quad (2-90b)$$

with

$$E_b^* = \frac{E_b}{\sqrt{gRD}} \quad (2-90c)$$

and

$$L_s^* = \frac{L_s}{D} \quad (2-90d)$$

In these relations  $E_b$  = volumetric rate of sediment entrainment per unit area; and  $L_s$  = particle step length (i.e., the particle travel distance from entrainment to deposition).

In a study of sand bed instability, Nakagawa and Tsujimoto (1980) found that the dimensionless entrainment rate  $E_b^*$  is a function of the Shields parameter  $\tau^*$  and tried to develop a probabilistic model for the dimensionless particle

step length  $L_s^*$  but did not find a simple way to characterize this parameter (Tsujimoto and Nakagawa 1983). Sechet and Le Guennec (1999) found experimentally that the particle step length is related to the bursting phenomenon (i.e., ejections and sweeps) which is in agreement with observations of near-wall particle-turbulence interactions made earlier by Sumer and Deigaard (1981), García et al. (1996), and Niño and García (1996). This might explain some of the difficulties encountered in trying to characterize Einstein's step length. Recently, Sumer et al (2003) were able to observe directly the influence of turbulence on bed load transport of sand ( $D_{50} = 0.22$  mm) with a set of carefully conducted lab experiments. The Shields parameter together with the root-mean-square value (RMS) of the streamwise velocity fluctuations, were correlated with the sediment transport rate. They found that the sediment transport rate increases markedly with increasing turbulence levels. A few years earlier, Drake et al (1988) observed a similar influence of the flow turbulence while observing bed load transport of fine gravel with motion-picture photography.

Recently, Wong and Parker (2006a) conducted a tracer study involving transport of uniform-size gravel in a large flume at St. Anthony Falls Laboratory, University of Minnesota. The sediment used in all the experiments was uniform gravel, with geometric mean size  $D_g = 7.2$  mm, geometric standard deviation  $\sigma_g = 1.2$ , median particle size  $D_{50} = 7.1$  mm, particle size for which 90% of the sediment is finer  $D_{90} = 9.6$  mm, and a specific gravity of 2.55 ( $R = 1.55$ ). Based on these observations they found empirical equations for the dimensionless entrainment rate  $E_b^*$  and particle step length  $L_s^*$  as functions of the Shields parameter  $\tau^*$ , as follows,

$$E_b^* = 0.06(\tau^* - 0.0549)^{1.97} \quad (2-90e)$$

and

$$L_s^* = 44.33(\tau^* - 0.0549)^{-0.47} \quad (2-90f)$$

Equation (2-90e) predicts values very close to those observed by Fernandez Luque and van Beek (1976). On the other hand, Eq. (2-90f) contradicts the original ideas of Einstein (1950) who did not include a critical shear stress for motion and assumed that the dimensionless step length  $L_s^* = 100$  for all flow conditions. Also of interest is the fact that the step length is found to decrease as the flow intensity characterized by  $\tau^*$ , increases.  $L_s^*$  takes values between 160 and 270 for the range of experimental conditions covered in the experiments. Wong and Parker (2006a) argued that since the chances of a given particle being captured and trapped into a resting position increases with sediment transport rate, it is reasonable to assume that the step length becomes smaller

when the excess dimensionless shear stress gets larger, as indicated by Eq. (2-90f). Substituting (2-90e) and (2-90f) into (2-90b), yields

$$q^* = 2.66(\tau^* - 0.0549)^{3/2} \quad (2-90g)$$

This empirical fit has a structure which is very similar to several formulations presented below.

Bagnold's approach is considered next. A dimensionless bed load transport equation, such as the one implied by Eq. (2-89), can be obtained by simply dividing both sides of Eq. (2-81) by a characteristic length given by the particle diameter  $D$  and a characteristic velocity given by  $\sqrt{gRD}$ , which yields

$$q^* = \frac{q_b}{D\sqrt{gRD}} = \frac{c_b\delta_b}{D} \frac{u_b}{\sqrt{gRD}} \quad (2-91)$$

Bagnold's (1956) hypothesis makes it possible to estimate the volumetric sediment concentration in the bedload layer per unit bed area, given by the product of sediment concentration  $c_b$  and the thickness of the bed load layer  $\delta_b$ , as follows

$$\frac{c_b\delta_b}{D} = \frac{\tau^* - \tau_c^*}{\mu_d} \quad (2-92)$$

where  $\mu_d$  is a dimensionless dynamic friction coefficient (Abott and Francis 1977; Sekine and Kikkawa 1992). Niño and García (1998) have used a Lagrangian particle-saltation model to estimate values of  $\mu_d$  and found that it takes values in the range between 0.25 and 0.4, which are smaller than  $\mu_d = \tan\phi = 0.63$  proposed by Bagnold (1973) but are in good agreement with laboratory observations of sand transport (Niño and García 1998c). Simulated values of  $\mu_d$  for the case of sand saltation are much closer to the corresponding observed values than in the case of saltation of gravel (Niño and García 1994). Bagnold's hypothesis used to obtain to Eq. (2-92) would be only valid for intense transport conditions involving very high sediment concentrations of sand-size material. The mean velocity of the particles in the bedload layer  $u_b$  can also be estimated with the help of numerical modeling and experimental observations of particle motion (Reizes 1978; Leeder 1979; Murphy and Hooshiari 1982; Bridge and Dominic 1984; van Rijn 1984a; Wiberg and Smith 1985, 1989; Sekine and Kikkawa 1992; Lee and Hsu, 1994; Niño and García 1994, 1998b, 1998c; Lee et al. 2000, 2006; Lukerchenko et al. 2006).

Ashida and Michiue (1972) presented a macroscopic analysis that does not account for the complexity of the saltation process, in particular the treatment of the particle collision

with the bed. In their analysis, a simplified particle equation of motion is used to obtain the following expression for the dimensionless mean particle velocity in the bedload layer:

$$\frac{u_b}{\sqrt{gRD}} = 8.5 \left[ (\tau^*)^{1/2} - (\tau_c^*)^{1/2} \right] \quad (2-93)$$

Upon substitution of Eqs. (2-92) and (2-93) into (2-91) and assuming a value for  $\mu_d$  of 0.5, the following final form for bed load transport is obtained

$$q^* = 17(\tau^* - \tau_c^*) \left[ (\tau^*)^{1/2} - (\tau_c^*)^{1/2} \right] \quad (2-94)$$

Ashida and Michiue recommend a value for  $\tau_c^*$  of 0.05 in their relation. It has been verified with uniform material ranging in size from 0.3 mm to 7 mm. The Ashida-Michiue bed load transport equation is a good example of a Bagnoldian formulation. It is very similar to the one developed independently by Engelund and Fredsøe (1976) and more recently by Niño and García (1998) using a Lagrangian particle-saltation model for bed load transport.

In addition to the relation of Ashida and Michiue (1972), the following bed load transport relations are of interest.

#### Meyer-Peter and Muller (1948):

$$q^* = 8(\tau^* - \tau_c^*)^{3/2} \quad (2-95a)$$

where  $\tau_c^* = 0.047$ . This formula is empirical in nature; it has been verified with data for uniform coarse sand and gravel. Even though it was developed for alpine streams in Switzerland, it enjoys wide use in coastal sediment transport (e.g. Soulsby, 1997). Recently, Wong and Parker (2006b) reanalysed the data used by Meyer-Peter and Muller and found that a better fit is provided by one of the two alternative forms;

$$q^* = 4.93(\tau^* - 0.047)^{1.6} \quad (2-95b)$$

$$q^* = 3.97(\tau^* - 0.0495)^{3/2} \quad (2-95c)$$

#### Einstein (1950):

$$q^* = q^*(\tau^*) \quad (2-96a)$$

where the functionality is implicitly defined by the relation

$$1 - \frac{1}{\sqrt{\pi}} \int_{-(0.413/\tau^*)-2}^{(0.413/\tau^*)-2} e^{-t^2} dt = \frac{43.5 q^*}{1+43.5 q^*} \quad (2-96b)$$

This relation constitutes the first attempt to derive a bed load function. Note that this relation contains no critical shear stress. It has been used for uniform sand and gravel. Gomez and Church (1989) recommend its use for cases where the local bed load transport rate needs to be calculated. Yang and Wan (1991) found that it could predict sediment transport rates in large rivers but not in small rivers and flumes.

#### Yalin (1963):

$$q^* = 0.635s(\tau^*)^{1/2} \left[ 1 - \frac{\ln(1+a_2s)}{a_2s} \right] \quad (2-97a)$$

where

$$a_2 = 2.45(R+1)^{0.4} \left( \tau_c^* \right)^{1/2} s = \frac{\tau^* - \tau_c^*}{\tau_c^*} \quad (2-97b)$$

and  $\tau_c^*$  is evaluated from the Shields curve. Two constants in this formula have been evaluated with the aid of data quoted by Einstein (1950), pertaining to 0.8 mm and 28.6 mm material. Wiberg and Smith (1985, 1989) were able to reproduce Yalin's relation, with their saltation-based bed load transport model.

#### Wilson (1966):

$$q^* = 12(\tau^* - \tau_c^*)^{3/2} \quad (2-98)$$

where  $\tau_c^*$  is determined from the Shields diagram. This relation is empirical in nature; most of the data used to fit it pertain to very high rates of bed load transport. It has been used extensively to estimate transport of sand and industrial materials such as nylon in pressurized flows (e.g., Wilson 1987).

#### Paintal (1971):

$$q^* = 6.56 \times 10^{18} \tau^{*16} \quad (2-99)$$

was obtained through extensive measurements of very low bed load transport rates. It is valid for  $0.007 < \tau^* < 0.06$  and sediment grain sizes between 1 mm (coarse sand) and 25 mm (gravel). This relation shows that for low shear stresses, the

sediment transport phenomenon is highly nonlinear. That is, for small changes in bed shear stress, the rate of bed load transport increases dramatically.

**Engelund and Fredsøe (1976):**

$$q^* = 18.74(\tau^* - \tau_c^*) \left[ (\tau^*)^{1/2} - 0.7(\tau_c^*)^{1/2} \right] \quad (2-100a)$$

where  $\tau_c^* = 0.05$ .

This formula resembles that of Ashida and Michiue because its derivation, albeit obtained independently, is almost identical. This relation was rederived by Fredsøe and Deigaard (1992, p. 214), resulting in a very similar relation,

$$q^* = \frac{30}{\pi \mu_d} (\tau^* - \tau_c^*) \left[ (\tau^*)^{1/2} - 0.7(\tau_c^*)^{1/2} \right] \quad (2-100b)$$

Fredsøe and Deigaard tested the formula for different values of the dynamic friction coefficient  $\mu_d$ . For  $\mu_d = 1.0$ , Eq. (2-96b) gives results very close to those of the Meyer-Peter and Muller formula (Eq. 2-95a). However, both formulations were found to overpredict bed load transport at high shear stresses.

**Fernandez-Luque and van Beek (1976):**

$$q^* = 5.7(\tau^* - \tau_c^*)^{3/2} \quad (2-101)$$

where  $\tau_c^*$  varies from 0.05 for 0.9-mm material to 0.058 for 3.3-mm material. The relation is empirical in nature and was obtained through laboratory observations.

**Parker (1979):**

$$q^* = 11.2 \frac{(\tau^* - 0.03)^{4.5}}{\tau^{*3}} \quad (2-102)$$

developed as a simplified fit to the relation of Einstein (1950) for the range of Shields numbers likely to be encountered in gravel-bed streams. This formula was used to analyze the hydraulic geometry of gravel-bed streams (Parker 1979).

**Van Rijn (1984a):**

$$q^* = 0.053 \frac{T^{2.1}}{D_*^{0.3}} \quad (2-103a)$$

can be used to estimate bed load transport rates of particles with mean sizes in the range between 0.2 and 2.0 mm. This

equation is based on a dimensionless particle diameter and the transport stage parameter  $T$ , defined, respectively, as

$$D_* = D_{50} \left( \frac{gR}{v^2} \right)^{1/3} = R_{ep}^{2/3} \quad (2-103b)$$

and

$$T = \frac{\tau_s^* - \tau_c^*}{\tau_c^*} \quad (2-103c)$$

Here  $\tau_s^*$  is the bed shear stress due to skin or grain friction, and  $\tau_c^*$  is the critical shear stress for motion from the Shields diagram.

**Madsen (1991):**

$$q^* = F_M (\tau^{*1/2} - 0.7\tau_c^{*1/2})(\tau^* - \tau_c^*) \quad (2-104a)$$

where  $F_M = 8 / \tan \phi$  for rolling/sliding sand grains and  $F_M = 9.5$  for saltating sand grains in water.

**Nielsen (1992):**

$$q^* = 12\tau^{*1/2}(\tau^* - \tau_c^*) \quad (2-104b)$$

obtained by fitting to uniform size sand and gravel bed load transport data. This relation was also independently derived by Soulsby (1997). Equations (2-104a) and (2-104b) have been used mainly in coastal engineering.

**Niño and García (1998b):**

$$q^* = \frac{12}{\mu_d} (\tau_* - \tau_{*c}) (\tau_*^{1/2} - 0.7\tau_{*c}^{1/2}) \quad (2-104c)$$

obtained with a Lagrangian description of bed load transport by saltating particles and tested with experimental observations of gravel transport (Niño and García 1994) and sand transport (Niño and García 1998c). A dynamic friction coefficient  $\mu_d = 0.23$  was determined, almost three times smaller than the value proposed for the same coefficient by Bagnold (1973). This relation basically has the same structure as Madsen's Eq. (2-104a).

**Cheng (2002):**

$$q^* = 13 \tau^{*3/2} \exp \left( -\frac{0.05}{\tau^{*3/2}} \right) \quad (2-104d)$$

This relation gives results similar to those obtained with Meyer-Peter and Muller (1948) and Einstein (1950) equation for moderate dimensionless shear  $\tau^*$  values. It also agrees

well with the values predicted with Paintal (1971) for weak transport conditions under low shear stresses.

For intense transport conditions associated with large values of the dimensionless Shields stress  $\tau^*$ , Eq. (2-104d) reduces to

$$q^* \equiv 13 \tau^{*3/2} \quad (2-104e)$$

In fact, most of the bed load transport equations display the same asymptotic behavior for high values of shear stress as can be observed in Fig. 2-33. That is, for  $\tau^* >> \tau_c^*$ ,  $q^* \approx \tau^{*3/2}$ . However, a word of caution is necessary because this does not seem to be the case according to the observations made by several investigators who have found a different relation for high transport rates. For instance, Rickenmann (1991) has indicated that for intense sediment transport conditions, when  $\tau^* > 0.4$ , grain flow (or sheet flow) conditions develop and  $q^*$  is actually proportional to  $\tau^{*5/2}$  as found by Hanes and Bowen (1985) with a granular fluid model for coastal sediment transport and Takahashi (1987) for debris flows on steep slopes. Hanes (1986) showed that under these conditions transport rates can be approximated with

$$q^* = 6 \tau^{*5/2} \quad (2-104f)$$

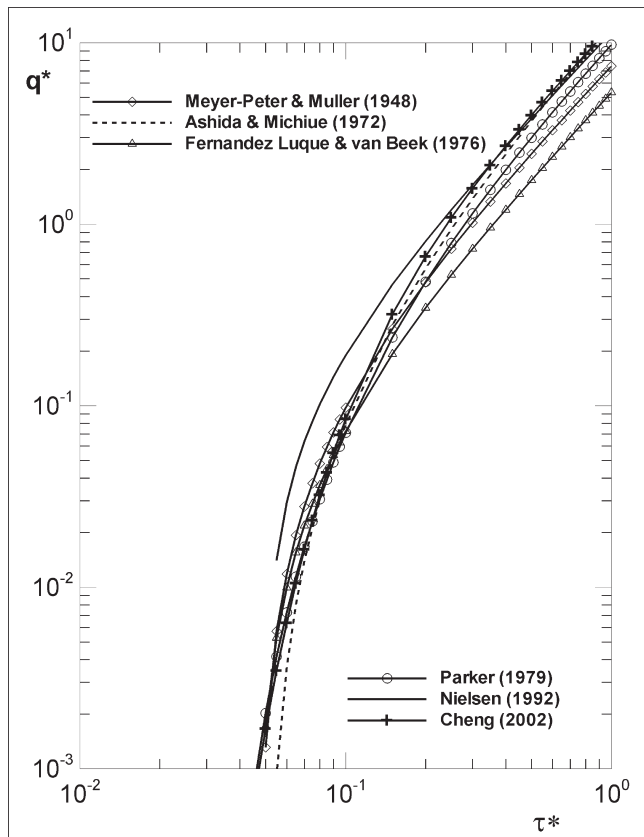


**Fig. 2-33.** Plot of several bed load functions found in the literature.

These findings indicate a stronger dependence of  $q^*$  on  $\tau^*$  at very high transport intensities than one might expect from bed load transport equations. In fact, Abrahams (2003) has recently revisited the concepts advanced by Bagnold (1973) and found that transport rates under sheet flow (grain flow) conditions are much higher than previously thought.

Most of the bed load equations shown above apply to the case of mild slopes or nearly horizontal flows. For steep channels, the effect of the downslope gravitational component cannot be neglected. Smart (1984), Bathurst et al. (1987), Graf and Suszka (1987), Tsujimoto (1989), Rickenmann (1991), Damgaard et al. (1997), and Aguirre-Pé and Fuentes (1995), among others, have proposed equations for bed load transport in steep slopes.

Only a few research groups have attempted complete derivations of the bed load function in water. They include Wiberg and Smith (1989); Sekine and Kikkawa (1992); Niño and García, (1994, 1998); Seminara et al (2002); and Parker et al (2003). These results are encouraging because they show that bed load transport can be predicted with a mechanics-based approach. More recently, discrete particle simulations of bed load transport which account for the effect of near-bed turbulence, particle location and particle-particle interaction, have been conducted, among others, by Jiang and Haff (1993), Drake and Calantoni (2001), Nelson et al. (2001) and Schmeeckle and Nelson (2003). Undoubtedly, the role played by turbulence in bed-load transport is still a subject that deserves more research (Nelson et al. 1995; García et al. 1996; Niño and García 1996; Best et al., 1997; Sechet and Le Guennec 1999; Schmeeckle et al., 2001; Papanicolaou et al. 2001; Sumer et al. 2003). It is also clear that direct field observations provide the best information for both developing and testing of new formulations (e.g., Almedej and Diplas 2003). Several bed-load transport relations for gravel and sediment mixtures are considered in Chapter 3.

## 2.6.5 Two-Dimensional Transport of Bed Load

The relations presented above for bed load transport are all one-dimensional in nature. That is, they provide the magnitude of a bed load transport vector that is oriented in the direction of the boundary shear stress. That is, if the  $s$  coordinate is directed along the bed parallel to the boundary shear stress and the  $n$  coordinate is directed along the bed and perpendicular to the  $s$  coordinate,

$$\vec{q} = (q_s, q_n) = (q, 0) \quad (2-105)$$

where  $\vec{q}$  denotes the two-dimensional vector of bed load transport rate and  $q$  denotes the magnitude of that vector, which is computed using one of the relations presented above.

In point of fact bed load transport is fundamentally two-dimensional in nature. This is illustrated in Fig. 2-34, which illustrates the bed at a river bend. In the diagram  $s$  is a boundary-embedded centerline streamwise component and  $n$  is a boundary-embedded transverse component. Because a bend generates secondary flow in addition to the downstream primary flow, the boundary shear stress vector  $\vec{\tau}_b$  is not parallel to the  $s$  direction, but is skewed somewhat inward. This drives a component of bed load transport in the negative  $n$  direction, i.e., inward (Brooks 1963). The bed itself slopes downward from inside to outside in the transverse direction with magnitude  $|\partial\eta / \partial n|$ . As a result, gravity pulls bed load particles down the slope, driving a component of bed load transport in the positive  $n$  direction. Depending on the magnitude of the forces involved, the bed load vector  $\vec{q}$  may have a positive or negative component in the transverse direction.

These competing transverse effects play an important role in determining the morphology of rivers in meander bends (Engelund 1974; Falcon and Kennedy 1983; Ikeda and Nishimura 1986; Bridge 1992). Secondary flow tends to drive erosion at the outside of a bend and deposition on the inside (Johanesson and Parker 1989a, 1989c). This creates a transverse component to the bed slope, which in turn acts to drive sediment down the slope from inside to outside. An equilibrium condition can be obtained in which secondary forces and gravity forces balance. The desire to understand bend morphodynamics has been one of the motivators in the development of two-dimensional bed load transport relations (van Bendegom 1947; Engelund, 1974; Ikeda and Parker (1989). Meandering channels are considered in more detail in Chapter 8.

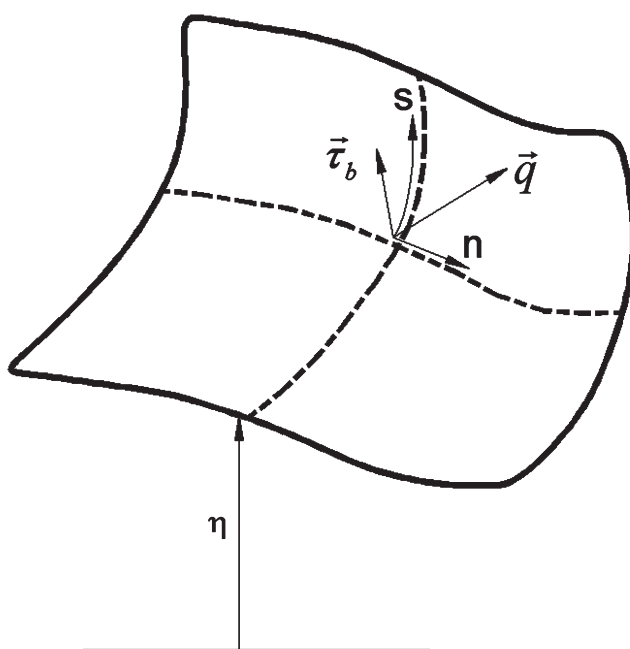


**Fig. 2-34.** Illustration of two-dimensional bed load transport in a river bend.

A second problem that has played a major role in the development of two-dimensional bed load relations is the quantification of the erosion of a river bank composed of noncohesive sediment. Banks in noncohesive material form side slopes; as bed load is moved downstream by the flow, gravity pulls it down the side slope, accomplishing bank erosion. Hirano (1973) was among the first to develop a quantitative formulation for this problem. Streambank erosion is addressed in Chapter 7.

Gravity can influence bed load transport in the downstream as well as transverse direction. In most cases of interest, however, gravity acts only indirectly to drive bed load transport. That is, gravity pulls the flow downslope, and the flow in turn drags the bed material downslope. If the streamwise slope of the bed is sufficiently high, however, the direct contribution of gravity acting on the bed load grains can increase the bed load transport rate (Fernandez-Luque and van Beek 1976).

The first generation of two-dimensional bed load relations was developed based on a linearized formulation for small transverse slope and streamwise bed slopes. These all take the general form

$$\vec{q} = |\vec{q}| \left[ \frac{\vec{\tau}_b}{|\vec{\tau}_b|} - \beta \left( \frac{\tau_{mag}^*}{\tau_c^*} \right)^{-n_0} \vec{\nabla} \eta \right] \quad (2-106a)$$

where the absolute values denote the magnitude of the vector in question,  $\beta$  and  $n_0$  are constants and

$$\vec{\tau}_b = (\tau_{bs}, \tau_{bn}) \quad (2-106b)$$

$$\tau_{mag}^* = \frac{|\vec{\tau}_b|}{\rho R g D} \quad (2-106c)$$

$$\vec{\nabla} \eta = \left( \frac{\partial \eta}{\partial s}, \frac{\partial \eta}{\partial n} \right) \quad (2-106d)$$

The derivations of these formulations are based on the following constraints, which allow linearizing an otherwise nonlinear formulation:

$$\frac{\tau_{bn}}{\tau_{bs}} \ll 1 \quad (2-107a)$$

$$\frac{\partial \eta}{\partial n} \ll 1 \quad (2-107b)$$

$$\frac{\partial \eta}{\partial s} \ll 1 \quad (2-107c)$$

If in turn the streamwise slope is  $\partial\eta/\partial s$  is so small that direct streamwise gravitational forces on bed load can be neglected, Eq. (2-106a) can be further cast in the approximate form

$$|\vec{q}| = q_s \quad (2-108a)$$

$$q_s = q_s \left[ \frac{\tau_{bn}}{\tau_{bs}} - \beta \left( \frac{\tau_s^*}{\tau_c^*} \right)^{-n_0} \right] \frac{\partial\eta}{\partial n} \quad (2-108b)$$

$$\tau_s^* = \frac{\tau_{bs}}{\rho R g D} \quad (2-108c)$$

Engelund (1974) proposed the following values of  $\beta$  and  $n_o$

$$\beta = \frac{1}{\mu_d}, \quad n_0 = 0 \quad (2-109a), (2-109b)$$

where  $\mu_d$  denotes a dimensionless coefficient of dynamic Coulomb friction for particles in bed load transport. Koch and Flokstra (1980) and Struiksma et al. (1985) proposed the form

$$\beta = \frac{1}{f_*}, \quad n_0 = 1 \quad (2-110a), (2-110b)$$

where  $f_*$  is a calibration coefficient between 1 and 2. Hasegawa (1989) proposed the form

$$\beta = \frac{1}{\sqrt{\mu_s \mu_d}}, \quad n_0 = \frac{1}{2} \quad (2-111a), (2-111b)$$

where  $\mu_s$  denotes a dimensionless coefficient of static Coulomb friction for bed particles. The Ikeda-Parker relation (Parker 1984, based on Ikeda 1982; see also Kikkawa et al., 1976) takes a very similar form (and in fact has a very similar derivation) to that of Hasegawa (1989),

$$\beta = \frac{1+r\mu_d}{\mu_d f_*}, \quad n_0 = \frac{1}{2} \quad (2-112a), (2-112b)$$

where  $r$  denotes the ratio of lift force to drag force on a particle in bed load motion and  $f_*$  is again a calibration coefficient. Johansson and Parker (1989b) obtained the following evaluations based on bend topography in rivers;

$$\mu_d = 0.43, \quad r = 0.85, \quad (2-112c), (2-112d), \\ f_* = 1.19 \quad (2-112e)$$

Sekine and Parker (1992) modeled the saltation trajectories of bed load grains over a bed sloping mildly in the transverse direction to obtain the evaluations

$$\beta = 0.75, \quad n_0 = \frac{1}{4} \quad (2-113a), (2-113b)$$

Olesen (1987) has suggested calibrating  $\beta$  and  $n_o$  to site-specific data.

In applying the above formulation the streamwise sediment transport  $q_s$  is evaluated using one of the one-dimensional formulations of the previous section and the transverse sediment transport is evaluated from Eq. (2-108b).

In recent years fully nonlinear formulations of two-dimensional bed load transport have become available. Kovacs and Parker (1994) used the underlying mechanics of the one-dimensional formulation of Ashida and Michiue (1972) for uniform material as a basis for a fully nonlinear generalization for arbitrary streamwise and transverse bed slopes. The analysis is involved and is beyond the scope of this chapter. It suffices to mention that (1) when applied to one-dimensional transport of bed load at low slopes it reduces to Eq. (2-66) of Ashida and Michiue (1972), and (2) when it is linearized to the form of Eq. (2-108b) the following evaluations are realized,

$$\beta = \frac{1}{\mu_d}, \quad n_0 = \frac{1}{2} \quad (2-114a), (2-114b)$$

with a value of  $\mu_d$  of 0.5. A treatment allowing the numerical implementation of the formulation can be found in Kovacs and Parker (1994).

The formulations of Ashida and Michiue (1972) and thus Kovacs and Parker (1994) employ forms of a criterion due to Bagnold (1956) that contains a conceptual error. Parker et al. (2003) have repeated the analysis using a bed load entrainment formulation due to Tsujimoto (e.g., 1991) (and ultimately due to Einstein 1950) that does not rely on the Bagnold criterion in question. Their two-dimensional bed load formulation is similarly involved; a source for software is referenced in their paper. When applied to one-dimensional transport of bed load at low slopes it reduces to a slightly modified form of Eq. (2-101) of Fernandez Luque and van Beek (1976), and when it is linearized to the form of Eq. (2-108b) the following evaluations are realized:

$$\beta = 0.7, \quad n_0 = \frac{1}{2} \quad (2-115a), (2-115b)$$

Despite very promising recent attempts (Kovacs and Parker 1994; Seminara et al. 2002; Dey 2003; Parker et al. 2003), prediction of bed load transport on arbitrarily sloping beds remains a challenge. This is mainly due to the fact that direct observations of transverse bed load transport are also very challenging (e.g., Talmon et al. 1995). To predict

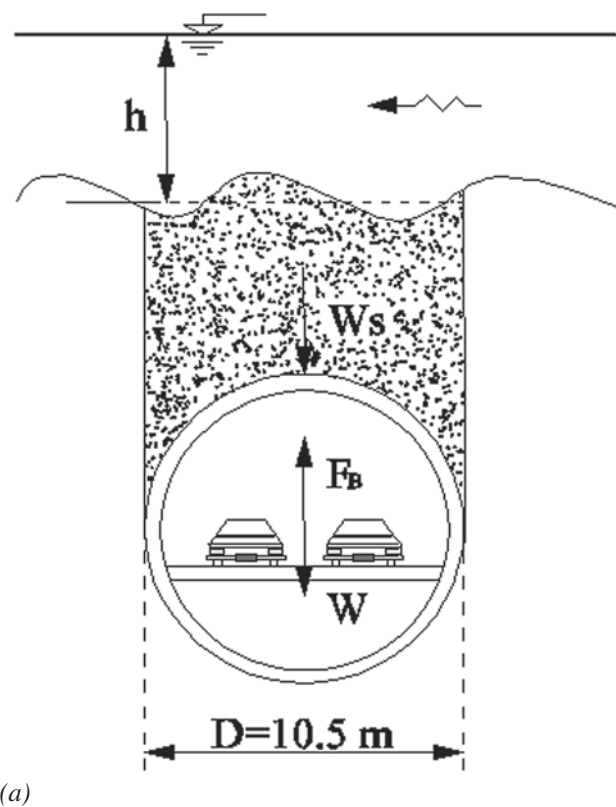
morphological changes in rivers, coastal areas, and estuaries, such technology is necessary and should be given priority in sediment transport research (Seminara and Blondeaux 2001; Parker and García 2006).

## 2.7 BED FORMS

Sediment waves produced by moving water are, in equal measure, intellectually intriguing and of great engineering importance. For example, seasonal water-temperature changes influence stage-discharge and depth-discharge relations in rivers (e.g., Missouri River) and in conveyance channels and navigation channels where water discharge is constant (Shen et al. 1978). The major influence is related to changes in bed configuration following changes in water temperature (Southard 1989). Large bed forms, such as megadunes, can make navigation difficult by increasing shoaling rates and endangering the stability of pipelines and tunnels (Kennedy and Odgaard 1991; Nemeth et al. 2002). The threat to infrastructure caused through sediment transport associated with dunes in the Rio Paraná, Argentina is highlighted by Amsler and García (1997), Amsler and Prendes (2000) and Amsler and Schreider (1999), who describe channel erosion near the city of Paraná as part of the disastrous floods of 1983 and 1992 (Best 2005). In one region of the river, where the Paraná narrows to ~1.5 km in width, a 2.4 km long subfluvial tunnel was built in 1968 and the depth of its placement was determined from a combination of regime theory and physical modeling, with a minimum sand cover thickness of 4 m above the tunnel (Amsler and García 1997). A cross section of the tunnel is shown in Fig. 2-35(a). However, the long duration of high floods in 1983 led to the formation of large dunes, up to 6.5 m in height and 320 m in length, that migrated through this river section (Fig. 2-35(b)). These large dunes caused temporary exposure of the tunnel to the flow over a distance of 250 m each time the trough of a large dune moved over the tunnel (Amsler and García 1997; Amsler and Schreider 1999), thus threatening its stability. Remedial actions were required to ensure the stability of the tunnel, involving placing trucks loaded with sand bags within the tunnel to prevent uplifting during most of the flood. This reach is now an area that is receiving much study and monitoring to assess the longer-term changes in bed elevation and the hysteresis effects of dune morphology through floods (e.g., Serra and Vionnet 2006). Shifting of the Paraná River thalweg makes the protection of both the tunnel itself and the river margin where one of the entrances to the tunnel is located (Santa Fe) even more challenging due to lateral migration experienced by the river (Ramonell et al. 2002).

Because of the important role they play in river sedimentation and their significance in ancient sedimentary structures, bed forms in general and dunes in particular have received extensive attention from engineers, sedimentologists and

geomorphologists (e.g., Ashley 1990; Southard 1991; Julien and Klaassen 1995, Julien et al. 2002, Bridge, 2003; Best 2005). Dunes are one of the most common depositional bed forms, forming in a range of sediment sizes from silt and sand to gravel (Dinehart 1992; Seminara 1995; Best 1996; Carling 1999; Kleinhans 2001, 2002). Recent studies of subsurface alluvium also demonstrate that dunes can form the majority of the deposits of sandy braided rivers (Best et al. 2003; Bridge 2003; Best 2005). The depositional patterns created by dunes can result in heterogeneous and anisotropic permeability fields in the subsurface, thus complicating prediction of subsurface flow in both aquifers and hydrocarbon reservoirs (Weber 1986). Shoaling rates and dredging times are largely controlled by the regeneration time of sand waves (Knaapen and Hulscher 2002), pointing to the practical significance of understanding the dynamics of bed forms. Experimental work has also shown the critical role of bed forms, and particularly dunes, in influencing convective flow within the bed sediment that is generated by the differential pressure gradient caused by the bed form (Thibodeaux and Boyle 1987). Packman and



(a)

**Fig. 2-35.** (a) Cross section of tunnel under Paraná River bottom that links Santa Fe and Paraná city, Argentina. The structure needs a sand cover about 4-m-thick on top of it to provide a safety weight  $W_s$  to counteract the net buoyancy force  $F_B - W$  (adapted from Serra and Vionnet 2006).

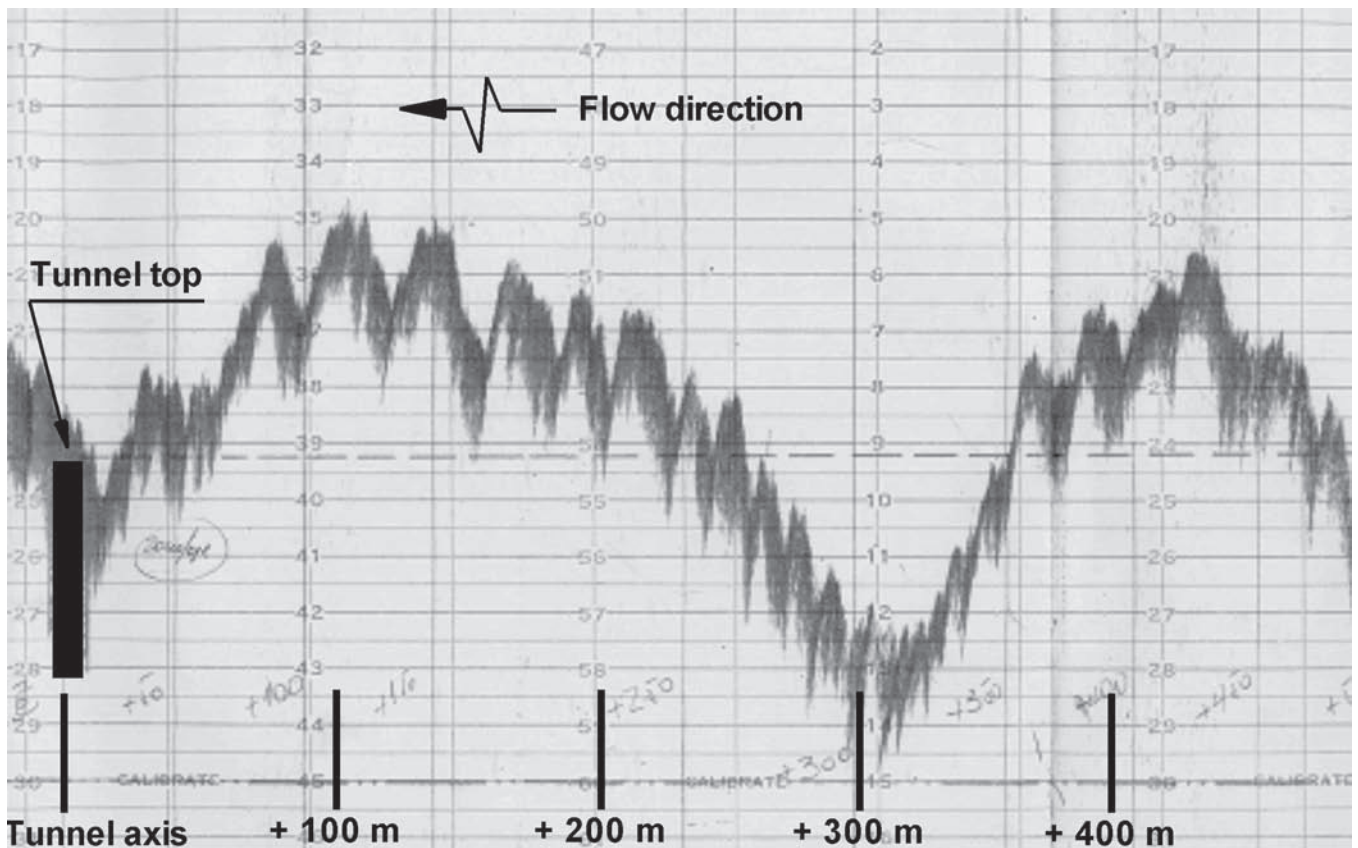


**Fig. 2-35.** (b) Echosound bottom profile of large dunes ( $\Delta_d \approx 6.5\text{m}$  and  $\lambda_d \approx 250\text{m}$ ) with superimposed smaller dunes ( $\Delta_d \approx 1\text{m}$  and  $\lambda_d \approx 10\text{m}$ ) passing by the tunnel during the flood of June 1992 in the middle reach of the Parana River. Each time the trough of a large dune moved over the tunnel, the sand-cover protection was removed and the tunnel was in danger of experiencing uplifting due to buoyancy effects (Echosound courtesy of Mario Amsler). (Continued)

Brooks (2001), Packman and Mackay (2003) and Packman et al. (2004) have also demonstrated the importance of bed forms in hyporheic exchange (i.e., the mixing of stream water with pore water beneath the sediment bed). They show the importance of dunes for both the clogging of the porous bed by finer grains, such as kaolinite, and that the exchange of solutes and colloids is also linked to the rate of bed form migration and scour, with faster-moving bedforms reworking the bed and leading to a greater turnover of sediment. Rutherford (1994, p. 316) has also analyzed the role of dune turnover on benthic oxygen uptake in the Tarawera River, New Zealand. This river receives treated pulp mill effluent and experiences high rates of deoxygenation. The role of dunes in contaminant exchange at sediment-water interfaces is also considered in Chapter 21.

### 2.7.1 Background Knowledge and Recent Advances

A major advance in the theory of alluvial channel flows has been the application of stability theory to identify the regions

of flow for which the stream bed would be stable, that is the flow conditions under which a small disturbance of an initially plane bed would be damped. The formation of sand waves is considered by most scientists as an instability problem (e.g., Fredsøe 1996). For instance, if a plane sand bed is slightly perturbed, the flow and sediment transport will be also affected. Two possibilities exist:

- (1) The changes in flow pattern and sediment transport will attenuate the amplitude of the perturbation and eventually the bed will go back to the original plane bed state (i.e., the bed is stable); or,
- (2) The flow and sediment transport changes cause the perturbation of the bed to grow in time, resulting in the formation of ripples, dunes, and/or antidunes (i.e., the bed is unstable).

In stability analysis, a plane bed is usually upset with a small sinusoidal bed perturbation having a certain amplitude and wave length. The goal of the analysis is to observe if the

perturbation will grow (unstable) or decay (stable) with time. In his pioneering work on morphodynamics, Exner (1920, 1925) studied the behavior of sand waves with a simple model that related the local sediment transport to the depth-averaged flow velocity, and predicted instability of the bed but no stable regions. Exner's work is described in Graf (1984, p. 289). Anderson (1953) improved upon Exner's flow description and was the first to apply stability theory to the analysis and prediction of bedforms (ripples, dunes, antidunes), although his analysis predicted only neutral instability. Kennedy (1961, 1963) was the first to advance a comprehensive theory to account for dunes, a plane bed, and antidunes by means of linear stability analysis. Kennedy used a potential flow model with an empirical relation between flow velocity and sediment transport; in later studies the theory was extended to the formation of ripples in closed ducts (Kennedy 1964) and to ripples formed in oscillatory flows (Kennedy and Falcon 1965). Potential flow models for bed stability analysis were also advanced by Reynolds (1965) and Gradowczyk (1968). Kennedy (1963) emphasized the need to include a lag between the local sediment transport rate and the local flow velocity. The main two factors causing Kennedy's lag in sand bed rivers are (1) fluid friction, and (2) delayed response of sediment transport to spatial changes in flow velocity. Hayashi (1970) made theoretical studies on bed form development using the St. Venant equations and further interpreted the lag distance introduced by Kennedy. A decade later, Engelund (1970) developed a model which did not require the lag distance and accounted for velocity and suspended sediment distribution as well as turbulent diffusion.

The instability due to bed friction was recognized independently by Frank Engelund (1970) and J. Dungan Smith (1970). Both applied an eddy-viscosity model to compute the flow over a wavy bottom. The Engelund-Smith approach succeeded in predicting the instability of the bed, but could not predict the wave length for which the perturbation growth rate was largest. In both of these cases the perturbation increases monotonically with decreasing wave length. Fredsøe (1974) improved this description by including a bed-slope effect (i.e., gravity) on the bed load movement. When gravitational effects are included, the sediment transport rate becomes smaller on the upslope part of the perturbation and larger on the downslope part. The net result is that less sediment makes it to the top of the perturbation and more sediment is transported downslope from the top of the perturbation, thus the bed-slope effect stabilizes the bed (Fredsøe 1996).

Different types of sand waves may occur simultaneously on a flat bed, but as the flow evolves only one type may reach fully-developed conditions. As will be described below, usually ripples and dunes are the most common bed forms observed for low Froude-number conditions (i.e., lower regime). Ripples are steeper and shorter than dunes and their length depends on particle diameter. Whereas dune height

and length are both mainly functions of the flow depth and display a more complex dependency on particle size. The co-existence of bed forms makes it more difficult to conduct a stability analysis capable of distinguishing between ripples and dunes. This problem was addressed by Richards (1980), who improved the eddy-viscosity description of the flow over a hydraulically-rough wavy bottom by introducing a one-equation turbulence model. His analysis discovered two peaks in the growth rate of the perturbations. The higher peak corresponds to the maximum found independently by Engelund and Smith in 1970, and later corroborated by Fredsøe (1974) when including the bed-slope (i.e., gravity) effect. Richards (1980) found that the location of this peak depends strongly on the flow depth indicating that it is related to the instability of dunes. The lower peak in perturbation amplification is not affected by changes in the flow depth, and according to Richards this maximum can be related to the instability of ripples. Sumer and Bakioglu (1984) considered only the ripple mode and extended the work of Richards to the case of hydraulically smooth and transition bed-roughness conditions. This extension is important since experimental observations have shown that ripples disappear and dunes are the prevailing bed form instability when the flow transitions from hydraulically-smooth to hydraulically-rough conditions.

The effect of sediment transport on bed stability was first included by Engelund (1970) for suspended load and by Parker (1975) for bed load to assess the role of sediment inertia on the development of antidunes. Reynolds (1976) indicated that Kennedy's lag was indeed related to the relaxation time associated with settling of suspended sediment and with less obvious adjustments in bed load. The stabilizing effect of sediment was used by Engelund and Fredsøe (1976) to explain the transition from dunes to plane bed in the lower flow regime. For low Froude numbers, bed load transport is the dominant mode due to low dimensionless Shields' numbers, thus giving place to the formation of dunes. At higher Shields' numbers, suspended load will become the predominant transport mode, resulting in a stable plane bed for sufficiently high shear stresses. The linear stability analysis of Engelund and Fredsøe (1976) was applied by Chen and Nordin (1976) to explain the transition from dunes to plane bed in the Missouri River. Recently, Coleman and Fenton (2000) have revisited potential flow analysis of bed instabilities.

Linear stability theories apply strictly to the inception of bed forms (Nakagawa and Tsujimoto 1984; Coleman and Melville 1996). They are only able to predict whether or not sand waves are generated. Another limitation is that the outcome is independent of the initial perturbation amplitude. Unsteady perturbations amplify or decay forever. Ji and Mendoza (1997) applied weakly nonlinear stability theory to the set of equations governing the motion of turbulent flow and transport of sediment in rivers proposed by Fredsøe (1974). They found that nonlinearities play an important

role in the formation of dunes. A comparison between the results of linear and nonlinear models indicated that for a nonlinear model, dunes are less unstable and less sensitive to changes in the intervening variables. Ji and Mendoza (1997) conducted a weakly nonlinear stability analysis to derive an equation of the Landau-Stuart type for the amplitude time evolution in steady, unidirectional turbulent flow over a movable boundary. It was found that nonlinear effects affect both dune growth and celerity, and the dune height reaches an equilibrium value at large time. A nonlinear model was also used by Zhou and Mendoza (2005) for analyzing the growth of sand wavelets from an initially flat bed. The results of the model were supported by the observations made by Coleman and Melville (1994, 1996). Stability analyses have also been used by Colombini et al. (1987) to study finite-amplitude bars and Seminara and Tubino (1989) to assess the role played by sediment bars on the initiation of river meandering, and by Seminara (1995) to study the effect of sediment sorting on the evolution and characteristics of bed forms. Komarova and Newell (2000) have also studied the nonlinear dynamics of sand banks and sand waves in the ocean. Coastal bed forms have been reviewed by Blondeaux (2001).

Recent years have seen great progress in our knowledge of bed form dynamics that has often been linked to significant advances in our ability to monitor flow and dune morphology in the laboratory and field, and the increasing sophistication of numerical modeling to capture not only the characteristics of the mean flow field but realistically simulate the origins and motions of coherent flow structures above dune beds (Best 2005). Most of this work has been summarized in several review articles, reports, and books, which have appeared since the publication of ASCE Manual 54 (Vanoni 1975). They include those by Reynolds (1976), Engelund and Fredsøe (1982), Ikeda and Parker (1989), McLean (1990), Southard (1991), Kennedy and Odgaard (1991), Seminara (1995), Best (1996), Seminara and Blondeaux (2001), Yalin and da Silva (2001), ASCE (2002), Bridge (2003), Best (2005), and Parker and García (2006).

As detailed in Best (2005), in recent years there has been great progress in our knowledge of bed form dynamics, which has often been linked to significant advances in our ability to monitor flow and dune morphology in the laboratory and field, and the increasing sophistication of numerical modeling to capture not only the characteristics of the mean flow field but realistically simulate the origins and motions of coherent flow structures above dune beds. Some of these advances are considered next.

Significant advances in our understanding have been achieved through studies that have been concerned both with the origin of bed forms (e.g. Yalin 1992; Nelson and Smith 1989; McLean 1990; Southard 1991; Bennett and Best 1996; Coleman and Melville 1996; Nikora and Hicks 1997; Gyr

and Kinzelbach 2004), their stability and transformations (Leeder 1983; Bennett and Best 1996; Robert and Ulhman 2001; Schindler and Robert 2004), uses in estimating bed load transport (e.g. Engel and Lau 1980; Mohrig and Smith 1996; Vionnet et al. 1998; Zhou and Mendoza 2005) and their role in determining flow resistance (e.g., Ogink 1988; Yoon and Patel 1996; Fedele and García 2001; Julien et al. 2002; Wilbers 2003). Additionally, these studies have been conducted both in increasingly sophisticated and quantitative laboratory studies (e.g. van Mierlo and de Ruiter 1988; Shen et al. 1990; Lyn 1993; McLean et al. 1994, 1996, 1999; Nelson et al. 1993; Bennett and Best 1995a; Bennett and Venditti 1997; Kadota and Nezu 1999; Nelson et al. 2001; Best and Kostaschuk 2002; Maddux 2002; Maddux et al. 2003a, 2003b; Coleman et al. 2003; Fernandez et al. 2006) and a growing quantification of bed forms within the natural environment (e.g., Kostaschuk 1989; Gabel 1993; Julien and Klaassen 1995; Kostaschuk and Church 1993; Kostaschuk and Ilersich 1995; Kostaschuk and Villard 1996; Roden 1998; Villard and Kostaschuk 1998; Carling et al. 2000a,b; Best et al. 2001; Williams et al. 2003; Sukhodulov et al. 2004; Parsons et al. 2005).

The simplified problem of flow over fixed (nonerodible) bedform shapes, motivated by the equilibrium problem, has received intense attention. Several laboratory studies have been conducted to elucidate the mean flow and turbulence characteristics above dunes (e.g., van Mierlo and de Ruiter 1988; Lyn 1993; Nelson et al. 1993; McLean et al. 1994; Nelson et al. 1995; Bennett and Best 1995; Best and Kostaschuk 2002; Fernandez et al. 2006). Flow resistance measurements over fixed bedforms have been made by Shen et al. (1990) and Maddux et al. (2003a, 2003b). Such studies have been restricted to flows without mobile-bed material; only recently studies of sediment-transporting flows over, though still artificial, bed forms have appeared (Cellino and Graf 2000; Venditti and Bennett 2000). Observations by Ikeda and Asaeda (1983) of a sediment-laden flow over a rippled bed are an exception.

Numerical simulations of flow over fixed-bed forms have been performed by, among others, Mendoza and Shen (1990); Yoon and Patel (1996); and Zedler and Street (2001). Recently, Tjerry and Fredsøe (2005) replaced the semi-empirical flow model used earlier by Fredsøe (1982) with a two-equation turbulence model, to compute numerically the morphology of dunes. More information on flow and turbulence modeling over dunes can be found in Chapter 16. Coherent turbulent structures in flows over bed forms have also received considerable attention (Ashworth et al 1996). Their dynamics, even in simpler flows such as uniform flat-bed flows, is still complicated (e.g. Nelson et al. 1995; García et al. 1996; Niño and García 1996). Some interpretations of suspended sediment flux measurements in the presence of dunes have been formulated within a coherent-structures conceptual framework (Lapointe

1992, 1996; Bennett et al. 1998; Nikora and Goring 2000; Venditti and Bennett 2000). Jackson (1976) was among the first to bring attention to the sedimentological effect of coherent structures, in particular the turbulent bursting phenomenon, in rivers.

Field studies (e.g., Kostachuk and Villard 1996; Holmes 2003; Kostachuk et al. 2004; Parsons et al. 2005) with detailed measurements not only of dune characteristics, but also of flow and transport, are valuable and daunting for the same reason: they indicate the complexity of the real problem, which, together with practical constraints on field measurements, make the analysis and interpretation of the data more difficult (van den Berg and van Gelder 1993). Field measurements present additional difficulties in interpretation and raise the question of how meaningful are direct comparisons between field and laboratory/theoretical results. Keulegan (1978) had to address this issue while attempting to estimate the channel roughness of interoceanic canals and recommended that reliance should be placed on field calibration of bed form predictors.

Accurate prediction of stage and flow developments during a flood event must recognize the transient nature of erodible-boundary roughness, implying clear knowledge about bed-form generation and development processes as flows increase and decrease in intensity (Julien and Klaasen, 1995; Julien et al. 2002). Amsler and García (1997) cite that large dunes on the Paraná River, Argentina, decreased in magnitude with increasing discharge, however, smaller superimposed dunes increased in size (Fig. 2-46). Large dunes with superimposed smaller dunes are shown in Fig. 2-35b.

For sedimentation engineering purposes, a minimum contribution desired of a theory or model for bed form development would be a reliable means of determining which equilibrium bed configuration would be established, i.e. delineating stability boundaries, as well as a reliable predictor for bed form dimensions under equilibrium conditions (i.e. wavelength and amplitude). As explained above, many attempts have been made to base such boundaries on theoretical stability models, but engineering approaches have been primarily based on dimensional analysis and empiricism.

Recent experimental and theoretical work (e.g., Coleman and Melville 1996; Coleman and Fenton 2000; Coleman et al. 2003; Zhou and Mendoza 2005) has focused on the bed form initiation process, in particular the conditions leading to the development of wavelets, the precursors of ripples (Coleman and Eling 2000). Although the mechanics of bed form development (e.g., Coleman and Melville 1994) and rates of bed form growth for steady flows (e.g., Nikora and Hicks 1997) have been clarified, practical implications and models accessible to the engineer remain to be elaborated. For example, how and at what rates bed forms change with increasing and decreasing flows remains to be quantified. Recent computations by Tjerry and Fredsøe (2005) of

dune morphology have shown promising results for laboratory-scale dunes. Particularly lacking, however, are similar bed form predictors for large alluvial rivers (Schumm and Winkley 1994; Sambrook-Smith et al. 2006). Research needs in this area have been recently addressed by an ASCE Task Committee (ASCE 2002), Best (2005), and Hulscher and Dohmen-Jansen (2005).

## 2.7.2 Dunes, Antidunes, Ripples, and Alternate Bars

The ripples, dunes, and antidunes illustrated in Fig. 2-36 are the classic bed forms of erodible-bed, open-channel flow. On the one hand, they are the product of flow and sediment transport, and on the other hand, they profoundly influence flow and sediment transport. In fact, all of the bed load equations quoted previously are strictly invalid in the presence of bed forms. The adjustment necessary to render them valid (i.e., removal of form drag) is discussed later in the chapter.

Ripples, dunes, and antidunes are undular (wavelike) features that have wavelength  $\lambda$  and wave height  $\Delta$  that scale with the flow depth  $H$ , as defined below.

**2.7.2.1 Dunes** Well-developed dunes tend to have wave heights  $\Delta$  scaling up to about one-sixth of the depth; i.e.,

$$\frac{\Delta}{H} \leq \frac{1}{6} \quad (2-116)$$

Dune wavelength can vary considerably. A fairly typical range can be quantified in terms of dimensionless wavenumber  $k$ , where

$$k = \frac{2\pi H}{\lambda} \quad (2-117)$$

This range is given by

$$0.25 < k < 4.0 \quad (2-118)$$

Dunes invariably migrate downstream. They are typically approximately triangular in shape and usually (but not always) possess a slip face, beyond which the flow is separated for a certain length.

A dune progresses forward as bed load accretes on the slip face. Generally, very little bed load is able to pass beyond the face without depositing on it, whereas most of the suspended load is not directly affected by it.

Dunes are characteristic of subcritical flow in the Froude sense. In a shallow-water (long-wave) model, the Froude criterion dividing subcritical ( $Fr < 1$ ) and supercritical ( $Fr > 1$ ) flow is

$$Fr = 1 \quad (2-119a)$$

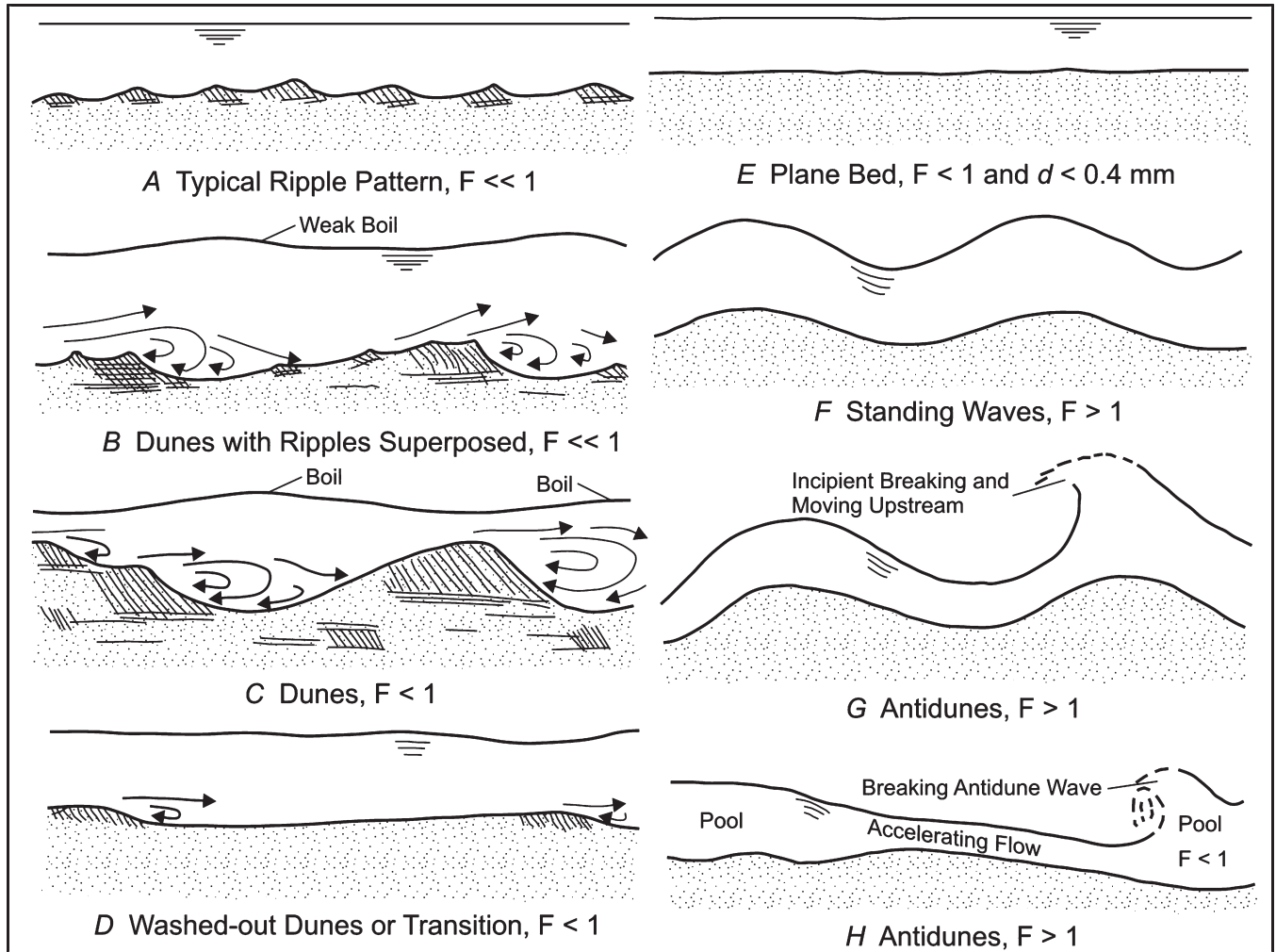


Fig. 2-36. Schematic of different bedforms. Note:  $F$  = Froude number;  $d$  = sediment size.

where the Froude number is given by,

$$Fr = \frac{U}{\sqrt{gH}} \quad (2-119b)$$

Dunes, however, do not qualify as long waves, in that their wavelength is of the order of the flow depth. A detailed potential flow analysis over a wavy bed yields the following (wave number-dependent) criterion for critical flow over a bedform (Kennedy 1963),

$$Fr^2 = \frac{1}{k} \tanh(k) \quad (2-120a)$$

Note that as  $k \rightarrow 0$  ( $\lambda \rightarrow \infty$ ),  $\tanh(k) \rightarrow k$ , and condition (2-119a) is recovered in the long-wave limit. For dunes to occur, then, the condition

$$Fr^2 < \frac{1}{k} \tanh(k) \quad (2-120b)$$

must be satisfied. Both dunes and antidunes cause the water surface to undulate as well as the bed. In the case of dunes, the undulation of the water surface is usually of much smaller amplitude than that of the bed; the two are nearly  $180^\circ$  out of phase.

Let  $c$  denote the wave speed of the dune. The bed load transport rate by dunes can be estimated as the volume of material transported forward per unit bed area per unit time by a migrating dune (Simons et al. 1965b). If the dune is approximated as triangular in shape, the following approximation holds (Engel and Lau 1980; Havinga 1983)

$$q \equiv \frac{1}{2} \Delta c (1 - \lambda_p) \quad (2-122)$$

where

- $\Delta$  and  $c$  = amplitude and celerity, respectively, of the bed form; and  
 $\lambda_p$  = porosity of the sediment bed.

Rubin and Hunter (1982) proposed that the transport rate given by Eq. (2-122) be called the bed form transport rate instead of the bed load transport rate. An elegant derivation of this equation can be found in Ten Brinke et al. (1999). The celerity of dunes  $c$  as a function of the Froude number  $Fr$  can be estimated with an empirical relation proposed by Kondap and Garde (1973),

$$\frac{c}{U} = 0.021 \times Fr^3 \quad (2-123)$$

The celerity of dunes is a small fraction of the mean flow velocity. Kondap and Garde found that for grain sizes in the range between 0.18 mm to 2.28 mm, sediment size seems to have a negligible effect on the celerity of dunes. The data were from laboratory experiments and low gradient streams having depths of less than 1 m. For the case of large sand bed rivers, Fedele (1995) obtained an empirical relation to estimate the velocity of dunes in the Paraná and Paraguay Rivers in South America. Vionnet et al (1998) have also proposed a methodology to compute sediment transport from dune celerity and amplitude based on kinematic-wave theory. More recently, Serra and Vionnet (2006) extended the analysis to account for the transport of smaller dunes superimposed on larger ones (see Fig. 2.35b).

**2.7.2.2 Antidunes** Antidunes are distinguished from dunes by the fact that the water surface undulations are nearly in phase with those of the bed. They are associated with supercritical flow, in the sense that

$$Fr^2 > \frac{1}{k} \tanh(k) \quad (2-124)$$

Antidunes may migrate either upstream or downstream. Upstream-migrating antidunes are usually rather symmetrical in shape and lack a slip face. Downstream-migrating antidunes are rather rarer; these have a well-defined slip face and look rather like dunes. The distinguishing feature is the water surface undulations, which are very pronounced in the case of antidunes.

The potential-flow criterion dividing upstream-migrating antidunes from downstream-migrating antidunes is (Kennedy 1963)

$$Fr^2 = \frac{1}{k \tanh(k)} \quad (2-125)$$

Values lower than the above are associated with upstream-migrating antidunes.

Relations (2-120a), (2-120b), (2-124) and (2-125) were obtained from a potential flow analysis over a wavy bed. A phase diagram showing these conditions is shown in Fig. 2-37. The boundaries they define are modified when turbulent shear flows transporting sediment are considered (e.g., Engelund and Fredsøe 1982). For instance, Wan and Wang (1994) have observed the absence of dunes for volumetric sediment concentrations greater than about 0.08.

**2.7.2.3 Ripples** Ripples are dune-like features that occur most of the time in the presence of a viscous sublayer. The existence of a viscous sublayer does not imply that the flow is either laminar or turbulent. Rather, when the flow is turbulent, the existence of a well-defined viscous sublayer implies flow in the turbulent smooth regime rather than the turbulent rough regime. Ripples look very much like dunes in that they migrate downstream and have a pronounced slip face. They generally are much more three-dimensional in structure than dunes, however, and have little effect on the water surface.

As mentioned earlier, many authors have suggested that a criterion for the existence of ripples is the existence of a viscous sublayer. Recalling that the thickness of the viscous sublayer is given by  $\delta_v = 11.6 v / u_*$ , it follows that ripples will form when

$$R_p = \frac{u_* D}{v} \leq 11.6 \quad (2-126)$$

Raudkivi (1990; 1997) indicates that ripples only develop in fine grained sediments having mean sizes of less than 0.7 to 0.9 mm, and for shear velocity Reynolds number ( $Re_* = u_* D / v$ ) of less than 10 to 27 (see Fig. 2-39b).

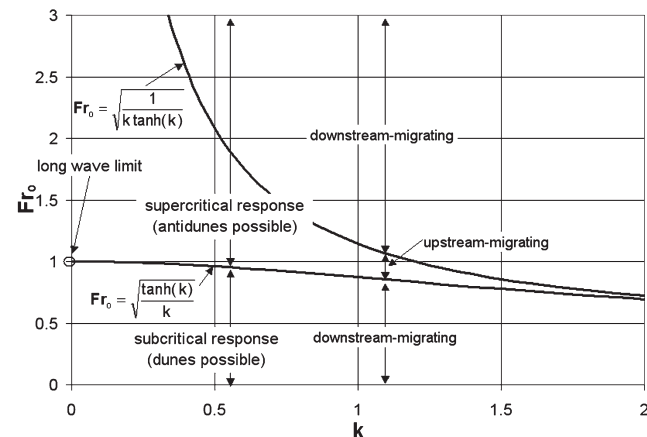


Fig. 2-37. Phase diagram for dunes and antidunes based on linear potential theory over a wavy bed (after Parker 2005).

Richards (1980) gave the following criteria for ripple formation

$$0.0007 < kz_0 < 0.16,$$

where  $k$  is the wave number ( $2\pi/\lambda$ ) and  $z_0$  is the Smith (1977) roughness-length parameter defined as

$$z_0 = 26.3 \frac{\tau_0 - \tau_c}{(\rho_s - \rho)g} + k_n \quad (2-127)$$

with  $k_n = 0.033 k_s$ , where  $k_s$  is the Nikuradse roughness height.

Karim (1999) proposed a relation for predicting ripples from laboratory data reported by Guy et al. (1966). He found that ripples would only occur if

$$N_* < 80 \quad (2-128a)$$

where  $N_* = \frac{u_* D_{50}}{v} \frac{U}{\sqrt{g R D_{50}}}$ ,  $U$  is the mean flow velocity, and  $D_{50}$  is the median grain size.

Coleman and Melville (1994) studied the relation between celerity of small bed forms (i.e., wavelets) as a function of bed-form height and found that such relation can be approximated by the expression

$$c'(\Delta - 3.5)^{1.3} = 40 \quad (2-128b)$$

where

$$c' = \text{dimensionless celerity} = c / [(u_* - u_{*c})(\tau^* - \tau_{*c}^*)];$$

$$H' = \text{dimensionless bed-form height} = \Delta / D_g; \text{ and}$$

$$D_g = \text{geometric mean sediment diameter}.$$

When plotted this relation results in a hyperbolic parabola, which indicates that as the bed form increases in height, its celerity decreases according to Eq. (2-128b).

**2.7.2.4 Alternate Bars** Alternate bars are bed forms most commonly found in straight alluvial channels (Bridge 2003). Their geometry is three-dimensional. Navigation conditions and streambank stability can be affected by alternate bars. When alternate bars are present, pools develop on alternate sides of the channel and the floor meanders from pool to pool. Under these conditions, the flow might start to attack the stream banks, eventually causing bank erosion (e.g., Jang and Shimizu 2005) and leading to the initiation of stream meandering (Blondeaux and Seminara 1985; Rhoads and Welford 1991). The pools formed by alternate bars also provide habitat and play an important role in stream ecology.

In straight streams, the minimum channel slope  $S$  necessary for alternate-bar formation is given by (Jaeggi 1984)

$$S > \frac{\exp \left[ 1.07 \left( \frac{B}{D_g} \right)^{0.15} + M_b \right]}{12.9 \left( \frac{B}{D_g} \right)} \quad (2-129a)$$

$B$  is the channel width,  $D_g$  is the geometric mean size of the bed sediment as given by Eq. (2-41a), and  $M_b$  is a parameter that varies from 0.34 for uniform-size bed material to 0.7 for poorly-sorted material. Scour depth ( $S_d$ ) due to alternate bar formation can be estimated with:

$$S_d = 0.76 \Delta_{AB} = \frac{B}{6 \left( \frac{B}{D_g} \right)^{0.15}} \quad (2-129b)$$

where  $\Delta_{AB}$  is the total height of the alternate bar.

Using dimensional analysis and experimental observations, Sukegawa (1973) found that the condition for the formation of alternate bars in straight channels is given by the following:

$$\frac{u_*^2}{u_{*c}^2} \leq 5 \left( \frac{\sqrt{gB}}{u_{*c}} S \right)^{2/3} \quad (2-130)$$

The wavelength of alternate bars is approximately six to ten times the channel width (i.e.,  $\lambda = 6$  to  $10B$ ; Yalin 1992). Channel sinuosity will affect the celerity of alternate bars (García and Niño 1993). As the sinuosity increases, the migration speed of alternate bars decreases with respect to that observed in a straight channel. In general, the celerity of alternate bars is always less than 0.01% of the mean flow velocity in the channel.

Most of the experimental and theoretical work done to characterize alternate bars in straight channels has been done for steady flow conditions (e.g. Sukegawa 1973; Ikeda 1984, Jaeggi 1984; Kuroki and Kishi 1985, Seminara and Tubino 1989; García and Niño 1993; Lanzoni 2000a, 2000b; Knaapen et al. 2001). One exception is the work of Tubino (1991), who analyzed the growth of alternate bars in unsteady flow. Tubino (1991) noted that the characteristic time scale for bar development and the time scale of natural unsteady flow events are typically of the same order of magnitude. The effect of sediment sorting on both the growth and dynamics

of alternate bars has been analyzed by Seminara (1995) and Lanzoni and Tubino (1999).

### 2.7.3 Progression of Bed Forms

Various bed forms are associated with various flow regimes. In the case of a sand-bed stream with a characteristic size less than about 0.5 mm, a clear progression is evident as flow velocity increases. This is illustrated in Fig. 2-36 presented above. The bed is assumed to be initially flat. At very low imposed velocity  $U$ , the bed remains flat because no sediment is moved. As the velocity exceeds the critical value, ripples are formed. At higher values, dunes form and coexist with ripples. For even higher velocities, well-developed dunes form in the absence of ripples. At some point, the velocity reaches a value near the short-wave critical value in the Froude sense, i.e., Eq. (2-120a). Near this point, the dunes are often suddenly and dramatically washed out. This results in a flat bed known as an upper-regime (supercritical) flat bed. Further increases in velocity lead to the formation of antidunes, and finally to the chute and pool pattern. The last of these is characterized by a series of hydraulic jumps.

The effect of bed forms on flow resistance can be explained as follows. As noted earlier for equilibrium flows in wide straight channels, the relation for bed resistance can be expressed in the form

$$\tau_b = \rho C_f U^2 \quad (2-131)$$

where  $C_f$  is bed friction coefficient. If the bed were rigid and the flow rough,  $C_f$  would vary only weakly with the flow, according to the logarithmic law embodied in Eq. (2-19). As a result, the relation between  $\tau_b$  and  $U$  is approximately parabolic for a flat rough bed.

The effect of bed forms is to increase the bed shear stress to values often well above that associated with the skin friction of a rough bed alone. In Fig. 2-38, a plot of  $\tau_b$  versus  $U$  is given for the case of an erodible bed. At very low values of  $U$ , the parabolic law is followed. As ripples and then dunes are formed, the bed shear stress rises to a maximum value (Robert and Uhlman 2001). At this maximum value, the value of  $C_f$  is seen to be as much as five times the value without dunes. It is clear that dunes play a very important role as regards bed resistance. The increased resistance results from form drag in the lee of the dune.

As the flow velocity increases further, dune wavelength gradually increases and dune height diminishes, leading to a gradual reduction in resistance. At some point, the dunes are washed out, and the parabolic law is again satisfied. At even higher velocities, the form drag associated with

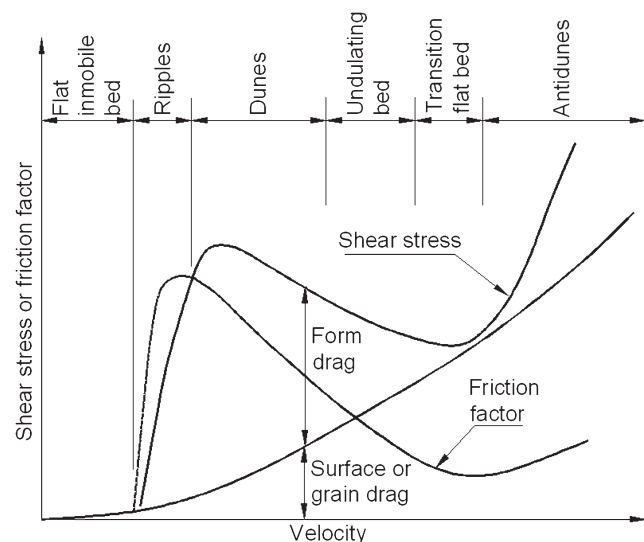


**Fig. 2-38.** Variations of bed shear stress  $\tau_b$  and Darcy-Weisbach friction factor  $f = 8 C_f$  with mean velocity  $U$  in flow over a fine-sand bed (after Raudkivi, 1990).

antidunes appears; it is usually not as pronounced as that of dunes.

In the case of a bed coarser than 1.0 mm, the ripple regime is replaced by a zone characterized by a lower-regime (subcritical) flat bed. Above this lie the ranges for dunes, upper-regime flat bed, and antidunes.

### 2.7.4 Dimensionless Characterization of Bed Form Regime

Based on the preceding arguments, it is possible to identify at least three dimensionless parameters that govern bedforms at equilibrium flow. These are Shields stress parameter  $\tau^*$ , shear Reynolds number  $R_p = u_* D / v$ , and Froude number  $Fr = U / \sqrt{gH}$ . A characteristic feature of sediment transport is the proliferation of dimensionless parameters (Vanoni 2006). This feature notwithstanding, Parker and Anderson (1977) have shown that equilibrium relations of sediment transport for uniform material in a straight channel can be expressed in terms of just two dimensionless hydraulic parameters, along with a particle Reynolds number (e.g.,  $R_p$  or  $R_{ep} = \sqrt{grDD}/v$ ) and a measure of density difference (e.g.,  $R = (\rho_s - \rho) / \rho$ ).

In the case of bed forms, then, the following classification can be proposed:

$$\text{bedform type} = f(\pi_1, \pi_2; R_{ep}, R) \quad (2-132)$$

Here, any independent pair of dimensionless hydraulic variables  $\pi_1, \pi_2$  applicable to the problem may be specified,

because any one pair can be transformed into any other independent pair. For example, the pair  $(\tau^*, Fr)$  might be used, or alternatively the pair  $(S, H/D)$ .

One of the most popular discriminators of bed form type is not expressed in dimensionless form at all. It is the diagram proposed by Simons and Richardson (1966), shown in Fig. 2-39a. In this diagram, regimes for ripples, dunes, transition to upper-regime plane bed, and upper-regime plane bed and antidunes are shown. The two hydraulic parameters are abbreviated to a single one, stream power  $\tau_b U$ , and particle Reynolds number is replaced by grain size  $D$ . The diagram is applicable only to sand-bed streams of relatively small scale. A similar bed phase discriminator which is popular in the geology community was proposed by Boguchwal and Southard (1990). An adaptation of the Boguchwal-Southard predictor made by Ashley (1990) is shown in Fig. 2-39b. It is a plot of laboratory observations of mean flow velocity against median sediment size covering the range of fine to coarse sand for flow depths between 0.20 and 0.40 m. Because the Boguchwal-Southard diagram uses a logarithmic scale for grain size instead of a normal scale like the Simons-Richardson discriminator, it shows that for finer grain sizes a marked increase in flow velocity can wash out existing ripples and transition abruptly to upper plane bed conditions without the appearance of dunes. The transition to the upper-regime is shown to take place for Froude numbers smaller

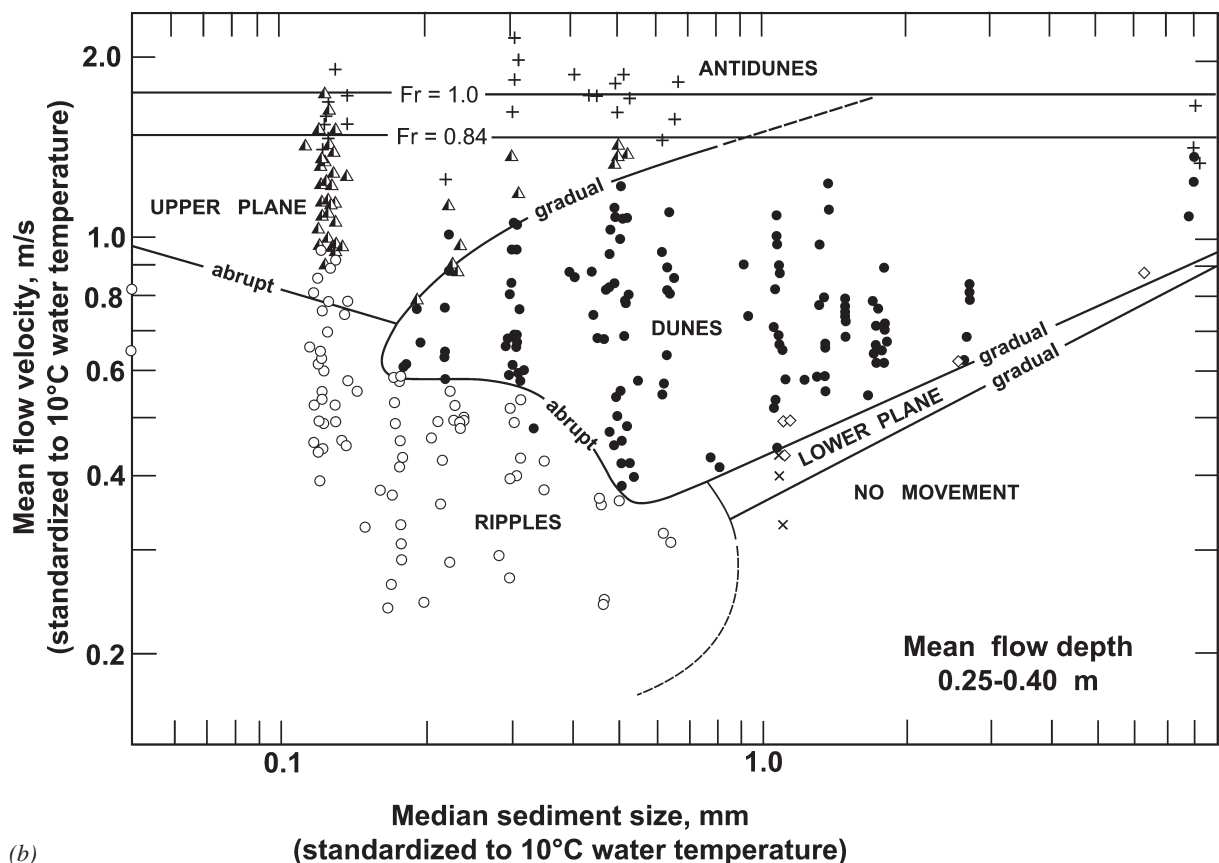
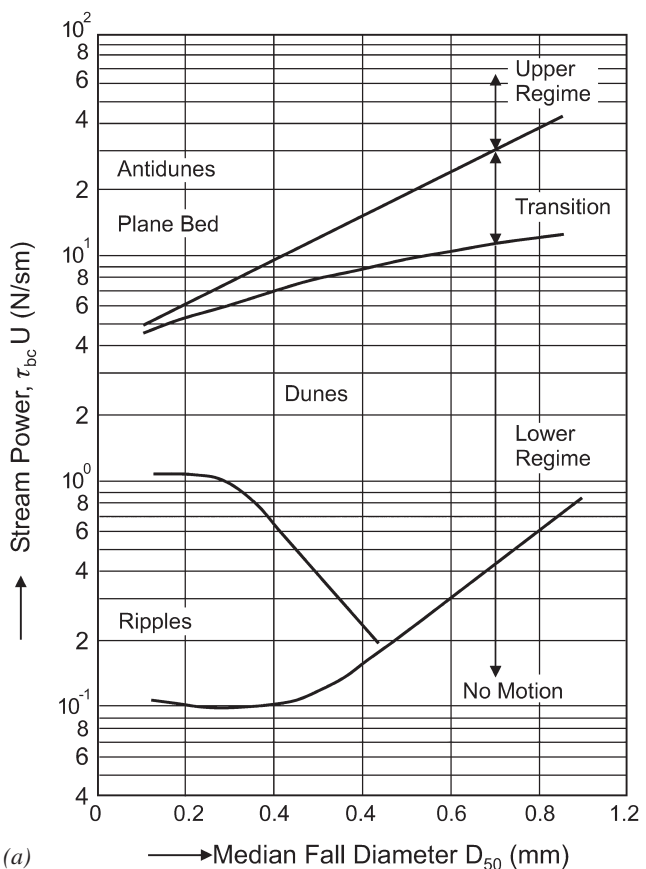


**Fig. 2-39.** Bed form discriminators proposed by (a) Simons and Richardson (1966) and (b) Boguchwal and Southard (adapted from Ashley 1990).

than one ( $Fr < 1$ ) depending on the sediment size. The fact that the bed phases shown in this diagram have been standardized to a given water temperature, highlights both the importance of accounting for temperature effects as well as the need to use dimensionless parameters to discriminate between bed-stability phases. Several dimensionless bed form and flow regime discriminators are presented next.

The discriminator originally proposed by Liu (1957) and later extended by Simons and Richardson (1961), is shown in Fig. 2-40. Liu's discriminator uses one dimensionless hydraulic parameter,  $u_* / v_s$  (a surrogate for  $\tau^*$ ), and the particle shear Reynolds number  $Re_* = u_* D / v$ . The diagram is of interest in that it covers sizes much coarser than those of Simons and Richardson and Boguchwal and Southard (Fig. 2-39). It is seen that the various regimes become compressed as grain size increases. For the case of very coarse material, the flow must be supercritical for any motion to occur. As a result, neither ripples nor dunes are to be expected. According to Simons and Senturk (1992), the Liu diagram does not give acceptable results for field conditions because few field data were used in the analysis. Nevertheless, the diagram should be useful for predictions of bed form type in

streams having mean flow depths less than 3 m (10 feet) and for the design of movable-bed laboratory experiments (e.g., Zwamborn 1966; 1981).

In fact, dunes can occur over a limited range in the case of coarse material (e.g., Dinehart 1989). This is illustrated in Figs. 2-41(a) and 2-41(b), which shows the discriminators originally advanced by Chaubert and Chauvin (1963) and Bonnefille-Pernecker (Vollmers and Giese 1970; Bechteler et al. 1991). The Chaubert-Chauvin diagram plots the Shields parameter ( $\tau^*$ ) versus the shear stress Reynolds number  $Re_*$ . A third parameter in this diagram is the Valenbois-Bonnefille dimensionless particle diameter given by

$$D^* = D \left( \frac{g R}{v^2} \right)^{1/3} \quad (2-133)$$

The Chaubert-Chauvin diagram shows that  $D^*$  must be less than about 15 for ripples to form. Employing  $R = 1.65$ ,  $g = 981 \text{ cm/s}^2$  and  $v = 0.01 \text{ cm}^2/\text{s}$ , it is seen that the condition  $D^* = 15$  corresponds to a value of  $D$  of approximately 0.6 mm.

For coarser grain sizes, the dune regime is preceded by a fairly wide range consisting of lower-regime flat bed. Many gravel-bed rivers never leave this lower-regime flat

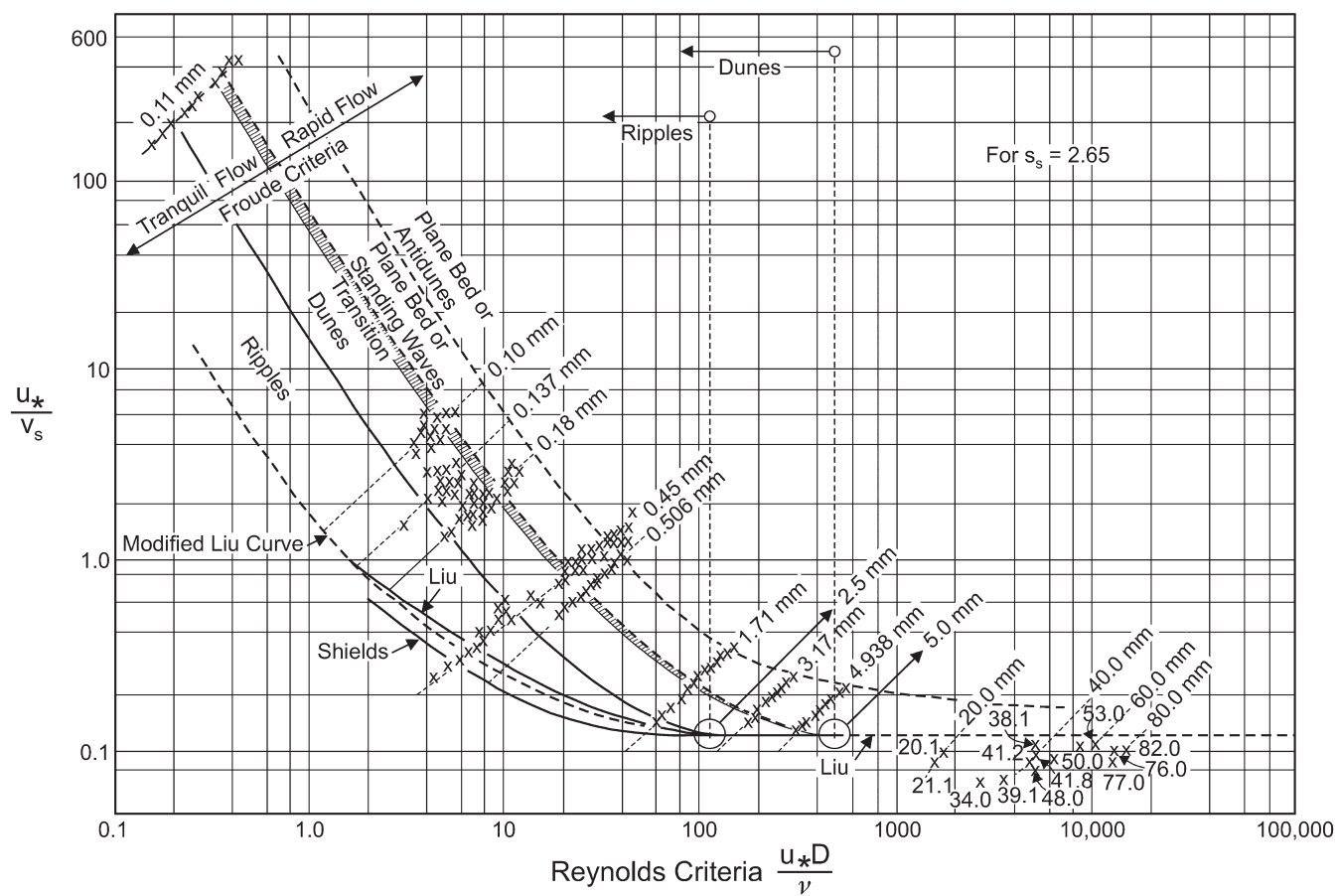


Fig. 2-40. Criteria for bed forms originally proposed by Liu (1957) and later extended by Simons and Richardson (1961).

bed region, even at bankfull flow. The Chabert-Chauvin diagram in Fig. 2-41(a) is not suited for the description of upper-regime flow.

The Bonnefille-Pernecker diagram displayed in Fig. 2-41(b) plots values of  $D^*$  versus  $Re_*$ . This diagram shows the transition from the lower regime (ripples) to flat bed condition and then to the upper regime ( antidunes), for  $D^* < 20$  as  $Re_*$  increases. For coarser sediment,  $D^* > 20$ , the diagram shows the lower regime conditions (dunes) following a narrow range of flat-bed transport conditions. An interesting aspect of this diagram is that it shows a narrow set of conditions, roughly defined by  $20 < Re_* < 45$  and  $7 < D^* < 20$ , for which ripples are superimposed on dunes. Bechteler et al. (1991) have used this diagram to analyze sediment transport conditions in alpine rivers.

A complete set of bed form diagrams for the case of sand is shown in Figs. 2-42(a) to 2-42(f); they are due to Vanoni (1974) and were not published in ASCE Manual 54. The two hydraulic parameters are the Froude number  $Fr$  and the relative flow depth  $H/D$  ( $= d/d_{50}$  in the diagram); the particle Reynolds number used in the plot is equal to the ratio  $R_{ep}/R^{1/2}$ , and the submerged specific gravity  $R$  is set constant at 1.65. Note how the transition to upper regime occurs at progressively lower values of  $Fr$  for relatively deeper flow (in the sense that  $H/D$  becomes large). Shen et al. (1978) confirmed that Vanoni's bedform discriminator fairly well captures temperature effects on river bottom configuration, such as those commonly observed in the Missouri River.

One of the most complete bed form classification schemes that includes both the lower and the upper regime

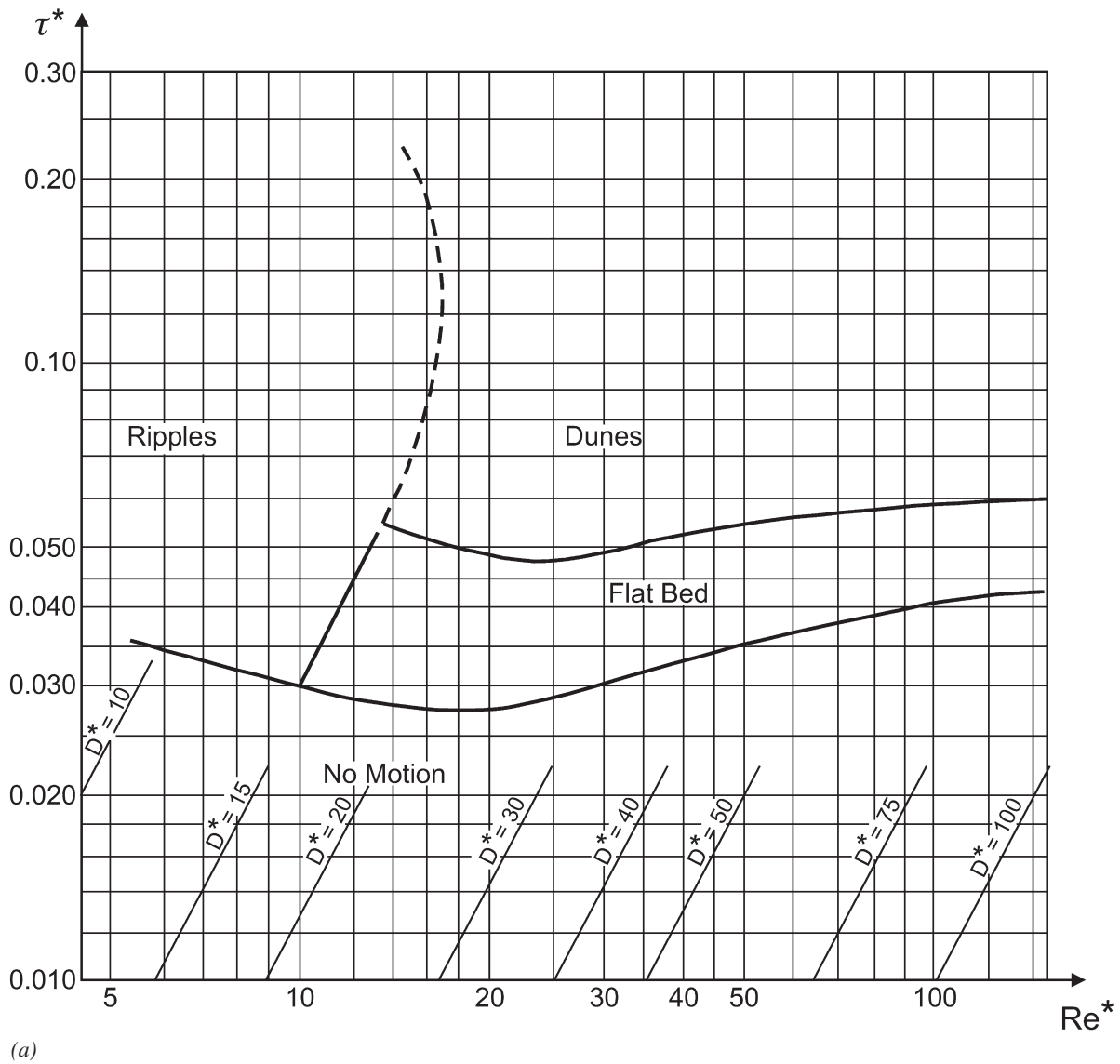
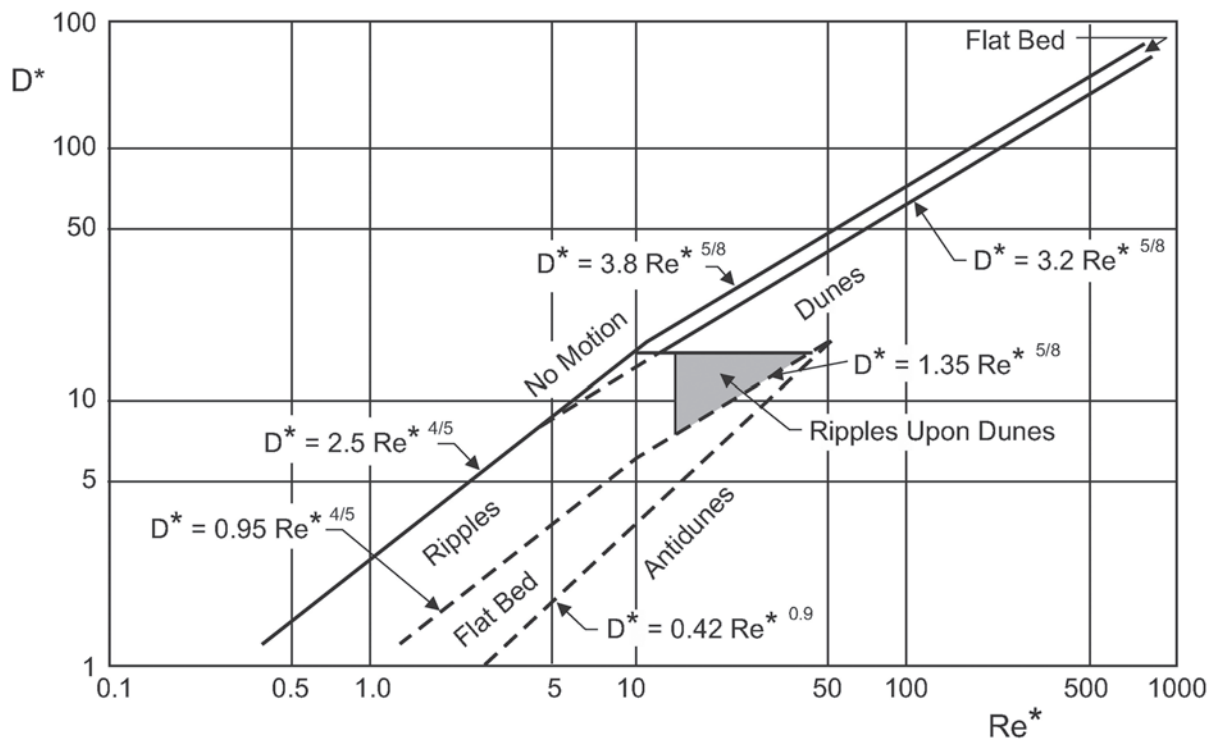
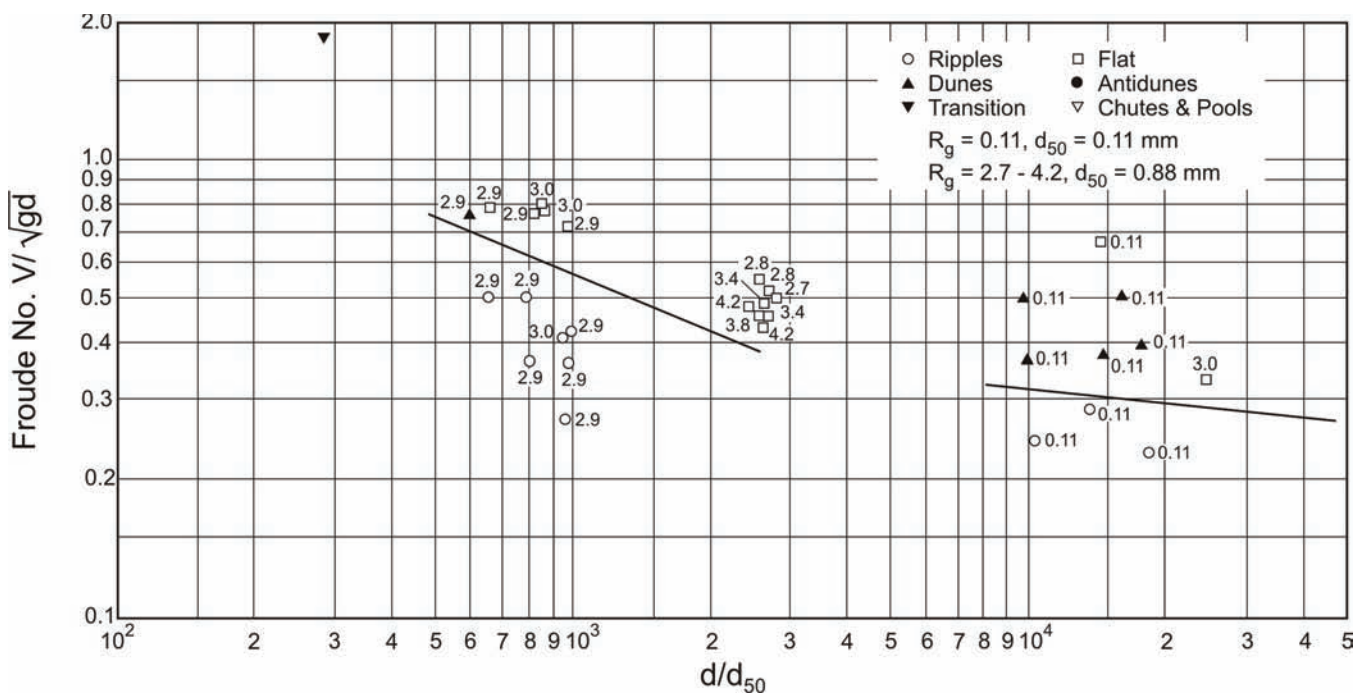


**Fig. 2-41.** Bed form classification diagrams (a) after Chabert and Chauvin (1963) and (b) Bonnefille-Pernecker (after Bechteler et al. 1991).



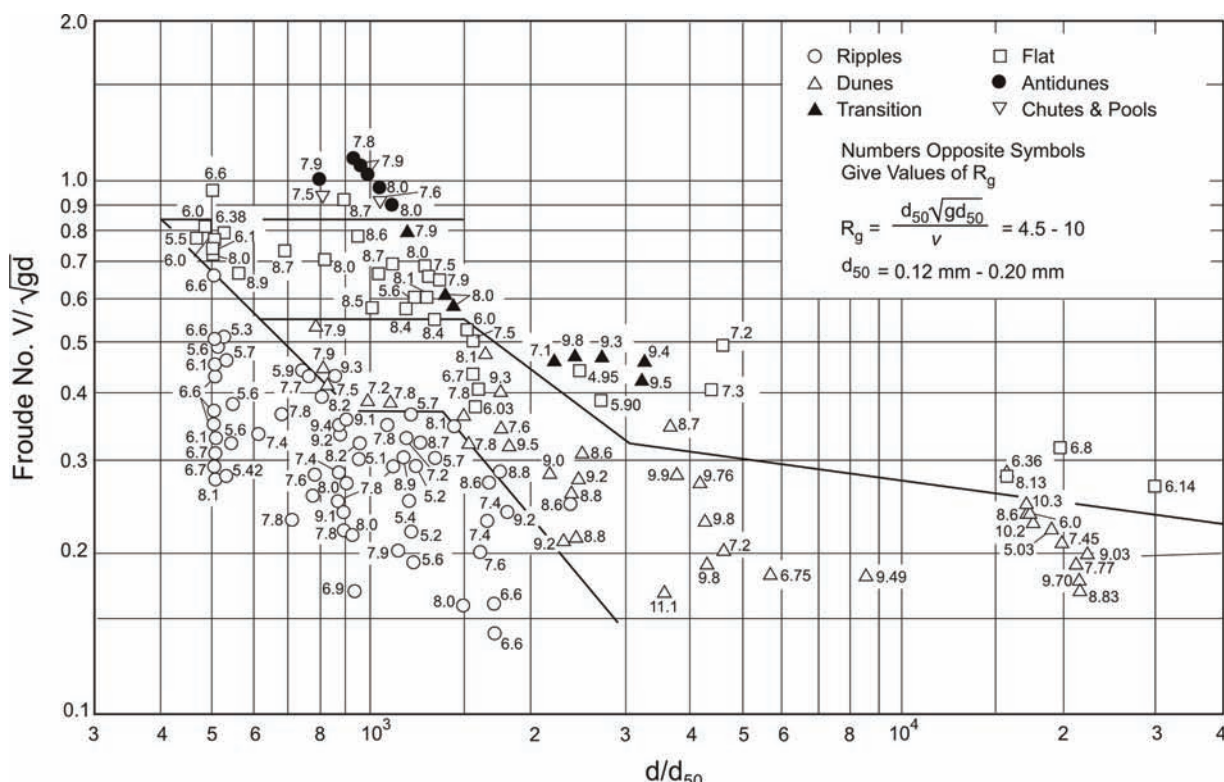
(b)

**Fig. 2-41.** Bed form classification diagrams (a) Chabert and Chauvin (1963) and (b) Bonnefille-Pernecker (after Bechteler et al. 1991). (Continued)

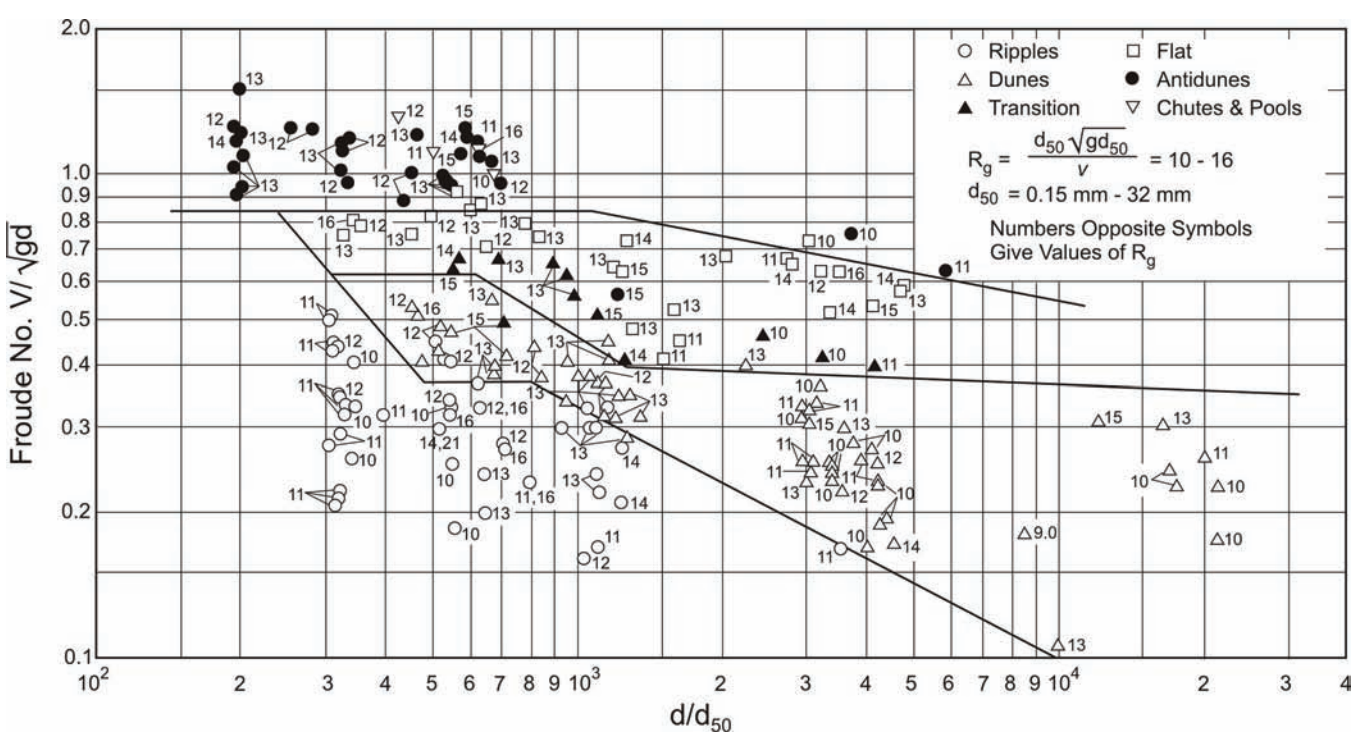


(a)

**Fig. 2-42.** Bed-form chart (a)  $R_g = 0.11$  and 2.7 to 4.2 ( $D_{50} = 0.1$  and 0.88 mm); (b)  $R_g = 4.5$  to 10 ( $D_{50} = 0.12$  to 0.20 mm); (c)  $R_g = 10$  to 16 ( $D_{50} = 0.15$  to 0.32 mm); (d)  $R_g = 16$  to 26 ( $D_{50} = 0.228$  to 0.45 mm); (e)  $R_g = 24$  to 48 ( $D_{50} = 0.40$  to 0.57 mm); (f)  $R_g = 82$  to 92, 130, 140 to 200 ( $D_{50} = 0.9, 1.20, 1.35 \text{ mm}$ ) (after Vanoni 1974).

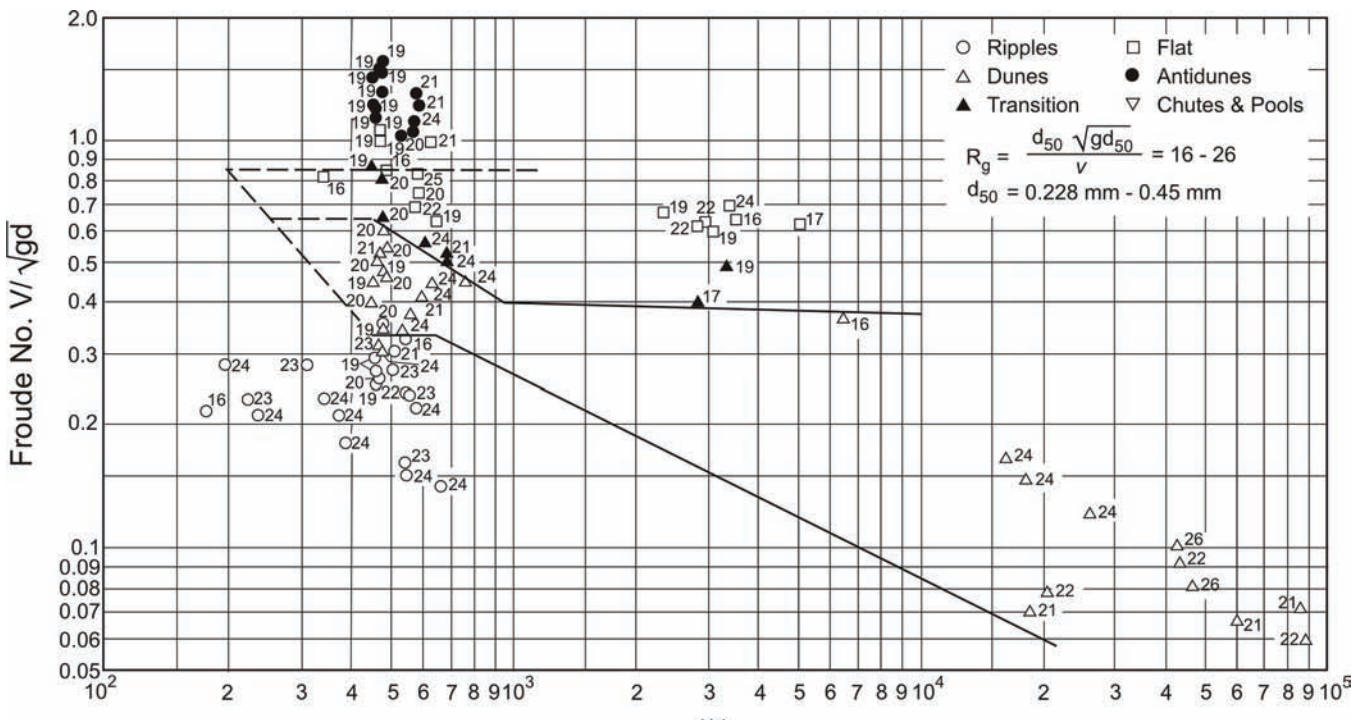


(b)

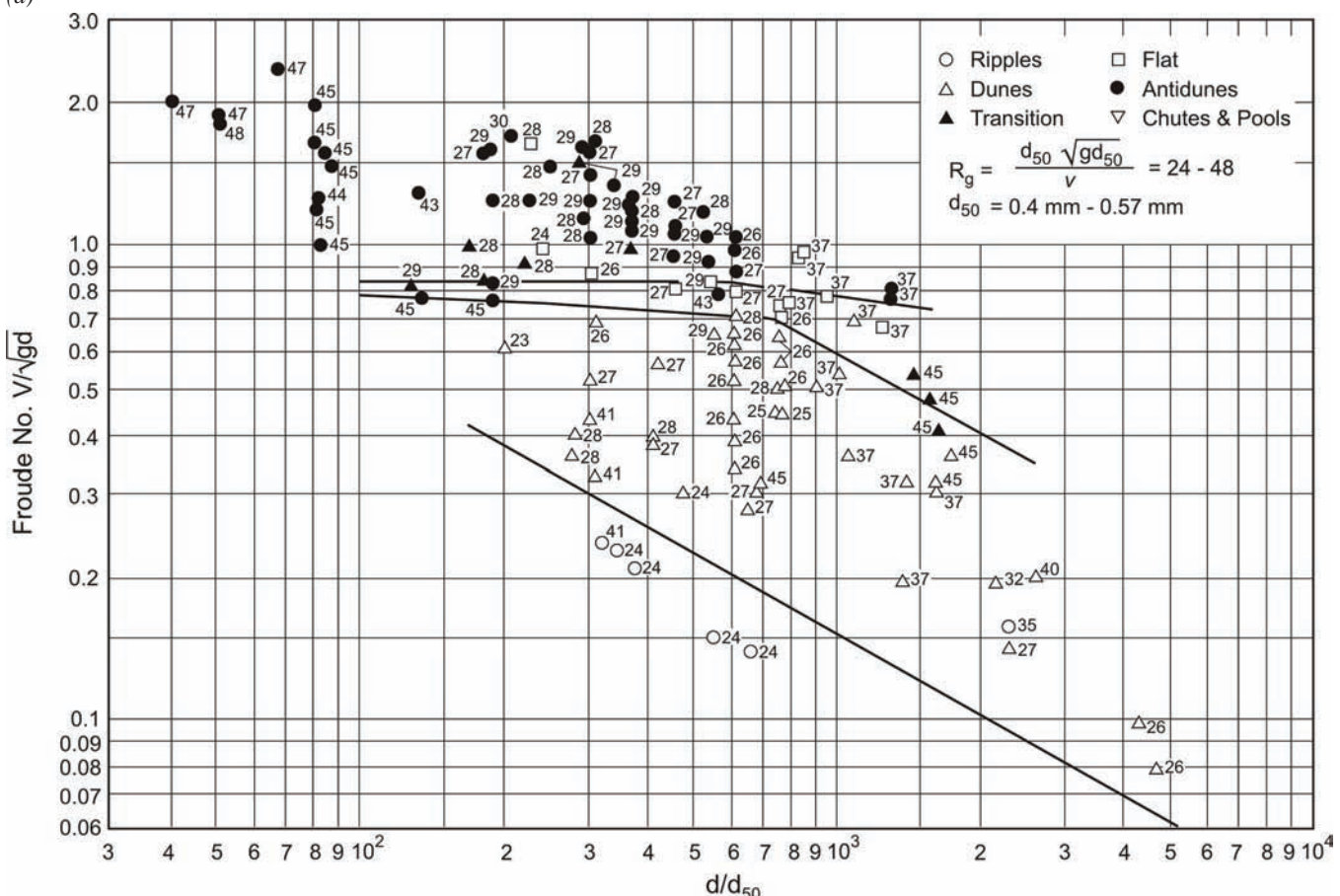


(c)

**Fig. 2-42.** Bed-form chart (a)  $Rg = 0.11$  and  $2.7$  to  $4.2$  ( $D_{50} = 0.1$  and  $0.88$  mm); (b)  $Rg = 4.5$  to  $10$  ( $D_{50} = 0.12$  to  $0.20$  mm); (c)  $Rg = 10$  to  $16$  ( $D_{50} = 0.15$  to  $0.32$  mm); (d)  $Rg = 16$  to  $26$  ( $D_{50} = 0.228$  to  $0.45$  mm); (e)  $Rg = 24$  to  $48$  ( $D_{50} = 0.40$  to  $0.57$  mm); (f)  $Rg = 82$  to  $92, 130, 140$  to  $200$  ( $D_{50} = 0.9, 1.20, 1.35$  mm) (after Vanoni 1974). (Continued)

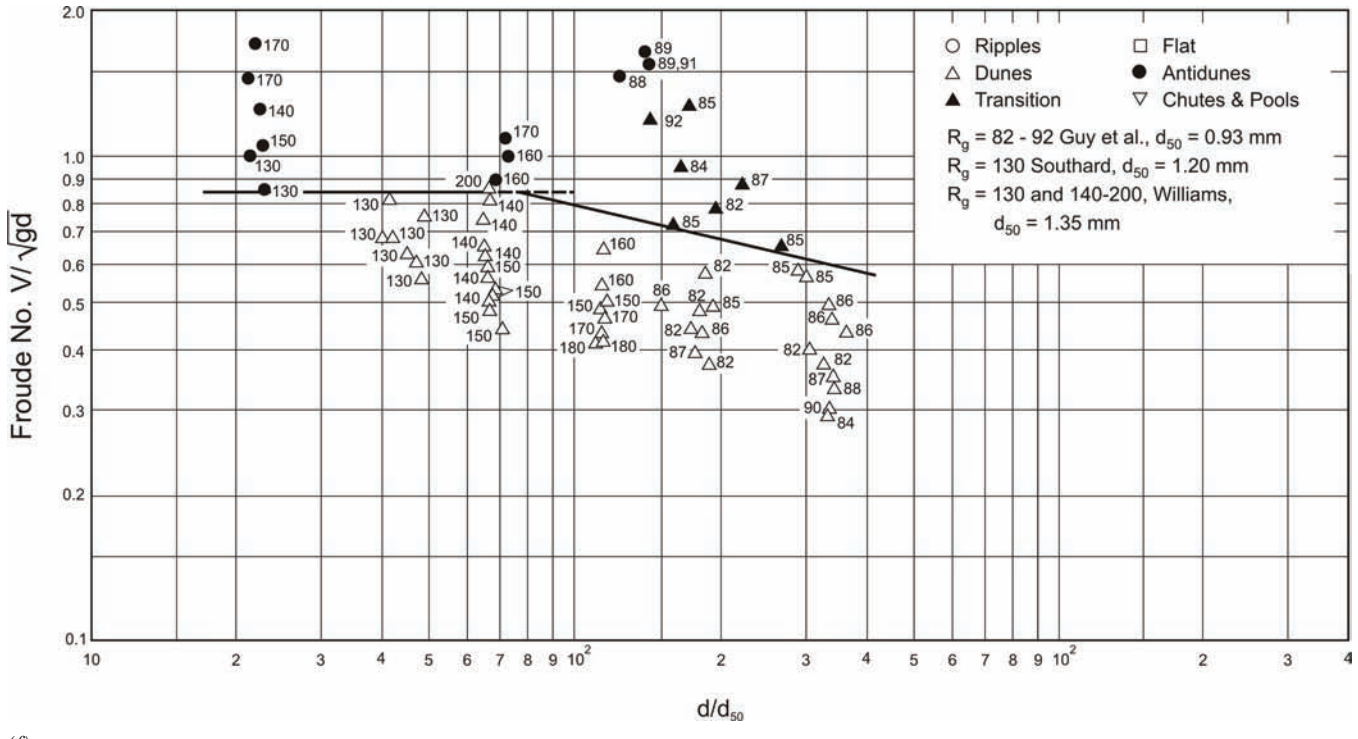


(d)



(e)

**Fig. 2-42.** Bed-form chart (a)  $Rg = 0.11$  and  $2.7$  to  $4.2$  ( $D_{50} = 0.1$  and  $0.88$  mm); (b)  $Rg = 4.5$  to  $10$  ( $D_{50} = 0.12$  to  $0.20$  mm); (c)  $Rg = 10$  to  $16$  ( $D_{50} = 0.15$  to  $0.32$  mm); (d)  $Rg = 16$  to  $26$  ( $D_{50} = 0.228$  to  $0.45$  mm); (e)  $Rg = 24$  to  $48$  ( $D_{50} = 0.40$  to  $0.57$  mm); (f)  $Rg = 82$  to  $92, 130, 140$  to  $200$  ( $D_{50} = 0.9, 1.20, 1.35$  mm) (after Vanoni 1974). (Continued)



$$\log \frac{N_s}{N_s^*} = \log 1.25 \quad \text{for } \frac{D_{50}}{\delta_v} > 2 \quad (2-136b)$$

Here  $N_s^* = 1.74 S^{-1/3}$  and  $S$  is the slope. For the upper limit of the lower regime, Brownlie proposed the following best-fit equations:

$$\log \frac{N_s}{N_s^*} = -0.2026 + 0.07026 \log \frac{D_{50}}{\delta_v} + 0.9330 \left( \log \frac{D_{50}}{\delta_v} \right)^2$$

for  $\frac{D_{50}}{\delta_v} < 2$  (2-137a)

$$\log \frac{N_s}{N_s^*} = \log 0.8 \quad \text{for } \frac{D_{50}}{\delta_v} > 2 \quad (2-137b)$$

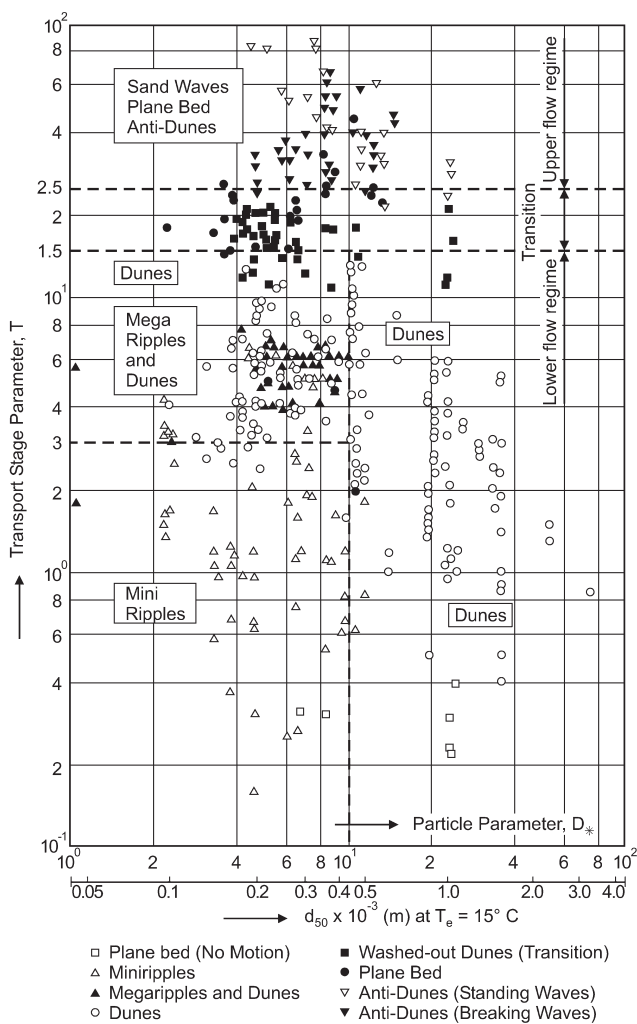


Fig. 2-43. Bedform clasification (after van Rijn 1984c, 1993).

These equations for the transition zone are shown in Fig. 2-44. It can be seen that the variable  $D_{50} / \delta_v$ , the ratio of grain size to viscous sublayer thickness, reflects the influence of viscous effects near the bed, thus indicating temperature dependence of the bedforms. A very similar flow-regime predictor, which accounts explicitly for viscous effects though the sediment fall velocity, was proposed earlier by Cruickshank and Maza (1973) and is presented below.

Karim (1995) developed bed form regime predictors in the form of limiting Froude numbers, defined as

$$F_t = 2.716 \left( \frac{H}{D_{50}} \right)^{-0.25}$$

$$F_u = 4.785 \left( \frac{H}{D_{50}} \right)^{-0.27} \quad (2-138a,b)$$

where  $F_t$  is the beginning of the transition regime (from the lower flow regime), and  $F_u$  gives the beginning of the upper regime. Based on these definitions for limiting Froude ( $Fr = U/\sqrt{gH}$ ) numbers proposed by Karim (1995), the bed form geometry type can be determined as follows:

Lower regime (ripples, dunes)

$$Fr \leq F_t$$

Transition regime (washed out dunes)

$$F_t \leq Fr \leq F_u$$

Upper regime (plane bed, antidunes)

$$Fr \geq F_u$$

Karim (1995) also used  $Fr \geq 0.8$  as a limit for the existence of antidunes.

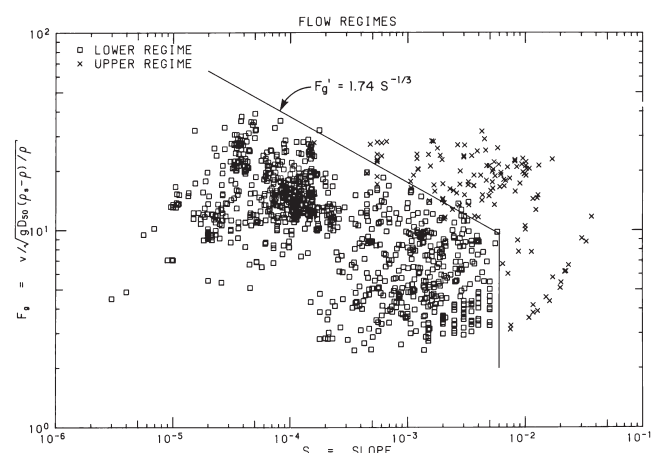


Fig. 2-44. Delineation of bedform transition zone from lower regime to upper regime (after Brownlie, 1983). This diagram generally agrees with the more detail diagrams of Vanoni (Fig. 2-42).

As part of a study on the transition of ripples to plane bed in flows over fine sand and silt, resembling Chinese rivers, van den Berg and van Gelder (1993) proposed a stability diagram (Fig. 2-45) that considers the bed shear stress component responsible for sediment transport. In the Van der Berg-Van Gelder diagram a mobility parameter related to grain roughness  $\theta'$ , as proposed by van Rijn (1984c), appears on the ordinate given by

$$\theta' = \frac{U^2}{gRD_{50}(C')^2} \quad (2-139a)$$

with

$$C' = 18 \log \frac{4H}{D_{90}} \quad (2-139b)$$

and the Valenbois-Bonnefille dimensionless particle diameter  $D_*$  in the abscissa

$$D_* = D_{50} \left( \frac{gR}{v^2} \right)^{1/3} \quad (2-139c)$$

where  $U$  is the mean flow velocity,  $H$  is the flow depth,  $R = (\rho_s - \rho) / \rho$  is the submerged specific gravity of the sediment,  $D_{50}$  and  $D_{90}$  are the sediment sizes for which 50% and 90% of the bed sediment is finer, respectively, and  $v$  is the kinematic viscosity of water. In all, 372 flume experiments with median particle diameters ranging from 11 to 4,080  $\mu\text{m}$  and flow depths up to 1 m, were used to produce the bed stability diagram shown in Fig. 2-45. A total of 262 field observations

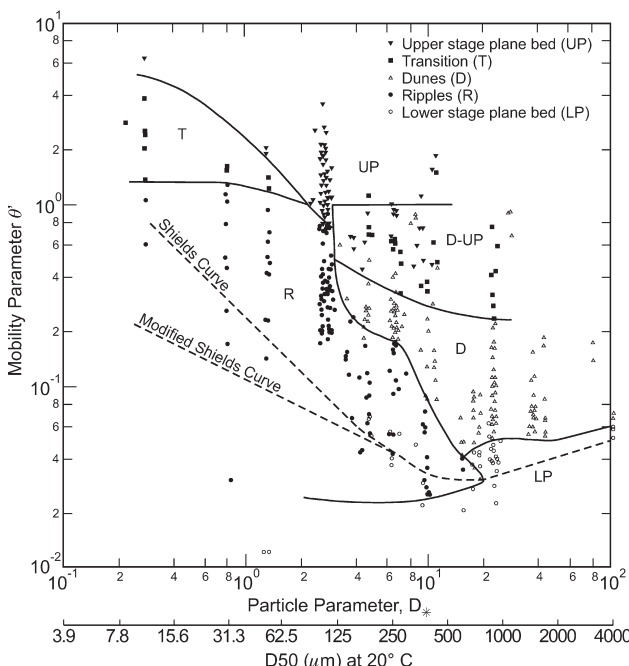


**Fig. 2-45.** Bed form in relation to grain mobility number and grain size parameter (after van den berg and van Gelder 1993).

with bed material particle sizes ranging from 80 to 5,100  $\mu\text{m}$  and flow depths ranging from 1 to 15 m were also included. This diagram shows the transition from lower regime (ripples) to upper-stage flat-bed conditions, taking place for  $D_* < 20$ . It appears that the position of the upper boundary of dune existence in fine sand as revealed from flume data is equally applicable to greater depths of natural river flows.

It is clear though that many more field observations using newer technology are needed in order to obtain more reliable bed stability diagrams (e.g., Parsons et al. 2005). The challenges associated with the production of a universal bed form stability diagram are discussed by Ashley (1990) and Best (1996).

## 2.7.5 Prediction of Equilibrium Bed Form Dimensions

The equilibrium dimensions of ripples have been studied for a wide range of sizes by a number of authors. Most studies indicate that ripple dimensions are controlled by sediment size and are independent of flow depth.

Baas (1999) proposed the following equations for ripple wavelength and height at equilibrium

$$\lambda = 75.4 \log D_{50} + 197 \quad (2-140a)$$

$$\Delta = 3.4 \log D_{50} + 18 \quad (2-140b)$$

or

$$\Delta = 18.16 D_{50}^{0.097} \quad (2-140c)$$

Raudkivi (1997) found that data on ripple length show a dependence on grain size as follows

$$\lambda = 245 D^{0.35} \quad (2-141a)$$

where the grain diameter  $D$  is in mm. According to Raudkivi (1997), the ripple steepness decreases with increasing grain size,

$$\Delta/\lambda = 0.074 D^{-0.253} \quad (2-141b)$$

Additional relations to estimate the characteristics of ripples can be found in Yalin (1985) and Mantz (1992). Coleman and Melville (1996), Nikora and Hicks (1997), Coleman and Eling (2000) and Coleman et al. (2003) provide details about the characteristics of sand wave development, in particular of wavelets, the precursors of ripples and dunes. Coleman et al. (2003) report that length of wavelets in open channels and closed conduits is a function only of particle size and

can be estimated with,  $\lambda = 175D^{0.75}$ , where both  $\Delta$  and  $\lambda$  are in mm.

For the case of dunes, Julien and Klaassen (1995) analyzed a large number of laboratory and field data and proposed the simple relation

$$\frac{\lambda}{H} = 6.25 \quad (2-143)$$

as a reasonable first approximation for dune length. They proposed the following equation for dune height;

$$\Delta = 2.5H \left( \frac{D_{50}}{H} \right)^{0.3} \quad (2-144)$$

In Julien and Klaassen's analysis, the dune length is described by

$$\lambda = 2.5\Delta \left( \frac{H}{D_{50}} \right)^{0.3} \quad (2-145)$$

In a discussion of the work of Julien and Klaassen (1995), Amsler and García (1997) noted that Julien and Klaassen's data indicate that large dune heights increased monotonically with increasing discharge (i.e., bed shear stress), which is contrary to what had been observed on the Paraná River, Argentina, and in other large rivers around the world. The Julien-Klaassen formulation implicitly assumes hydraulically rough flow conditions and does not account for the existence of viscous effects. Schreider and Amsler (1992) proposed an empirical set of curves for dune steepness which includes viscous effects. They used laboratory observation as well as data from the Missouri River, USA, the Paraná River, Argentina, and the ACOP channels in Pakistan. Their analysis implicitly accounts for the existence of smaller dunes superimposed on large dunes (see Fig. 2-35b).

In the lower regime, the geometry of bed forms refers to representative dune height  $\Delta$  and wavelength  $\lambda$  as a function of the average flow depth  $H$ , median bed particle diameter  $D_{50}$ , and other flow parameters such as the transport-stage parameter  $T$ , and the grain shear Reynolds number  $R_p$ . The bedform height and steepness predictors proposed by van Rijn (1984c) are

$$\frac{\Delta}{H} = 0.11 \left( \frac{D_{50}}{H} \right)^{0.3} (1 - e^{-0.5T}) (25 - T) \quad (2-146a)$$

and

$$\frac{\Delta}{\lambda} = 0.015 \left( \frac{D_{50}}{H} \right)^{0.3} (1 - e^{-0.5T}) (25 - T) \quad (2-146b)$$

The bed form length obtained by dividing these two equations,  $\lambda = 7.3H$ , is close to the value,  $\lambda = 2\pi H$ , proposed by Yalin (1964). The agreement with laboratory data was found to be quite good, but both curves tend to underestimate the bedform height and steepness of field data (Julien 1992; Julien and Klaassen 1995). As mentioned above, lower-regime bedforms are observed in the Mississippi River at values of  $T$  well beyond 25. Van Rijn's curves largely underpredict the dimensions of bed forms in large rivers (van Rijn 1996).

Field measurement of bed forms in large sand-bed rivers such as the Paraná in South America, the branches of the Rhine in the The Netherlands, and the Mississippi in the USA, show that the flows never leave the lower flow regime and while large dunes might elongate and disappear as the flow discharge increases, the smaller bed forms, originally superimposed on the larger sand waves, do remain along the bottom. This behavior can be observed in Fig. 2-46 for the case of the Paraná River, where the amplitude  $\Delta_D$  and steepness  $\Delta / \lambda_D$  of large dunes as well as the amplitude  $\Delta_d$  and steepness of smaller dunes  $\Delta / \lambda_d$  are plotted as a function of mean flow discharge  $Q$  for the year 1987 (Amsler and García 1997). The smaller dunes are seen to readily respond to variations in flow discharge, reaching a maximum amplitude and steepness around the peak flow discharge. On the other hand, the larger dunes display more inertia with respect to flow change, responding with an increase in amplitude just before the peak discharge and a minimum in steepness when the flow discharge reaches its largest value. It is clear that bed form predictors that have been mainly developed with laboratory data cannot be expected to capture the non-linear behavior displayed in Fig. 2-46. More research using emerging technologies (e.g., ADCP, multibeam sonars' etc.) is needed to be able to understand the morphodynamics of bed forms in large alluvial rivers (e.g., Parsons et al. 2005).

Karim (1999) used an approach similar to that of Kennedy and Odgaard (1991) whereby energy loss because of form drag is related to the head loss across a sudden expansion in an open channel. Essentially this is Carnot's formula for head loss, which had been applied earlier to bed forms by Engelund and Hansen (1967) and by Fredsøe (1989) to estimate stage-discharge relations in sand bed streams. Karim (1999) presents the following equation for the geometry of ripples, dunes, and transition bedforms as

$$\frac{\Delta}{H} = \left[ \frac{\left\{ S_e - 0.0168 \left( \frac{D_{50}}{H} \right)^{0.33} F^2 \right\} \left( \frac{\lambda}{H} \right)^{1.20}}{0.47F^2} \right]^{0.73} \quad (2-147)$$

where  $S_e$  is the energy slope. Karim further recommends solving for  $\lambda / H$  using: the equation of Julien and Klaassen

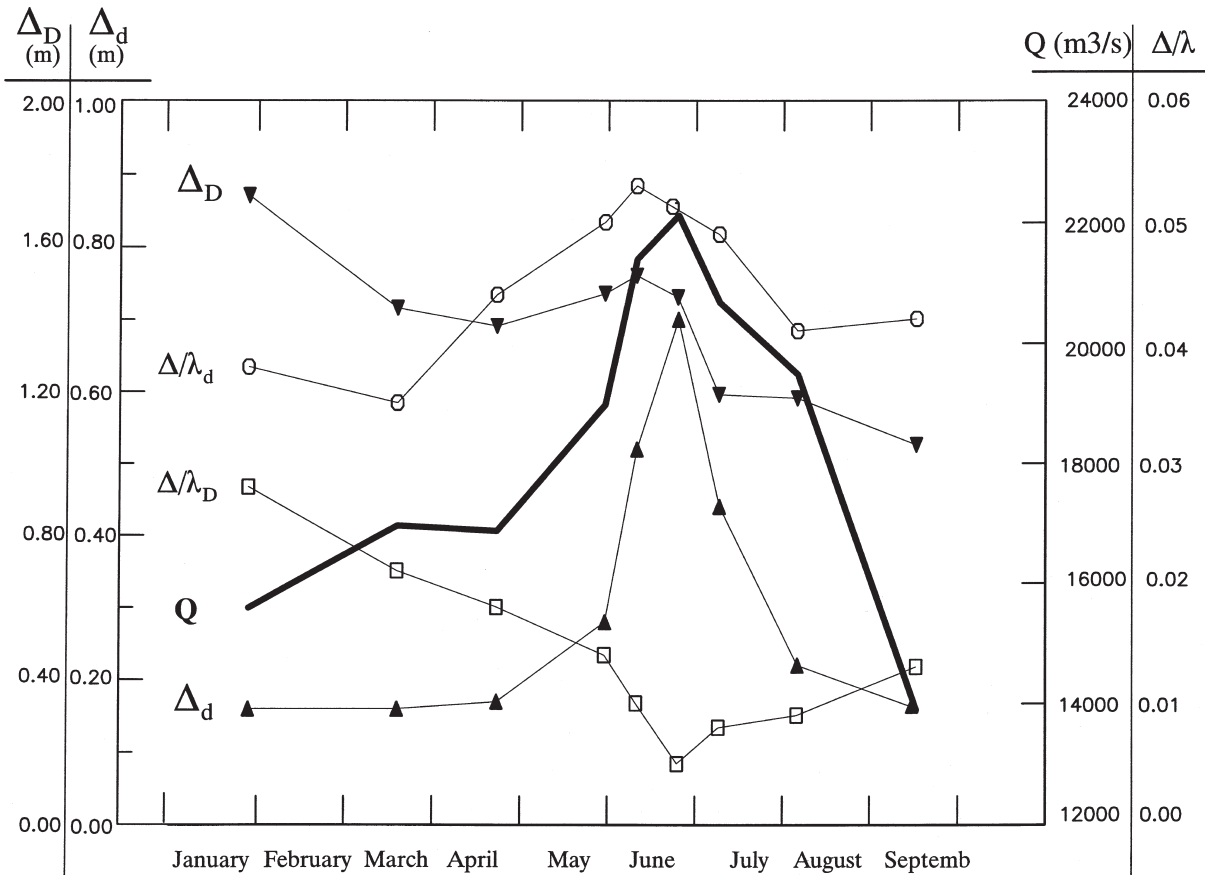


**Fig. 2-46.** Variation of bed form characteristics, large dunes with superimposed smaller dunes, with flow discharge for a reach of the middle Paraná River (After Amsler and García 1997).

(1995), i.e.,  $\lambda / H = 6.25$  for dunes; Yalin's (1964) relation for ripples, i.e.,  $\lambda = 1000 D$ ; and Kennedy's equation for the wavelength of antidunes, i.e.,  $\lambda / H = 2\pi Fr^2$ , where  $Fr$  is the Froude number. Karim (1999) compares his approach (Eq. 2-147) with the relations of Yalin (1964), Ranga Raju and Soni (1976), Allen (1978), van Rijn (1984), Kennedy and Odgaard (1991), Julien and Klaassen (1995), and Karim (1995). Karim's method performs as well as or better than the rest of the relations tested. However, although it performs fairly well when tested with laboratory data, it does not capture the behavior observed in the field. At the same time, Karim's approach is one of the few available methods for predicting sand wave equilibrium dimensions over a wide range of conditions. It can be applied to various bed forms, i.e., ripples, dunes, antidunes/standing waves, and transitional bed regimes. However, it needs to be tested with more observations from large alluvial rivers.

Most of the work in the literature has concentrated on obtaining equilibrium dimensions of ripples and dunes. One exception is the approach proposed by Fredsøe (1982) to estimate the evolution of dunes, all the way from inception

to fully developed stage. Using observations of flow over a negative bottom step, Fredsøe (1982) made an analogy with the flow separation that takes place over the top of a dune. Fredsøe's model accounts for the effect of suspended load and bed load on the dimensions of dunes as the flow intensity increases. Using computations of bed shear stress along a dune profile (e.g., McLean and Smith 1986; Mendoza and Shen 1990), Fredsøe's model was used to solve an approximate analytical expression for dune shape (Fredsøe and Deigaard 1992, p267). Recently, Tjerry and Fredsøe (2005) estimated the bed shear stress needed in Fredsøe's dune model with a two-equation turbulence model, and used these results to investigate the shape and dimensions of dunes caused by a turbulent flow over an erodible bed. Other attempts at developing analytical expressions similar to Fredsøe's for the shape of dunes and ripples include the work among others of Haque and Mahmood (1985, 1986).

The evolution from wavelets to ripples to dunes and to megadunes seems to suggest that there is self-similarity in the mechanics of sand waves, as implied by the work of Raudkivi and Witte (1990), Coleman and Melville (1994),

Nikora and Hicks (1997), and Jerolmack et al. (2006). This hypothesis is supported by the work of Flemming (2000) who prepared a log-log plot of height ( $\Delta$ ) versus wavelength ( $\lambda$ ) for 1,491 observations of subaqueous bedforms. The collapse of the data was rather remarkable and a single “discontinuity” could be observed in the continuum of lengths at slightly less than 1 m, which provides support for the distinction between current ripples and large-scale bed forms. The best fit to the data yields

$$\Delta = 0.0677 \lambda^{0.81} \quad (2-148)$$

where both the wavelength  $\lambda$  and the wave height  $\Delta$  are in meters. The sandwave length covers the range from wavelets (a few centimeters long) observed in the laboratory to megadunes (several hundred meters long) observed in large alluvial rivers (Fig. 2-35b).

The development of a reliable bed form predictor for large alluvial flows is one of the outstanding problems in river sedimentation (e.g., Schumm and Winkley 1994). In order to more completely understand the morphodynamics of river dunes, a fuller appreciation is needed of the complex links between flow turbulence, bed morphology, and sediment transport (ASCE 2002; Best 2005; Parker and García 2006). Future research on relations between sediment transport mechanics and dune morphology should focus on:

- Numerical modeling applied to a wide range of flow and bed-material conditions that would allow an analysis of the adjustment of dune morphology, particularly steepness and lee slope angle, to both bed load and suspended load (e.g., Zedler and Street 2001; Tjerry and Fredsøe 2005).
- Detailed field studies of flow, sediment transport and the evolving morphology of individual dunes using modern technology such as acoustic Doppler current profilers and velocimeters, *in-situ* particle size transmissometers and multibeam echosounders to capture the three-dimensional river-bed morphology shown in the cover of this manual (e.g., Parsons et al. 2005).
- Laboratory experiments on and numerical simulations of fundamental processes such as sediment entrainment into suspension and particle-turbulence interaction in the presence of bed forms (e.g. Maddux et al. 2003a; Coleman et al. 2003; Schmeekle and Nelson 2003).
- Relations amongst dune celerity, crest planform, dune profile shape, water temperature, and sediment transport mechanics (e.g., Kostaschuk 2006; Serra and Vionnet 2006).

## 2.7.6 Effect of Bed Forms on River Stage

The presence or absence of bed forms on the bed of a river can lead to curious effects on river stage. According to the

standard Manning-type relation for a nonerodible bed, the following should hold:

$$U = \frac{1}{n} H^{2/3} S^{1/2} \quad (2-149a)$$

Here, the channel is assumed to be wide enough to allow the hydraulic radius to be replaced with the depth  $H$ . According to Eq. (2-149a), if energy slope remains relatively constant, depth should increase monotonically with increasing velocity. This would indeed be the case for a rigid bed. In a sand-bed stream, however, resistance decreases as  $U$  increases over a wide range of conditions.

At equilibrium,

$$\tau_b = \rho C_f U^2 = \rho g H S \quad (2-149b)$$

This decrease in resistance implies that depth does not increase as rapidly in  $U$  in a movable-bed stream as it would for a rigid-bed open channel. In fact, as the transition to upper regime is approached, the bed forms can be wiped out quite suddenly, resulting in a dramatic decrease in resistance. The result can be an actual decrease in depth as velocity increases. This phenomenon was documented for the case of the Padma River, Bangladesh, by Stevens and Simons (1973) and predicted numerically by Chollet and Cunge (1980), as shown in Fig. 2-47. This plot shows how Manning's  $n$  decreases as the flow discharge increases and the dunes are first elongated and finally washed out. Notice that the numerical model predictions agree very well with the observations for the lower regime conditions but overestimate the value of Manning's  $n$  in the upper regime where most of the flow resistance should be mainly due to grain friction. Even for one-dimensional computations, this remains a challenging problem for river engineers as shown in Chapter 14.

The effect of the transition phenomenon on flow-stage discharge is best illustrated with a flow resistance diagram first proposed by Cruickshank and Maza (1973) and shown in Fig. 2-48(a). Flume and river data were used to develop this dimensionless diagram showing the transition from the lower regime to the upper regime. In the transition region the flow depth is seen to decrease as the flow velocity increases. The straight part of the curves in the diagram can be expressed with exponential curves obtained by a least square regression analysis. The original Cruickshank-Maza empirical relations have been adapted to follow the notation used in this chapter.

For the lower regime, the mean flow velocity  $U$  can be estimated with

$$\frac{U}{\sqrt{gRD_{50}}} = 6.03 \frac{v_{s50}}{\sqrt{gRD_{50}}} \left( \frac{H}{D_{84}} \right)^{0.634} S^{0.456} \quad (2-150a)$$

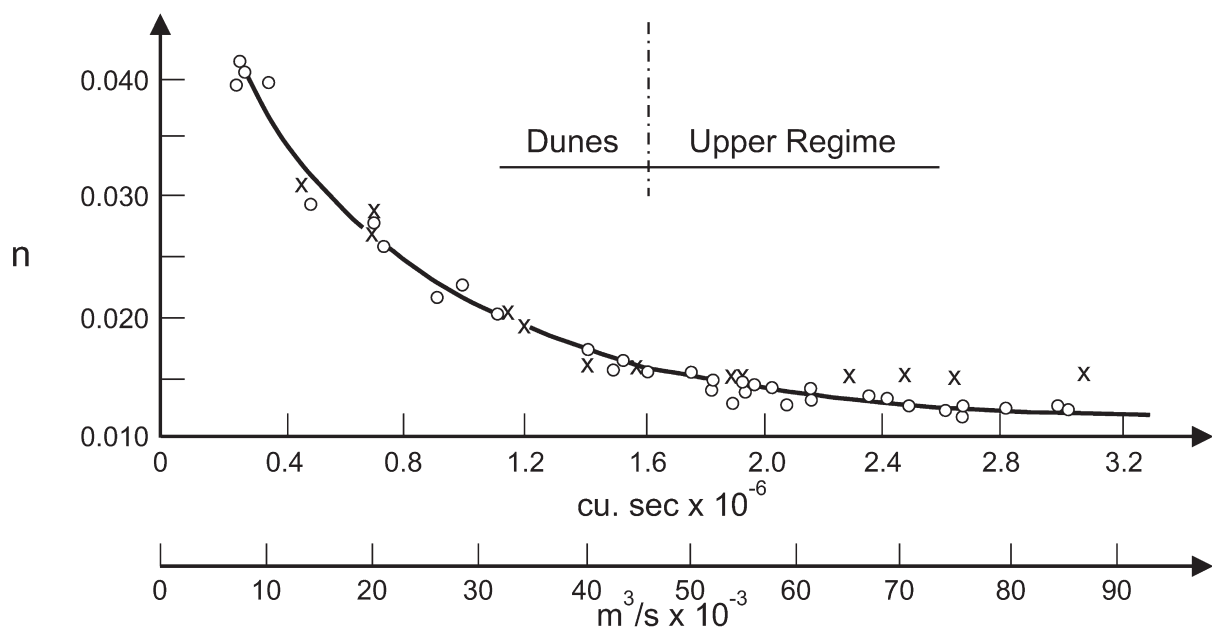
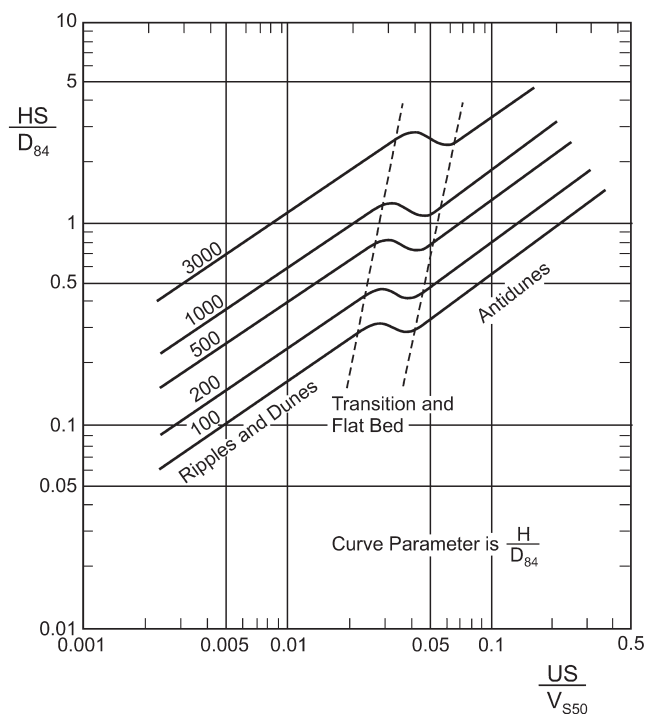
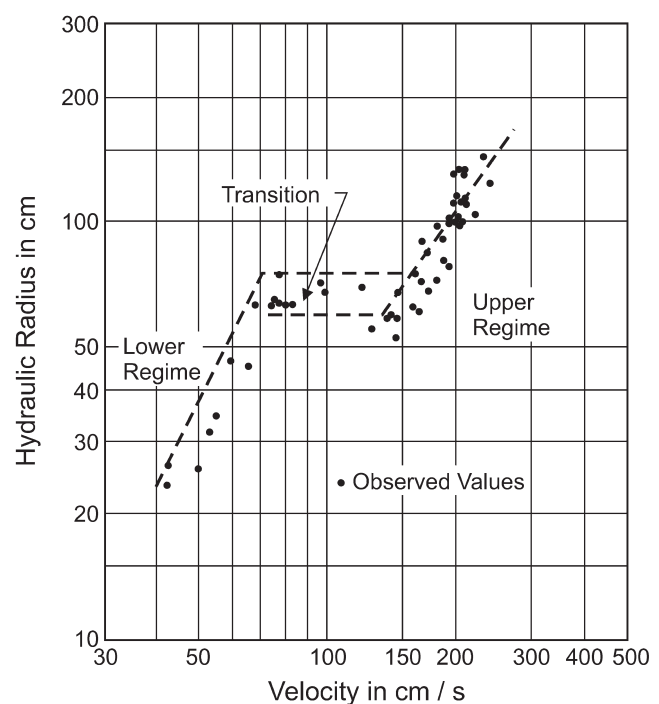


**Fig. 2-47.** Variation of Manning's  $n$  with flow discharge for the Padma River, Bangladesh. (o) observations of Stevens and Simmons and (x) computations of Chollet and Cunge (1980).



(a)



(b)

**Fig. 2-48.** (a) Cruickshank-Maza Flow Resistance Predictor, and (b) Stage-Discharge curve for Rio Grande near Bernalillo, New Mexico, estimated with Cruickshank-Maza predictor.

which is valid for,

$$\frac{1}{S} \geq 70 \left( \frac{H}{D_{84}} \right)^{0.350} \quad (2-150b)$$

For the upper regime, the mean flow velocity  $U$  can be estimated with

$$\frac{U}{\sqrt{gRD_{50}}} = 5.45 \frac{v_{s50}}{\sqrt{gRD_{50}}} \left( \frac{H}{D_{84}} \right)^{0.644} S^{0.352} \quad (2-150c)$$

$$\frac{1}{S} \leq 55 \left( \frac{H}{D_{84}} \right)^{0.382} \quad (2-150d)$$

where,

$U$  = mean flow velocity;

$H$  = flow depth;

$S$  = energy slope (same as channel slope for uniform flow);

$v_{s50}$  = fall velocity for sediment size  $D_{50}$ ;

$D_{50}$  = median grain size used to determine the fall velocity  $v_{s50}$ ; and

$D_{84}$  = sediment size for which 84% of bed-material is finer;

These relations are recommended for median grain sizes ( $D_{50}$ ) in the range from 0.2 to 2 mm. The range of geometric standard deviation ( $\sigma_g$ ) of the bed-material size distribution data, went from 1.2 to 2.5. The submerged specific gravity was the same for all the data ( $R=1.65$ ). The exponents for the flow depth ( $H$ ) and energy slope ( $S$ ) are similar to those reported by Simmons and Albertson (1963) for stable alluvial channels. In fact, the exponents are not very different from those found in Manning's equation (Eq. 2-149a).

Cruickshank and Maza used these relations to compute the stage-discharge relation shown in Fig. 2-48(b). The data shown correspond to the Rio Grande near Bernalillo, New Mexico. It is seen that the Cruickshank-Maza relations capture the behavior of the hydraulic radius, which increases with flow velocity along the lower regime (ripples and dunes), remains almost constant for a wide range of flow velocities during the transition (flat bed), and continues to increase again in the upper regime due to the development of antidunes.

It is often found that the discharge at which the dunes are obliterated is a little below bank-full in sand-bed streams with medium to high bed slopes. As a result, flooding is not as severe as it would be otherwise. The precise point of transition is generally different, depending on whether the discharge is increasing or decreasing. This behavior can lead to double-valued stage-discharge relations as shown in

Fig. 2-48(b). The same behavior does not seem to occur in large, low-slope sand-bed streams, because such streams never enter upper-regime conditions, even at or above bank-full discharge (e.g., Amsler and Prendes 2000; Wright and Parker 2004b). In the case of the Paraná River, Argentina, shown in Fig. 2-46, it is observed that the larger dunes elongate and their steepness decreases as the flow discharge increases. On the other hand, the smaller dunes, originally superimposed on the larger ones (see Fig. 2-35b), persist along the bottom of the river and their steepness reaches a maximum for the peak flow discharge. The Froude number  $Fr$  is in general less than 0.25, even during large floods, hence the flow never leaves the lower regime (Amsler and García 1997).

In the case of the Missouri River, temperature effects seem to control the transition from plane bed to a bed with dunes (Shen et al 1978). Southard (1989) used the observations of Shen et al to produce a flow velocity versus sediment size diagram, showing that as the water gets colder and the temperature drops, dunes vanish and plane bed conditions are observed in the Missouri River. Temperature effect on the dynamics of bed forms is a topic that needs to be addressed in the future so that flood stages can be estimated for different climate conditions.

## 2.8 BED FORMS, FLOW RESISTANCE, AND SEDIMENT TRANSPORT

### 2.8.1 Form Drag and Skin Friction

As has been seen, bed forms can have a profound influence on flow resistance, and thus on sediment transport in an alluvial channel. To characterize the importance of bed forms in this regard, it is of value to consider the forces that contribute to the drag force on the bed.

Consider, for example, the case of normal flow in a wide, rectangular channel. In the presence of bed forms, Eq. (2-1) must be amended to

$$\bar{\tau}_b = \rho g H S \quad (2-151)$$

where  $\bar{\tau}_b$  is an effective boundary shear stress, where the overbar denotes averaging over the bed forms, and can be defined as the streamwise drag force per unit area, where  $H$  now represents the depth averaged over the bed forms.

In most cases of interest, the two major sources of the effective boundary shear stress  $\bar{\tau}_b$  are skin friction, which is associated with the local shear stresses, and form drag, which is associated with the pressure. That is,

$$\bar{\tau}_b \equiv \tau_{bs} + \tau_{bf} \quad (2-152)$$

where  $\tau_{bs}$  is the shear stress component due to skin friction and  $\tau_{bf}$  is the shear stress component due to form drag.

The important thing to realize is that form drag results from the net pressure distribution over an entire bed form. At any given point along the surface of the bed form, the pressure force acts normal to the body. For this reason, form drag is directly effective neither in moving sediment as bed load nor in entraining sediment into suspension. In the case of dunes in rivers, the flow usually separates in the lee of the crest, so that form drag is often substantial. The part of the effective shear stress that governs sediment transport is thus seen to be the skin friction.

To render any of the bed-load formulas presented in Section 2.6.4 valid in the presence of bed forms, it is necessary to replace the Shields stress  $\tau^*$  by the Shields stress  $\tau_s^*$  associated with skin friction only:

$$\tau_s^* = \frac{\tau_{bs}}{\rho g RD} \quad (2-153)$$

The fact that the form drag needs to be excluded for the purposes of computing sediment transport does not by any means imply that it is unimportant. It is often the dominant source of boundary resistance, and thus plays a crucial role in determining the depth of flow (e.g., Brownlie 1983). This will be considered in more detail below.

## 2.8.2 Shear Stress Partitions

**2.8.2.1 The Einstein Partition** Einstein (1950) was the first to recognize the necessity of distinguishing between skin friction and form drag. He proposed the following simple scheme to partition the two. Eq. (2-131) is amended to represent an effective boundary shear stress averaged over bed forms,

$$\bar{\tau}_b = \rho C_f U^2 \quad (2-154)$$

where  $C_f$  now represents a resistance coefficient that includes both skin friction and form drag. For given flow velocity  $U$ , Einstein computes the skin friction as

$$\tau_{bs} = \rho C_{fs} U^2 \quad (2-155)$$

where  $C_{fs}$  is the frictional resistance coefficient that would result if bed forms were absent. For example, in the case of rough turbulent flow, Eq. (2-19) may be used:

$$C_{fs} = \left[ \frac{1}{\kappa} \ln \left( 11 \frac{H_s}{k_s} \right) \right]^{-2} \quad (2-156)$$

In fact, Einstein presents a slightly different formula, which allows for turbulent smooth and transitional flow as well. Here the analysis is only done for rough flow conditions

without any loss of generality. The parameter  $H_s$  denotes the depth that would result in the absence of bedforms (but with  $U$  held constant). This depth is necessarily less than  $H$ , because the resistance is less in the absence of bed forms. The remaining problem is how to calculate  $H_s$ . Einstein restricts his arguments to the case of normal (steady, uniform) flow. In this case, Eq. (2-151) holds; that is,

$$\bar{\tau}_b = \rho C_f U^2 = \rho g H S \quad (2-157a)$$

$$\tau_{bs} = \rho C_{fs} U^2 = \rho g H_s S \quad (2-157b)$$

Now between Eqs. (2-154) and (2-157b), the following relation is obtained for  $H_s$ :

$$H_s = \frac{U^2}{gS} \left[ \frac{1}{\kappa} \ln \left( 11 \frac{H_s}{k_s} \right) \right]^{-2} \quad (2-158)$$

For given values of  $U$ ,  $k_s$ , and  $S$  (averaged over bedforms), Eq. (2-158) is easily solved iteratively for  $H_s$ . Once  $H_s$  is known, it is not difficult to complete the partition. From Eq. (2-152), it follows that

$$\tau_{bf} = \bar{\tau}_b - \tau_{bs} \quad (2-159)$$

In analogy to Eqs. (2-152), (2-153), and (2-155), the following definitions are made,

$$\tau_{bf} = \rho C_{ff} U^2 = \rho g H_f S \quad (2-160)$$

from which it follows that

$$C_f = C_{fs} + C_{ff} \quad (2-161a)$$

$$H = H_s + H_f \quad (2-161b)$$

Here  $C_{ff}$  denotes the resistance coefficient associated with form drag, and  $H_f$  denotes the extra depth (compared to the case of skin friction alone) that results from form drag.

Up to this point, it is assumed that  $U$ ,  $S$ , and  $k_s$  are given. If, for example,  $H$  is also known,  $\bar{\tau}_b$  can be calculated from Eq. (2-151). After  $H_s$ ,  $C_{fs}$ , and  $\tau_{bs}$  are computed from Eqs. (2-156) to (2-158), it is possible to compute  $\tau_{bf}$ ,  $H_f$ , and  $C_{ff}$  from Eqs. (2-159) and (2-161).

For example, consider a sand-bed stream at a given cross section with a slope of 0.0004, a mean depth of 2.9 m, a median bed sediment size of 0.35 mm, and a discharge per unit width  $q = U \times H = 4.4 \text{ m}^2/\text{s}$ . Assume that the flow

is under near-normal conditions. Compute values of  $\tau_{bs}$ ,  $\tau_{bf}$ ,  $C_{fs}$ ,  $C_{ff}$ ,  $H_s$ , and  $H_f$ .

The mean flow velocity is given by  $U = 4.4/2.9 = 1.52$  m/s. An appropriate estimate of  $k_s$  for a sand-bed stream is  $k_s = 2.5 D_{50}$ .

By solving Eq. (2-158) by successive approximations, it is found that  $H_s = 1.047$  m. The following values then hold:

$$\tau_{bs} = 4.11 \text{ N/m}^2 \quad (\tau_s^* = 0.725)$$

$$\tau_{bf} = 7.27 \text{ N/m}^2 \quad (\tau_f^* = 1.283)$$

$$\bar{\tau}_b = 11.38 \text{ N/m}^2 \quad (\tau^* = 2.008)$$

$$C_{fs} = 0.00178$$

$$C_{ff} = 0.00315$$

$$C_f = 0.00493 \quad (C_f^{-1/2} = 14.5)$$

$$H_s = 1.047 \text{ m}$$

$$H_f = 1.842 \text{ m}$$

$$H = 2.9 \text{ m}$$

In these relations,

$$\tau_f^* = \frac{\tau_{bf}}{\rho g R D} \quad (2-162)$$

denotes a form-induced Shield stress. In this case, only some 30% of the total Shields stress (skin + form) contributes to the transport of sediment.

The Einstein method provides a way of partitioning the boundary shear stress if the flow is known. It does not provide a direct means of computing form drag. A method proposed by Nelson and Smith (1989) overcomes this difficulty when dune height and wavelength are known.

**2.8.2.2 The Nelson-Smith Partition** Nelson and Smith (1989) consider flow over a dune; the flow is taken to separate in the lee of the dune. This method builds on the work of Smith and McLean (1977) and is very similar to the method proposed independently by Kikkawa and Ishikawa (1979). Based on experimental observations in the Columbia River, Nelson and Smith use the following relation for form drag:

$$D_{ffs} = \frac{1}{2} \rho c_D B \Delta U_r^2 \quad (2-163)$$

Here  $D_{ffs}$  denotes that portion of the streamwise drag force  $D_{fs}$  that is due to form drag,  $B$  is the channel width, and  $U_r$  denotes a reference velocity to be defined below.

They estimate the drag coefficient as  $c_D = 0.21$  from measurements taken in the Columbia River (Smith and McLean 1977).

It follows that

$$\tau_{bf} = \frac{1}{2} \rho c_D \frac{\Delta}{\lambda} U_r^2 = \frac{D_{ffs}}{B \lambda} \quad (2-164)$$

The reference velocity  $U_r$  is defined to be the mean velocity that would prevail between  $z = k_s$  and  $z = \Delta$  if the bed forms were not there. From the logarithmic profile represented by Eq. (2-17a), this is found to be given by

$$\frac{U_r}{\sqrt{\tau_{bs}/\rho}} = \frac{1}{\kappa} \left[ \ln \left( 30 \frac{\Delta}{k_s} \right) - 1 \right] \quad (2-165)$$

It is now assumed that a rough logarithmic law with roughness  $k_s$  prevails from  $z = k_s$  to  $z = \Delta$ , and a different rough logarithmic law with roughness  $k_c$  prevails from  $z = \Delta$  to  $z = H$ . Here  $k_c$  represents a composite roughness length, including the effects of both skin or grain friction and form drag. The two flow velocity distribution laws are thus given by

$$\frac{\bar{u}(z)}{\sqrt{\tau_{bs}/\rho}} = \frac{1}{\kappa} \ln \left( 30 \frac{z}{k_s} \right), \quad k_s < z < \Delta \quad (2-166a)$$

$$\frac{\bar{u}(z)}{\sqrt{(\tau_{bs} + \tau_{bf})/\rho}} = \frac{1}{\kappa} \ln \left( 30 \frac{z}{k_c} \right), \quad \Delta < z < H \quad (2-166b)$$

Nelson and Smith match the above two laws at the level  $z = \Delta$  (i.e., the top of the dune). After some manipulation, it is found that

$$\frac{\tau_{bs} + \tau_{bf}}{\tau_{bs}} = \left[ \frac{\ln(30 \Delta / k_s)}{\ln(30 \Delta / k_c)} \right]^2 \quad (2-167a)$$

The partition requires a prior knowledge of total boundary shear stress  $\bar{\tau}_b = \tau_{bs} + \tau_{bf}$ , as well as roughness height  $k_s$ , dune height  $\Delta$ , and dune wavelength  $\lambda$ . Between Eqs. (2-163) and (2-164),

$$\tau_{bf} = \bar{\tau}_b - \tau_{bs} = \frac{1}{2} c_D \frac{\Delta}{\lambda \kappa^2} \left[ \ln \left( 30 \frac{\Delta}{k_s} \right) - 1 \right]^2 \tau_{bs} \quad (2-167b)$$

This equation can be solved for  $\tau_{bs}$ , and thus  $\tau_{bf}$ . The value of the composite roughness  $k_c$  is then obtained from Eq. (2-167a).

For example, chosen to be rather similar to the previous one, let  $H = 2.9$  m,  $S = 0.0004$ ,  $k_s = 2.5 D_{50}$ ,  $D_{50} = 0.35$  mm,

$\Delta = 0.4$  m, and  $\lambda = 15$  m. The technique, which requires no iteration, yields the following results:

$$\tau_{bs} = 4.45 \text{ N/m}^2 \quad (\tau_s^* = 0.785)$$

$$\tau_{bf} = 6.93 \text{ N/m}^2 \quad (\tau_f^* = 1.223)$$

$$\bar{\tau}_b = 11.38 \text{ N/m}^2 \quad (\tau^* = 2.008)$$

$$k_c = 0.0311 \text{ m}$$

$$C_{fs} = 0.00130$$

$$C_{ff} = 0.00203$$

$$C_f = 0.00333 \quad (C_f^{-1/2} = 17.3)$$

$$H_s = 1.134 \text{ m}$$

$$H_f = 1.766 \text{ m}$$

$$H = 2.9 \text{ m}$$

In computing friction coefficients, the Keulegan relationship was used for the depth-averaged flow velocity:

$$\frac{U}{\sqrt{(\tau_{bs} + \tau_{bf})/\rho}} = \frac{1}{\kappa} \ln \left( 11 \frac{H}{k_c} \right) \quad (2-168a)$$

From this equation, an expression for the composite roughness is obtained,

$$k_c = \frac{11H}{e^{(\kappa U/u_*)}} \quad (2-168b)$$

Here the shear velocity includes the effect of grain friction and form drag, i.e.,  $u_* = \sqrt{(\tau_{bs} + \tau_{bf})/\rho}$ .

The Nelson-Smith method does not require the assumption of quasi-normal flow; the user must, however, have information about the bedform dimensions. This method has been extended by García and Parker (1993) to the case where the boundary is hydraulically smooth (i.e.,  $k_s < \delta_v = 11.6v/u_*$ ) and viscous effects are present. In this case, the bed shear stress associated with form drag can be estimated with

$$\tau_{bf} = \bar{\tau}_b - \tau_{bs} = \frac{1}{2} C_D \frac{\Delta}{\lambda \kappa^2} \left[ \ln \left( 9 \frac{u_{*s} \Delta}{v} \right) - 1 \right]^2 \tau_{bs} \quad (2-168c)$$

This expression was used to remove the effect of ripples in laboratory experiments on eroding density currents. It can also be applied to remove the effect of ripples on flow

resistance in open channel flows (e.g., Ikeda and Asaeda 1983).

**2.8.2.3 The Engelund-Fredsøe Partition** This method is based on the ideas of Engelund, who first suggested that the head loss due to the expansion of the flow right after a dune's crest, and thus form drag, could be estimated with Carnot's head loss formula (Fredsøe and Deigaard 1992, p. 280). Similar to the Einstein partition method, the total dimensionless bed stress due to skin friction plus form drag (Fredsøe 1982), is expressed as

$$\tau^* = \tau_s^* + \tau_f^* \quad (2-169a)$$

In this method, the component of the dimensionless shear stress due to skin (grain) friction is

$$\tau_s^* = \frac{u_{*s}^2}{gRD} = \frac{U^2}{RgD} \left( \frac{u_{*s}}{U} \right)^2 \quad (2-169b)$$

Here,  $R = (\rho_s / \rho) - 1$  = submerged specific gravity of sediment ( $R = 1.65$  for sand), and  $C_{fs} = (u_{*s} / U)^2$  = skin friction coefficient (Eq. 2-156). The contribution to the dimensionless shear stress by the form drag is estimated with Carnot's formula,

$$\tau_f^* = \frac{1}{2} \frac{U^2}{RgD} \frac{\Delta}{H} \frac{\Delta}{\lambda} \quad (2-169c)$$

Combining Eqs. (2-169a), (2-169b), and (2-169c), yields

$$\tau^* = \tau_s^* + \tau_f^* = \tau_s^* \left[ 1 + \frac{1}{2} \frac{\Delta}{H} \frac{\Delta}{\lambda} C_{fs}^{-1} \right] \quad (2-169d)$$

Fredsøe (1982) tested the relationship implied in Eq. (2-169d) between total dimensionless shear stress  $\tau^*$  and contribution made by skin friction  $\tau_{bs}^*$  with the experimental observations made by Guy et al. (1966) at Fort Collins, Colorado. Fredsøe (1989) has also used this approach to compute stage-discharge curves in small sand-bed streams.

Fredsøe (1982) and Fredsøe and Deigaard (1992) have formulated equations to estimate the dune parameters (i.e.,  $\Delta / H$  and  $\Delta / \lambda$ ) in Eq. (2-169d). Following the example presented earlier, let  $H = 2.9$  m,  $C_{fs} = 0.00178$  (from Eq. 2-156),  $\Delta = 0.4$  m, and  $\lambda = 15$  m. Substituting these values into Eq. (2-169d), yields  $\tau^* / \tau_s^* = 2.03$ . This value is close to those estimated for the same ratio with the Einstein ( $\tau^* / \tau_s^* = 2.77$ ) and Nelson-Smith ( $\tau^* / \tau_s^* = 2.56$ ) partitions. This is not surprising because the Engelund-Fredsøe partition combines elements of both of these approaches.

### 2.8.3 Empirical Techniques for Stage-Discharge Relations

To use either the Einstein, Nelson-Smith, or Engelund-Fredsoe partition, it is necessary to know in advance the total effective boundary shear stress  $\bar{\tau}_b$ . In general, this is not known. As a result, the relations in themselves cannot be used to predict the boundary shear stress (as well as the contributions from skin friction and form drag), and thus depth  $H$ , for a flow of, say, given slope  $S$  and discharge per unit width  $q_w$ .

A number of empirical techniques have been proposed to accomplish this. Only a few selected ones are presented herein; they are known to perform at least reasonably well for sand-bed streams with dune resistance.

**2.8.3.1 The Einstein-Barbarossa Method** The method of Einstein and Barbarossa (1952) is applicable for the case of dune resistance in sand-bed streams. It is of historical value and this is the main motivation for presenting it here. This method assumes an empirical relation of the following form:

$$C_{ff} = f(\tau_{s35}^*) \quad (2-170a)$$

Here

$$\tau_{s35}^* = \frac{\tau_{bs}}{\rho g R D_{35}} \quad (2-170b)$$

$$B = B(H) \quad (2-171)$$

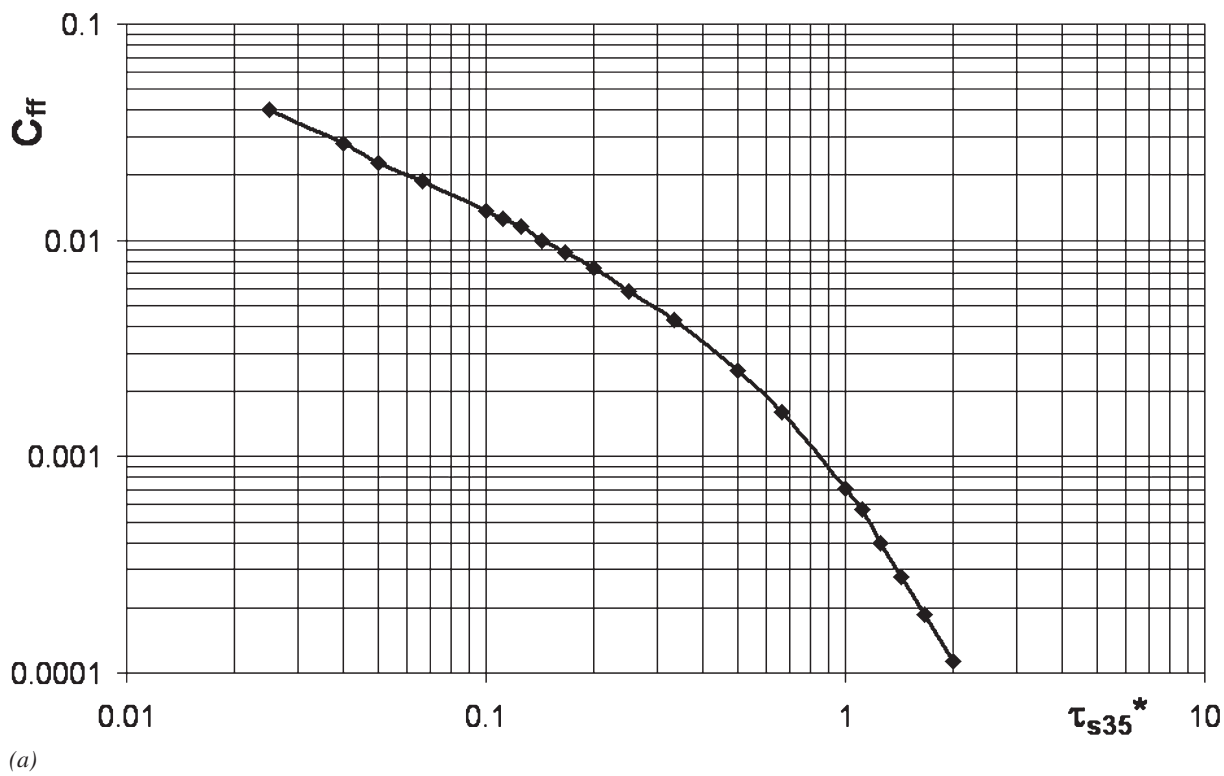
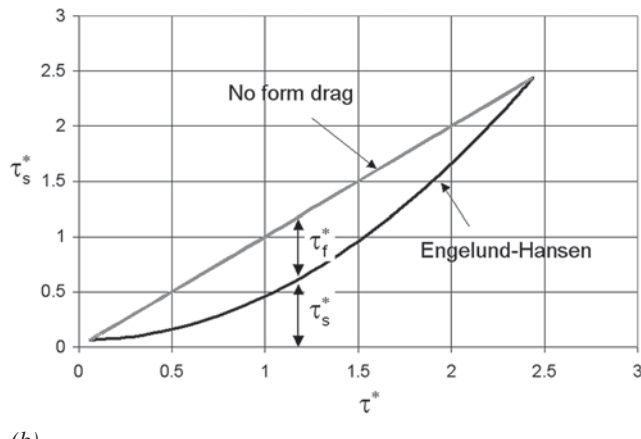


**Fig. 2-49.** Flow resistance diagrams (a) Einstein and Barbarossa (1952) and (b) Engelund and Hansen (1967).

An adaptation of the original Einstein-Barbarossa bar-resistance diagram, given implicitly by Eq. (2-170a), is shown in Fig. 2-49(a). Note that it implies that the friction coefficient for the bed forms  $C_{ff}$  declines for increasing  $\tau_{s35}^*$ . That is, the relation applies in the range for which increased intensity of flow causes a decrease in form drag (i.e., the transition from dunes to flat bed). A flow resistance diagram like the one shown in Fig. 2-49(a) can be developed for any sand-bed or gravel-bed stream provided that flow stage and discharge observations for a wide range of conditions, as well as bed-material characteristics, are available.

In the Einstein-Barbarossa method,  $C_{ff}$  is computed from a relation very similar to Eq. (2-156). That relation is used here to illustrate the method, which employs the Einstein partition for skin friction and form drag.

The method is now used to synthesize a depth-discharge relation; that is, a relation between  $H$  and water discharge  $Q$  is obtained. It is assumed that the river slope  $S$  and the sizes  $D_{50}$  and  $D_{35}$  are known. The river is taken to be sufficiently wide so that the hydraulic radius  $R_h \equiv H$ ; otherwise,  $R_h$  should be used in place of  $H$ . In addition, cross-sectional shape is known, allowing for specification of channel width as a function of flow depth:



(b)

**Fig. 2-49.** Flow resistance diagrams (a) Einstein and Barbarossa (1952) and (b) Engelund and Hansen (1967). (*Continued*)

It is also assumed that auxiliary relations for area  $A$ , wetted perimeter  $P$  and hydraulic radius  $R_h$  as functions of  $H$  are known. A range of values of  $H_s$  is arbitrarily assumed, ranging from a very shallow depth to near-bankfull depth (recall that  $H_s < H$ ). For each value of  $H_s$ , the calculation proceeds as follows:

$$H_s \rightarrow C_{fs} \quad \text{Eq. (2-156)}$$

$$C_{fs}, H_s \rightarrow U \quad \text{Eq. (2-158)}$$

$$H_s \rightarrow \tau_{bs} \rightarrow \tau_{s35}^* \quad \text{Eqs. (2-157b), (2-170b)}$$

$$\tau_{s35}^* \rightarrow C_{ff} \quad \text{Eq. (2-170a); use the diagram in Fig. 2-49a}$$

$$C_{ff}, U \rightarrow H_f \quad \text{Eq. (2-160)}$$

$$H = H_s + H_f \quad \text{Eq. (2-161b)}$$

$$Q = U H B \quad \text{Eq. (2-171)}$$

The result may be plotted in terms of  $H$  versus  $Q$  for the desired depth-discharge relation.

The analysis may be continued for bed load transport rates. That is, the parameter  $\tau_{bs}$  may be computed from

$$\tau_s^* = \frac{\tau_{bs}}{\rho g R D_{50}} \quad (2-172)$$

and this parameter may be substituted into an appropriate bed load transport equation to obtain  $q_b$ . The volumetric bed load transport rate  $Q_b$  is then computed as

$$Q_b = q_b B \quad (2-173)$$

Most depth-discharge predictors have been developed for sand-bed streams. One exception is the predictor

proposed by Parker and Peterson (1980) for gravel-bed streams. They obtained an empirical bar-resistance equation that displays the same behavior as the bedform resistance of Fig. 2-49a developed for sand-bed streams. The Parker-Peterson equation reads  $C_{ff} = 2.33 \times 10^{-6} \tau_s^{*-1.744}$ , and as expected it yields values that are at least an order of magnitude smaller than those predicted with the Einstein-Barbarossa relation for sand-bed streams. This is mainly due to the absence of dunes in most gravel-bed streams. Parker and Peterson (1980) found that for high flows, little of the resistance is due to alternate bars, but for the lowest stages bar resistance can reach 56% of the total. More information on flow-resistance predictors for gravel-bed streams can be found in Chapter 3.

**2.8.3.2 The Engelund-Hansen Method** The method of Engelund and Hansen (1967) also specifically applies to sand-bed streams. It is generally more accurate than the method of Einstein and Barbarossa, to which it is closely allied. The method assumes quasi-uniform material size; it is necessary to know only a single grain size  $D$ . Roughness height is estimated as  $k_s = 2.5 D_{50}$ .

The method uses the Einstein partition. Skin friction is computed via Eq. (2-153). Form drag is computed from the empirical relation

$$\tau_s^* = f(\tau^*) \quad (2-174)$$

$$\tau^* = \frac{\bar{\tau}_b}{\rho R g D} \quad (2-175a)$$

$$\tau_s^* = \frac{\tau_{bs}}{\rho R g D} \quad (2-175b)$$

Relation (2-174) is shown graphically in Fig. 2-58 in Vanoni (2006, p.81). It has two branches, corresponding to lower-regime and upper-regime flows. The two do not meet smoothly, implying the possibility of a sudden transition. The point of transition is not specified, suggesting the possibility of double-valued rating curves as shown in Fig. 2-48(b).

The lower-regime branch is given by

$$\tau_s^* = 0.06 + 0.4 (\tau^*)^2 \quad (2-176a)$$

The upper branch satisfies the relation

$$\tau_s^* = \tau^* \quad (2-176b)$$

over a range; this implies on upper-regime plane bed. For higher values of Shields stress,  $\tau^*$  again exceeds  $\tau_s^*$ , implying form drag due to the development of antidunes.

The procedure rather closely parallels that of the Einstein-Barbarossa method. It is assumed that values of  $S$  and  $D$  are known, as well as cross-sectional geometry. Values of  $H_s$  are selected, ranging from a low value to near bank-full. The calculation then proceeds as follows:

$$H_s \rightarrow C_{fs} \rightarrow U \quad \text{Eqs. (2-156) and (2-158)}$$

$$H_s \rightarrow \tau_{bs} \rightarrow \tau_s^* \quad \text{Eqs. (2-157b) and (2-175a)}$$

$$\tau_s^* \rightarrow \tau^* \quad \text{Eq. (2-174); use Equation (2-176a) or Fig. 2-49b}$$

$$\tau^* \rightarrow \bar{\tau}_b \rightarrow H \quad \text{Eq. (2-175b) and (2-157a)}$$

$$Q = U H B \quad \text{Eq. (2-171)}$$

The value of  $\tau_s^*$  can be used to calculate bed load transport rates, in a fashion completely analogous to the procedure outlined for the Einstein-Barbarossa method.

**2.8.3.3 The Wright-Parker Method** The method of Engelund and Hansen (1967) was developed using data from laboratory flumes (Guy et al. 1966), and verified in the field using relatively small sand-bed streams (Fredsøe 1989). Posada (1995) found that Eq. (2-176a) did not perform well for the large river data collected in her study. It was found that the relation tends to overpredict the skin-friction shear stress for large rivers at high flows, indicating that large rivers do not make the transition from dunes to a flat bed at shear stresses as low as those observed in laboratory flumes. A recent reanalysis of the problem by Wright and Parker (2004a, 2004b) indicates that the Engelund-Hansen method does indeed provide good results for laboratory flumes and small- to medium-scale sand-bed streams, but does not perform well for large, low-slope sand-bed streams such as the lower Mississippi River. They found, as mentioned earlier, that such streams rarely if ever enter the upper regime. The following modified relation not only provides good results for small and medium-sized sand-bed streams such as the Niobrara River, Middle Loup River, and Rio Grande, but also performs well for such large, low-slope sand-bed streams as the Mississippi River, Atchafalaya River and Red River. It reads

$$\tau_s^* = 0.05 + 0.7(\tau^* Fr^{0.7})^{0.8} \quad (2-177)$$

In this relation  $Fr$  denotes the Froude number of the flow, given as Eq. (2-119b).

The relationship between depth and discharge appropriate for lower-regime conditions is developed by first assuming

that the velocity profile over a rough bed with dunes has approximately the same shape as that over a flat bed. Instead of using the logarithmic velocity distribution, a power law is used for the mean flow velocity,

$$\frac{U}{u_*} = \frac{8.32}{\alpha_{st}} \left( \frac{H}{k_c} \right)^{1/6} \quad (2-178a)$$

$$\frac{U}{u_{*s}} = \frac{8.32}{\alpha_{st}} \left( \frac{H_s}{k_s} \right)^{1/6} \quad (2-178b)$$

Here

$$u_* = \sqrt{gHS};$$

$$u_{*s} = \sqrt{gH_s S};$$

$k_s = 3 D_{90}$  = roughness height due to skin friction; and  $k_c$  = composite roughness accounting for both skin friction and form drag.

Also,  $\alpha_{st}$  is a stratification parameter that can be estimated as a function of near-bed sediment concentration and channel slope as follows (Wright and Parker, 2004b),

$$\alpha_{st} = 1 - 0.06 \left( \frac{\bar{c}_b}{S} \right)^{0.77} \quad \text{for } \frac{\bar{c}_b}{S} \leq 10 \quad (2-179a)$$

$$\alpha_{st} = 0.67 - 0.0025 \left( \frac{\bar{c}_b}{S} \right) \quad \text{for } \frac{\bar{c}_b}{S} > 10 \quad (2-179b)$$

Here

$\bar{c}_b$  = volumetric sediment concentration at a distance  $b = 0.05H$  above the bed; and  
 $S$  = channel slope.

In the case of a sediment mixture, this concentration would be the total concentration for all sizes. Wright and Parker (2004b) used a somewhat modified version of the equation proposed by García and Parker (1991) to estimate  $\bar{c}_b$  (Eq. 2-224a), as given in Eq. (3-143e) of Chapter 3. Using the water continuity equation,  $q_w = UH$ , Eq. (2-178a) can be re-arranged into the dimensionless depth-predictor form

$$\frac{H}{D_{50}} = \left[ \frac{\alpha_{st}}{8.32} \frac{\tilde{q}}{\sqrt{S}} \left( \frac{k_c}{D_{50}} \right)^{1/6} \right]^{3/5} \quad (2-180)$$

Here  $\tilde{q} = q_w / \sqrt{gRD_{50}} D_{50}$  is a dimensionless water discharge. The composite roughness is related to the sand-grain roughness by eliminating  $U$  between Eqs. (2-178a) and (2-178b),

$$\frac{k_c}{k_s} = \left( \frac{H}{H_s} \right)^4 = \left( \frac{\tau^*}{\tau_s^*} \right)^4 \quad (2-181)$$

The relationship between  $\tau^*$  and  $\tau_s^*$  is given by the modified Engelund-Hansen formulation, Eq. (2-177), which provides all the information needed to solve for the flow depth.

The required known parameters are the unit flow discharge  $q_w$ , the river slope  $S$ , and the grain size distribution. To do the computations, guess the depth  $H$  and calculate  $\tau^*$  and the Froude number  $Fr$ . Then calculate  $\tau_s^*$  from Eq. (2-177) and  $k_c$  from Eq. (2-181), using  $k_s = 3D_{90}$ . Then compute the near-bed concentration with Eq. (3-143e) of Chapter 3, which allows computation of the stratification correction  $\alpha_{st}$  from Eqs. (2-179a) and (2-179b). Finally, compute the flow depth  $H$  with Eq. (2-180) and iterate to convergence.

The method has been tested with the large river data set of Toffaleti (1968) with excellent results (Wright and Parker 2004b). The depth predictor was then used to support the development of a suspended-load relation for mixtures which will be presented in Chapter 3.

The partition of bed shear stress into skin-friction and form-drag components is largely motivated by the hypothesis that sediment transport is directly linked to the former component. Recently McLean et al. (1999) have used detailed laboratory measurements to challenge the assumed linkage between sediment transport and bed shear stress due to skin friction. They suggest that the flow velocity at the crest of a bedform may be a better parameter with which to correlate sediment transport.

#### 2.8.3.4 The Brownlie & Cruickshank-Maza Methods

An empirical method offered by Brownlie (1981) has proved to be quite accurate (Brownlie 1983). Like the Cruickshank-Maza (1973) method presented earlier (Section 2.7.6), Brownlie's approach does not involve a decomposition of bed shear stress, but rather gives a direct predictor of depth-discharge relations based on nonlinear regression analysis of hundreds of data points from laboratory and field observations.

The complete method can be found in Section 2.10.3. Here the relation is presented only for the case of lower-regime dune resistance in sand-bed streams. It takes the form

$$\frac{HS}{D_{50}} = 0.3724 (\tilde{q} S)^{0.6539} S^{0.09188} \sigma_g^{0.1050} \quad (2-182a)$$

Here  $\sigma_g$  denotes the geometric standard deviation of the bed material, and  $\tilde{q}$  denotes dimensionless water discharge per unit width, given by

$$\tilde{q} = \frac{q_w}{\sqrt{g D_{50} D_{84}}} \quad (2-182b)$$

For known values  $S$ ,  $D_{50}$ , and  $\sigma_g$ ,  $q_w$ , and thus  $Q = q_w \times B$  can be computed directly as functions of depth  $H$  with the help of Eqs. (2-182a) and (2-182b). The water discharge per unit width is given by  $q_w = UH$  where  $U$  is the mean flow velocity and  $H$  is the flow depth.

Because of its similarity with Brownlie's relation, the empirical relation for lower regime proposed by Cruickshank and Maza (Eq. 2-150a), is reintroduced here. It can be used as a stage-discharge predictor by rewriting it as

$$\tilde{q} = 7.75 R_f \left( \frac{H}{D_{84}} \right)^{1.634} S^{0.456} \quad (2-182c)$$

where the dimensionless specific flow discharge (i.e., flow discharge per unit width) is

$$\tilde{q} = \frac{q_w}{\sqrt{g D_{50} D_{84}}} = \frac{UH}{\sqrt{g D_{50} D_{84}}} \quad (2-182d)$$

and the dimensionless fall velocity is

$$R_f = \frac{v_{s50}}{\sqrt{g R D_{50}}} \quad (2-182e)$$

Notice that the dimensionless fall velocity  $R_f$  is a function of the particle Reynolds number  $R_{ep} = (\sqrt{g R D_{50}} D_{50}) / v$ , and can be estimated with Dietrich's fall velocity relation (Eq. 2-47a), the Jimenez-Madsen relation (Eq. 2-48a), or from Fig. 2-11.

For known values  $S$ ,  $D_{50}$ ,  $D_{84}$ , and kinematic viscosity of water  $v$ ,  $q_w$ , and channel width  $B$ ,  $Q = q_w B$  can be computed directly as functions of depth  $H$  with the help of Eqs. (2-182c), (2-182d), (2-182e), and (2-47). The water discharge per unit width is given by  $q_w = UH$  where  $U$  is the mean flow velocity and  $H$  is the flow depth.

Notice that the Cruickshank-Maza relation accounts for water temperature effects through the dimensionless fall velocity parameter (Eq. 2-182e). This approach can also be used to obtain a stage-discharge predictor for the upper-flow regime by rewriting Eq. (2-150c),

$$\tilde{q} = 7.0 R_f \left( \frac{H}{D_{84}} \right)^{1.644} S^{0.352} \quad (2-182f)$$

Equations (2-182c) for lower-flow regime and (2-182f) for upper-regime apply to the range of conditions defined by Eqs. (2-150b) and (2-150d), respectively. Although the Cruickshank-Maza method has not been tested as thoroughly as Brownlie's, it has been found to provide an effective approximation for both the design of movable-bed models as well as for computing stage-discharge relations in several Mexican sand-bed rivers with flows depths in the range from 1 to 8 m, and with bed-material size in the range from 0.2 to 2.0 mm (Berezowsky and Lara 1986).

**2.8.3.5 The Karim-Kennedy Method** An approach similar to the one used by Brownlie (1983) was employed by Karim and Kennedy (1981) to develop a depth-discharge predictor for alluvial streams. Nonlinear regression analysis was applied to a database consisting of 339 river flows and 608 flume flows to determine the most significant dimensionless variables affecting depth-discharge as well as sediment transport relationships. The flow resistance was formulated in terms of the ratio of friction factors  $f/f_o$ , in which  $f$  is the friction factor for flow over a moving sediment bed, and  $f_o$  is a reference friction factor for flow over a fixed sediment bed given by a Keulegan-type resistance relation as

$$f_o = \frac{8}{[5.75 \log(12H/k_s)]} \quad (2-183a)$$

in which  $k_s = 2.5 D_{50}$ . It was assumed, based on Engelund's analysis of flow in the lower regime that  $f/f_o$  varies linearly with the ratio of ripple or dune height to flow depth as follows:

$$\frac{f}{f_o} = 1.20 + 8.92 \frac{\Delta}{H} \quad (2-183b)$$

Karim and Kennedy used an expression proposed by Allen (1978) for the ratio of bed form height to flow depth, given by

$$\begin{aligned} \frac{\Delta}{H} &= 0.08 + 2.24 \left( \frac{\tau^*}{3} \right) - 18.13 \left( \frac{\tau^*}{3} \right)^2 \\ &\quad + 70.9 \left( \frac{\tau^*}{3} \right)^3 - 88.33 \left( \frac{\tau^*}{3} \right)^4 \end{aligned} \quad (2-183c)$$

for  $\tau^* < 1.5$  and  $\Delta / H = 0$  for  $\tau^* > 1.5$ . They applied regression analysis to the data to obtain an relationship for dimensionless flow velocity as a function of relative roughness  $H/D_{50}$ , slope  $S$ , and  $f/f_o$ , given by

$$\frac{U}{\sqrt{gRD_{50}}} = 6.683 \left( \frac{H}{D_{50}} \right)^{0.626} S^{0.503} \left( \frac{f}{f_o} \right)^{-0.465} \quad (2-183d)$$

For a given flow depth, the mean flow velocity can be computed directly from Eq. (2-183d). The bed forms are identified as being in the lower regime for  $\tau^* < 1.2$ , transition for  $1.2 < \tau^* < 1.5$ , and upper regime for  $\tau^* > 1.5$ .

**2.8.3.6 Other Stage-Discharge Predictors** There are almost as many empirical resistance predictors for rivers as there are sediment transport relations. A fairly comprehensive summary of older methods can be found in ASCE Manual 54 (Vanoni 2006). Other flow-resistance predictors for sand-bed streams worth considering, besides the ones presented above, are those of van Rijn (1984c), Camacho and Yen (1991), and Bennett (1995).

## 2.9 SUSPENDED LOAD

### 2.9.1 Mass Conservation of Suspended Sediment

A phenomenon of considerable interest in river mechanics is the erosion, transport, and deposition of noncohesive material by turbulent open-channel flow. Suspended sediment differs from bed load sediment in that it may be diffused throughout the vertical column of fluid via turbulence. As long as the suspended sediment under consideration is sufficiently coarse not to undergo Brownian motion, molecular effects can be neglected. Suspended particles are transported solely by convective fluxes. These sediment fluxes have two components: one associated with the mean flow motion and one associated with the turbulence of the flow. A complete derivation of the mass conservation equation for suspended sediment can be found in García (2001). More material can also be found in Chapter 16. Here, only the main elements of the theory of equilibrium suspensions needed to estimate suspended load are presented.

The equation describing mass conservation of suspended sediment of uniform size and constant material density in a turbulent flow can be written as follows (García and Parker 1991)

$$\frac{\partial \bar{c}}{\partial t} + \frac{\partial F_i}{\partial x_i} = 0 \quad (2-184a)$$

where

$$F_i = (u_i - v_s \delta_{i3}) \bar{c} + \overline{u'_i c'} \quad (2-184b)$$

$x_i$  = Cartesian coordinate system such that  $x_3$  is directed upward vertically;

$t$  = time;

$u_i$  = fluid velocity field averaged over turbulence,

$u'_i$  = turbulent fluctuations;

$\bar{c}$  = volume suspended-sediment concentration averaged over turbulence;

$c'$  = instantaneous fluctuation in concentration;

$F_i$  = volume flux vector of suspended sediment averaged over turbulence;  
 $v_s$  = fall velocity of sediment in quiescent water; and  
 $\delta_{ij}$  = Kronecker delta (i.e.,  $\delta_{ij} = 1$  for  $i = j$  and  $\delta_{ij} = 0$  otherwise).

Equations (2-184a) and (2-184b) are valid only for dilute suspensions (i.e.,  $\bar{c} \ll 1$ ) of particles that are not too coarse (i.e., size is less or equal than 0.5 mm). The mean volumetric sediment concentration  $\bar{c}$  is defined as the ratio between the volume of sediment and the volume of sediment-water mixture.

If  $x_3 = z$  is upward vertical, Eqs. (2-184a) and (2-184b) reduce to

$$\begin{aligned}\frac{\partial \bar{c}}{\partial t} + \bar{u} \frac{\partial \bar{c}}{\partial s} + \bar{v} \frac{\partial \bar{c}}{\partial n} + (\bar{w} - v_s) \frac{\partial \bar{c}}{\partial z} \\ = - \frac{\partial \bar{u}' c'}{\partial s} - \frac{\partial \bar{v}' c'}{\partial n} - \frac{\partial \bar{w}' c'}{\partial z}\end{aligned}\quad (2-185)$$

where

$\bar{u}$ ,  $\bar{v}$ , and  $\bar{w}$  = mean flow velocities in the  $s$ ,  $n$ , and  $z$  directions, respectively; and  
 $\bar{u}' c'$ ,  $\bar{v}' c'$ , and  $\bar{w}' c'$  = sediment fluxes due to turbulence, also known as Reynolds fluxes.

The main assumption here is that the sediment particles follow the fluid particles (i.e., have the same velocity as the fluid), except in the vertical  $z$  direction, where the effect of gravity introduces a slip velocity denoted by the sediment fall velocity  $v_s$  in quiescent water (see section 2.3.8).

It is seen from Eq. (2-184b) that the mean flux of suspended sediment  $F_i$  is composed of two components, i.e., a mean convective flux and a Reynolds flux. The Reynolds flux  $\bar{u}' c'$  in the above relation is clearly diffusive in nature. The simplest closure assumption to represent the Reynolds sediment fluxes is to assume these fluxes proportional to gradients in sediment concentration

$$\bar{u}_i' c' = -D_d \frac{\partial \bar{c}}{\partial x_i} \quad (2-186a)$$

In this equation, the kinematic eddy diffusivity  $D_d$  is assumed to be a scalar quantity. For the case of nonisotropic turbulence, Equation (2-186a) must be generalized to the form (García 2001)

$$\bar{u}_i' c' = -D_{dij} \frac{\partial \bar{c}}{\partial x_j} \quad (2-186b)$$

Here  $D_{dij}$  is a tensor quantity. It is often assumed to represent a diagonal matrix, such that  $D_{dij} = 0$  if  $i \neq j$ , and  $D_{d11} \neq D_{d22} \neq D_{d33}$ . Notes on tensor notation and turbulence can be found in the appendix at the end of Chapter 16.

The kinematic eddy diffusivity  $D_d$  has dimensions of  $L^2/T$ . Common practice is to treat the eddy diffusivity as a scalar. However, this is the case only for isotropic, homogeneous turbulence, as realized in the pioneering experiments conducted by Rouse (1938) on equilibrium suspensions with grid-generated turbulence in a jar (Ettema 2006). More insight into turbulence in sediment-laden flows can be found in Chapter 16. To solve Eq. (2-185), appropriate boundary conditions are needed. These are presented next.

## 2.9.2 Boundary Conditions for Sediment Advection-Diffusion Equation

Equation (2-185), coupled with a Fickian closure approximation such as Eqs. (2-186a) or (2-186b), represents an advection-diffusion equation for suspended sediment (García 2001). The condition of vanishing flux of suspended sediment across (normal to) the water surface defines the upper boundary condition.

If steady, uniform, turbulent flow over a flat bed (when averaged over bed forms) is considered, the water surface boundary condition for the net vertical flux of sediment reduces to

$$\bar{F}_{sz}|_{z=H} = 0 \quad (2-187a)$$

where

$$\bar{F}_{sz} = -v_s \bar{c} + \bar{w}' c' \quad (2-187b)$$

gives the net vertical flux of sediment.

The boundary condition at the bed differs from the one at the water surface, in that it must account for entrainment of sediment into the flow from the bed and deposition of sediment from the flow onto the bed. For a flat (averaged over bedforms) bed, the mean depositional flux of suspended sediment onto the bed is given by  $-D_r$ , which needs to be evaluated at a distance  $z = b$  near the bed,

$$D_r = v_s \bar{c}_b \quad (2-188)$$

denotes the volume rate of deposition of suspended sediment per unit time per unit bed area. Here  $\bar{c}_b$  denotes a near-bed value of mean volumetric sediment concentration.

The component of the Reynolds flux of suspended sediment near the bed that is directed upward normal to the bed may be termed the rate of erosion, or more accurately, entrainment of bed sediment into suspension per unit bed area per unit time. The entrainment rate  $E_r$  is thus given by

$$E_r = \bar{w}' c' \quad (2-189)$$

where

$w'$  and  $c'$  = turbulent fluctuations around both the mean vertical fluid velocity and the mean sediment concentration, respectively.

The ‘overbar’ denotes averaging over turbulence. The terminology “near-bed” is employed to avoid possible singular behavior at the bed (located at  $z = 0$ ).

It is seen from these equations that the net-upward, normal flux of suspended sediment at (or rather just above) the bed is given by

$$\bar{F}_{sz}|_{z=b} = E_r - D_r = v_s (E_s - \bar{c}_b) \quad (2-190a)$$

where

$$E_s \equiv \frac{E_r}{v_s} \quad (2-190b)$$

denotes a dimensionless rate of entrainment of bed sediment into suspension (i.e., volume of entrained sediment per unit bed area per unit time). The required bed boundary condition, then, involves a specification of  $E_s$ , which can be used to estimate the sediment entrainment flux at the bed (i.e., Eq. 194b). Typically a relation is assumed of the form

$$E_s = E_s(\tau_{bs}, \text{other parameters}) \quad (2-191)$$

where  $\tau_{bs}$  denotes the boundary shear stress due to skin friction.

If it is furthermore assumed that an equilibrium steady, uniform suspension has been achieved. It follows that there should be neither net deposition on ( $\bar{F}_{sz} < 0$ ) nor erosion from ( $\bar{F}_{sz} > 0$ ) the bed. That is,  $\bar{F}_{sz}|_{z=b} = 0$ , yielding the result

$$E_s = \bar{c}_b \quad (2-192)$$

This relation simply states that the entrainment rate equals the deposition rate at equilibrium; thus there is no net normal flux of suspended sediment at the bed. García and Parker (1991) took advantage of this relation and developed a sediment entrainment formulation presented below.

Sediment entrainment and deposition fluxes were directly measured in Central Long Island Sound by Bedford et al. (1987) with the help of acoustic transducers. A control volume approach was used to estimate settling fluxes as well as Reynolds sediment fluxes. The sediment entrainment measurements correlated well with near-bed turbulent kinetic energy. Sediment resuspension has also been backcalculated from in-situ flow observations in the continental shelf off California by Wiberg et al. (1994).

### 2.9.3 Equilibrium Suspension in a Wide Channel

Consider normal flow in a wide, rectangular open channel. The bed is assumed to be erodible and has no curvature when averaged over bed forms such as ripples and dunes. The  $z$ -coordinate is quasi-vertical, implying low channel slope  $S$ . The suspension is likewise assumed to be in equilibrium. That is,  $\bar{c}$  is a function of  $z$  alone, as shown in Fig. 2-50. The flow and suspension are uniform in  $s$  (streamwise direction) and  $n$  (transverse direction) and steady in time, so that Eq. (2-185) reduces to

$$\frac{d}{dz} (\bar{w}' \bar{c}') - v_s \bar{c} = 0 \quad (2-193a)$$

indicating that for equilibrium conditions,  $(\bar{w}' \bar{c}') - v_s \bar{c}$  = constant for all values of  $z$  in the range  $z = b$  to  $z = H$ . It follows from the boundary condition at the water surface, given by Eqs. (2-187a) and (2-187b), that the constant = 0, thus Eq. (2-193a) reduces to

$$\bar{w}' \bar{c}' - v_s \bar{c} = 0 \quad (2-193b)$$

It is appropriate to close this equation with the assumption of an eddy diffusivity as in Eq. (2-186a) so that Eq. (2-193b) becomes (Rouse 1937, Vanoni 1946)

$$D_d \frac{d\bar{c}}{dz} + v_s \bar{c} = 0 \quad (2-194a)$$

According to the literature, this equation was first developed by Wilhelm Schmidt in the mid 1920s for studies of dust transport in atmospheric flows and by M. P. O’Brien in the early 1930s for studies of suspended sediments in streams. It has a simple physical interpretation. The term  $v_s \bar{c}$  represents the rate of deposition of suspended sediment under the influence of gravity; it is always directed downward. If all of the sediment is not to settle out, there

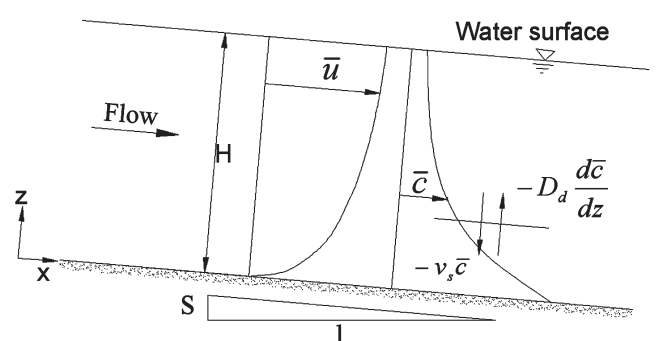


Fig. 2-50. Definition diagram for sediment entrainment from and deposition on channel bed.

must be an upward flux that balances this term. The upward flux is provided by the effect of turbulence, acting to yield a Reynolds flux. According to Eq. (2-186a), this flux will be directed upward as long as  $d\bar{c}/dz < 0$ . It follows that the equilibrium suspended sediment concentration decreases for increasing  $z$ , so that turbulence diffuses sediment from zones of high concentration (near the bed) to zones of low concentration (near the water surface). Thus the general boundary conditions for Eq. (2-194a) are given by (Parker 1978; Fredsøe and Deigaard 1992, p. 246)

$$-D_d \frac{d\bar{c}}{dz} \Big|_{z=b} = v_s E_s \quad (2-194b)$$

$$D_d \frac{d\bar{c}}{dz} + v_s \bar{c} \Big|_{z=H} = 0 \quad (2-194c)$$

The first of these specifies the near-bed rate of entrainment of sediment into suspension, and the second specifies the condition of vanishing upward normal sediment flux at the water surface. It follows that at equilibrium, the flux boundary condition given by Eq. (2-194b) is equivalent to the identity given by Eq. (2-192). However, for nonequilibrium conditions, Eq. (2-194b) should be used as the near-bed boundary condition (Parker 1978; Fredsøe and Deigaard 1992; Admiraal and García 2000).

#### 2.9.4 Form of Eddy Diffusivity (Prandtl analogy)

Further progress requires an assumption for the kinematic eddy diffusivity  $D_d$ . The simple approach taken here is that of Rouse (1937). It involves the use of the Prandtl analogy. The argument is as follows. Fluid mass, heat, momentum, etc., should all diffuse at the same kinematic rate due to turbulence and thus have the same kinematic eddy diffusivity, because each is a property of the fluid particles, and it is the fluid particles that are being transported by Reynolds fluxes.

The Prandtl analogy is by no means exact but has been found to be a reasonable approximation for many turbulent flows. Its application to sediment is more problematic (e.g., Coleman 1970; Kerssens et al. 1979; Nielsen 1992). Inertial effects might cause the sediment particles to lag behind the fluid, resulting in lower eddy diffusivity for sediment than for the fluid (Niño and García 1998a). Furthermore, the mean fall velocity of sediment grains should reduce their residence time in any given eddy, again reducing the diffusive effect (Nielsen 1992). If the particles are not too large, however, it may be possible to equate the vertical diffusivity of the sediment with the vertical eddy viscosity (eddy diffusivity of momentum) of the fluid, as a first approximation. This is done here.

The velocity profile is approximated as logarithmic throughout the depth. To account for the possible

existence of bed forms, the turbulent rough law embodied in Eq. (2-166b) is employed.

$$\frac{\bar{u}}{u_*} = \frac{1}{\kappa} \ln \left( 30 \frac{z}{k_c} \right) \quad (2-195)$$

Here  $k_c$  is a composite roughness chosen to include the effect of bed forms, as outlined in Section 2.8.2.2. Furthermore, according to Eq. (2-2), the bed shear stress is given by

$$\tau_b = \rho u_*^2 \quad (2-196)$$

where  $b$  is chosen to be very close to the bed, i.e.,

$$\frac{b}{H} \ll 1 \quad (2-197)$$

Now the kinematic eddy viscosity  $D_d$  is defined such that

$$\tau = D_d \frac{d\bar{u}}{dz} \quad (2-198)$$

where the distribution of fluid shear stresses  $\tau$  is given by Eq. (2-3)

$$\tau = \tau_b \left( 1 - \frac{z}{H} \right) \quad (2-199)$$

From the above equations, the following equation is obtained

$$D_d = \kappa u_* z \left( 1 - \frac{z}{H} \right) \quad (2-200)$$

If  $D_d$  is averaged in the vertical, the following result is obtained:

$$\bar{D}_d = \frac{\kappa}{6} u_* H \approx \frac{1}{15} u_* H \quad (2-201a)$$

This relation provides a good approximation to estimate the longitudinal dispersion of fine-grained sediment and contaminants in rivers and streams (e.g., Rutherford 1994; Huang and García 2000).

In the early 1940s, Lane and Kalinske tried to obtain a simple method to estimate suspended sediment load in the field. To this end, they used the average value for the eddy diffusivity given by Eq. (2-201a) to integrate Eq. (2-194a),

resulting in the following equation for suspended sediment distribution

$$\frac{\bar{c}}{\bar{c}_b} = \exp \left\{ -\frac{15v_s}{u_*} \left( \frac{z-b}{H} \right) \right\} \quad (\text{Eq. 201b})$$

where  $\bar{c}_b$  is a near-bed reference concentration measured at a distance  $z = b$  from the bed. This simple exponential equation provides a reasonable approximation to estimate the suspended sediment distribution in wide rivers (i.e.,  $H/B << 1$ ). It also yields a finite value of sediment concentration at the water surface (i.e.,  $z = H$ ), which is one weakness of the Rousean distribution presented below. The exponential decay in suspended sediment concentration with distance from the bed given by the Lane-Kalinske relation was the solution originally obtained by Rouse in his turbulence jar experiments. In Rouse's jar, however, the eddy diffusivity was also constant in the vertical direction but the turbulence was generated by an oscillating grid and not by a velocity gradient (i.e., shear stress) as in the case of Eq. (2-201a).

Equation (2-200) is known as the Rousean formulation for the vertical kinematic eddy viscosity. The form predicted is parabolic in shape. Although strictly applying to the turbulent diffusion of fluid momentum, it is equated to the eddy diffusivity of suspended sediment mass below. Coleman (1970) was among the first to estimate the variation of  $D_d$  with distance from the bed  $z$ , from laboratory and field observations of suspended sediment. He found that its variation is parabolic only in the lower portion of the flow and then it remains constant up to the water surface. Van Rijn (1984b), among others, has argued that the ratio between the diffusivity of sediment and the kinematic eddy viscosity is slightly larger than 1 and has proposed an empirical coefficient to adjust the values of  $D_d$  accordingly. On the other hand, Bennett et al. (1998) have found with the help of turbulence measurements in sediment-laden flow that  $D_d$  is a good surrogate for the sediment diffusivity as long as it is directly measured and not back-calculated from Eq. (2-194a). Nielsen (1992) argues that diffusion models do not capture the physics of the problem in coastal sediment transport. Muste and Patel (1997) have done detailed laboratory measurements that can be used to understand sediment diffusion in open-channel flows. Through an analysis of the turbulent kinetic energy budget, Niño and García (1998a) have found that near the bed, fine particles reduce the kinetic energy of the flow but coarser particles enhance turbulence because of the production of turbulent kinetic energy through vortex shedding mechanisms. Cellino and Graf (2000) have analyzed the effect of bed forms on open channel suspensions, showing that the turbulent diffusion is enhanced in the presence of bed forms. Greimann and Holly (2001) have used a two-phase flow model to estimate the role of cross trajectories on eddy diffusivity. A review of most of the experimental work, including sources of error, which has been done on

suspended sediment transport to determine parameters such as the eddy diffusivity, can be found in Muste (2002). Different approaches to estimate numerically the eddy diffusivity in sediment-laden flows are discussed in Chapter 16. In large, low-gradient, sand-bed streams, the diffusion coefficient has to be adjusted for stratification effects. This adjustment to account for stratification effects is presented below.

## 2.9.5 Rouse-Vanoni-Ippen Suspended Sediment Distribution

To integrate Eq. (2-194a) in the vertical, the nominal "near bed" elevation in applying the bottom boundary condition is taken to be  $z = b$ , where  $b$  is a distance taken to be very close to the bed (i.e., satisfying condition Eq. (2-197)). In the Rousean analysis, this value cannot be taken as  $z = 0$ , because Eq. (2-195) is singular there.

Equation (2-200) is now substituted into Eq. (2-194a), which is then integrated from the nominal bed level to distance  $z$  above the bed in  $z$ . The resulting form can be cast as

$$\int_b^H \frac{d\bar{c}}{\bar{c}} = -Z_R \int_b^z \frac{H dz}{z(H-z)} = \ln \left[ \left( \frac{H-z}{z} \right)^{Z_R} \right]_b^z \quad (2-202)$$

where  $Z_R$  denotes the dimensionless Rouse Number, given as

$$Z_R = \frac{v_s}{\kappa u_*} \quad (2-203)$$

Integration yields the profile

$$\frac{\bar{c}}{\bar{c}_b} = \left[ \frac{(H-z)/z}{(H-b)/b} \right]^{Z_R} \quad (2-204)$$

Equation (2-204) is commonly recognized as the Rousean distribution for suspended sediment and is one of the milestones in the mechanics of sediment transport (Vanoni 1984). Profiles of suspended sediment obtained from laboratory observations are plotted in Rousean form in Fig. 2-51 (Vanoni 2006). It has also been found to work well in several large alluvial rivers. Sediment concentration profiles of suspended sediment observed in the Amazon River, Brazil, are plotted in Rousean coordinates (i.e.,  $(H-z)/z = (d-y)/y$ ) in Fig. 2-52 (Vanoni 1980). The slope of the straight lines in log-log paper corresponds to the Rouse number  $Z_R$  for a given grain size range. If the mean fall velocity of the particles in each size range can be estimated, it is possible to backcalculate the shear velocity  $u_*$ . Despite the wide range of sediment sizes present in the water column and the large

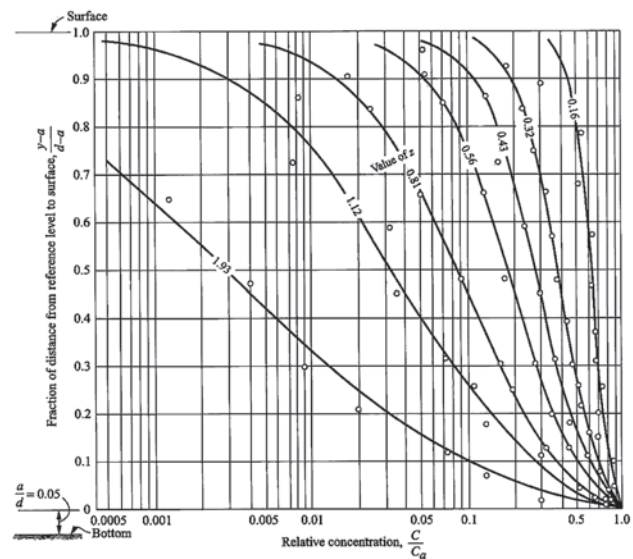


**Fig. 2-51.** Laboratory observations of suspended sediment distribution (Vanoni 2006).

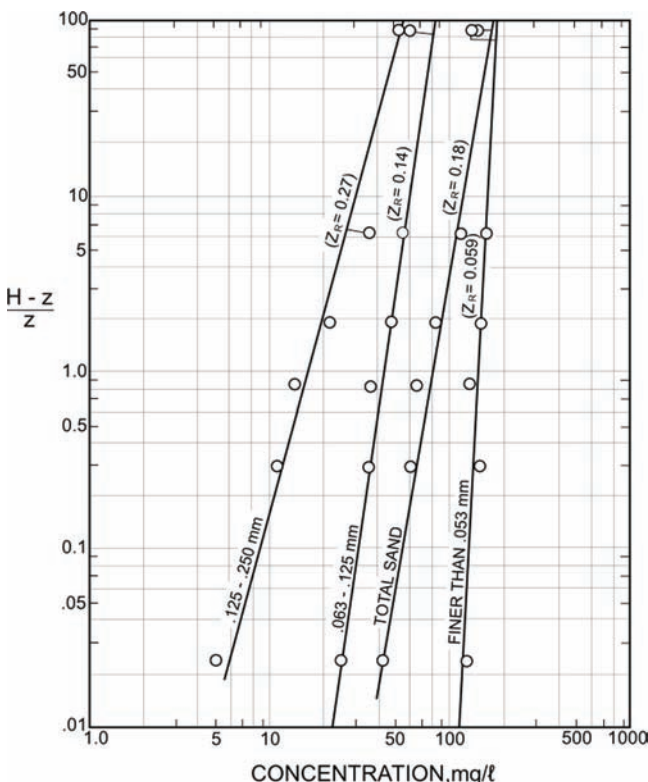


**Fig. 2-52.** Distribution of Suspended Sediment plotted in Rousean Coordinates for the Amazon River at Manacapuru, where the flow depth is 44 m. Each line shows the particle size range and the corresponding value of the Rouse number (adapted from Vanoni 1980).

water depth (44 m), it is clear that the concentration profiles follow the vertical distribution given by Eq. (2-204). The Rousean distribution has also been found to work well for the analysis of sediment transport in vegetated channels (Lopez and García 1998). In this particular case, the eddy diffusivity is enhanced by the presence of the vegetation, resulting in vertical sediment concentration distributions that are slightly more uniform than those predicted by the Rousean formulation.

Although strictly speaking the credit for the above relation should go to Hunter Rouse, Kennedy (1983) argued that Eq. (2-204) should be named the Rouse-Vanoni-Ippen equation for suspended sediment distribution, because all of these researchers contributed either directly or indirectly to its development and subsequent testing. The seminal idea of using the logarithmic flow velocity distribution and the Prandtl analogy to estimate the eddy diffusivity was suggested independently to both Hunter Rouse and Arthur Ippen by Professor Theodore von Karman at the California Institute of Technology. Rouse used the Karman-Prandtl logarithmic velocity distribution that led to the development of the classic relation that now bears his name, while Ippen used the velocity distribution proposed earlier by Krey instead of the Karman-Prandtl relation. Thus, the Rousean formulation predicts sediment concentration relative to a near-bed concentration  $\bar{c}_b$ , which has to be estimated as a function of flow parameters and sediment characteristics, as will be shown below.

Starting with his PhD dissertation completed at Caltech in 1940, Vito Vanoni spent a substantial amount of effort studying open-channel suspensions, in particular the predictions made by the Rousean formulation both in the laboratory (Fig. 2-51) and in the field (Fig. 2-52). By the time ASCE Manual 54 was first published, the Rouse-Vanoni-Ippen formulation had already reached prominence and since then it has become one of the most important milestones in the field of sediment transport (Vanoni 1984).

**2.9.5.1 Modification of the Rousean Formulation to Include Flow Stratification Effects** River flows carrying suspended sediment are self-stratifying. As illustrated in Fig. 2-51, the Rousean profile predicts a concentration of suspended sediment that decreases with increasing elevation above the bed. It follows that the density of the water-sediment mixture also decreases with increasing elevation above the bed. This stable stratification inhibits turbulent mixing of both flow momentum and sediment mass in the vertical. The result is a modification of the vertical distributions of both streamwise momentum and suspended sediment concentration. More specifically, stratification effects lead to a streamwise velocity profile that increases more rapidly in the vertical than the logarithmic profile, and a suspended sediment profile that decreases more rapidly in the vertical than the Rousean profile.

Starting with his seminal contribution to the subject of sediment transport by currents and waves in continental

shelves (Smith 1977), J. Dungan Smith has been a tireless advocate of the importance of self-stratification by flows with suspended sediment. Smith and McLean (1977a), Smith and McLean (1977b), Gelfenbaum and Smith (1986), McLean (1990), and McLean (1992) offer quantitative formulations of stratification effects based on simple algebraic closures. The kinematic eddy diffusivity  $D_d$  given in Eq. (2-200) is now denoted as  $D_{do}$ , where the subscript “*o*” denotes the absence of stratification effects. The value of  $D_d$  in the presence of stratification effects is given as

$$D_d = D_{do} F_{strat}(RI_g) \quad (2-205a)$$

$$D_{do} = \kappa u_* z \left(1 - \frac{z}{H}\right) \quad (2-205b)$$

$$RI_g = \frac{-Rg \frac{d\bar{c}}{dz}}{\left(\frac{d\bar{u}}{dz}\right)^2} \quad (2-205c)$$

Here  $RI_g$  denotes a gradient Richardson number and  $F_{strat}$  is a function that decreases with increasing gradient Richardson number, thus capturing the effect of damping of the turbulence due to flow stratification. Smith and McLean (1977) offer the following form for the function  $F_{strat}$ :

$$F_{strat}(RI_g) = 1 - 4.7 RI_g \quad (2-206)$$

Note that  $F_{strat}$  equals unity for a gradient Richardson number of zero (no stratification effects) and decreases to zero as  $RI_g$  increases to a value of 0.21, at which turbulent mixing is extinguished.

Smith and McLean (1977a) approximate the equation of streamwise momentum balance for the case of equilibrium flow in a wide channel Eq. (2-199) to the form

$$D_d \frac{d\bar{u}}{dz} = u_*^2 \left(1 - \frac{z}{H}\right) \quad (2-207)$$

An appropriate near-bed boundary condition on Eq. (2-207) at  $z = b$  is obtained by matching the velocity profile to the logarithmic law (Eq. 2.17a) there:

$$\frac{\bar{u}|_{z=b}}{u_*} = \frac{1}{\kappa} \ln \left( 30 \frac{b}{k_c} \right) \quad (2-208)$$

Here  $k_c$  is the composite roughness length accounting for both grain resistance and form-induced drag introduced

earlier. The corresponding boundary condition on Eq. (2-194a) is

$$-D_d \frac{d\bar{c}}{dz} \Big|_b = v_s E_s \quad (2-209)$$

Solving Eqs. (2-194a) and (2-207) subject to the boundary conditions (2-209) and (2-208) and the relations (2-205a), (2-205b), and (2-205c) results in the forms

$$\bar{c} = E_s \exp \left[ - \frac{v_s}{\kappa u_* z \left(1 - \frac{z}{H}\right) F_{strat}(RI_g)} dz \right] \quad (2-210)$$

and

$$\bar{u} = \frac{u_*}{\kappa} \left[ \ln \left( \frac{b}{z_o} \right) + \int_b^z \frac{1}{z F_{st}(RI_g)} dz \right] \quad (2-211)$$

These two equations do not constitute an explicit solution for the concentration and velocity profiles, because  $RI_g$  is a function of the concentration gradient  $d\bar{c}/dz$  in accordance with Eq. (2-205c). In the limit, as  $RI_g \rightarrow 0$ , however, Eq. (2-210) converges to the Rousean solution of Eq. (2-204) and Eq. (2-211) converges to the logarithmic profile of Eq. (2-195). These two unstratified profiles can be used as base forms for an iterative solution of Eqs. (2-210) and (2-211).

The first step in this iterative process can be illustrated as follows. Let  $\bar{c}_o(z)$  denote the Rousean solution for the profile of suspended sediment concentration and let  $\bar{u}_o$  denote the logarithmic profile of streamwise velocity. The first iteration, including the effect of stratification yields the forms  $\bar{c}_1(z)$  and  $\bar{u}_1(z)$ , where

$$\bar{c}_1 = E_s \exp \left\{ - \frac{v_s}{\kappa u_* z \left(1 - \frac{z}{H}\right) \left[ 1 + 4.7 \frac{Rg \frac{d\bar{c}_o}{dz}}{\left(\frac{d\bar{u}_o}{dz}\right)^2} \right]} dz \right\} \quad (2-212)$$

$$\bar{u}_1 = \frac{u_*}{\kappa} \left\{ \ln \left[ \frac{b}{z_o} \right] + \int_b^z \frac{1}{z} \left[ \frac{Rg \frac{dc_o}{dz}}{1 + 4.7 \left( \frac{du_o}{dz} \right)^2} \right] dz \right\} \quad (2-213)$$

A sample calculation illustrates the procedure. The following values are used:  $R = 1.65$ ,  $v_s = 0.748$  mm/s ( $D = 0.1$  mm for  $v = 1 \times 10^{-6}$  m<sup>2</sup>/s),  $H = 2$  m,  $k_c = 5$  mm,  $u_* = 0.02$  m/s,  $b = 0.05 H$ , and  $E_s = \bar{c}_b = 0.0001$ . Fourteen iterations are needed to converge to a solution based on a convergence criterion of less than 0.1 % of error. The Rousean and stratification-modified profiles of suspended sediment concentration are shown in Fig. 2-53(a). The logarithmic and stratification-modified profiles of streamwise velocity are shown in Fig. 2-53(b).

Recently, Wright and Parker (2004) have shown that sediment-induced stratification effects are important in large, low-gradient, sand-bed streams. Using an approach similar to the one presented here, they have estimated velocity profiles for the Red and the Atchafalaya Rivers, showing the difference between clear-water and stratified flow velocity profiles as shown in Figure 2-54.

Other approaches in the literature to account for the effect of sediment-induced stratification on velocity profiles not mentioned earlier include the work of Itakura and Kishi (1980), Adams and Weatherly (1981), Coleman (1981), and Soulsby and Wainright (1987). With the exception of Coleman (1981) who also used the Richardson number to quantify the effect of stratification, the rest of the formulations have made an analogy with stratified atmospheric flows, introducing the so-called Monin-Obukhov length into their analyses.

### 2.9.6 Vertically Averaged Concentrations: Suspended Load

Often times it is useful to know the average concentration in the water column. Assuming that a value of near-bed elevation  $b$  is selected, Eq. (2-204) can be used to evaluate a depth-averaged volume suspended sediment concentration  $C$ , defined by

$$\bar{C} = \frac{1}{H} \int_b^H \bar{c}(z) dz \quad (2-214)$$

Using  $\delta = \frac{z}{H}$  and  $\delta_b = \frac{b}{H}$ , where  $b$  denotes a location just above the bed, Eq. (2-214) can be expressed as:

$$\bar{C} = \bar{c}_b J_1 = \bar{c}_b \int_{\delta_b}^{Z_R} \left[ \frac{(1-\delta)/\delta}{(1-\delta_b)/\delta_b} \right] d\delta \quad (2-215)$$

Einstein (1950) proposed a relation for the depth-averaged sediment concentration as

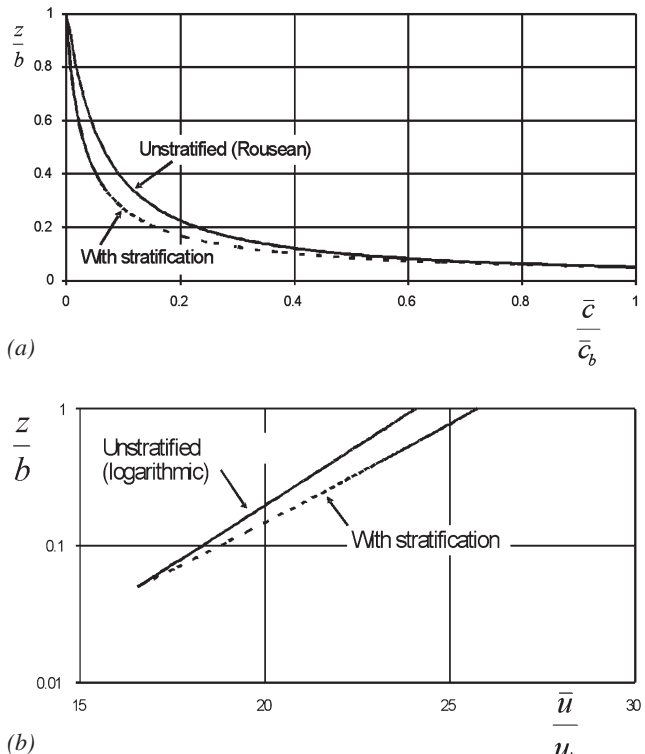


Fig. 2-53. (a) Concentration profiles and (b) streamwise velocity profiles without and with stratification.

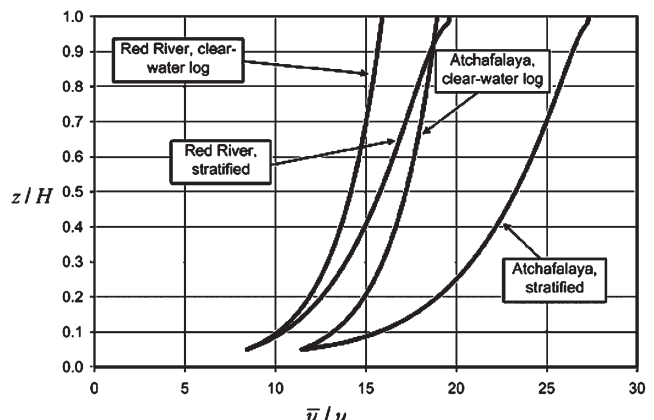


Fig. 2-54. Velocity profiles for Red and Atchafalaya Rivers with and without stratification effects (Wright and Parker 2004).

$$\bar{C} = \bar{c}_b \frac{\delta_b}{0.216} I_1 \quad (2-216)$$

Here,  $I_1$  is given in graphical form by Fig. 2-55(a). It follows from Eqs. (2-215) and (2-216) that

$$J_1 = \frac{\delta_b}{0.216} I_1 = \int_{\delta_b}^1 \left[ \frac{(1-\delta)/\delta}{(1-\delta_b)/\delta_b} \right]^{Z_R} d\delta \quad (2-217)$$

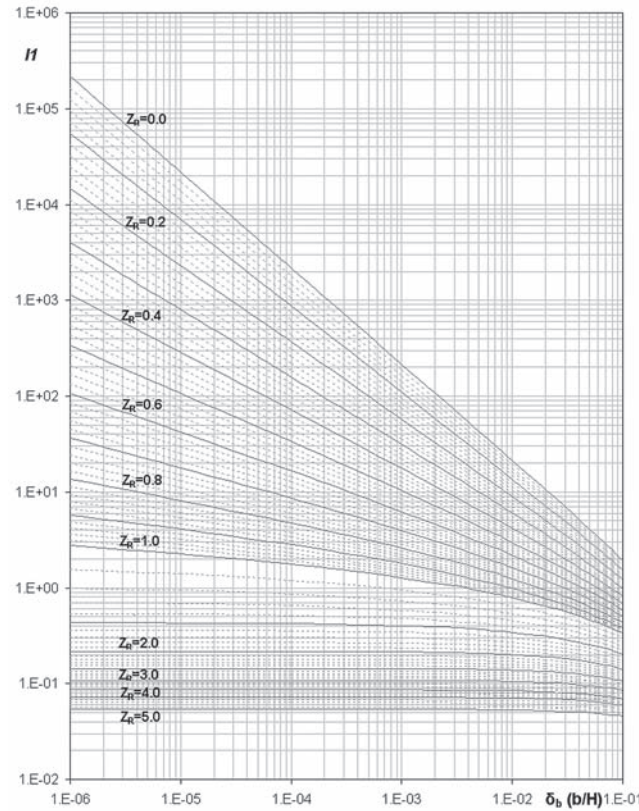
The streamwise suspended load  $q_s$  was seen in Eq. (2-85) to be given by the relation

$$q_s = \int_b^H \bar{c}_b \bar{u} dz \quad (2-218)$$

Reducing with the aid of Eqs. (2-195) and (2-204), it is found that Eq. (2-218) can be expressed as (García 1999)

$$q_s = \frac{1}{\kappa} \bar{c}_b u_* H \left[ J_1 \ln \left( 30 \frac{H}{k_c} \right) + J_2 \right] \quad (2-219)$$

This equation indicates that to compute the rate of volumetric suspended sediment transport per unit width under



(a)

uniform, equilibrium flow conditions, it is necessary to know the near-bed concentration  $\bar{c}_b$ , the total friction velocity  $u_* = \sqrt{(\tau_{bs} + \tau_{bf})/\rho}$ , the flow depth  $H$ , the value of the composite roughness which can be computed from Eq. (2-168b) as  $k_c = 11H \exp \left\{ -\frac{\kappa U}{u_*} \right\}$ , and the values of

the integral parameters  $J_1$  and  $J_2$ . Assuming that the flow discharge per unit  $q_w$  width is known, the mean flow velocity can be estimated as  $U = q_w / H$ .

$J_1$  is defined above and  $J_2$  is given by

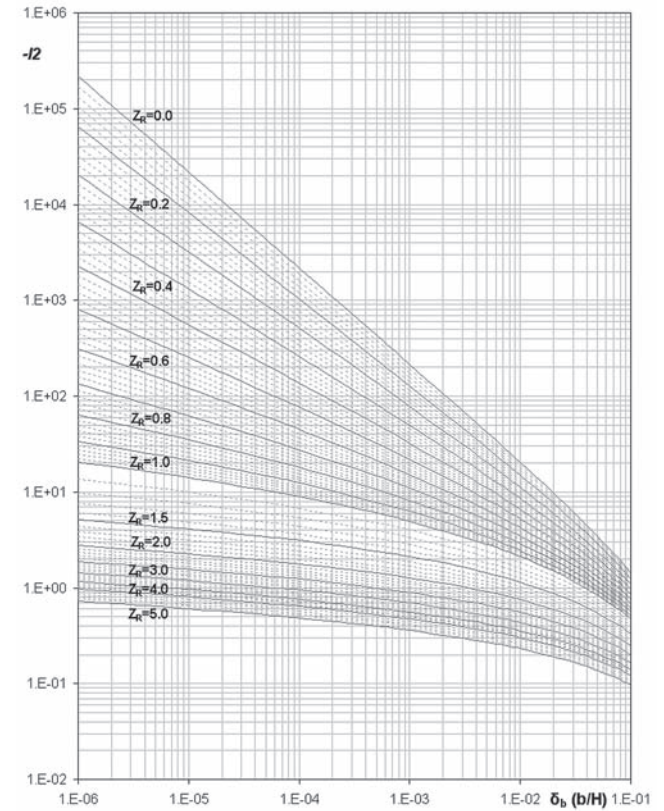
$$J_2 = \int_{\delta_b}^1 \left[ \frac{(1-\delta)/\delta}{(1-\delta_b)/\delta_b} \right]^{Z_R} \ln(\delta) d\delta \quad (2-220a)$$

Again, Einstein (1950) stated another relation for this integral as

$$J_2 = \frac{\delta_b}{0.216} I_2 \quad (2-220b)$$

where  $-I_2$  is also given in tabular form by Fig. 2-55(b).

There have been a number of attempts at finding analytical expressions to estimate the integrals, first presented by Einstein (1950), and shown graphically in Figures 2-55a and



(b)

Fig. 2-55. Einstein integrals (a)  $I_1$  and (b)  $-I_2$ .

**Table 2-5 Coefficients from Regression Analysis for (a)  $J_1$  and (b)  $J_2$** 

$\delta_b$	$C_0$	$C_1$	$C_2$	$C_3$	$C_4$	$C_5$	$C_6$
0.001	8.0321	-26.273	-114.69	501.43	-229.51	41.94	-2.7722
0.005	2.1142	-3.4502	12.491	60.345	-29.421	5.4215	-0.3577
0.01	1.4852	0.2025	14.087	20.918	-10.91	2.034	-0.1345
0.05	1.1038	2.6626	5.6497	0.3822	-0.6174	0.1315	-0.0091
0.1	1.1266	2.6239	3.0838	-0.3636	-0.0734	0.0246	-0.0019

$\delta_b$	$C_0$	$C_1$	$C_2$	$C_3$	$C_4$	$C_5$	$C_6$
0.001	2.5779	-12.418	47.353	17.639	-13.554	2.8392	-0.2003
0.005	1.2623	1.033	13.543	0.7655	-1.6646	0.3803	-0.0275
0.01	1.151	2.1787	7.6572	-0.2777	-0.57	0.1424	-0.0105
0.05	1.2574	2.3159	1.9239	-0.3558	0.0075	0.0064	-0.0006
0.1	1.4952	2.2041	1.0552	-0.2372	0.0265	-0.0008	-0.00005

2-55b (e.g., Nakato 1984; Guo and Wood 1995; Guo and Julien 2004). Recently, Abad and García (2006) have proposed an approach that should be of practical use because it is easy to implement in computational models.

With the help of series analysis and appropriate software, Abad and García (2006) obtained expressions for  $J_1$  and  $J_2$  that are well approximated by the following regression-analysis equations:

$$J_1 = \frac{1}{c_0 + c_1 Z_R + c_2 Z_R^2 + c_3 Z_R^3 + c_4 Z_R^4 + c_5 Z_R^5 + c_6 Z_R^6} \quad (2-221a)$$

and

$$J_2 = \frac{-1}{c_0 + c_1 Z_R + c_2 Z_R^2 + c_3 Z_R^3 + c_4 Z_R^4 + c_5 Z_R^5 + c_6 Z_R^6} \quad (2-221b)$$

All the coefficients in Eqs. (2-221a) and (2-221b) are functions of the parameter  $\delta_b = b / H = z_b / H$  where the near-bed concentration  $c_b^-$  is evaluated. The values of such coefficients for both equations are presented in Tables 5a and 5b.

It is apparent from Eq. (2-219) that further progress is predicated on a method for evaluating the near-bed reference concentration  $c_b^-$ , or equivalently (for the case of equilibrium suspensions) the sediment entrainment rate  $E_s$  (García and Parker 1991; Zyserman and Fredsøe 1994). Such a relation is necessary to model transport of suspended sediment in non-equilibrium situations (Celik and Rodi 1988; Alonso and Mendoza 1992; Admiraal and García 2000).

### 2.9.7 Functions for Sediment Entrainment or Equilibrium Near-Bed Sediment Concentration

A number of relations are available in the literature for estimating the entrainment rate of sediment into suspension  $E_s$  (and thus the reference concentration  $c_b^-$  for the equilibrium

case). Table 2-6 summarizes most of the available relations. It includes the formulations proposed by Einstein (1950); Engelund and Fredsøe (1976); Smith and McLean (1977a), Itakura and Kishi (1980), van Rijn (1984), Engelund and Fredsøe (1982); Celik and Rodi (1984), Akiyama and Fukushima (1986), García and Parker (1991), Zyserman and Fredsøe (1994), and Cao (1999). García and Parker (1991) performed a detailed comparison of eight such relations against data. The relations were checked against a carefully selected set of data pertaining to equilibrium suspensions of uniform sand. In such case, it is possible to measure  $c_b^-$  directly at some near-bed elevation  $z = b$ , and to equate the result to  $E_s$  according to Eq. (2-192).

The data consisted of some 64 sets from 10 different sources, all pertaining to laboratory suspensions of uniform sand with a submerged specific gravity  $R = (\rho_s - \rho) / \rho$  near 1.65. Information about the bed forms was typically not sufficient to allow for a partition of boundary shear stress in accordance with Nelson and Smith (1989). As a result, the shear stress due to skin friction alone  $\tau_{bs}$ , and the associated shear velocity due to skin friction  $u_{*s}$ , given by

$$\tau_{bs} = \rho u_{*s}^2 \quad (2-222a)$$

were computed with Eq. (2-156) with the following relation for roughness height  $k_s$

$$k_s = 2 D_{50} \quad (2-222b)$$

The data covered the following ranges:

$E_s$ : 0.0002 to 0.06

$u_{*s}/v_s$ : 0.70 to 7.50

$H/D$ : 240 to 2400

$R_{ep}$ : 3.50 to 37.00

The range of values of  $R_{ep} = (\sqrt{gRDD}/v)$  corresponds to a grain size range from 0.09 mm to 0.44 mm. Except for

**Table 2-6 Existing Relations to Estimate Sediment Entrainment or Near-Bed Concentration Under Equilibrium Conditions**

Author	Formula	Parameters	Reference height
Einstein (1950)	$\bar{c}_b = \frac{q_*}{23.2(\tau_s^*)^{0.5}}$		$b = 2D_s$
Engelund and Fredsøe (1976; 1982)	$\bar{c}_b = \frac{0.65}{(1 + \lambda_b^{-1})^3}$	$\lambda_b = \left[ \frac{\tau_s^* - 0.06 - \frac{\beta p \pi}{6}}{0.027(R+1)\tau_s^*} \right]^{0.5}; p = \left[ 1 + \left( \frac{\beta \pi}{6} \right)^4 \right]^{-0.25}; \beta = 1.0$	$b = 2D_s$
Smith and McLean (1977)	$\bar{c}_b = \frac{0.65\gamma_o T}{1 + \gamma_o T}$	$T = \frac{\tau_s^* - \tau_c^*}{\tau_c^*}; \gamma_o = 2.4 \cdot 10^{-3}$	$b = \alpha_o (\tau_s^* - \tau_c^*) D_s + k_s$ $\alpha_o = 26.3$
Itakura and Kishi (1980)	$\bar{c}_b = k_1 \left( k_2 \frac{u_*}{v_s} \frac{\Omega}{\tau^*} - 1 \right)$	$\Omega = \frac{\tau^*}{k_3} \left( k_4 + \left[ \frac{\exp(-A_o^2)}{\int_{A_o}^{\infty} \exp(-\xi^2) d\xi} \right] \right) - 1; A_o = \frac{k_3}{\tau^*} - k_4;$ $k_1 = 0.008; k_2 = 0.14; k_3 = 0.143; k_4 = 2.0; v_s = \text{fall velocity}$	$b = 0.05H$
Van Rijn (1984)	$\bar{c}_b = 0.015 \frac{D_s}{b} \frac{T^{1.5}}{D_*^{0.3}}$	$D_* = D_s \left( \frac{gR}{V^2} \right)^{1/3}; \Delta_b \text{ is the mean dune height}$	$b = \frac{\Delta_b}{2}$ if $\Delta_b$ known else $b = k_s, b_{min} = 0.01H$
Celik and Rodi (1984)	$\bar{c}_b = \frac{k_o C_m}{I}$	$C_m = 0.034 \left[ 1 - \left( \frac{k_s}{H} \right)^{0.06} \right] \frac{u_*^2}{gRH} \frac{U_m}{v_s}; I = \int_{0.05}^1 \left( \frac{1-\eta}{\eta} \cdot \frac{\eta_b}{1-\eta_b} \right)^{v_s/0.4u_*} d\eta;$ $h = z/H; h_b = 0.05; k_o = 1.13$	$b = 0.05H$
Akiyama and Fukushima (1986)	$E_s = 0; Z < Z_c$ $E_s = 3 \cdot 10^{-12} Z^{10} \left( 1 - \frac{Z_c}{Z} \right); Z_c < Z < Z_m$ $E_s = 0.3; Z > Z_m$	$Z = \frac{u_*}{v_s} R_p^{0.5}; Z_c = 5; Z_m = 13.2$	$b = 0.05H$
García and Parker (1991)	$E_s = \frac{AZ_u^5}{1 + \frac{A}{0.3} Z_u^5}$	$Z_u = \frac{u_{*s}}{v_s} R_p^n; u_{*s} = \frac{g^{0.5}}{C'} U_m; C' = 18 \cdot \log \left( \frac{12R_b}{3D_s} \right); n = 0.6; A = 1.3 \cdot 10^{-7}$	$b = 0.05H$
Zyserman and Fredsøe (1994)	$\bar{c}_b = \frac{0.331(\tau_s^* - 0.045)^{1.75}}{1 + \frac{0.331}{0.46}(\tau_s^* - 0.045)^{1.75}}$	$\tau_s^* = \frac{(u_{*s})^2}{RgD_s}$	$b = 2D_s$

the somewhat small values of  $H/D$ , the values cover a range that includes typical field sand-bed streams. Three of the relations for  $E_s$  (or  $\bar{c}_b$  at equilibrium) performed particularly well and are presented here. The first of these presented is the relation of García and Parker (1991). The reference level is taken to be 5 % of the depth; that is,

$$\frac{b}{H} = \delta_b = 0.05 \quad (2-223)$$

The relation takes the form

$$E_s = \frac{AZ_u^5}{\left(1 + \frac{A}{0.3}Z_u^5\right)} \quad (2-224a)$$

where

$$A = 1.3 \times 10^{-7} \quad (2-224b)$$

$$Z_u = \frac{u_* s}{v_s} R_{ep}^{0.6} \quad (2-224c)$$

García and Parker (1993) have found that for fine-grained, non-cohesive sediments, Eq. (2-224a) performs well, provided that the similarity variable given by Eq. (2-224c) is modified to

$$Z_u = 0.708 \frac{u_*}{v_s} R_{ep}^{0.6} \text{ for } R_{ep} < 3.5 \quad (2-225)$$

A plot of the García-Parker entrainment function, including data from open-channel flows as well as turbidity currents, is shown in Fig. 2-56. The equation has been used to assess the impact of navigation on sediment resuspension in the Mississippi River basin (García et al. 1999; Admiraal et al. 2000) as well as the inception of channels in submarine fans (Imran et al., 1998). Of all the formulations in the literature, this equation is one of the few that has been generalized to handle sediment mixtures. This generalization of the formula is shown in Eq. (3-143a) of Chapter 3. Because the equation was developed with data from small-sized to medium-sized sand-bed streams, Wright and Parker (2004; 2005b) have found that it needs to be slightly modified for the case of large, low-slope sand-bed rivers. This modification of the formula is shown in Eq. (3-143e) of Chapter 3.

Another relation that has been found to perform well is that of van Rijn (1984b). This relation takes the form,

$$\bar{c}_b = 0.015 \frac{D}{b} \frac{\left(\tau_s^*/\tau_c^* - 1\right)^{1.5}}{D_*^{0.3}} \quad (2-226)$$

Here  $D_* = D(gR/v^2)^{1/3}$  and  $\tau_s^*$  denotes the Shields stress due to skin friction. Van Rijn computes  $\tau_{bs}$  from relations

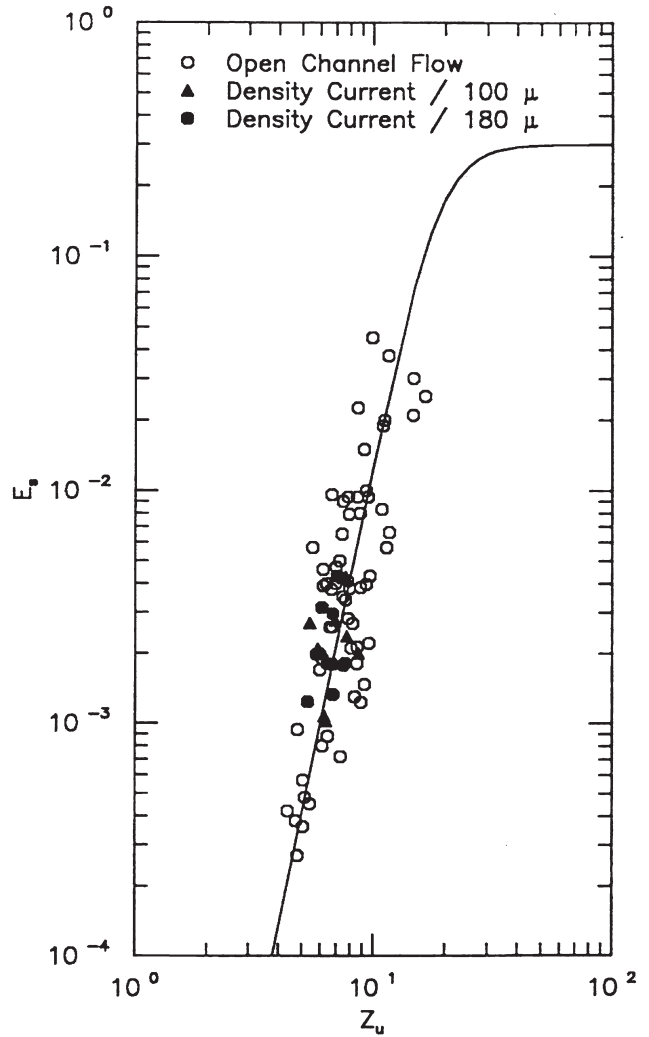


**Fig. 2-56.** Sediment entrainment function of García and Parker (1991, 1993).

that are similar to Eqs. (2-155) and (2-156). Van Rijn's relations are

$$C_{fs} = \frac{1}{\kappa} \ln \left( 12 \frac{H}{k_s} \right)^{-2} \quad (2-227)$$

where for uniform material  $k_s = 3D$ . In this equation, the reference level  $b = 1/2\Delta$ , where  $\Delta$  = bed form height or  $b = k_s$  when the bed form height is not known. Note that in Eq. (2-227), the total depth  $H$  is used, in contrast to Eq. (2-156) where  $H_s$  is used. Van Rijn's formulation has been used extensively in numerical models of suspended sediment transport and bed morphology (e.g., Duan et al. 2001; Zeng et al. 2006). Its application for two-dimensional and three-dimensional sediment transport modeling is illustrated in Chapter 15.

A third relation that performs well is that of Smith and McLean (1977). Its origin can be traced back to the early work of Yalin (1963) on bed load transport and was first proposed by Smith (1977). It can be expressed as

$$\bar{c}_b = 0.65 \frac{\gamma_o (\tau_s^*/\tau_c^* - 1)}{1 + \gamma_o (\tau_s^*/\tau_c^* - 1)} \quad (2-228a)$$

where

$$\gamma_o = 0.0024 \quad (2-228b)$$

The value  $b$  at which  $\bar{c}_b$  is to be evaluated is given by the relation below:

$$b = 26.3 (\tau_s^*/\tau_c^* - 1) D + k_s \quad (2-228c)$$

Here  $k_s$  denotes the equivalent roughness height (i.e., Nikuradse's roughness) for a fixed bed. The Smith-Mclean formulation is used extensively in benthic boundary layer flows and oceanic sedimentation (e.g., Wiberg et al. 1994; Hill and McCave 2001).

After the comparative analysis of different entrainment formulations by García and Parker (1991), Zyberman and Fredsøe (1994) proposed an empirical relation using the Fort Collins experimental data. It reads

$$\bar{c}_b = \frac{0.331(\tau_s^* - \tau_c^*)^{1.75}}{1 + 0.72(\tau_s^* - \tau_c^*)^{1.75}} \quad (2-229)$$

In this formulation the near-bed equilibrium concentration  $\bar{c}_b$  is assigned to a reference level  $b = 2D_{50}$ . Even though this relation was developed with laboratory data, it has been used to estimate near-bed sediment concentration in coastal sediment transport (e.g., Soulsby 1997).

### 2.9.8 Example of Depth-Discharge and Sediment Load Computation

Consider the example stream of Section 2.8.2. For this stream,  $S = 0.0004$  and  $D = 0.35$  mm (uniform material). At bankfull flow, the stream width is 75 m. For flows below bankfull, the following sample relation is assumed (Parker and Peterson 1980):

$$\frac{B}{B_{bf}} = \left( \frac{Q}{Q_{bf}} \right)^{0.1}$$

A more precise relation can be worked out for any cross section using measured cross-sectional profiles in a stream. Here the subscript  $bf$  denotes bank-full. Assume that the stream is wide enough to equate the hydraulic radius  $R_h$  with the cross-sectionally averaged depth  $H$ .

1. Compute depth-discharge relations for flows up to bank-full (lower regime only) using the Engelund-Hansen method. Plot  $H$  versus  $Q$ . Use the results of the Engelund-Hansen method to compute values of  $\tau_s^*$  as well.

2. Use the values of  $\tau_s^*$  to compute the bed load discharge  $Q_b = q_b B$  using the Ashida-Michiue formulation (Eq. 2-94). For each value of  $H$  and  $U$ , back-calculate the composite roughness  $k_c$ . Then compute the suspended load  $Q_s = q_s B$  from the Einstein formulation and the relation for  $E_s$  due to García and Parker. Plot  $Q_b$ ,  $Q_s$ , and  $Q_T = Q_b + Q_s$  as functions of water discharge  $Q$ .

For example, compute the flow depth, bed load discharge, and suspended load discharge as a function of flow discharge for a stream with the following properties:

$$S = 0.0004$$

$$D_s = 0.35 \text{ mm} = 3.5 \times 10^{-4} \text{ m}$$

$$R = 1.65$$

$$B = 75 \text{ m at bankfull}$$

$$H = 2.9 \text{ m at bankfull}$$

The calculations are performed for flows up to bank-full. For flows below bank-full, the following relation is used to calculate the stream width:

$$(i) \quad \frac{B}{B_{bf}} = \left( \frac{Q}{Q_{bf}} \right)^{0.1} = \left( \frac{U H B}{Q_{bf}} \right)^{0.1}$$

where the subscript  $bf$  indicates bankfull values. Solving for the stream width  $B$  yields:

$$(ii) \quad B = \left[ B_{bf} \left( \frac{U H}{Q_{bf}} \right)^{0.1} \right]^{1/0.9}$$

The methods used to determine  $Q$ ,  $Q_b$ ,  $Q_s$ , and  $Q_{bf}$  are described below. A computer program can be written or a spreadsheet can be used to perform the necessary calculations. All computations and results are summarized in Table 2-7.

**2.9.8.1 Depth-Discharge Calculations** The depth-discharge relation is computed using the Engelund-Hansen method. The calculations are performed by assuming a value for  $H_s$  (the flow depth that would be expected in the absence of bedforms), and then calculating the actual flow depth ( $H$ ) and the flow discharge ( $Q$ ).  $H_s$  is varied between 0.22 m and the bank-full value of 2.9 m. The first step in calculating the depth-discharge relation is to compute the resistance coefficient due to skin drag ( $C_{fs}$ ) from  $H_s$ :

**Table 2-7 Computation of Depth-Discharge Relation and Total Sediment Load**

Hs (m)	U Cfs	Width B (m/s)	H $\tau_s^*$	Discharge $\tau^*$	Depth (m)	Q (m <sup>3</sup> /s)	$q_b$ $q_b^*$	$Q_b$ (m <sup>3</sup> /s)	$k_c$ (m)	$Z_u$	$E_s$ (m/s)	$u^*$	Rouse#	$J_1$	$J_2$	$q_s$ (m <sup>2</sup> /s)	$Q_s$ (m <sup>3</sup> /s)	$Q_t$ (m <sup>3</sup> /s)		
0.10	0.003	0.353	0.069	0.152	0.220	45.282	3.516	0.01296	0.00000	0.00002	0.00192	2.51992	0.00001	0.02936	4.76463	0.01219	-0.03363	0.00000	0.00000	0.00002
0.20	0.003	0.548	0.139	0.443	0.640	53.541	18.781	0.22362	0.00001	0.00032	0.00280	3.56370	0.00007	0.05010	2.79237	0.02417	-0.06165	0.00000	0.00005	0.00036
0.30	0.002	0.706	0.208	0.608	0.878	57.038	35.358	0.62296	0.00002	0.00094	0.00256	4.36462	0.00021	0.05868	2.38406	0.03008	-0.07401	0.00001	0.00031	0.00124
0.40	0.002	0.844	0.277	0.737	1.064	59.434	53.359	1.16862	0.00003	0.00183	0.00233	5.03983	0.00042	0.06460	2.16564	0.03447	-0.08272	0.00002	0.00106	0.00289
0.50	0.002	0.969	0.346	0.846	1.221	61.284	72.500	1.83808	0.00005	0.00297	0.00214	5.63470	0.00074	0.06923	2.02077	0.03809	-0.08962	0.00004	0.00269	0.00566
0.60	0.002	1.083	0.416	0.943	1.361	62.801	92.588	2.61681	0.00007	0.00433	0.00199	6.17251	0.00116	0.07309	1.91423	0.04122	-0.09539	0.00009	0.00569	0.01002
0.70	0.002	1.190	0.485	1.031	1.488	64.093	113.487	3.49443	0.00009	0.00590	0.00186	6.66707	0.00170	0.07641	1.83093	0.04400	-0.10040	0.00017	0.01065	0.01655
0.80	0.002	1.291	0.554	1.111	1.605	65.220	135.098	4.46304	0.00012	0.00767	0.00176	7.12740	0.00237	0.07935	1.76309	0.04652	-0.10484	0.00028	0.01825	0.02592
0.90	0.002	1.387	0.623	1.187	1.713	66.221	157.342	5.51640	0.00015	0.00962	0.00167	7.55975	0.00318	0.08200	1.70620	0.04883	-0.10884	0.00044	0.02925	0.03887
1.00	0.002	1.478	0.693	1.258	1.816	67.124	180.160	6.64937	0.00018	0.01176	0.00159	7.96868	0.00412	0.08441	1.65745	0.05098	-0.11249	0.00066	0.04449	0.05625
1.10	0.002	1.566	0.762	1.325	1.912	67.947	203.503	7.85765	0.00021	0.01407	0.00152	8.35762	0.00521	0.08663	1.61496	0.05299	-0.11585	0.00095	0.06488	0.07894
1.20	0.002	1.651	0.831	1.388	2.005	68.704	227.329	9.13758	0.00024	0.01654	0.00146	8.72925	0.00645	0.08869	1.57740	0.05488	-0.11898	0.00133	0.09138	0.10792
1.30	0.002	1.732	0.900	1.450	2.093	69.404	251.603	10.48599	0.00028	0.01917	0.00141	9.08569	0.00784	0.09062	1.54385	0.05667	-0.12189	0.00180	0.12503	0.14421
1.40	0.002	1.811	0.970	1.508	2.177	70.057	276.297	11.90008	0.00031	0.02196	0.00136	9.42866	0.00938	0.09243	1.51358	0.05837	-0.12463	0.00238	0.16689	0.18885
1.50	0.002	1.888	1.039	1.564	2.259	70.669	301.385	13.37737	0.00035	0.02490	0.00132	9.75959	0.01109	0.09414	1.48607	0.05999	-0.12722	0.00309	0.21805	0.24295
1.60	0.002	1.963	1.108	1.619	2.337	71.244	326.844	14.91565	0.00039	0.02799	0.00128	10.07967	0.01294	0.09577	1.46089	0.06155	-0.12967	0.00392	0.27963	0.30762
1.70	0.002	2.036	1.177	1.671	2.413	71.788	352.654	16.51293	0.00044	0.03123	0.00124	10.38988	0.01496	0.09731	1.43770	0.06304	-0.13200	0.00491	0.35277	0.38400
1.80	0.002	2.107	1.247	1.722	2.487	72.303	378.798	18.16739	0.00048	0.03460	0.00121	10.69110	0.01712	0.09878	1.41625	0.06447	-0.13421	0.00607	0.43860	0.47320
1.90	0.002	2.176	1.316	1.772	2.558	72.793	405.260	19.87737	0.00052	0.03812	0.00118	10.98406	0.01944	0.10019	1.39631	0.06585	-0.13634	0.00739	0.53825	0.57637
2.00	0.002	2.244	1.385	1.820	2.628	73.260	432.026	21.64136	0.00057	0.04177	0.00115	11.26941	0.02190	0.10155	1.37769	0.06719	-0.13837	0.00891	0.65283	0.69460
2.10	0.002	2.311	1.455	1.867	2.696	73.706	459.083	23.45795	0.00062	0.04555	0.00112	11.54771	0.02451	0.10285	1.36026	0.06848	-0.14032	0.01063	0.78342	0.82897
2.20	0.002	2.376	1.524	1.913	2.762	74.134	486.419	25.32585	0.00067	0.04946	0.00110	11.81946	0.02726	0.10410	1.34387	0.06973	-0.14220	0.01256	0.93107	0.98053
2.30	0.002	2.440	1.593	1.958	2.826	74.544	514.024	27.24386	0.00072	0.05350	0.00108	12.08510	0.03014	0.10531	1.32843	0.07094	-0.14401	0.01471	1.09677	1.15027
2.40	0.002	2.502	1.662	2.001	2.890	74.939	541.887	29.21083	0.00077	0.05767	0.00105	12.34502	0.03315	0.10648	1.31384	0.07212	-0.14575	0.01710	1.28147	1.33914

$$(iii) \quad C_{fs} = \left[ \frac{1}{\kappa} \ln \left( 11 \frac{H_s}{k_s} \right) \right]^{-2}$$

where  $\kappa$  is the von Karman constant (0.4) and  $k_s$  is given by

$$(iv) \quad k_s = 2.5 D_s = 2.5 (3.5 \cdot 10^{-4}) = 8.75 \times 10^{-4} \text{ m}$$

The depth-averaged flow velocity ( $U$ ) can be found from  $C_{fs}$  and  $H_s$

$$(v) \quad U = \sqrt{\frac{g H_s S}{C_{fs}}}$$

The Shields stress due to skin friction ( $\tau_s^*$ ) is given by

$$(vi) \quad \tau_s^* = \frac{\tau_{bs}}{\rho g R D_s} = \frac{H_s S}{R D_s}$$

According to Engelund-Hansen, the total Shields stress for the lower regime can be found from the following relation:

$$(vii) \quad \tau^* = \sqrt{\frac{\tau_s^* - 6}{0.4}}$$

The flow depth can be calculated from the total Shields stress as follows:

$$(viii) \quad H = \frac{\tau^* R D_s}{S}$$

Finally, the discharge can be calculated from the results of Eqs. (v) and (viii):

$$(ix) \quad Q = U H B$$

where  $B$  must be adjusted according to Eq. (ii) for flows less than bankfull. A plot of the depth-discharge relation is shown in Fig. 2-57(a).

**2.9.8.2 Bed Load Discharge Calculations** The dimensionless bed load transport rate ( $q^*$ ) is found from the Ashida-Michiue formulation:

$$(x) \quad q^* = 17(\tau_s^* - \tau_c^*) [(\tau_s^*)^{0.5} - (\tau_c^*)^{0.5}]$$

where  $\tau_s^*$  is calculated in Eq. (vi) and  $\tau_c^*$  is taken to be 0.05. The bed load transport rate per unit width  $q_b$  is given by

$$(xi) \quad q_b = q^* \sqrt{g R D_s} D_s$$

Therefore, the bedload transport rate (in  $\text{m}^3/\text{s}$ ) is given by

$$(xii) \quad Q_b = q_b B$$

Again,  $B$  must be adjusted according to Eq. (ii) for flows less than bank-full.

**2.9.8.3 Sediment Load Discharge Calculations** The Einstein formulation is used to compute the suspended load transport rate per unit width  $q_s$ ,

$$(xiii) \quad q_s = \frac{1}{\kappa} \bar{c}_b u_* H \left[ J_1 \ln \left( 30 \frac{H}{k_c} \right) + J_2 \right]$$

where

$$(xiv) \quad u_* = \sqrt{g H S}$$

If the suspension is assumed to be at equilibrium,  $\bar{c}_b = E_s$ . The dimensionless rate of entrainment ( $E_s$ ) is calculated with the relation of García and Parker (1991),

$$(xv) \quad E_s = \frac{A Z_u^5}{\left( 1 + \frac{A}{0.3} Z_u^5 \right)}$$

where  $A$  is equal to  $1.3 \times 10^{-7}$  and

$$(xvi) \quad Z_u = \frac{u_{*s}}{v_s} R_{ep}^{0.6}$$

$$(xvii) \quad u_{*s} = \sqrt{g H_s S}$$

$$(xviii) \quad R_{ep} = \frac{\sqrt{R g D_s D_s}}{v}$$

Notice that for the entrainment formulation, the shear velocity associated with skin friction  $u_{*s}$  has to be used. The temperature is assumed to be about  $20^\circ\text{C}$ ; therefore, the kinematic viscosity  $v$  is about  $10^{-6} \text{ m}^2/\text{s}$ . An iterative method, or Eq. (2-47a), is used to calculate the terminal fall velocity of the sediment particles  $v_s$ , which is found to be  $5.596 \times 10^{-2} \text{ m/s}$ . The composite roughness ( $k_c$ ) is calculated according to the following relation:

$$(xix) \quad k_c = 11 H \exp \left\{ - \frac{\kappa U}{u_*} \right\}$$

The Einstein integral parameters  $J_1$  and  $J_2$  are found for  $\delta_b = 0.05$  with the help of Equations (2-221a) and (2-221b).

The suspended load transport rate per unit width calculated according to Eq. (xiii) is used to compute the suspended load transport rate suspended load per unit width  $q_s$ , so that the total suspended load can be obtained (in  $\text{m}^3/\text{s}$ ) with

$$(xx) \quad Q_s = q_s B$$

For flows less than bankfull flow, the channel width  $B$  must be adjusted according to Eq. (ii).

**2.9.8.4 Determination of Bank-Full Flow Discharge ( $Q_{bp}$ )** The flow discharge at bankfull ( $Q_{bp}$ ) is determined by assuming that up to bank-full flow, lower regime conditions exist. The bank-full flow depth for this stream is assumed to

be 2.9 m. Then for bank-full flow, the total shear stress  $\tau^*$  is given by

$$(xxi) \quad \tau^* = \frac{HS}{RD_s} = \frac{2.9 \cdot 0.0004}{1.65 \cdot 3.5 \times 10^{-4}} = 2.01$$

From Engelund and Hansen,

$$(xxii) \quad \tau_s^* = 0.06 + 0.4(\tau^*)^2 = 0.06 + 0.4(2.01)^2 = 1.67$$

$$(xxiii) \quad H_s = \frac{\tau_s^* RD_s}{S} = \frac{1.67 \times 1.65 \times (3.5 \times 10^{-4})}{0.0004} = 2.42 \text{ m}$$

$$C_{fs} = \left[ \frac{1}{\kappa} \ln \left( 11 \frac{H_s}{k_s} \right) \right]^{-2}$$

$$(xxiv) \quad = \left[ \frac{1}{0.4} \ln \left( 11 \frac{2.42}{8.75 \times 10^{-4}} \right) \right]^{-2} = 1.5 \times 10^{-3}$$

$$(xxv) \quad U = \sqrt{\frac{g H_s S}{C_{fs}}} \\ = \sqrt{\frac{9.81 \times 2.42 \times 0.0004}{1.5 \times 10^{-3}}} = 2.51 \text{ m/s}$$

$$(xxvi) \quad Q_b = UHB = 2.51 \times 2.9 \times 75 = 546.35 \text{ m}^3/\text{s}$$

A plot of  $Q_b$ ,  $Q_s$ , and  $Q_T = Q_b + Q_s$  as functions of water discharge is shown in Fig. 2-57(b). For flows up to 100  $\text{m}^3/\text{s}$ , the bed load discharge is larger than the suspended load discharge. As the flow discharge increases, the suspended load becomes much larger than the bed load all the way up to bank-full flow conditions.

Notice also that the composite roughness  $k_c$  (grain-friction plus form drag) first increases with flow discharge for low flows, but from then on it decreases monotonically as the bedforms begin to be washed out by the flow. For bank-full conditions, the bedforms have a small effect on flow resistance in this particular example.

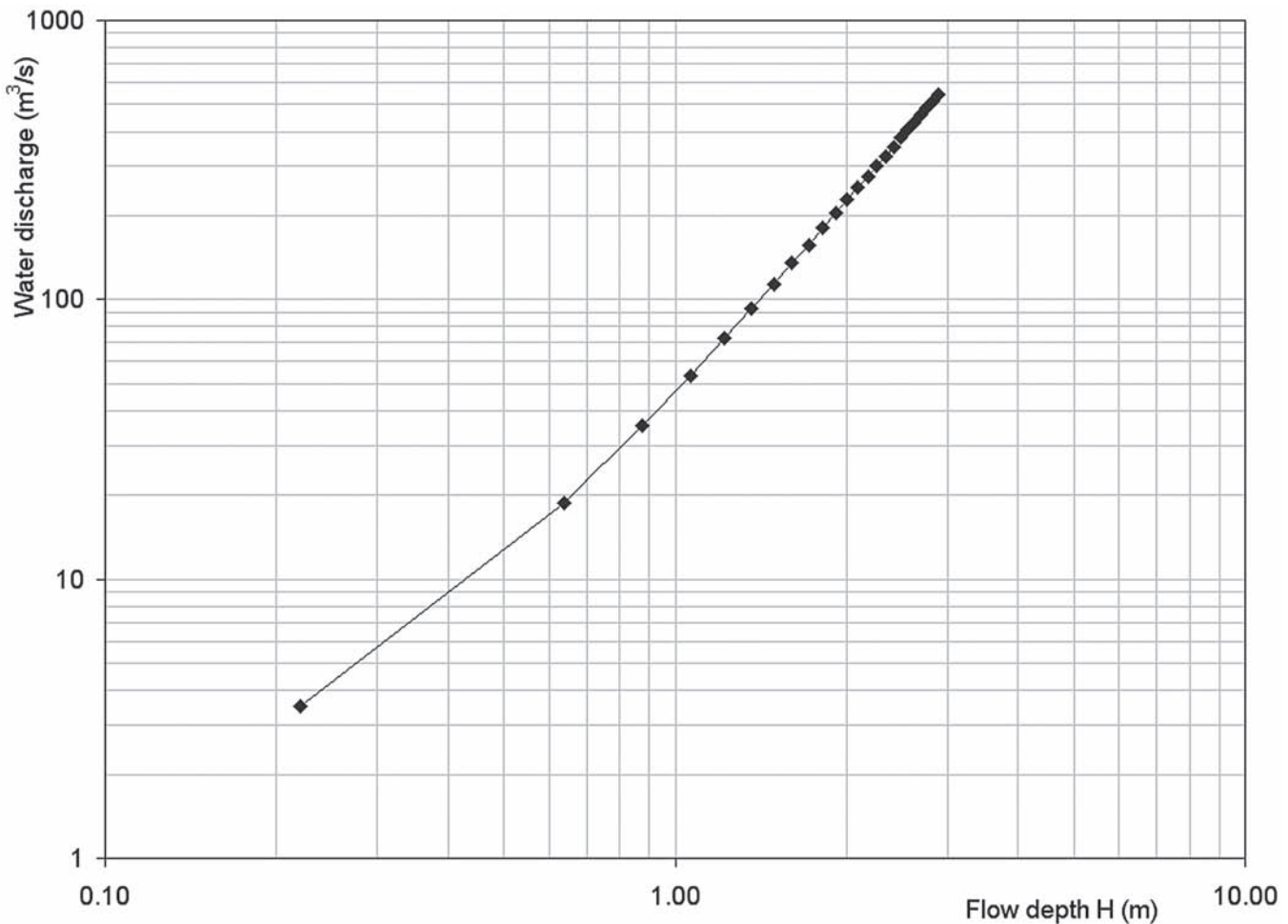
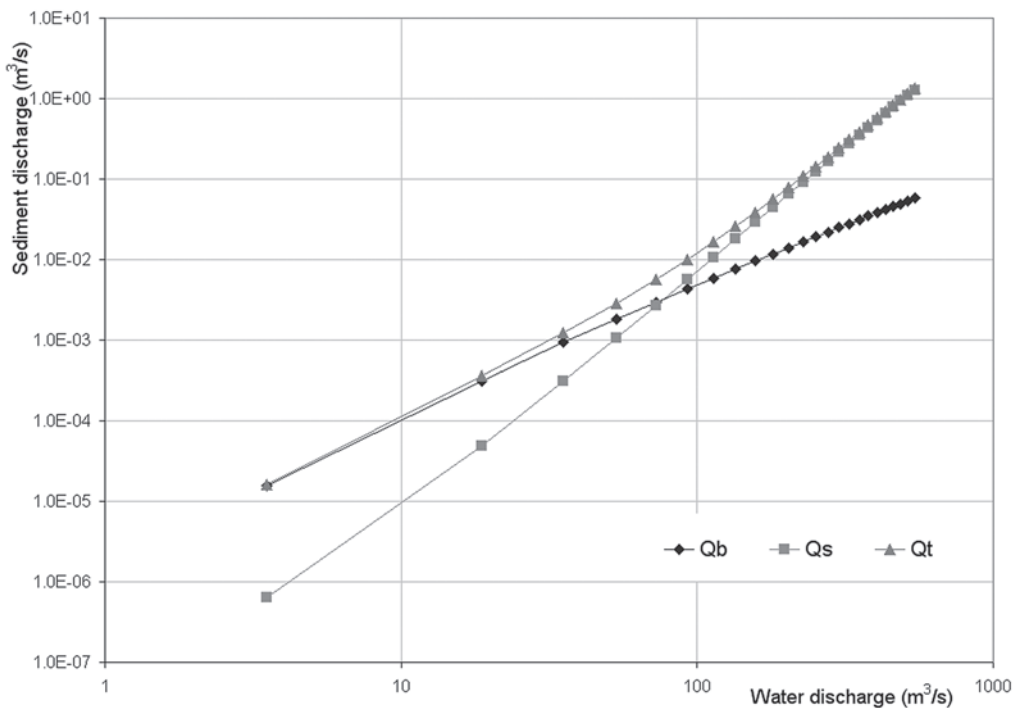


Fig. 2-57. (a) flow discharge rating curve, and (b) sediment discharge rating curves for bed load, suspended load and total load.



**Fig. 2-57.** (a) flow discharge rating curve, and (b) sediment discharge rating curves for bed load, suspended load and total load. (*Continued*)

## 2.10 DIMENSIONLESS RELATIONS FOR TOTAL BED-MATERIAL LOAD IN SAND-BED STREAMS

### 2.10.1 Form of the Relations

In the analysis presented in previous sections, the guiding principle has been the development of mechanistically accurate models of the bed load and suspended load components of bed-material load. The total bed-material load is then computed as the sum of the two. That is, where  $q_b$  denotes the volume bed load transport rate per unit width, and  $q_s$  denotes the volume suspended load transport rate per unit width (bed material only), the total volume transport rate of bed material per unit width  $q_t$  is given by

$$q_t = q_b + q_s \quad (2-229)$$

Another, simpler approach is to ignore the details of the physics of the problem, and instead use empirical techniques such as regression analysis to correlate dimensionless parameters involving  $q_t$  to dimensionless flow parameters inferred to be of importance for sediment transport. This can be implemented in the strict sense only for equilibrium or quasi-equilibrium flows, i.e., near-normal flow conditions. The resulting relations are no better than the choice of dimensionless parameters to be correlated. They are also less versatile than physically based relations, because their application to non-steady, nonuniform flow fields is not obvious. On the other hand, they have the advantage of being relatively simple to use and of having been calibrated to sets of both laboratory and field data often deemed to be trustworthy.

Here six such relations are presented, those due to Engelund and Hansen (1967); Ackers and White (1973); Yang (1973); Brownlie (1981b); Karim and Kennedy (1981; 1990); and Molinas and Wu (2001).

They apply only to sand-bed streams with relatively uniform bed sediment. The Engelund and Hansen relation together with the relations of Brownlie and Karim and Kennedy, are the most complete ones, as each is presented as a pair of relations for total load and hydraulic resistance. Ackers and White (1973), Yang (1973), and Molinas and Wu (2001) are presented as relations for total load only. In most cases, it will also be necessary for the user to specify a relation for hydraulic resistance in order to perform actual calculations. Computations for one-dimensional river modeling using the Ackers-White, Engelund-Hansen, and Yang transport relations are presented in Chapter 14.

As stated earlier, the importance of using transport and hydraulic resistance relations as pairs cannot be overemphasized (e.g., Parker and Anderson 1977). Consider, for example, the simplest generalization beyond the assumption of normal flow, the case of quasi-steady, gradually varied one-dimensional flow. The governing equations for a wide rectangular channel with flow in the streamwise  $x$  direction, can be written as (Chow 1959)

$$\frac{d}{dx} \left( \frac{V^2}{2g} + H \right) = S - S_f \quad (2-230a)$$

$$q_w = UH \quad (2-230b)$$

Here the friction slope  $S_f$  is given as

$$S_f = \frac{\tau_b}{\rho g H} = C_f \frac{U^2}{g H} \quad (2-231)$$

A slightly more general form for non-rectangular channels is

$$\frac{d}{dx} \left( \frac{1}{2} \frac{Q^2}{g A^2} + \xi_b \right) = S - S_f \quad (2-232a)$$

$$Q = U A \quad (2-232b)$$

where

$A$  = channel cross-sectional area,

And the friction slope  $S_f$  is given as

$$S_f = \frac{\tau_b}{\rho g R_h} = C_f \frac{U^2}{g R_h} \quad (2-233)$$

In the above equations,  $R_h$  denotes the hydraulic radius and  $\xi_b$  denotes the water surface elevation above the deepest point in the channel, as shown in Fig. 2-58.

Note that in the case of normal flow, the momentum equations reduce to  $S_f = S$ , or  $\tau_b = \rho g H S$  for the wide rectangular case and  $\tau_b = \rho g R_h S$  for the non-rectangular, natural case. In the case of gradually varied flow, however,  $S_f \neq S$ , in which case the bed slope  $S$  cannot be used as a basis for calculating sediment transport. The appropriate choice is  $S_f$ , so that from Eq. (2-233), for example,

$$\tau_b = \rho g R_h S_f \quad (2-234)$$

It should be apparent for the case of gradually varying flow, then, that the friction slope necessary to perform sediment

transport calculations must be obtained from a predictor of hydraulic resistance. Chollet and Cunge (1979) demonstrate a useful approach to estimate friction slopes for unsteady flow computations (i.e., head losses) using two hydraulic resistance predictors developed for steady, normal flow conditions (i.e., Einstein-Barbarossa and Engelund-Hansen). Chapter 14 also presents relevant information on how the friction slope is estimated for one-dimensional computational modeling.

A few parameters are introduced here. Let  $Q$  denote the total water discharge, and  $Q_{st}$  the total volume of bed-material sediment discharge. Furthermore, let  $B_a$  denote the active width of the river over which bed material is free to move as described in Fig. 2-58. In general,  $B_a$  is usually somewhat less than water surface width  $B$  due to the common tendency for the banks to be cohesive, vegetated, or both.

It follows then that

$$Q = B q_w \quad (2-235a)$$

$$Q_{st} = B_a q_t \quad (2-235b)$$

One dimensionless form for dimensionless total bed material transport per unit width is  $q_t^*$  where

$$q_t^* = \frac{q_t}{\sqrt{R g D D}} \quad (2-236)$$

where

$D$  = grain size usually equated to  $D_{50}$ .

Another commonly used measure is concentration by weight in parts per million, here called  $C_s$ . This can be given as

$$C_s = 10^6 \frac{\rho_s Q_{st}}{\rho Q + \rho_s Q_{st}} \quad (2-237)$$

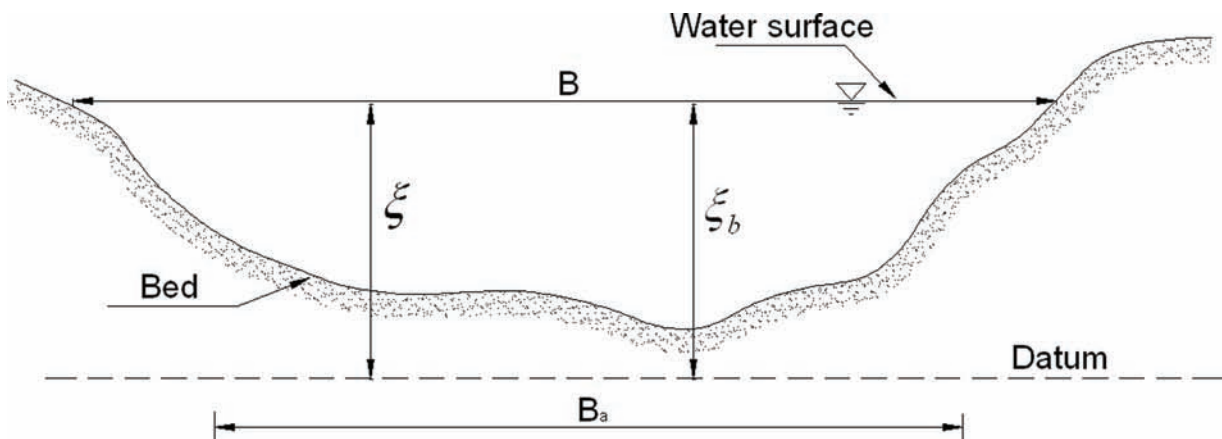


Fig. 2-58. Definition diagram for channel parameters.

## 2.10.2 The Engelund-Hansen Relation

**2.10.2.1 Sediment Transport** This relation is one of the simplest to use for sediment transport, and also one of the most accurate. It was determined from a rather small set of laboratory data (Guy et al. 1966), but performs quite well as a field predictor as well. It takes the form

$$C_f q_t^* = 0.05 (\tau^*)^{5/2} \quad (2-238)$$

where

$C_f$  = total resistance coefficient (skin friction plus form drag); and

$\tau^*$  = total (skin friction plus form drag) Shields stress based on the size  $D_{50}$ .

**2.10.2.2 Hydraulic Resistance** The hydraulic resistance relation of Engelund and Hansen has already been introduced above. It must be written in several parts. The key relation for skin friction is

$$C_{fs}^{-1/2} = \frac{U}{\sqrt{g R_{hs} S}} = 2.5 \ln \left( 11 \frac{R_{hs}}{k_s} \right) \quad (2-239a)$$

where

$$k_s = 2 \text{ to } 2.5 D_{50}$$

Here,  $R_{hs}$  denotes the hydraulic radius due to skin friction, which often can be approximated by  $H_s$ . The relation for form drag can be written in the form

$$\tau_s^* = f(\tau^*) \quad (2-239b)$$

where for the lower regime

$$\tau_s^* = 0.06 + 0.4(\tau^*)^2 \quad (2-239c)$$

and for the upper regime

$$\tau_s^* = \begin{cases} \tau^* & ; \tau^* < 1 \\ \left[ 0.298 + 0.702 - (\tau^*)^{-1.8} \right]^{-(1/1.8)} & ; \tau^* > 1 \end{cases} \quad (2-239d)$$

An approximate condition for the transition between the lower and upper regimes is given by

$$\tau_s^* = 0.55 \quad (2-239e)$$

The Engelund-Hansen relation has been found to be a good predictor of both laboratory and field data in spite of its simplicity.

### 2.10.2.3 Computational Procedure for Normal Flow

The water discharge  $Q$ , slope  $S$ , and grain size  $D_{50}$  must be known. In addition, channel geometry must be known, so that  $B$ ,  $B_a$ ,  $A$ ,  $H$ ,  $P$ , and  $R_h$  are all known functions of stage (water surface elevation)  $\xi$ . The procedure is best outlined assuming that  $R_{hs}$  is known and  $Q$  is to be calculated, rather than vice versa. For any given value of  $R_{hs}$  (or  $H_s$ ),  $U$  can be computed from Eq. (2-239a). Noting that  $\tau_s^* = R_{hs} S / (R D_{50})$  and  $\tau^* = R_h S / (R D_{50})$ ,  $\tau_s^*$ , and thus,  $R_h$  can be computed from Eqs. (2-239b-e). The plot of  $R_h$  versus water surface elevation  $\xi$  is used to determine  $\xi_b$ , which is then used to determine  $B$ ,  $B_a$ ,  $H$ ,  $A$ ,  $P$ , etc. Discharge  $Q$  is then given by  $Q = U B H$ . In an actual implementation, this process is reversed ( $Q$  is given and  $R_{hs}$ , etc., is computed). This requires an iterative technique; Newton-Raphson is not difficult to implement (e.g., Parker 2005).

Once the calculation of hydraulic resistance is complete, it is possible to proceed with the computation of total bed material load  $Q_{st}$ . The friction coefficient  $C_f$  is given by  $(g R_h S) / U^2$ . Placing the known values of  $C_f$  and  $\tau^*$  into (2-238),  $q_t^*$ , and thus,  $q_t$  can be computed. It follows that  $Q_{st} = q_t B_a$ .

**2.10.2.4 Computational Procedure for Gradually Varied Flow** To implement the method for gradually varied flow, it is necessary to recast the above formulation into an algorithm for friction slope  $S_f$ , which replaces  $S$  everywhere in the formulation of Eqs. (2-239a) to (2-239e). The formulation is then solved in conjunction with Eqs. (2-230a) and (2-230b) or Eqs. (2-232a) and (2-232b) to determine the appropriate backwater curve. Once  $C_f$  and  $\tau_b$  are known everywhere, the sediment transport rate can be calculated from Eq. (2-238). Computations for gradually-varied flow with the Engelund-Hansen relations are presented in Chapter 14.

## 2.10.3 The Brownlie Relation

**2.10.3.1 Sediment Transport** The Brownlie relations are based on regressions of over 1000 experimental and field data points. For normal or quasi-normal flow, the transport relation takes the form

$$C_s = 7115 c_f (F_g - F_{go})^{1.978} S^{0.6601} \left( \frac{R_h}{D_{50}} \right)^{-0.3301} \quad (2-240a)$$

where

$$F_g = \frac{U}{\sqrt{R g D_{50}}} \quad (2-240b)$$

$$F_{go} = 4.596 (\tau_c^*)^{0.5293} S^{-0.1045} \sigma_g^{-0.1606} \quad (2-240c)$$

$$\tau_c^* = 0.22 Y + 0.06 \cdot 10^{-7.7Y} \quad (2-240d)$$

$$Y = R_{ep}^{-0.6} \quad (2-240e)$$

In Eq. (2-240a),  $c_f = 1$  for laboratory flumes and 1.268 for field channels. The parameters  $\tau_c^*$  and  $R_{ep}$  are the ones previously introduced in this chapter.

**2.10.3.2 Hydraulic Resistance** The Brownlie relations for hydraulic resistance were determined by regression from the same set of data used to determine the relation for sediment transport. The relation for lower regime flow is

$$\frac{R_h}{D_{50}} S = 0.3724 (\tilde{q})^{0.6539} S^{0.09188} \sigma_g^{0.1050} \quad (2-241a)$$

The corresponding relation for upper regime flow is

$$\frac{R_h}{D_{50}} S = 0.2836 (\tilde{q})^{0.6248} S^{0.08750} \sigma_g^{0.08013} \quad (2-241b)$$

In these relations,

$$\tilde{q} = \frac{q_w}{\sqrt{g D_{50} D_{50}}} \quad (2-241c).$$

The distinction between lower and upper regime is made as follows (see Fig. 2-44). For  $S > 0.006$ , the flow is assumed always to be in the upper regime. For  $S < 0.006$ , the largest value of  $F_g$  at which the lower regime can be maintained is taken to be

$$F_g = 0.8 F'_g \quad (2-241d)$$

And the smallest value of  $F_g$  for which upper regime can be maintained is taken to be

$$F_g = 1.25 F'_g \quad (2-241e)$$

In the above relations

$$F'_g = 1.74 S^{-1/3} \quad (2-241f)$$

**2.10.3.3 Computational Procedure for Normal Flow** It is necessary to know  $Q$ ,  $S$ ,  $D_{50}$ ,  $\sigma_g$ , and cross-sectional geometry as a function of stage. The computation is explicit, although trial and error may be required in order to determine the flow regime. Hydraulic radius is computed from Eq. (2-241a) or Eq. (2-241b), and the result can be substituted

into Eq. (2-240a) in order to determine the concentration  $C_s$  in parts per million by weight. The transport rate  $Q_{st}$  is then computed from Eq. (2-237).

**2.10.3.4 Computation for Gradually Varied Flow** The Brownlie relation is not presented in a form that obviously allows extension to gradually varied flow. The most unambiguous procedure, however, is to replace  $S$  with  $S_f$  in the resistance relation and to couple it with a backwater calculation to determine  $S_f$ . The friction slope is then substituted into Eq. (2-240a) in place of the bed slope in order to determine the sediment transport rate.

## 2.10.4 The Ackers-White Relation

Based on Bagnold's stream power concept, Ackers and White (1973) applied dimensional analysis to express the mobility and transport rate of sediment in terms of dimensionless parameters. Several years later a corresponding relation for hydraulic resistance was also presented (White et al. 1980; 1982). Only the sediment load equation is presented here. It takes the form

$$C_s = 10^6 c \frac{\rho_s}{\rho} \frac{D_{50}}{R_h} \left( \frac{U}{u_*} \right)^n \left( \frac{F_{gr}}{A_{aw}} - 1 \right)^m \quad (2-242a)$$

where the so-called Ackers-White mobility number is given by

$$F_{gr} = \frac{u_*^n u'_*^{1-n}}{\sqrt{R g D_{50}}} \quad (2-242b)$$

$$u'_* = \frac{U}{\sqrt{32} \log \left( 10 \frac{R_h}{D_{50}} \right)} \quad (2-242c)$$

The parameters  $n$ ,  $m$ ,  $c$ , and  $A_{aw}$  were determined with best-fits of laboratory data, as functions of a dimensionless grain size  $D_{gr}$ , where

$$D_{gr} = R_{ep}^{2/3} \quad (2-242d)$$

in the following fashion. If  $D_{gr} > 60$ , then

$$n = 0 \quad (2-242e)$$

$$m = 1.5 \quad (2-242f)$$

$$A_{aw} = 0.17 \quad (2-242g)$$

$$c = 0.025 \quad (2-242h)$$

If  $1 < D_{gr} < 60$ , then

$$n = 1 - 0.56 \log(D_{gr}) ; \quad m = \frac{9.66}{D_{gr}} + 1.34 \quad (2-242i)$$

$$m = \frac{9.66}{D_{gr}} + 1.34 \quad (2-242j)$$

$$A_{aw} = \frac{0.23}{\sqrt{D_{gr}}} + 0.14 \quad (2-242k)$$

$$\log(c) = 2.86 \log(D_{gr}) - [\log(D_{gr})]^2 - 3.53 \quad (2-242l)$$

Note that all logarithms here are base 10;  $u_*$  retains its previously introduced meaning as shear velocity.

The procedure for the computation of sediment transport rate using Ackers and White's approach can be summarized as follows:

1. Determine the value of  $D_{gr}$  with Eq. (2-242d) from known values of  $D$ ,  $R = (\rho_s - \rho) / \rho$ , and kinematic viscosity  $\nu$ .
2. Determine the value of  $n$ ,  $A_{aw}$ ,  $m$ , and  $c$  corresponding to the value of  $D_{gr}$  from Eqs. (2-242e) to (2-242l).
3. Determine the total sediment concentration  $C_s$  by weight in parts per million (ppm) with Eq. (2-242a).
4. Determine the total sediment transport rate  $Q_{st}$  with Eq. (2-237) and a known value of flow discharge  $Q$ .

Computations for gradually-varied flow in a river with the Ackers-White relations are presented in Chapter 14. Brownlie (1981a) found that the Ackers-White sediment load relation predicted laboratory observations quite well but field observations were underestimated. In 1990, HR Wallingford adjusted the coefficients in the Ackers-White relation, because the original formula predicted transport rates which were too large for fine sediments ( $D_{50} < 0.2$  mm). More recently, Niño et al. (2002) has found that the Ackers-White relation provides a good predictor for coarse sand and gravel transport in the rivers of Chile, and used this relation to predict longitudinal grain-size variation. The Ackers-White formulation is extended for application to sediment mixtures in Chapter 3.

### 2.10.5 The Yang Relation

To determine total sediment concentration, Yang (1973) also used dimensional analysis and the fundamental concept of unit stream power given by the product of mean flow

velocity and channel slope. Coefficients in Yang's equation were determined by a multiple regression analysis of laboratory flume data. The relation takes the form

$$\log(C_s) = a_1 + a_2 \log \left( \frac{U_s}{v_s} - \frac{U_c S}{v_s} \right) \quad (2-243a)$$

where

$$a_1 = 5.435 - 0.286 \log \left( \frac{v_s D_{50}}{\nu} \right) - 0.457 \log \left( \frac{u_*}{v_s} \right) \quad (2-243b)$$

$$a_2 = 1.799 - 0.409 \log \left( \frac{v_s D_{50}}{\nu} \right) - 0.314 \log \left( \frac{u_*}{v_s} \right) \quad (2-243c)$$

and  $U_c$  denotes a critical mean flow velocity for initiation of motion given by

$$\frac{U_c}{v_s} = \begin{cases} 2.05 & \text{if } \frac{u_* D_{50}}{\nu} > 70 \\ \frac{2.5}{\log \left( \frac{u_* D_{50}}{\nu} \right) - 0.06} & \text{if } 1.2 < \frac{u_* D_{50}}{\nu} < 70 \end{cases} \quad (2-243d)$$

Note that the logarithms are all base 10, and that  $v_s$  retains its previous meaning as fall velocity. Computations using Yang's approach for gradually-varied flow are presented in Chapter 14.

Yang and Molinas (1982) compared the Yang's formula with 1093 laboratory data and 166 river data, yielding a value of 95% of the predicted transport rates within a factor of 2 of measured transport rates. Large-scale river data were not included in this comparison. Recently, Yang and Simoes (2005) have used Yang's unit stream power approach (Yang 1979; Yang et al. 1996) to predict total bed-material load as well as wash load in the Yellow River, China.

### 2.10.6 The Karim-Kennedy Relation

The Karim and Kennedy (1981, 1990) methodology for depth-discharge predictors described previously in Section 2.8.3.5 also includes a total sediment discharge formula obtained from nonlinear regression using a database of 339

river flows and 608 flume flows. The uncoupled sediment load and resistance relations they obtained are given by

$$\log \frac{q_t}{\sqrt{gRD_{50}^3}} = -2.279 + 2.972 \log \left[ \frac{U}{\sqrt{gRD_{50}}} \right] + 1.060 \log \left[ \frac{U}{\sqrt{gRD_{50}}} \right] \log \left[ \frac{u_* - u_{*c}}{\sqrt{gRD_{50}}} \right] + 0.299 \log \left( \frac{H}{D_{50}} \right) \log \left[ \frac{u_* - u_{*c}}{\sqrt{gRD_{50}}} \right] \quad (2-244a)$$

and

$$\frac{U}{\sqrt{gRD_{50}}} = 2.822 \left[ \frac{q_w}{\sqrt{gRD_{50}}} \right]^{0.376} S^{0.310} \quad (2-244b)$$

in which

$q_t$  = total volumetric sediment discharge per unit width.

The rest of the variables have been defined above. Equation (2-244b) can be used for flows well above incipient sediment motion. If it is necessary to take into account the bed configuration changes, Eq. (2-244b) should be replaced with Eq. (2-183d).

More recently, Karim (1998) proposed a simpler power relation for the sediment transport equation using the same data sets employed in the Karim-Kennedy analysis, with the results given by

$$\frac{q_t}{\sqrt{gRD_{50}^3}} = 0.00139 \left[ \frac{U}{\sqrt{gRD_{50}}} \right]^{2.97} \left[ \frac{u_*}{v_s} \right]^{1.47} \quad (2-244c)$$

Both relations yield approximately the same results but Eq. (2-244c) would be easier to implement than the original Eq. (2-244a). Karim (1998) applied his equation to laboratory and field data having non-uniform sediments by dividing the sediment into size fractions. More on this application can be found on Chapter 3.

### 2.10.7 The Molinas-Wu Relation

This empirical relation is based on Velikanov's gravitational power theory, which assumes that the power available in flowing water is equal to the sum of the power required to overcome flow resistance and the power required to keep sediment in suspension against gravitational forces. In fact, this is equivalent to the simplified energy balance presented

earlier (Eq. 2-72a) for the discussion of wash load and bed-material load. The formulation proposed by Celik and Rodi (1984) to estimate sediment transport capacity (see Table 2-6) is also based on Velikanov's theory. Molinas and Wu (2001) argued that the predictors of Engelund-Hansen, Ackers and White, and Yang have been developed with flume experiments representative of shallow flows and cannot be applied to large rivers having deep-flow conditions. Average depths vary between 12 and 68 m in the Amazon River, and between 3 and 22 m in the Mississippi River (Posada 1995). These flow depths are much larger than those commonly found in laboratory experiments ( $< 1$  m). At the same time, under laboratory conditions Reynolds numbers are much smaller, Froude numbers are larger, and water surface (energy) slopes are steeper than those observed in large natural rivers. Motivated by the need for having a total bed-material load predictor for application to large sand-bed rivers, they used stream power and energy considerations together with data from large rivers (e.g., Amazon, Atchafalaya, Mississippi, Red River), to obtain an empirical fit for the total bed-material load concentration (Eq. 2-237) in ppm,

$$C_s = \frac{1430(0.86 + \sqrt{\Psi})\Psi^{1.5}}{0.016 + \Psi} \quad (2-245a)$$

where

$\Psi$  = stream power, which is defined by

$$\Psi = \frac{U^3}{g R H v_{s50} \left[ \log_{10} \left( \frac{H}{D_{50}} \right) \right]^2} \quad (2-245b)$$

Where

$U$  = mean flow velocity;

$g$  = acceleration of gravity,

$H$  = flow depth,

$v_{s50}$  = fall velocity for sediment size  $D_{50}$ ; and

$R$  = submerged specific gravity of sediment.

Most parameters in this empirical relation can be measured and/or estimated in the field, making it a useful formulation for practical use in large sand-bed rivers. One advantage of this approximation is that the energy slope ( $S$ ) does not have to be measured directly, which is always a challenge in large alluvial rivers. On the other hand, since Molinas and Wu (2001) do not mention how the wash load was separated from the bed-material load and the same large river data were used both to develop and to test their formulation, Eq. (2-245) might overestimate bed-material load concentrations when applied to other large rivers not included in the calibration. More testing of this formulation with independent data

sets is needed. Such data should be forthcoming given the new technologies that are now available for flow and sediment measurements in large rivers.

#### 2.10.8 Other Relations for Total Bed-Material Load

Several other total sand-discharge formulae can be found in the literature, including those of Shen and Hung (1972), Kikkawa and Ishikawa (1978), Ranga-Raju et al. (1981), van Rijn (1984), and Pacheco-Ceballos (1989; 1992) among others. A more complete review and evaluation and ranking of various relations can be found in Alonso (1980), Brownlie (1981), Yang and Molinas (1982), Gomez and Church (1989), Yang and Wan (1991), Maza-Alvarez and García-Flores (1996), Yang (1996), and Bravo-Espinosa et al. (2003), and Yang (2005).

In general, sediment transport predictors should be applied within the range of flow conditions and sediment characteristics for which they were developed (Williams and Julien 1989). Of paramount importance is to realize that sediment transport and flow resistance relations should be specified in pairs (Parker and Anderson 1977). The most reliable predictors for sediment load and flow resistance will continue to rely on direct observations in the field. Some guidance regarding the estimation of sediment discharge in the field can be found in Appendix D.

### 2.11 MORPHODYNAMICS OF RIVERS AND TURBIDITY CURRENTS

#### 2.11.1 Introduction

Turbidity currents are bottom currents of water laden with suspended sediment that move downslope in otherwise still bodies of water (García 1992). Turbidity currents are very similar to river flows, except for one important difference. In the case of a river, gravity pulls the water downslope, and the water drags the sediment with it. In the case of turbidity current in a body of still water, there would be no flow if there were no suspended sediment. Gravity acts to pull the suspended sediment in the bottom water downslope, and the sediment then drags the water with it. Turbidity currents occur in lakes, reservoirs, and the ocean. They provide major mechanisms for moving sediment into deep water.

Knowledge about sediment transport by turbidity currents was limited when ASCE *Manual 54* was first published. Manual 54 cited frequent observations of turbidity currents in Lake Mead induced by the high sediment loads of the Colorado River, suggesting that these flows could play an important role in lake and reservoir sedimentation (Vanoni 2006, p.166). In China, the impact of turbidity currents on reservoir sedimentation has long been recognized and attempts have been made to use the transport capacity of these underflows to preserve storage capacity (Fan and Morris 1992a, 1992b). One of the first attempts at modeling turbidity in reservoirs with a simple one-dimensional

approach, including their venting to prevent siltation, was made by Fan (1986). A few years later, Sloff (1994) used the method of characteristics to model turbidity currents in reservoirs, but did not address the morphodynamics of reservoir sedimentation. More recently, De Cesare et al. (2001) also indicated that turbidity currents have played an important role in the siltation of many Swiss reservoirs. Thus, the main reason for introducing turbidity currents in this section is to motivate a succeeding section on the modeling of lake and reservoir sedimentation. No attempt is made here to provide a detailed discussion of either turbidity currents or reservoir sedimentation. The latter issue is addressed in more detail in Chapter 12. Rather, the goal here is to guide the reader in understanding the processes involved in the morphodynamics of lake and reservoir sedimentation.

#### 2.11.2 Equations Governing the Morphodynamics of Rivers

Rivers evolve over time in accordance with the interaction between the flow and sediment-transport fields over an erodible bed (which changes the bed) and the changing morphology of the bed (which changes the flow and sediment-transport fields). This co-evolution is termed “morphodynamics” (Parker and García 2006). It is useful to introduce the relations governing the morphodynamics of turbidity currents in analogy to the morphodynamics of one-dimensional flow in a river of constant width. The parameters  $h$ ,  $U$  and  $\eta$  denote flow depth, depth-averaged flow velocity, and bed elevation, respectively. Depth-averaged flow velocity is defined as

$$Uh = \int_0^h \bar{u} dz \quad (2-246)$$

where

$z$  = upward normal coordinate with its origin at the bed;

and

$\bar{u}$  = local streamwise flow velocity averaged over turbulence at  $z$ .

Under appropriate simplifying assumptions, the one-dimensional St. Venant shallow-water equations take the form

$$\frac{\partial h}{\partial t} + \frac{\partial Uh}{\partial x} = 0 \quad (2-247a)$$

$$\frac{\partial Uh}{\partial t} + \frac{\partial U^2 h}{\partial x} = -gh \frac{\partial h}{\partial x} + ghS - C_f U^2 \quad (2-247b)$$

where

$t$  = time;

$x$  = boundary-attached (bed-attached) streamwise coordinate;

$g$  = gravitational acceleration;  
 $\rho$  = water density;  
 $S$  = bed slope, given as

$$S = -\frac{\partial \eta}{\partial x} \quad (2-248a)$$

and

$C_f$  = bed friction coefficient such that the bed shear stress  $\tau_b$  is given as

$$\tau_b = \rho C_f U^2 \quad (2-248b)$$

Here Eq. (2-247a) describes water-mass conservation and Eq. (2-247b) describes water-momentum conservation.

The river is assumed to carry a dilute suspension of sediment. Let the depth-flux averaged volume concentration  $C$  of suspended sediment be given by the relation

$$q_s = UCh = \int_0^h \bar{u} \bar{c} dz \quad (2-249)$$

where  $\bar{c} \ll 1$  is the local volume suspended-sediment concentration averaged over turbulence at elevation  $z$ , and  $q_s$  denotes the volume transport rate per unit width of suspended sediment. An approximate form for depth-averaged conservation of suspended sediment is as follows:

$$\frac{\partial Ch}{\partial t} + \frac{\partial UCh}{\partial x} = v_s (E_s - \bar{c}_b) \quad (2-250)$$

where

$v_s$  = sediment fall velocity;  
 $E_s$  = dimensionless rate of entrainment of bed sediment into suspension; and  
 $\bar{c}_b$  = near-bed value of  $\bar{c}$ ,

all of which were introduced earlier in this chapter. The Exner equation of conservation of bed sediment presented earlier takes the form

$$(1 - \lambda_p) \frac{\partial \eta}{\partial t} = -\frac{\partial q_b}{\partial x} + v_s (\bar{c}_b - E_s) \quad (2-251)$$

where  $q_b$  denotes the volume bedload transport rate per unit width and  $\lambda_p$  denotes the bed porosity.

Equations (2-247a), (2-247b), (2-250), and (2-251) are the basic equations describing the one-dimensional morphodynamics of rivers. The equations need to be closed by specifying relations for (1) volume bed load transport  $q_b$ ,

(2) dimensionless rate of entrainment of bed sediment into suspension  $E_s$ , and (3) near-bed suspended-sediment concentration  $\bar{c}_b$ . Numerous relations for  $q_b$  and  $E_s$  have been introduced in this chapter. In addition, if the flow and suspension do not deviate too strongly from equilibrium (i.e., logarithmic and Rousean profiles), the following approximate relation for  $\bar{c}_b$  is obtained from Eqs. (2-195), (2-204), and (2-249):

$$\bar{c}_b = r_o C \quad (2-252a)$$

$$r_o = \frac{\ln\left(11 \frac{h}{k_c}\right)}{\int_{\xi_b}^1 \left[ \frac{(1-\zeta)/\zeta}{(1-\zeta_b)/\zeta_b} \right]^{Z_R} \ln\left(30 \frac{h}{k_c} \zeta\right) d\zeta} \quad (2-252b)$$

$$Z_R = \frac{v_s}{\kappa u_*} \quad (2-252c)$$

$$\zeta = \frac{z}{h} \quad (2-252d)$$

where  $\zeta_b \ll 1$  is a near-bed parameter. When  $\xi_b = b/h = 0.05$ , which is the commonly used value for this parameter, the shape factor  $r_o$  can be estimated with a simple fit to the Rousean profile (Parker et al. 1987)

$$r_o = 1 + 31.5 \left( \frac{u_*}{v_s} \right)^{-1.46} \quad (2-252e)$$

Thus, Eqs. (2-250) and (2-251) take the respective forms

$$\frac{\partial Ch}{\partial t} + \frac{\partial UCh}{\partial x} = v_s (E_s - r_o C) \quad (2-253)$$

$$(1 - \lambda_p) \frac{\partial \eta}{\partial t} = -\frac{\partial q_b}{\partial x} + v_s (r_o C - E_s) \quad (2-254)$$

Alternatively, between Eqs. (2-249), (2-250), and (2-251) it is found that

$$(1 - \lambda_p) \frac{\partial \eta}{\partial t} + \frac{\partial Ch}{\partial t} = -\frac{\partial q_b}{\partial x} - \frac{\partial q_s}{\partial x} \quad (2-255a)$$

For the case of a dilute suspension ( $C \ll 1$ ), the amount of sediment stored in suspension can be neglected compared to

the amount of sediment stored in the bed, so that the above equation accurately approximates to

$$(1 - \lambda_p) \frac{\partial \eta}{\partial t} = -\frac{\partial q_b}{\partial x} - \frac{\partial q_s}{\partial x} = -\frac{\partial q_t}{\partial x} \quad (2-255b)$$

Where  $q_t$  denotes the total volume bed-material load per unit width. The formulation of Eq. (2-255b) can be implemented by assuming an appropriate relation for the volume bed-load transport rate per unit width  $q_b$ , and estimating the volume suspended-load transport rate per unit width  $q_s$  for disequilibrium flow by the means of the local application of a formulation for equilibrium flow (based on, e.g., a logarithmic velocity profile and the Rousean profile for suspended sediment).

In point of fact the forms for Eqs. (2-247) and (2-251) are only approximate. The more general forms of Eq. (2-247) and (2-251) are, respectively,

$$\frac{\partial Uh}{\partial t} + \frac{\partial \alpha_1 U^2 h}{\partial x} = -gh \frac{\partial h}{\partial x} + ghS - C_f U^2 \quad (2-256a)$$

where

$$\alpha_1 = \int_0^1 \left( \frac{\bar{u}}{U} \right)^2 d\zeta \quad (2-256b)$$

and

$$\frac{\partial \alpha_2 Ch}{\partial t} + \frac{\partial UCh}{\partial x} = v_s(E_s - r_o C) \quad (2-257a)$$

where

$$\alpha_2 = \int_0^1 \frac{\bar{c}}{C} d\zeta = \frac{\left( \int_0^1 \bar{u} d\zeta \right) \left( \int_0^1 \bar{c} d\zeta \right)}{\left( \int_0^1 \bar{u} \bar{c} d\zeta \right)} \quad (2-257b)$$

where  $\zeta$  is given by Eq. (2-252d). Here  $\alpha_1$  and  $\alpha_2$  are dimensionless shape factors governing the velocity and concentration profiles. Were  $\bar{u}$  and  $\bar{c}$  constant in the vertical, both shape factors would be equal to unity (i.e., top-hat approximation). They are often approximated to unity for simplicity.

### 2.11.3 Equations Governing the Morphodynamics of Turbidity Currents

A turbidity current is illustrated in Fig. 2-59. Let  $x$  denote a boundary-attached (bed-attached) streamwise coordinate

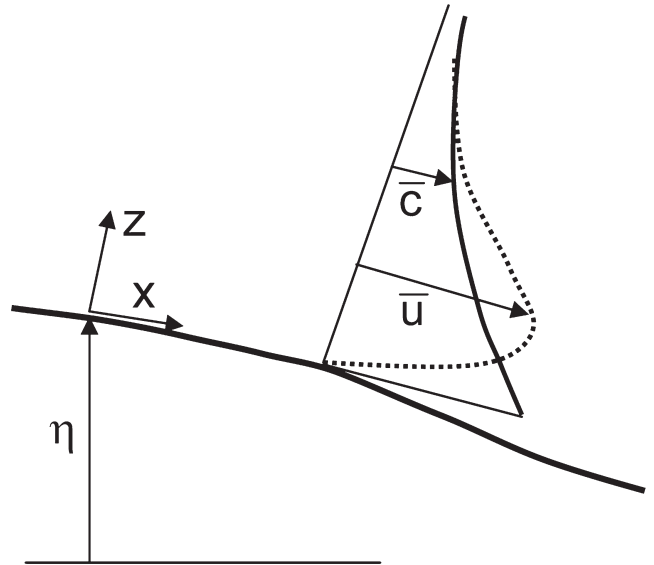


Fig. 2-59. Definition diagram for turbidity current.

and  $z$  denote an upward vertical coordinate from the bed. Just as in the case of rivers, the streamwise flow velocity  $\bar{u}$  and volume concentration of suspended sediment  $\bar{c}$ , both averaged over turbulence, show notable variation in the  $z$  direction. Note, however, that because a turbidity current is a bottom flow, it can be expected that both  $\bar{u}$  and  $\bar{c}$  become vanishingly small as  $z \rightarrow \infty$ , where here “ $\infty$ ” is shorthand for “high above the bottom current.”

The turbidity current flows because it is laden with sediment, which renders it heavier than the ambient water above. Let  $\rho$  denote the density of water and  $\rho_s$  denote the density of sediment. The density  $\rho_t(z)$  of the turbidity current at level  $z$  is thus given as

$$\rho_t = \rho(1 - \bar{c}) + \rho_s \bar{c} = \rho(1 + R\bar{c}) \quad (2-255)$$

where

$$R = \frac{\rho_s}{\rho} - 1 \quad (2-256)$$

denotes the “submerged specific gravity” of the sediment, taking the value 1.65 for quartz. The turbidity current is driven downslope due to gravity acting on the density excess of the turbidity current relative to the ambient water. The fractional density excess is given as

$$\frac{\rho_t - \rho}{\rho} = R\bar{c} \quad (2-257)$$

Here the case of dilute turbidity currents is considered, so that  $\bar{c} \ll 1$  and thus  $R\bar{c} \ll 1$ .

One-dimensional layer-averaged equations governing the flow of turbidity currents can be derived in analogy to the St. Venant equations of shallow water flow in rivers. The suspended sediment that drives the turbidity current is characterized here in terms of a single fall velocity  $v_s$ . Layer thickness  $h$  and layer-averaged flow velocity  $U$  and volume concentration of suspended sediment  $C$  are defined in terms of the following three moments (e.g., Ellison and Turner 1959):

$$Uh = \int_0^\infty \bar{u} dz \quad (2-258a)$$

$$U^2 h = \int_0^\infty \bar{u}^2 dz \quad (2-258b)$$

$$UCh = \int_0^\infty \bar{u} \bar{c} dz \quad (2-258c)$$

Note that Eqs. (2-258a) and (2-258c) for turbidity currents are almost identical in form to the corresponding Eqs. (2-245) and (2-249) used to define the layer-averaged (more precisely depth-averaged) quantities  $U$  and  $C$  in a river. The only difference is that the upper limit  $y = h$  in a river is replaced with  $y = \infty$  in a turbidity current. That is, turbidity currents have no “layer thickness” in the precise sense of the word. The extra relation of Eq. (2-258b) specifies a momentum-based equivalent layer thickness  $h$ .

A complete derivation of the one-dimensional flow equations for turbidity currents are given in Parker et al. (1986). The one-dimensional equations contain a number of dimensionless shape factors analogous to  $\alpha_1$  and  $\alpha_2$  of Eqs. (2-256b) and (2-257b), all of which take the value unity for the special case of the velocity and concentration profiles

$$\frac{\bar{u}}{U} = \frac{\bar{c}}{C} = \begin{cases} 1 & ; 0 < z \leq h \\ 0 & ; z > h \end{cases} \quad (2-259)$$

Parker et al. (1987) and García (1993, 1994) have evaluated these shape factors for experimental turbidity currents. Because the values so determined do not deviate strongly from unity, values of unity are assumed below as well.

The one-dimensional layer-averaged equation of conservation of water mass takes the form

$$\frac{\partial h}{\partial t} + \frac{\partial Uh}{\partial x} = e_w U \quad (2-260)$$

where

$e_w$  = coefficient of entrainment of ambient (sediment-free) water from above into the turbidity current.

The one-dimensional layer-averaged equation of conservation of streamwise flow momentum is

$$\frac{\partial Uh}{\partial t} + \frac{\partial U^2 h}{\partial x} = -\frac{1}{2} g \frac{\partial Ch}{\partial x} + gRChS - C_f U^2 \quad (2-261)$$

The one-dimensional layer-averaged equations for conservation of suspended and bed sediment are given by the same forms as for a river, that is, Eqs. (2-250) and (2-251), respectively.

The governing equations of turbidity currents are thus seen to be very similar to those governing flow and sediment transport in a river. There is, however, one important difference. A river that carries no suspended sediment continues to flow, because the pull of gravity acts directly on the water. This effect is embodied in the term  $ghS$  in Eq. (2-247). So gravity pulls the water downhill, and the water pulls the sediment with it. In the case of a turbidity current, the corresponding downslope impelling term in Eq. (2-261) is  $gRChS$ . If the concentration of suspended sediment  $C$  drops to zero, the downslope impelling force also drops to zero, and the current must eventually die. In a turbidity current, then, gravity pulls the sediment downslope, and the sediment drags the water with it. In a river, the dynamics of the flow is essentially decoupled from the dynamics of suspended sediment. In a turbidity current, the two are intimately linked (García 1992).

Equations (2-260) and (2-261), along with Eqs. (2-250) and (2-251), can be closed with functional relations for  $E_s$ ,  $q_b$  and  $r_o$  that are similar to those used for rivers. In addition, however, an equation for the entrainment coefficient of ambient water  $e_w$  must be specified. Parker et al. (1987) suggest the following functional form

$$e_w = \frac{0.075}{(1 + 718 \times Ri^{2.4})^{0.5}} \quad (2-262)$$

where  $Ri$  denotes the bulk Richardson number, given as

$$Ri = \frac{RgCh}{U^2} \quad (2-263)$$

The bulk Richardson number is related to the densimetric Froude number  $Fr_d$  as

$$Fr_d = \frac{U}{\sqrt{gRCh}} = Ri^{-1/2} \quad (2-264)$$

A turbidity current is supercritical if  $Fr_d > 1$  ( $Ri < 1$ ) and subcritical if  $Fr_d < 1$  ( $Ri > 1$ ). (In fact the precise borderline between subcritical and supercritical flow depends upon the shape factors discussed above, but a value of unity is generally an acceptable approximation.) Supercritical turbidity currents

tend to entrain ambient water from above, in analogy to the tendency of supercritical open channel flows to entrain air on spillways. In accordance with Eq. (2-262), highly subcritical turbidity currents tend to entrain little ambient water (García 1994). More material on water entrainment by underflows, including the role played by bottom slope and roughness, can be found in Fernandez and Imberger (2006).

## 2.12 MORPHODYNAMICS OF LAKE AND RESERVOIR SEDIMENTATION

The following material is intended to provide a brief summary of the morphodynamics of sedimentation in lakes and reservoirs. More detail on reservoir sedimentation is given in Chapter 12.

### 2.12.1 Introduction: Topset, Foreset, and Bottomset of Delta

As a river enters the slack water of a lake or reservoir, the flow decelerates and its sediment drops out. The result is the formation of a delta (Fig. 2-60). The coarser sediment (typically sand and/or gravel) deposits fluvially to form an aggrading topset and deposits by avalanching to form a prograding foreset. The finer sediment (typically mud, i.e., silt and clay) deposits in deeper water to form a bottomset (e.g., Morris and Fan 1997).

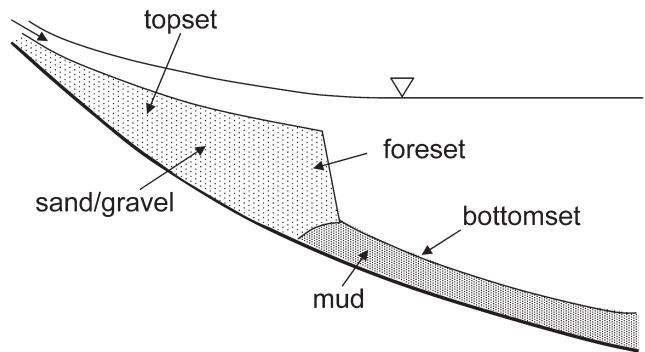


Fig. 2-60. Definition diagram for a fluvial delta.

These characteristic features are seen for the case of Lake Mead in Fig. 2-61 (Grover and Howard 1938; Smith et al. 1954). The figure shows the history of reservoir sedimentation from the closing of the dam in 1936 to 1948. The topset, foreset, and bottomset deposits are clearly visible in the figure. It is of interest to note that the maximum slope of the foreset is less than 1°. An inset in Fig. 2-61 is expanded in Fig. 2-62. This inset shows that the topset and foreset are predominantly composed of sand, and the bottomset is predominantly composed of mud (silt and clay). The foreset-bottomset interface clearly defines a moving boundary. This feature is exploited in the modeling described here.

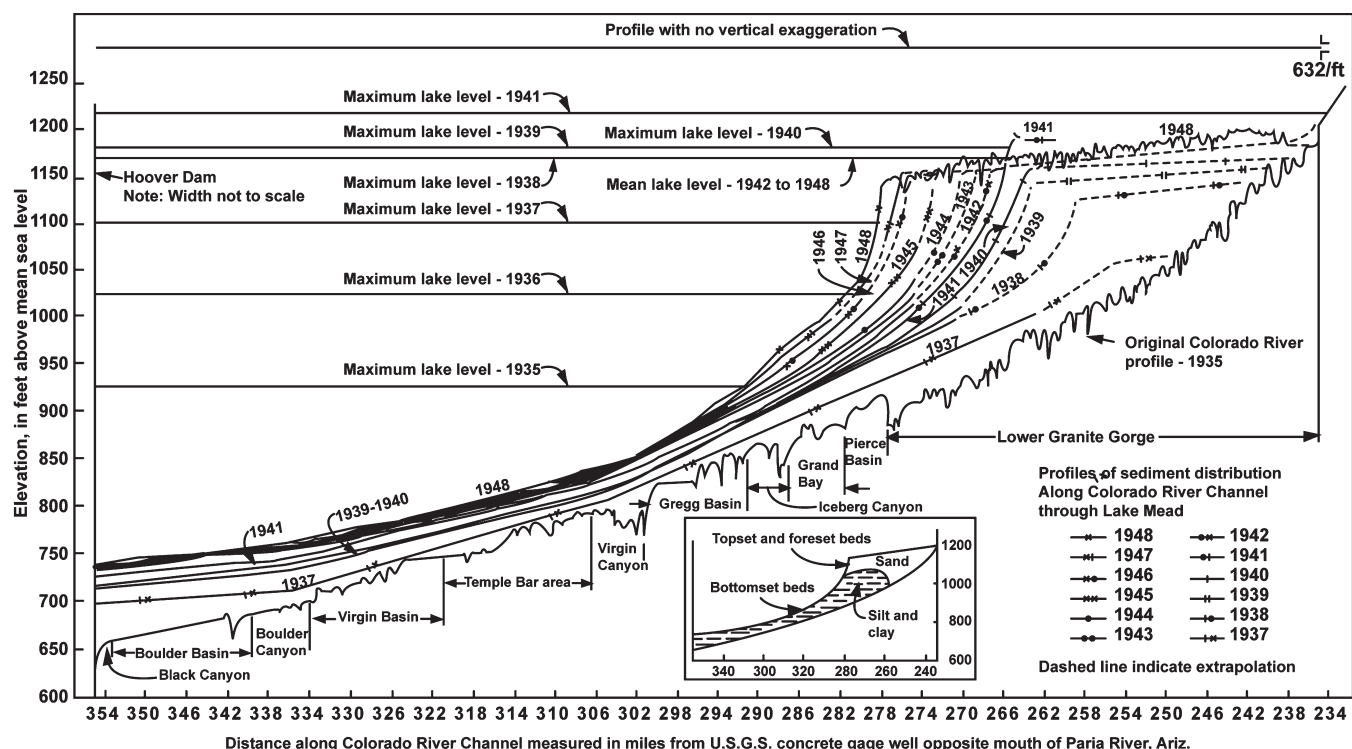
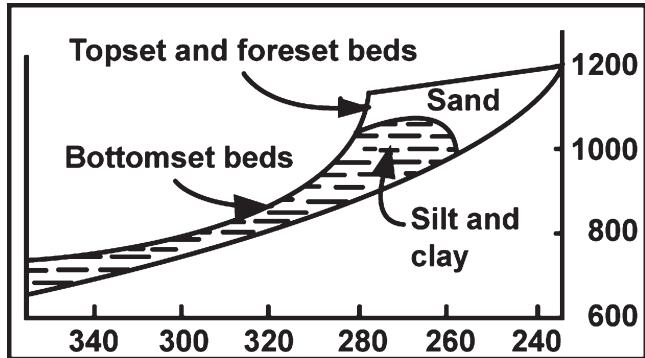


Fig. 2-61. Formation of fluvial delta in Lake Mead, USA. Adapted from Smith et al. (1954).



**Fig. 2-62.** Inset of Fig. 2-61 showing the moving boundary between the muddy bottomset and the sandy topset-foreset.

The bottomset can be emplaced in three ways. If the sediment-laden river water is lighter than the lake water, a muddy surface plume extends out into the lake from the delta front. Mud gradually rains out of this plume and deposits to form the bottomset, as shown in Fig. 2-63a. Lakes are often stratified, however, so that the surface water is warmer and lighter than the water at a depth. If the sediment-laden river water has a density that is intermediate between that of the surface and bottom water in the lake, the muddy plume partially plunges to form an interflow, as shown in Fig. 2-63b. During floods, when rivers are likely to carry their highest concentrations of mud as wash load, the river water is often sufficiently dense to plunge to the bottom of the reservoir and form a turbidity current, as shown in Fig. 2-63c (Bell 1942; Fan and Morris 1992a).

### 2.12.2 Fluvial Deposition of Topset and Foreset

A simple one-dimensional morphodynamic model of delta topset and foreset evolution is first considered. A river of constant width flows into a lake of the same width and infinite streamwise extent. The water surface elevation  $\xi_o$  in the lake is held constant. The river transports sand as bed-material load; this sand is approximated with a single grain size  $D_s$ . The hydrograph of the river is approximated in the following way; for a constant fraction  $I_f$  of the year the river is in flood, carrying a constant floodwater discharge per unit width  $q_w$ . Otherwise, the river is assumed to be morphodynamically inactive. During floods sand enters the river at  $x = 0$  at volume rate per unit width  $q_{tf}$ , where the subscript  $t$  denotes total bed material load and  $f$  denotes flood. The porosity of the sandy bed deposit is denoted as  $\lambda_{ps}$ , where  $s$  denotes sand. Since the flood flow is assumed to be steady, Eqs. (2-246) and (2-247) can be reduced to the backwater equation

$$\frac{\partial h_f}{\partial x} = -\frac{\partial \eta_f}{\partial x} - C_{ff} Fr^2 \quad (2-265a)$$

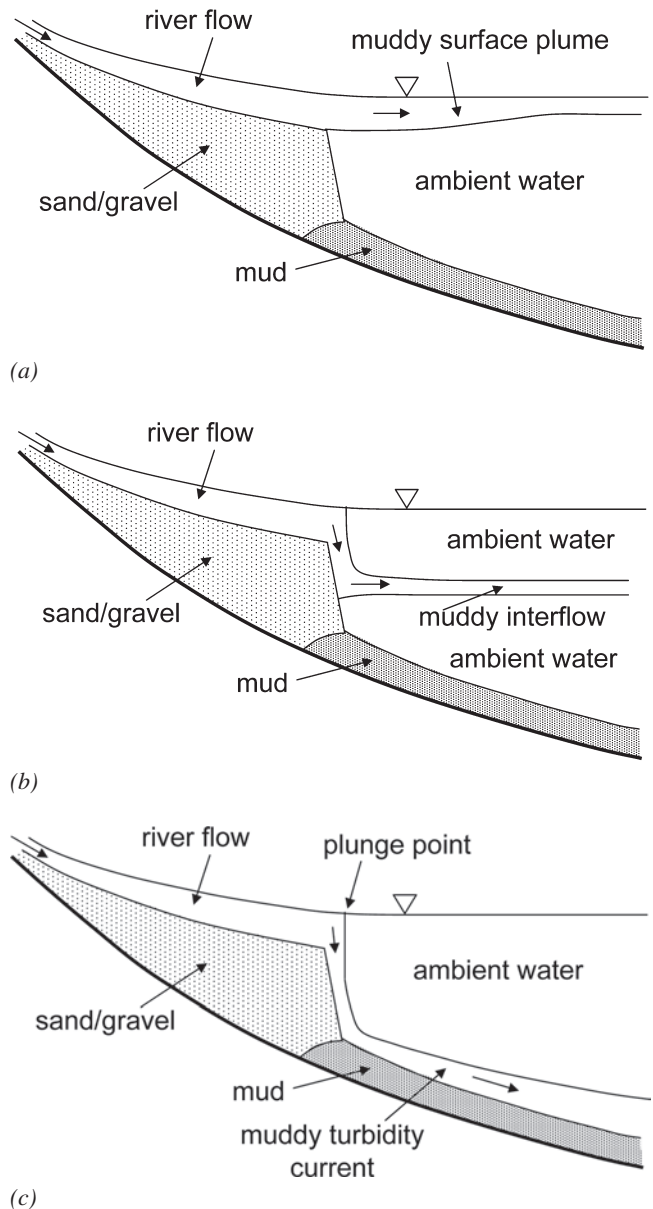


**Fig. 2-63.** Illustration of the formation of a muddy surface plume (a), a muddy interflow (b), and a muddy bottom turbidity current (c).

$$Fr^2 = \frac{q_w^2}{gh_f^3} \quad (2-265b)$$

In this backwater equation,

$h_f$  and  $\eta_f$  = flow depth and bed elevation in a fluvial zone that includes the topset and foreset regions but excludes the bottomset;

$Fr$  = Froude number of the fluvial flow; and  
 $C_{ff}$  = bed friction coefficient in the fluvial region.

The boundary condition on this equation is expressed in terms of the flow depth at a point  $x = s_{\text{stand}}$  where standing water elevation  $\xi_o$  is maintained. Let  $\eta_f(x, t)$  denote the bed elevation at any point  $x$  and time  $t$ . The boundary condition is then

$$h_f(x,t) \Big|_{x=s_{\text{stand}}} = \xi_o - \eta_f(x,t) \Big|_{x=s_{\text{stand}}} \quad (2-265c)$$

The flow is assumed to be everywhere subcritical ( $Fr < 1$ ), so that Eq. (2-265a) is integrated in the upstream (negative  $x$ ) direction from  $x = s_{\text{stand}}$ . The solution of Eq. (2-265a) subject to Eq. (2-265c) constitutes the standard backwater formulation; in a consideration of reservoir sedimentation the backwater curve of interest is the M1 curve (Chow 1959).

The Shields number  $\tau^*$  of the fluvial flow is given as

$$\tau^* = \frac{\tau_b}{\rho R_s g D_s} = \frac{C_f q_w^2}{R_s g D_s h_f^2} \quad (2-266)$$

where  $R_s$  denotes the submerged specific gravity for the sand. In all following calculations, the total volume bed material load per unit width of the river  $q_t$  is estimated using the relation of Engelund and Hansen (1967) introduced earlier in the chapter,

$$q_t^* = \frac{q_t}{\sqrt{R_s g D_s D_s}} = \frac{0.05}{C_{ff}} (\tau^*)^{5/2} \quad (2-267)$$

Here the friction coefficient  $C_{ff}$  is assumed to be a specified constant for simplicity. At any given time  $t$ , then, the total volume bed material transport rate per unit width of sand  $q_t(x,t)$  can be computed by (1) solving Eq. (2-265a) subject to Eq. (2-265c) to determine  $h_f(x,t)$  over a known bed  $\eta_f(x,t)$ , and then (2) using Eqs. (2-266) and (2-267) to determine  $q_t(x,t)$ .

The bed evolution or morphodynamics driven by the backwater of the lake is computed from the Exner equation of sediment continuity. Modifying Eq. (2-255b) for the fluvial region so as to account for the fact that the river is morphologically active only  $I_f$  fraction of the time, it is seen that

$$(1 - \lambda_{ps}) \frac{\partial \eta_f}{\partial t} = -I_f \frac{\partial q_t}{\partial x} \quad (2-268)$$

The boundary condition on Eq. (2-268) is a specified feed rate of sand, here taken to be constant;

$$q_t \Big|_{x=0} = q_{tf} \quad (2-269)$$

The initial condition on the problem is here simplified to a bed with constant slope  $S_{\text{base}}$  and a bed elevation  $\eta_f = 0$  at  $x = s_{\text{stand}}$ .

The problem defined by Eqs. (2-265) to (2-269) has been solved numerically by many authors, e.g., Hotchkiss and Parker (1991). Here techniques outlined in Parker (2005) are used to solve the problem. A predictor-corrector method is used to solve the backwater equation over the bed at any given time, and the Euler step method is used to compute the bed elevation at a later time from the above Exner formulation. The input parameters are given as those of Case A of Table 2-8. The size  $D_s$  of the sand is seen there to be 0.4 mm, or 400  $\mu\text{m}$ .

The results of a computer simulation of Case A for a simulated run time  $t_{\text{run}}$  of 30 years are shown in Fig. 2-64. The

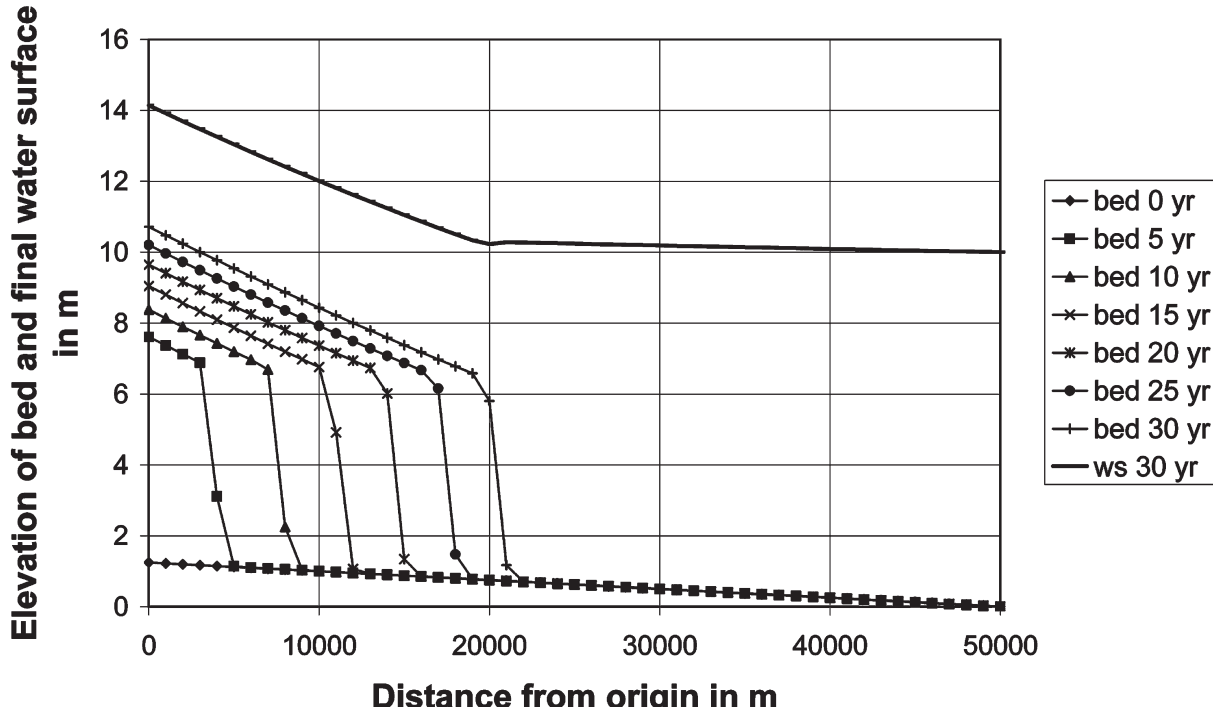


Fig. 2-64. Simulation of formation of sandy topset and foreset in a lake using a shock-capturing formulation and the input of Case A of Table 2.7.

**Table 2-8 Parameters Used in Numerical Modeling of Lake/Reservoir Sedimentation**

Parameter	Units	Case A	Case B	Case C	Case D	Case E
$q_w$	$\text{m}^2/\text{s}$	6	6	6	6	2
$q_{ff}$	$\text{m}^2/\text{s}$	0.001	0.001	0.001	0.001	0.000625
$D_s$	$\mu\text{m}$	400	400	400	400	400
$C_{ff}$	1	0.0025	0.0025	0.0025	0.0025	0.00694
$I_f$	1	0.1	0.1	0.1	0.1	1
$S_{base}$	1	0.000025	0.000025	0.005	0.005	0.016
$R_s$	1	1.65	1.65	1.65	1.65	1.65
$\lambda_{ps}$	1	0.4	0.4	0.4	0.4	0.4
$\xi_o$	m	10	10	53	53	203
$s_{stand}$	m	50,000	—	—	—	—
$t_{run}$	yrs	30	600	45	3000	0.246
$\eta_{sl}$	m	—	6.304	50	50	200
$\eta_{bl}$	m	—	0.931	0	0	100
$S_a$	1	—	0.05	0.05	0.05	0.2
$S_{fl}$	1	—	0.00023	0.00023	0.00028	0.00073
$s_{sl}$	m	—	13,000	10,000	10,000	1000
$q_{mf}$	$\text{m}^2/\text{s}$	—	—	0.003	0.003	0.00625
$D_m$	$\mu\text{m}$	—	—	10, 15, 25	10	50
$C_{ft}$	1	—	—	0.00111	0.00111	0.00111
$R_m$	1	—	—	1.65	1.65	1.65
$\lambda_m$	1	—	—	0.6	0.6	0.6
$s_{max}$	m	—	—	30,000	30,000	6000
$B_c$	m	—	—	—	80	—
$\theta_f$	°	—	—	—	90	—
$\theta_t$	°	—	—	—	10	—

method is fundamentally shock-capturing (the delta front being the shock); a delta forms of its own accord, steepens, and progrades downstream. The topset and foreset are clearly visible in Fig. 2-64. There is no bottomset because mud has not been included in the formulation. Although this formulation clearly captures the mechanism of formation and progradation of the delta topset and foreset, it does not correctly describe foreset slope. In a shock-capturing method, the slope of the foreset is entirely dependent on the spatial step length.

Once the delta has formed, it becomes possible to change the formulation to a shock-fitting formulation, in which the foreset has a prescribed slope of avalanching  $S_a$  that can be selected based on physical considerations. Swenson et al. (2000) have developed such a formulation. The delta is defined in terms of a topset-foreset break and a foreset-basement break, as shown in Fig. 2-65. The foreset progrades over a subaqueous basement of prescribed morphology. The distance from the sediment feed point at  $x = 0$  to the topset-foreset break is denoted as  $s_s(t)$  (the subscript s being shorthand for shoreline),

and the corresponding distance to the foreset-bottomset break is denoted as  $s_b(t)$ . Both these parameters define boundaries that move as the delta evolves. Likewise, the bed elevation at the topset-foreset break is defined as  $\eta_s(t)$ , and the bed elevation at the foreset-basement break is defined as  $\eta_b(t)$ .

In a shock-fitting formulation, delta progradation is described in terms of a shock condition determined by integrating the Exner equation (2-268) from the topset-foreset break to the foreset-bottomset break, under the condition of constant foreset slope  $S_a$ . Kostic and Parker (2003a) generalized the work of Swenson et al. (2000) to obtain the condition

$$\dot{s}_s = \frac{1}{(S_a - S_s)} \left[ \frac{I_f q_t|_{x=s_s}}{(1 - \lambda_{ps})(s_b - s_s)} - \frac{\partial \eta_f}{\partial t} \Big|_{x=s_s} \right] \quad (2-270)$$

In this relation  $\dot{s}_s$  denotes the speed of migration of the topset-foreset break, and

$$S_s = - \frac{\partial \eta_f}{\partial x} \Big|_{x=s_s} \quad (2-271)$$

i.e., the slope of the topset at the topset-foreset breaks. Eq. (2-270) indicates that the foreset progrades at a speed that is commensurate with the rate of delivery of bed-material load (sand in the simulations reported here) to the topset-foreset break.

The shock condition of Eq. (2-270) is augmented with an elevation continuity condition at the foreset-basement break, which reduces to the following condition; where  $\dot{s}_b$  denotes the speed of migration of the foreset-basement break,

$$(S_a - S_b) \dot{s}_b = (S_a - S_s) \dot{s}_s + \frac{\partial \eta_f}{\partial t} \Big|_{x=s_s} \quad (2-272)$$

In the above relation  $S_b$  denotes the slope of the subaqueous basement at the foreset-basement break.

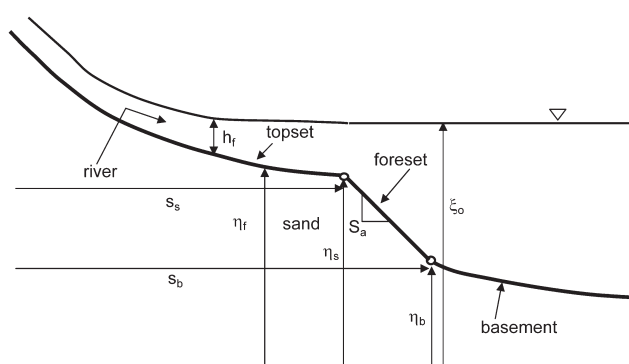


**Fig. 2-65.** Definition diagram for a moving-boundary shock-fitting formulation of delta topset-foreset evolution.

The problem is conveniently solved numerically in terms of moving boundary coordinates, according to which

$$\hat{x}_f = \frac{x}{s_s(t)} \quad (2-273a)$$

$$\hat{t}_f = t \quad (2-273b)$$

That is, Eqs. (2-265) and (2-268) are transformed according to Eqs. (2-273a) and (2-273b) and solved in conjunction with Eqs. (2-270) and (2-272). The transformed problem is stated here in terms of the backwater formulation,

$$\frac{1}{s_s} \frac{\partial h_f}{\partial \hat{x}_f} = \frac{-\frac{1}{s_s} \frac{\partial \eta_f}{\partial \hat{x}_f} - C_{ff} \frac{q_w^2}{gh_f^3}}{1 - \frac{q_w^2}{gh_f^3}} \quad (2-274a)$$

$$h_f \Big|_{\hat{x}_f=1} = \xi_o - \eta_f(1, \hat{t}) \quad (2-274b)$$

the Exner equation of sediment continuity,

$$(1 - \lambda_{ps}) \left[ \left( \frac{\partial \eta_f}{\partial \hat{t}_f} - \frac{\dot{s}_s}{s_s} \hat{x} \frac{\partial \eta_f}{\partial \hat{x}_f} \right) \right] = -\frac{1}{s_s} I_f \frac{\partial q_t}{\partial \hat{x}_f} \quad (2-275)$$

the shock condition for foreset progradation,

$$\dot{s}_s = \frac{1}{S_a} \left[ \frac{I_f q_t(1, \hat{t}_f)}{(s_b - s_s)(1 - \lambda_{ps})} - \frac{\partial \eta_f}{\partial \hat{t}_f} \Big|_{x_f=1} \right] \quad (2-276)$$

and the continuity condition at the foreset-basement break.

$$\dot{s}_b = \dot{s}_s + \frac{1}{S_a} \frac{\partial \eta_f}{\partial \hat{t}_f} \Big|_{\hat{x}_f=1} \quad (2-277)$$

Details are given in Kostic and Parker (2003a; 2003b). The calculation is implemented here as Case B, the input parameters for which are given in Table 2-8. Case B is chosen to be very close to Case A. Case B requires initial values  $s_{sI}$ ,  $\eta_{sI}$  and  $\eta_{bI}$  for  $s_s$ ,  $\eta_s$  and,  $\eta_b$ , respectively, as well as an initial fluvial bed slope  $S_{ff}$ . These values have been estimated from the output of Case A at  $t = 15$  years. Basement slope  $S_{base}$  is the same in Case B as that of Case A; because it is constant,  $S_b$  in Eq. (2-272) is always equal to  $S_{base}$ . The foreset avalanche slope  $S_a$  has been set equal to 0.05, i.e.,  $2.86^\circ$ .

The results of 600 years of simulation of Case B are shown in Fig. 2-66. Progradation forces the evolution of a topset with an upward-concave long profile, i.e., one for which slope declines in the streamwise direction. After 600 years the delta front has prograded well over 150 km. It should be noted that the progradation predicted by a one-dimensional model is considerably exaggerated as compared to nature. This is because in a one-dimensional model the

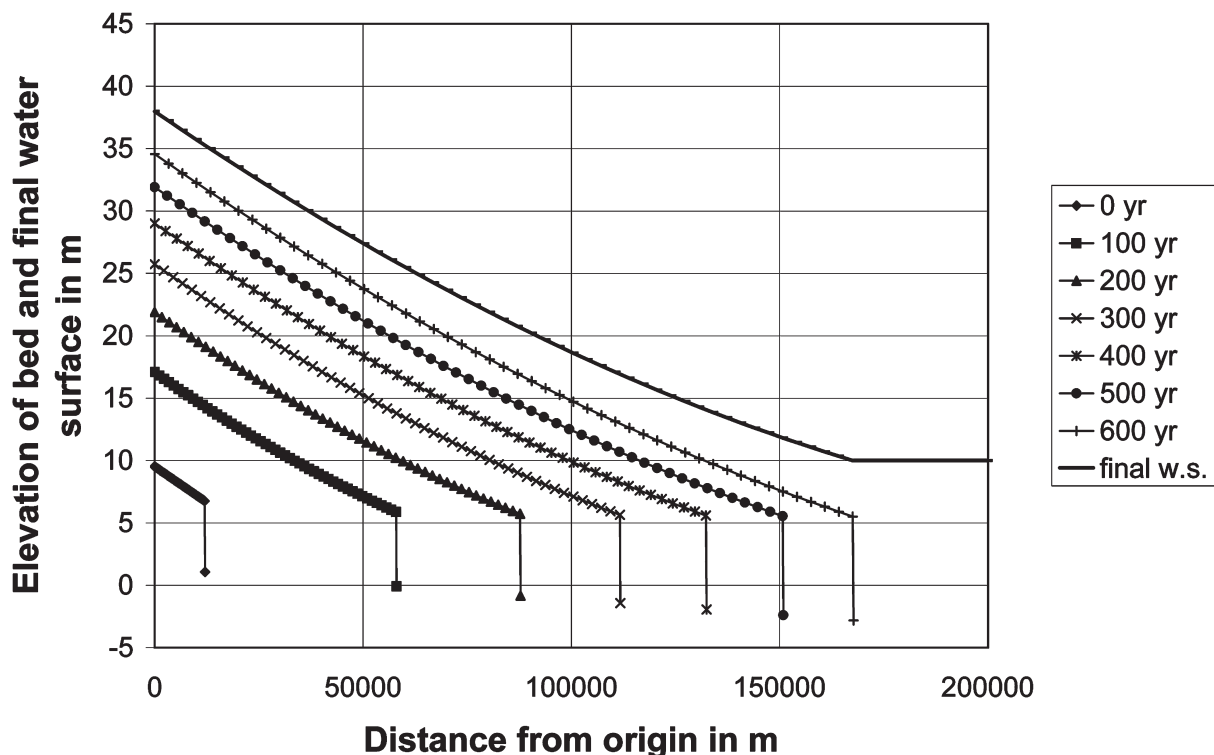


**Fig. 2.66.** Simulation of progradation of sandy topset and foreset in a lake using a shock-fitting formulation and the input of Case B of Table 2-7.

only place for the topset sediment to deposit is in the channel, whereas in nature sediment deposits on the surface of a much wider fan-delta over which the river channel avulses. The two-dimensional case is considered below.

### 2.12.3 Plunging of a Muddy Turbidity Current

Up to now the muddy bottomset has been excluded from the formulation. Sand- and gravel-bed rivers often carry copious amounts of mud (sand and silt) as wash load, i.e., material that is carried in suspension but constitutes only a negligible fraction of the bed sediment. An example is the Colorado River, USA (Smith et al. 1954). Because the mud does not deposit in the bed of the river, it may be neglected in a first model of the evolution of the topset and foreset.

As seen in Figs. 2-63, however, when river meets the standing water of a lake or reservoir, the sand is left behind on the topset-foreset and the remaining muddy water continues as a surface plume, interflow, or bottom turbidity current. The case considered here is the one for which the muddy water is sufficiently dense to plunge and form a bottom turbidity current.

When muddy river water is denser than lake water at every level of the lake, the river water plunges somewhere above the foreset to create the bottom turbidity current schematized in Fig. 2-67. A number of relations are available to predict plunging of muddy water in a lake; these are reviewed in Parker and Toniolo (2007). Here the treatment of Parker and Toniolo (2007) is offered as a sample.

The analysis is applied to muddy water flowing into a lake with no ambient stratification. The flow near the plunge point is illustrated in Fig. 2-68. Except for the mud, the river water is assumed to have the same density as the sediment-free lake water. The flow velocity, depth, and volume mud concentration in the river water just upstream of the plunge point are denoted as  $U_p$ ,  $h_p$  and  $C_{mp}$ , respectively; the corresponding flow velocity, layer thickness and volume mud concentration in the turbidity current just downstream of the plunge point are denoted as  $U_d$ ,  $h_d$ , and  $C_{md}$ , respectively. The

submerged specific gravity of the mud is denoted as  $R_m$ . As the river flow plunges, it invariably draws into it some ambient water from the lake. The velocity at which this ambient water enters the muddy flow is denoted as  $U_a$ .

The coefficient of mixing of ambient water into the muddy flow,  $\gamma$ , is defined as

$$\gamma = \frac{U_a(h_p - h_d)}{U_p h_p} \quad (2-278)$$

A value  $\gamma > 0$  is required for the muddy flow to plunge. The flow discharge per unit width just downstream of plunging is related to that just upstream of plunging as

$$U_d h_d = U_p h_p (1 + \gamma) = q_w (1 + \gamma) \quad (2-279)$$

The depth ratio  $\varphi$  and the densimetric Froude numbers  $Fr_{dp}^2$  and  $Fr_{dd}^2$  just upstream and downstream of the plunge point are defined as

$$\varphi = \frac{h_d}{h_p} \quad (2-280a)$$

$$Fr_{dp}^2 = \frac{U_p^2}{R_m C_{mp} g h_p} = \frac{q_w^2}{R_m C_{mp} g h_p^3} \quad (2-280b)$$

$$Fr_{dd}^2 = \frac{U_d^2}{R_m C_{md} g h_d} \quad (2-280c)$$

Parker and Toniolo (2007) obtain the following relations for these parameters:

$$Fr_{dd}^2 = Fr_{dp}^2 \frac{(1+\gamma)^3}{\varphi^3} \quad (2-281)$$

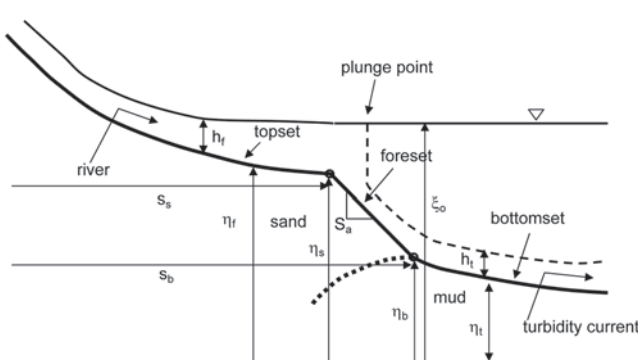


Fig. 2-67. Definition diagram illustrating plunging.

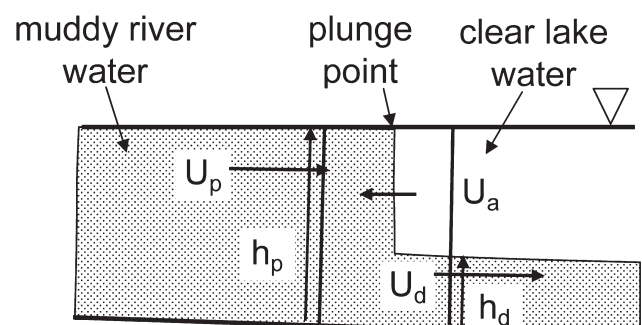


Fig. 2-68. Detailed illustration of flow near the plunge point with definitions.

$$Fr_{dp}^2 = \frac{1}{2\gamma^2} (1-\varphi)^3 \quad (2-282)$$

$$\frac{1}{\gamma^2} (1-\varphi)^3 - \frac{1}{\gamma^2} \frac{(1-\varphi)^3}{\varphi} (1+\gamma)^2 - (1-\varphi)^2 + 1 - \frac{\varphi^2}{(1+\gamma)} = 0 \quad (2-283)$$

Once the mixing coefficient  $\gamma$  is specified, these equations allow the determination of the plunge point and the flow below it. Let  $q_{mf}$  denote the volume feed rate of mud per unit width. Because the mud does not settle out upstream of the plunge point, the volume concentration of mud,  $C_{mp}$ , just upstream of the plunge point (and, indeed, everywhere upstream of the plunge point) is given from the relation

$$q_{mf} = q_w C_{mp} \quad (2-284)$$

The ratio  $\varphi = h_d/h_p$  is obtained from Eq. (2-283). Once this value is known,  $h_p$  is computed from Eqs. (2-282) and (2-280b) and  $h_d$  is further computed from this value and the previously computed value of  $\varphi$ . The value of  $U_d$  is then computed from Eq. (2-279), and the value of  $C_{md}$  is computed from  $U_d$ ,  $h_d$ , and Eqs. (2-280c) and (2-281).

Plunging occurs at the point of the foreset where the fluvial depth  $h_f$  becomes equal to the value  $h_p$  predicted from the above relations. It can be verified from these relations that a necessary condition for plunging is a mixing coefficient  $\gamma > 0.14$ . Under such conditions, the river flow just upstream of the plunge point is subcritical in the sense of the densimetric Froude number, i.e.,  $Fr_{dp} < 1$ , and the turbidity current just downstream of the plunge point is supercritical, i.e.,  $Fr_{dd} > 1$ .

#### 2.12.4 Linked One-Dimensional Model of Topset, Foreset and Bottomset Evolution

As noted above, Eqs. (2-260), (2-261), (2-253), and (2-254) describe, respectively, flow mass balance, momentum balance, suspended-sediment mass balance, and conservation of bed sediment for the case of a turbidity current. Here the following assumptions are made to simplify the problem.

- The turbidity current is assumed to be steady and driven by the steady inflow from the river.
- The turbidity current is assumed to be flowing over a bed that is sufficiently steep to render it everywhere supercritical in the densimetric sense.
- The turbidity current is purely depositional, so the term  $E_s$  in Eqs. (2-253) and (2-254) can be neglected.
- The turbidity current is allowed to run out infinitely in the streamwise direction.
- Bed load transport is neglected.

Under these assumptions, Eqs. (2-253), (2-260) and (2-261) can be reduced to the forms

$$\frac{\partial h_t}{\partial x} = \frac{Ri \frac{\partial \eta_t}{\partial x} + e_w \left( 2 - \frac{1}{2} Ri \right) + C_{ft} - \frac{1}{2} Ri r_o \frac{v_{sm}}{U_t}}{1 - Ri} \quad (2-285a)$$

$$\frac{\partial U_t}{\partial x} = \frac{Ri \frac{\partial \eta_t}{\partial x} - e_w \left( 1 + \frac{1}{2} Ri \right) - C_{ft} + \frac{1}{2} Ri r_o \frac{v_{sm}}{U_t}}{1 - Ri} \frac{U_t}{h_t} \quad (2-285b)$$

$$\frac{\partial q_m}{\partial x} = -r_o \frac{v_{sm}}{U_t} \frac{q_m}{h_t} \quad (2-285c)$$

Where

- $\eta_t$  = elevation of the bed below the turbidity current;
- $h_t$  = layer thickness of the turbidity current;
- $U_t$  = layer-averaged velocity of the turbidity current; and
- $q_m$  = volume discharge of mud per unit width of the turbidity current, related to the layer-flux averaged mud concentration  $C_t$  as

$$q_m = U_t h_t C_t \quad (2-286)$$

In addition,  $v_{sm}$  denotes the fall velocity of the mud and  $C_{ft}$  denotes the coefficient of bed resistance of the turbidity current, here approximated as constant. Finally, the Richardson number  $Ri$  is given from Eqs. (2-263) and (2-286) as

$$Ri = \frac{R_m g C_t h_t}{U_t^2} = \frac{R_m g q_m}{U_t^3} \quad (2-287)$$

The assumption of supercritical flows implies that  $Ri < 1$  everywhere. This assumption allows Eqs. (2-285a), (2-285b), and (2-285c) to be integrated downstream from the plunge point. Let  $x = s_p$  denote the position of the plunge point. The boundary conditions on (2-285a), (2-285b), and (2-285c) are then

$$h_t|_{x=s_p} = h_d \quad (2-288a)$$

$$U_t|_{x=s_p} = U_d \quad (2-288b)$$

$$q_m|_{x=s_p} = U_d h_d C_{md} \quad (2-288c)$$

where  $h_d$ ,  $U_d$  and  $C_{md}$  are obtained from the calculation of plunging.

Once the flow over the bed is solved, the morphodynamic evolution of the lake bed is solved from Eq. (2-251) subject to these assumptions, which reduce it to the form

$$(1 - \lambda_{pm}) \frac{\partial \eta_t}{\partial t} = -I_f r_o \frac{v_{sm}}{U_t} \frac{q_m}{h_t} \quad (2-289)$$

where  $\lambda_{pm}$  denotes the porosity of the mud deposit. The solution of Eqs. (2-285a), (2-285b), and (2-285c) subject to Eqs. (2-288a), (2-288b), and (2-288c) for the flow over the bed, and Eq. (2-289) for the bed evolution describes the evolution of a bottomset emplaced by a purely depositional one-dimensional muddy turbidity current.

Kostic and Parker (2003a, 2003b) have devised a moving-boundary formulation that dynamically links the moving-boundary model of the topset-foreset evolution described in Section 2.12.2 with the model of the bottomset evolution described in this section. All the equations describing topset-foreset evolution remain the same except for Eq. (2-272) describing the evolution of the foreset-basement break. In a linked model the foreset-basement break is replaced with a foreset-bottomset break located at  $x = s_b$ , as described in Fig. 2-66. The modified relation is

$$(S_a - S_b) \dot{s}_b = (S_a - S_s) \dot{s}_s + \left. \frac{\partial \eta_f}{\partial t} \right|_{s_s} - \left. \frac{\partial \eta_t}{\partial t} \right|_{s_s} \quad (2-290)$$

where  $S_b$  is now given as the slope of the bottomset at the foreset-bottomset break:

$$S_b = - \left. \frac{\partial \eta_t}{\partial x} \right|_{x=s_b} \quad (2-291)$$

The moving boundary formulation for topset/foreset evolution remains the same as that of Section 2.12.2, except for Eq. (2-277), which takes the amended form

$$\dot{s}_b = \dot{s}_s + \frac{1}{S_a} \left( \left. \frac{\partial \eta_f}{\partial \hat{t}_f} \right|_{\hat{x}_f=1} - \left. \frac{\partial \eta_t}{\partial \hat{t}_t} \right|_{\hat{x}_t=0} \right) \quad (2-292)$$

where the moving boundary coordinates for the bottomset region are given as

$$\hat{t}_t = t \quad \hat{s}_t = \frac{x - s_b}{s_{max} - s_b} \quad (2-293)$$

and  $x = s_{max}$  denotes the downstream limit of the range on which the calculation is to be performed.

Sample calculations of the coevolution of the sandy topset-foreset and muddy bottomset of a one-dimensional delta are presented as Case C, which has three subcases Ca, Cb, and Cc, corresponding to mud size  $D_m = 10$ , 15, and 25  $\mu\text{m}$ , respectively. The relevant modeling parameters are given in Table 2-8; for these cases  $S_{base}$  corresponds to the slope of the antecedent subaqueous bed over which the turbidity current deposits mud. Fall velocities  $v_{sm}$  have been computed using the values of  $R_m$  and  $D_m$  listed in Table 2-8, the kinematic viscosity  $\nu$  of water at 20°C and the relation of Dietrich (1982) presented in Eq. (2-47a). Water entrainment has been computed using Eq. (2-262). The coefficient  $r_o$  has been set equal to 2 (García 1994). The plunging formulation used in the computation is a highly simplified version that is less rigorous than the one presented in the previous section. It serves, however, to illustrate the morphodynamics of coevolution. In the calculation the turbidity current runs a short distance down the foreset from the plunge point before debouching onto the bottomset. It is assumed that the foreset is too steep to allow for the deposition of mud. Mud deposition commences at the foreset-bottomset break.

The results of the calculations for Cases Ca, Cb and Cc are presented in Fig. (2-69). In Case Ca with 10- $\mu\text{m}$  material, the bottomset is quite thin due to the small fall velocity of the mud. (The bottomset extends far beyond the point  $s_{max} = 30,000$  m in Cases Ca, Cb, and Cc.) Progradation of the foreset simply pushes the bottomset lakeward. In Case Cb with 15- $\mu\text{m}$  material the foreset and bottomset are seen to interact: progradation of the foreset pushes the bottomset lakeward, and aggradational of the bottomset reduces the elevation drop of the foreset. The interaction is seen to be even stronger for the 25- $\mu\text{m}$  material of Case Cc. Note that as the mud becomes coarser it falls out more rapidly from the turbidity current, so that deposition on the bottomset becomes more proximal to the foreset.

Figure 2-69(c) in particular bears a remarkable resemblance to the delta of Lake Mead shown in Fig. 2-61. In both images the interface between the sand and mud (foreset-bottomset break) is first seen to move upward and lakeward, and then to move downward and lakeward.

The restriction to supercritical flow means that the backwater formulation of Eqs. (2-285a), (2-285b), and (2-285c) for the turbidity (actually a frontwater formulation, because supercritical flow dictates integration in the downstream direction) can only be implemented on relatively high subaqueous bed slopes. On lower slopes the turbidity current undergoes a hydraulic jump to subcritical flow (García 1993). The problem can still be solved, but steady forms of Eqs. (2-285a), (2-285b), and (2-285c) must be replaced by their corresponding unsteady forms, even when the incoming flow is constant. The unsteady forms of the equations allow automatic shock capturing of any hydraulic jump. Kostic and Parker (2003a, 2003b) have implemented such calculations using a moving-boundary formulation that adds an extra moving boundary. In addition to the moving boundaries of the topset-foreset and foreset-bottomset breaks, the model also captures the

migration of the front of the turbidity current until such time as it exits the calculational domain. Tracking the front propagation constitutes a challenging problem (e.g., Choi and García 1995, 2001). Finally, a quasi-steady state turbidity current is achieved in a relatively short amount of time when the inflow conditions are steady.

#### 2.12.5 Linked Quasi-Two-Dimensional Model of Topset, Foreset and Bottomset Evolution

Most real deltas at the upstream end of lakes are fan-deltas. That is, they spread out in the transverse direction. Fig. 2-70 shows an example of such a fan-delta: the Eau Claire River flowing into Lake Altoona, a reservoir in Wisconsin. As the river channel on a fan-delta aggrades, it migrates and avulses to fill the available surface of the fan-delta as it progrades. That is, it fills the area of the fan rather than the area of the channel in Fig. 2-71. Since the river fills a much wider area than just the bed of the channel itself, the rate of delta progradation is greatly slowed compared to the one-dimensional case.

The two-dimensional morphodynamics of a fan-delta can be approximated using a one-dimensional model in the following way. The river on the fan is assumed to have an effective constant width  $B_c$  for transporting sediment. In the long-term average, however, the sediment is assumed to be

deposited across the entire fan by gradual channel shift and avulsion. Here an axially symmetric fan with angle  $\theta_f$  is considered, as illustrated in Fig. 2-71. A radial coordinate  $r$  is defined from the apex of the fan. The equations governing flow in the channel remain unchanged from the one-dimensional formulation (except for the transformation from  $x$  to radial coordinate  $r$ ).

The radial width  $B_f$  is given as

$$B_f = \theta_f r \quad (2-294)$$

The appropriate form of the Exner equation of sediment conservation for the topset and foreset is

$$(1 - \lambda_{ps}) B_f \frac{\partial \eta_f}{\partial t} = -I_f B_c \frac{\partial q_t}{\partial r} \quad (2-295a)$$

or rearranging,

$$(1 - \lambda_{ps}) \frac{\partial \eta_f}{\partial t} = -I_f \frac{B_c}{B_f} \frac{\partial q_t}{\partial r} \quad (2-295b)$$

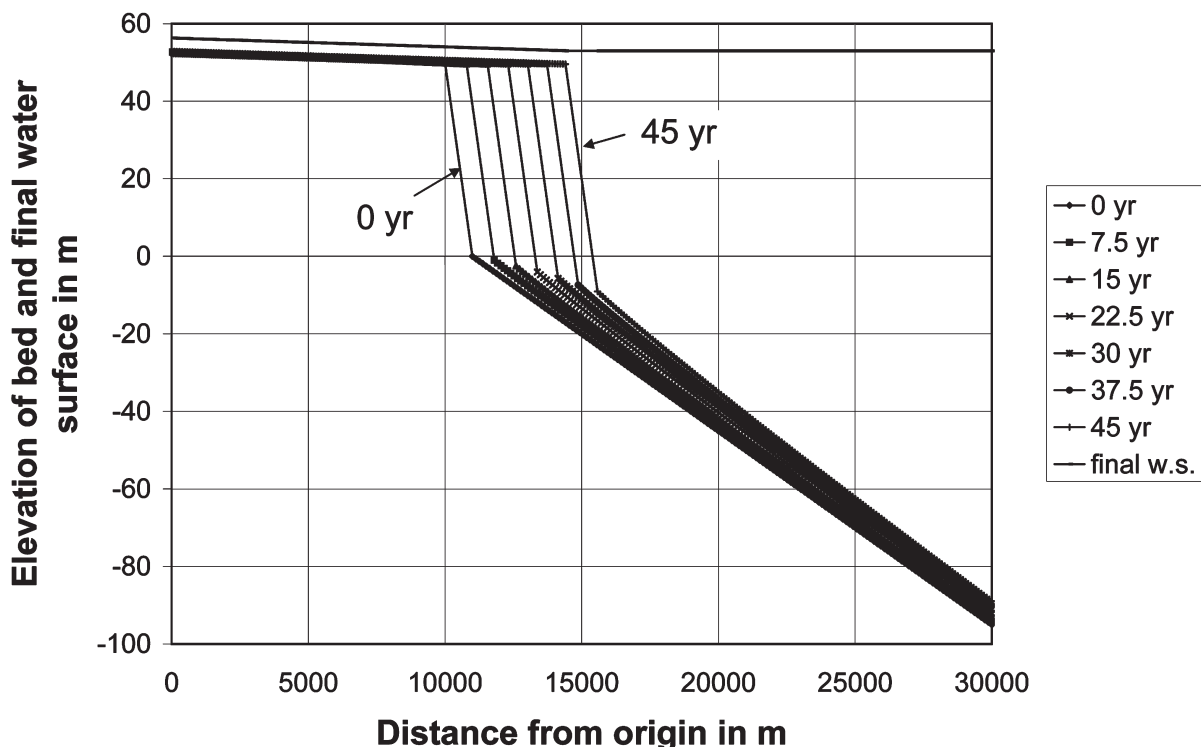


**Fig. 2-69.** Simulation of coevolution of a sandy topset-foreset and a muddy bottomset foreset in a lake using a shock-fitting formulation and the input of Cases Ca(a),Cb(b), and Cc(c) of Table 2-8. The mud has a size of (a)10  $\mu\text{m}$ , (b) 15  $\mu\text{m}$ , and (c) 25  $\mu\text{m}$ .

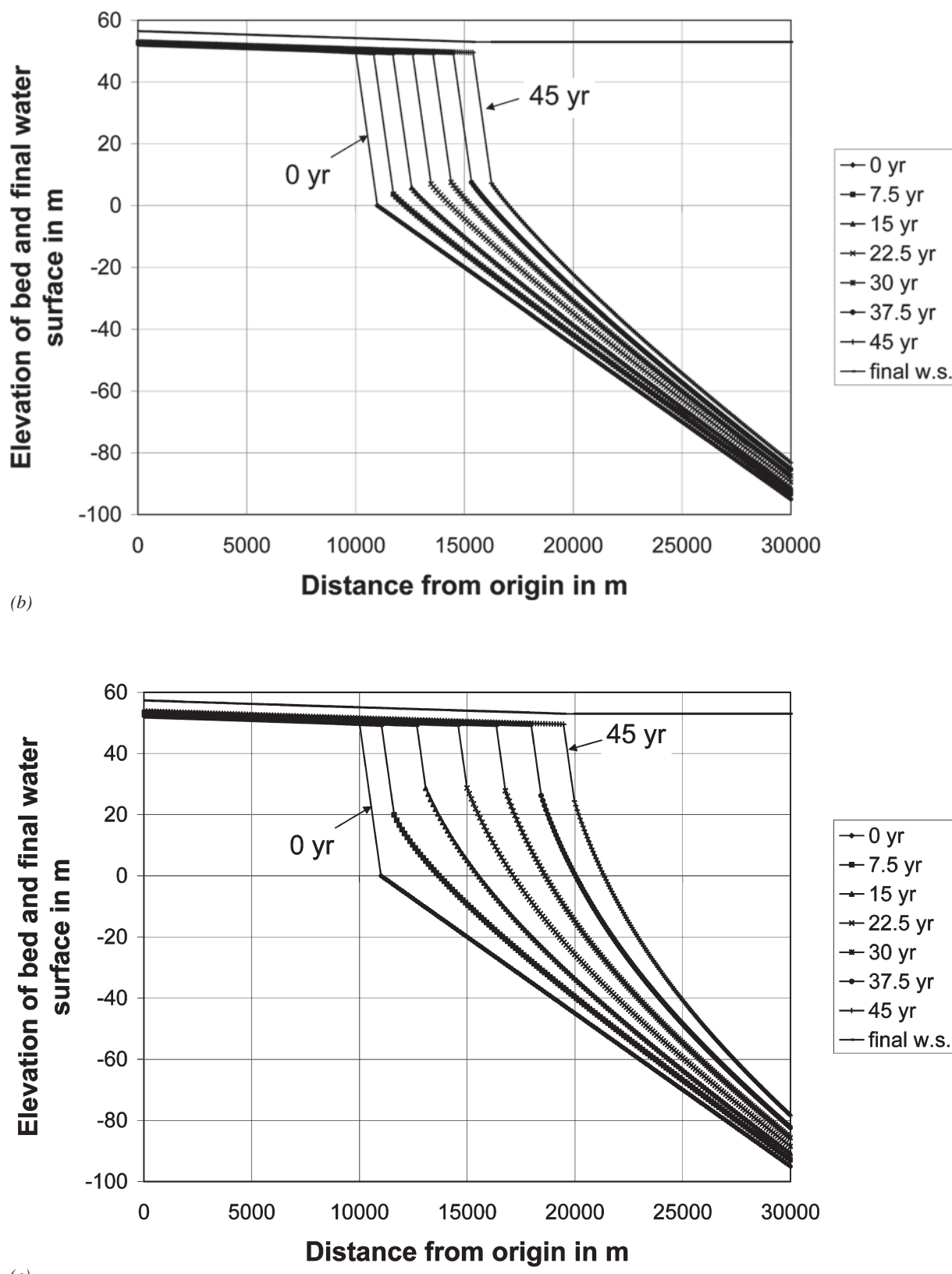


**Fig. 2-69.** Simulation of coevolution of a sandy topset-foreset and a muddy bottomset foreset in a lake using a shock-fitting formulation and the input of Cases Ca(a), Cb(b), and Cc(c) of Table 2-8. The mud has a size of (a) 10  $\mu\text{m}$ , (b) 15  $\mu\text{m}$ , and (c) 25  $\mu\text{m}$ . (*Continued*)

As the fan progrades the ratio  $B_c/B_f$  must become small in accordance with Eq. (2-294). The result is a greatly suppressed rate of delta progradation and aggradational compared to a purely one-dimensional formulation in which all the topset sand deposits within the channel.

As illustrated in Fig. 2-71, the topset-foreset break is located at  $r = s_s(t)$  and the foreset-bottomset break is located at  $r = s_b(t)$ ; both define moving boundaries. The shock condition at the foreset now takes the form

$$\frac{1}{2}(s_b^2 - s_s^2)\theta_f \left[ \frac{\partial \eta_f}{\partial t} \Big|_{s_s} + (S_a - S_s)\dot{s}_s \right] = \frac{I_f B_c q_t \Big|_{r=s_s}}{(1 - \lambda_{ps})} \quad (2-296)$$



**Fig. 2-70.** Fan-delta of the Eau Claire River as it flowed into Lake Altoona, a reservoir in Wisconsin, in 1988.

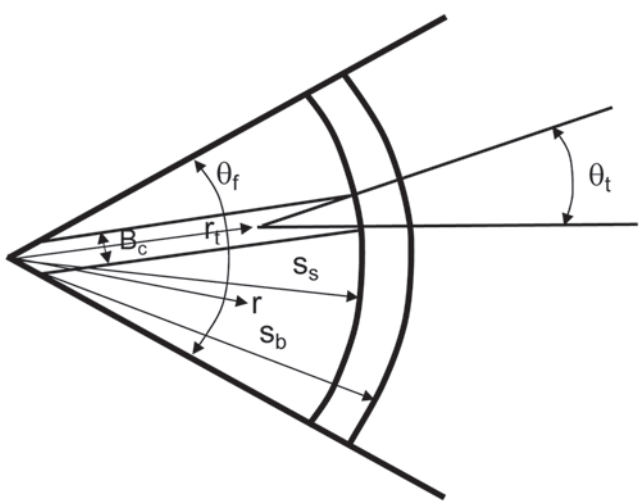


**Fig. 2-71.** Definition diagram for a two-dimensional fan-delta.

where

$$S_s = -\left. \frac{\partial \eta_f}{\partial r} \right|_{r=s_s} \quad (2-297)$$

The continuity condition at the foreset-bottomset break remains unaltered from the one-dimensional case (except for the transformation  $x \rightarrow r$ ).

The turbidity current is assumed to spread out axially at angle  $\theta_t$ . It is assumed to have an upstream width equal to that of the effective river channel, as described in Fig. 2-71. Let  $r_t$  denote the position of the virtual origin of the wedge of the turbidity current with angle  $\theta_t$  in Fig. 2-71. The governing equations of a steady, axially symmetric, purely depositional turbidity current can be reduced to the forms

$$\frac{dh_t}{d\tilde{r}} = \frac{Ri \frac{\partial \eta_t}{\partial \tilde{r}} Ri + e_w \left( 2 - \frac{1}{2} Ri \right) + C_{ft} - \frac{h_t}{\tilde{r}} \left( 1 - \frac{1}{2} Ri \right) - \frac{1}{2} Ri r_o \frac{v_{sm}}{U_t}}{1 - Ri} \quad (2-298a)$$

$$\frac{dU_t}{d\tilde{r}} = \frac{Ri \frac{\partial \eta_t}{\partial \tilde{r}} - e_w \left( 1 + \frac{1}{2} Ri \right) - C_{ft} + \frac{1}{2} Ri \frac{h_t}{\tilde{r}} + \frac{1}{2} Ri r_o \frac{v_{sm}}{U_t}}{1 - Ri} \frac{U_t}{h_t} \quad (2-298b)$$

$$\frac{dq_m}{d\tilde{r}} = -\frac{q_m}{\tilde{r}} - r_o \frac{v_{sm}}{U_t} \frac{q_m}{h_t} \quad (2-298c)$$

where

$$\tilde{r} = r - r_t \quad (2-299)$$

The turbidity current is assumed to migrate across the subaqueous fan, filling it in a manner analogous to that of a subaerial fan-delta. That is, the turbidity current deposits over an area that is much larger than that of the turbidity current itself at any given time. The appropriate form of the Exner equation of sediment continuity becomes

$$(1 - \lambda_{pm})\theta_f r \frac{\partial \eta_t}{\partial t} = r_o \frac{v_{sm}}{U_t} \frac{q_m}{h_t} \theta_t (r - r_t) \quad (2-300)$$

This quasi-two-dimensional formulation can be cast into a moving-boundary framework and solved in a manner that is completely analogous to the one-dimensional case. The input parameters for the calculation are shown as Case D in Table 2-8. As in all previous cases, the sand size  $D_s$  is 0.4 mm (400  $\mu\text{m}$ ); the mud size is 10  $\mu\text{m}$ . The fan angle  $\theta_f$  is taken to be  $90^\circ$  and the angle of spread of the turbidity current  $\theta_t$  is taken to be  $10^\circ$ .

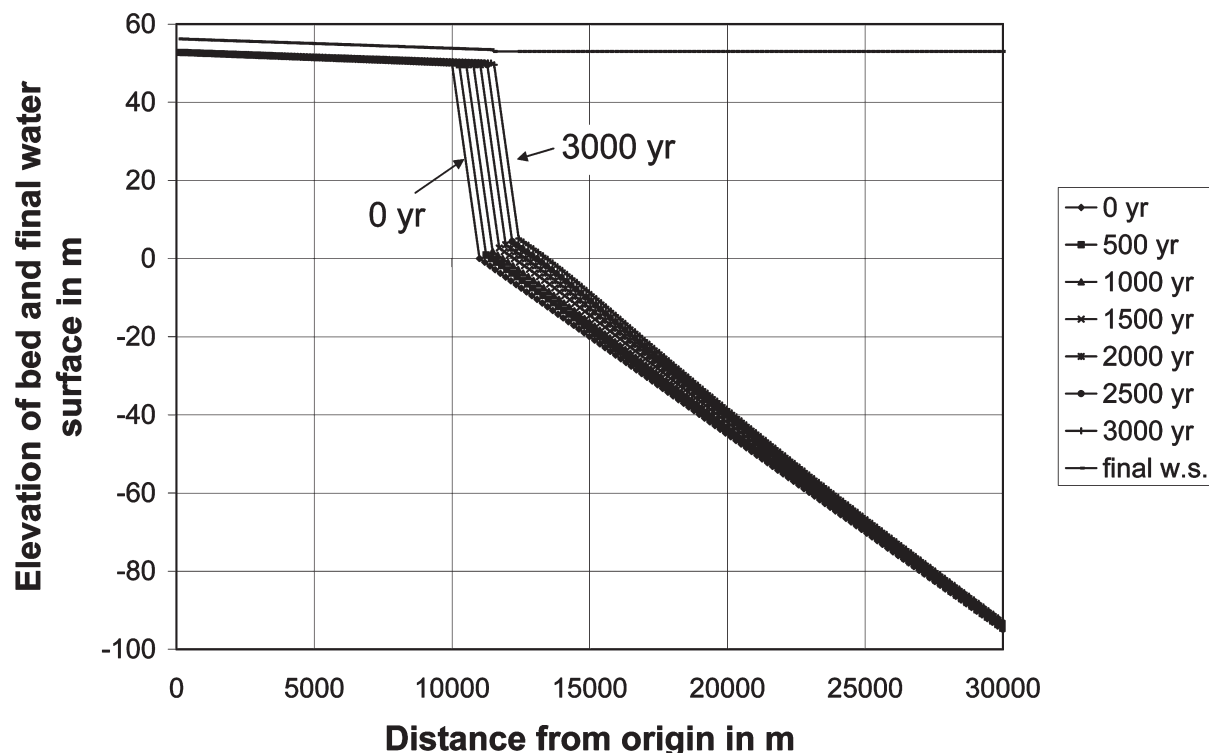


**Fig. 2-72.** Simulation of coevolution of a sandy topset-foreset and a muddy bottomset foreset in a lake using a quasi-2D shock-fitting formulation and the input of Case D of Table 2-8. The mud has a size of 10  $\mu\text{m}$ .

The results of the quasi-two-dimensional calculation of Case D are shown in Fig. 2-72. The analogous one-dimensional case is that of Case Cc. It is seen that after 3000 years the quasi-two-dimensional fan-delta has prograded out much less than in the corresponding one-dimensional case over 45 years. The effect of the two-dimensional geometry in limiting the rate of progradation is clearly apparent.

#### 2.12.6 Formation of a Muddy Pond in a Reservoir: Detrainment and Sediment Trap Efficiency

In the calculations presented in the previous two sections the turbidity current has been allowed to run out infinitely in the streamwise direction. In a reservoir, however, a sustained turbidity current eventually hits the dam and reflects off it.

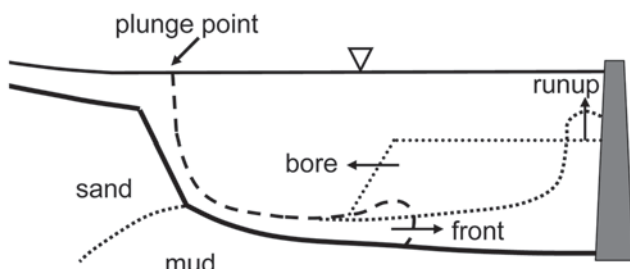


**Fig. 2-73.** Process by which a muddy pond is set up in a reservoir.

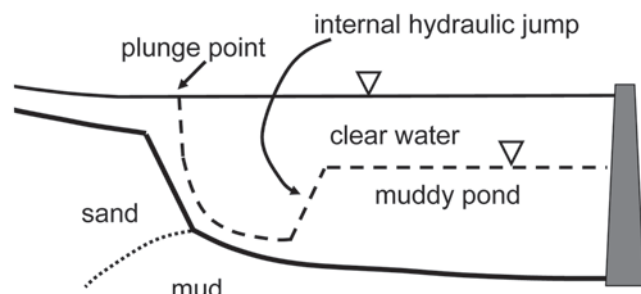


**Fig. 2-74.** Quasi-steady flow in a reservoir after the establishment of an internal hydraulic jump and a muddy pond.

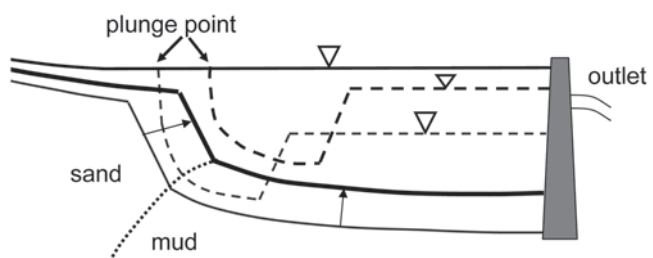


**Fig. 2-75.** Diagram illustrating the gradual decline in trap efficiency of a reservoir as the level of the muddy interface gradually rises above an outlet.

This creates an upstream-migrating bore that eventually stabilizes upstream as an internal hydraulic jump (García and Parker 1989; García 1993). The result is the formation of a deep, slow-moving muddy pond downstream of the hydraulic jump (Lamb et al. 2006). The setup process is illustrated in Fig. 2-73, and the resulting quasi-steady flow after setup of the muddy pond is illustrated in Fig. 2-74.

The muddy pond is a zone containing a nearly stagnant turbidity current, for which the densimetric Froude number  $Fr_d$  satisfies the condition

$$Fr_d \ll 1 \quad (2-301)$$

It is subject to a phenomenon which Toniolo (2002) and Lamb et al. (2004) have called "water detrainment." In the absence of incoming flow from upstream, the interface between the muddy pond and the clear water above would gradually migrate downward at a rate equal to the fall velocity  $v_{sm}$  of the mud. Thus muddy water is converted to clear water at a detrainment discharge equal to  $v_{sm} A$ , where  $A$  is equal to the surface area of the interface. When muddy water is constantly being replaced from upstream as it passes through the hydraulic jump, however, the elevation of the muddy pond

can stabilize well below the water surface of the reservoir, while water continues to detrain at the discharge  $v_{sm} A$ .

Initially the interface of the muddy pond may stabilize at a level that is below any outlet, as shown in Fig. 2-75. In such a case the trap efficiency of the reservoir is 100 %. As the foreset progrades and the bottomset upgrades, however, the interface should rise in time, so that mud is washed out of a reservoir outlet. This process is illustrated in Fig. 2-75. The result is a trap efficiency that gradually drops below 100 percent.

Toniolo et al. (2007) have developed a moving boundary numerical model to describe the coevolution of a sandy topset-foreset and a muddy bottomset, in which a dam forces the formation of a muddy pond. The model is one-dimensional, but it could easily be adapted to a quasi-twodimensional configuration. The model requires a fully unsteady treatment of the flow in order to capture the hydraulic jump (e.g., Choi and García 1995). Once its position is stabilized, however, a quasi-steady flow is maintained in the presence of slow delta progradation and bottomset. Again, the turbidity current is treated as purely depositional.

The equations governing flow mass and momentum conservation and conservation of suspended sediment must be adapted to include water detrainment from a stagnant, muddy pond for which  $Fr_d \ll 1$ . The forms of these relations used in the analysis are

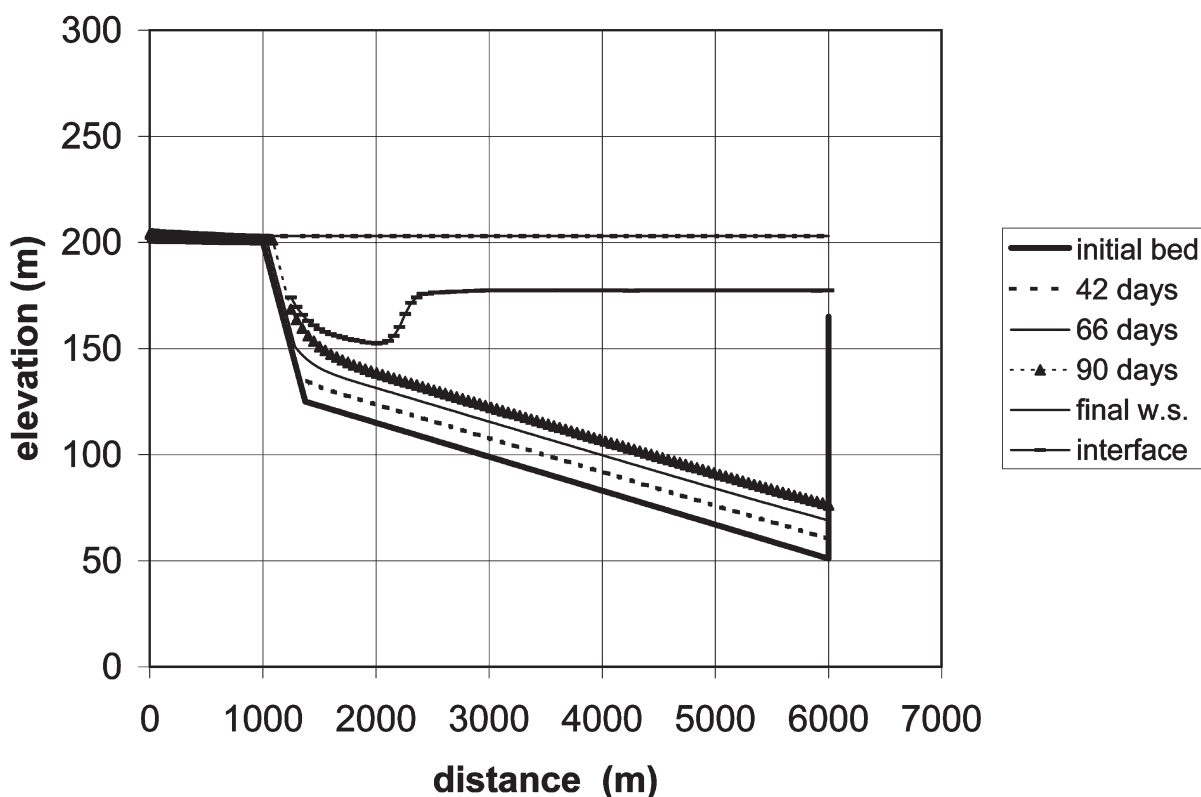


**Fig. 2-76.** Simulation of coevolution of a sandy topset-foreset and a muddy bottomset foreset in a reservoir using a one-dimensional shock-fitting formulation and the input of Case E of Fig. 2-77. Prediction of reservoir trap efficiency for Case E of Table 2-8. The mud has a size of 50  $\mu\text{m}$ . Note the presence of the internal hydraulic jump and the muddy pond.

$$\frac{\partial h_t}{\partial t} + \frac{\partial U_t h_t}{\partial x} = (1 - \delta)e_w U_t - \delta v_{sm} \quad (2-302a)$$

$$\begin{aligned} \frac{\partial U_t h_t}{\partial t} + \frac{\partial U_t^2 h_t}{\partial x} + \delta U_t v_{sm} \\ = -\frac{1}{2} R_m g \frac{\partial C_t h_t^2}{\partial x} + R_m g C_t h_t S - C_f U_t^2 \end{aligned} \quad (2-302b)$$

$$\frac{\partial C_t h_t}{\partial t} + \frac{\partial U_t C_t h_t}{\partial x} = -\delta r_o v_{sm} C_t \quad (2-302c)$$

Here the parameter  $\delta$  is set equal to 1 in the muddy pond, but is set equal to 0 elsewhere. The details of the moving-boundary analysis can be found in Toniolo et al. (2007). The treatment uses the plunging formulation of Parker and Toniolo (2007) with a value of  $\gamma$  of 1.3.

Toniolo et al. (2007) have applied the model at field scale. The parameters are given as Case E of Table 2-8. Note that  $r_o$  is set equal to 1 in the analysis, because the hydraulic jump should render the ponded zone well-mixed up, to the interface with the clear water above. The distance  $s_{max}$  from the origin to the wall of the dam is 6000 m. The flow intermittency  $I_f$  has been set equal to unity. This means that the 90 days of calculation time corresponds to 90 days of continuous flood, which might translate to, e.g., 2 to 10 years of real time.

The results of the calculation are shown in Fig. 2-76. Note that the bottomset deposit in the ponded zone is of nearly uniform thickness. This feature is driven by the ponding itself. In performing the calculation, water was vented from the reservoir at an elevation that was 38 m below the level of the water surface. As shown in Fig. 2-77, the trap efficiency was initially 100 percent because the settling interface was below the outlet. Reservoir sedimentation caused the level of the interface to rise in time, however, leading to a gradual reduction in trap

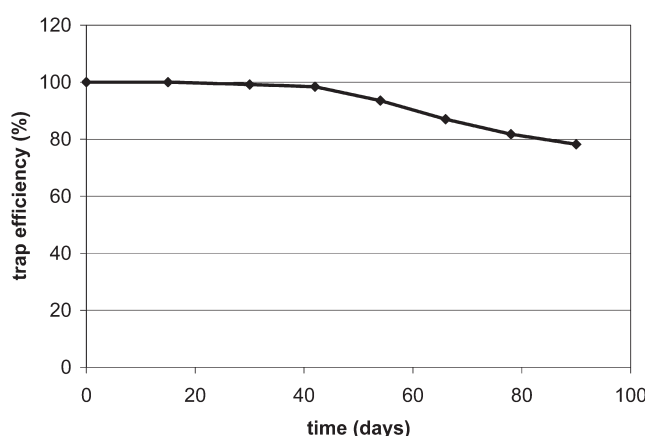


Fig. 2-77. Prediction of reservoir trap efficiency for Case E of Table 2-8.

efficiency. It should be pointed out that all the sediment escaping the model reservoir was mud, not sand.

Venting of turbidity currents through bottom outlets to prevent reservoir sedimentation has been considered around the world, particularly in China where the sediment loads of rivers are extremely large (e.g., Bruk 1985; Fan and Morris 1992b). For instance, the effectiveness of bottom outlets to discharge sediment-laden water will be greatly influenced by the characteristics of turbidity currents reaching the dam where they are placed (Toniolo and Schultz 2005). The location and frequency of operation of bottom outlets will also be influenced by sediment-laden underflows. The approach presented here, which is based on the dynamics of plunging turbidity currents, provides a way to assess how effective and useful different technologies might be for extending the life of reservoirs.

## 2.12.7 Remarks in Closing

The analyses of lake and reservoir sedimentation presented here are highly simplified. They should, however, serve to illustrate the main processes by which sedimentation occurs. They also should provide guidelines for the numerical prediction of lake and reservoir sedimentation as well as the operation of reservoirs to reduce sediment deposition by open-channel flows and turbidity currents. A more practical analysis of reservoir sedimentation is given in Chapter 12. One-dimensional modeling of sedimentation processes in rivers is addressed in Chapter 14, while two-dimensional and three-dimensional sediment transport models are covered in Chapter 15. Turbulence models for sediment-laden flows are considered in Chapter 16, while numerical modeling of sediment transport associated with dam removal is presented in Chapter 22.

## REFERENCES

- Abad, J. D., and García, M. H. (2006) Discussion of “Efficient algorithm for Computing Einstein Integrals by Junke Guo and Pierre Y. Julien.” (*Journal of Hydraulic Engineering*, Vol. 130, No. 12, pp. 1198–1201, 2004). *Journal of Hydraulic Engineering, ASCE*, 132(3), 332–334.
- Abbott, J. E. and Francis, J.R.D. (1977). “Saltation and suspension trajectories of solid grains in a water stream.” *Philosophical Transactions of the Royal Society of London, Series A*, 284, 225–254.
- Abrahams, A. D. (2003). “Bed-load transport equation for sheet flow.” *Journal of Hydraulic Engineering, ASCE*, 129(2), 159–163.
- Ackers, P., and White, W. R. (1973). “Sediment transport: New approach and analysis.” *Journal of Hydraulic Engineering, ASCE*, 99(11), 2041–2060.
- Adams, C. E., and Weatherly, G. L. (1981). “Some effects of suspended sediment stratification on an oceanic bottom boundary layer.” *Journal of Geophysical Research*, 86, 4161–4172.

- Admiraal, D., García, M. H., and Rodriguez, J. F. (2000). "Entrainment Response of Bed Sediment to Time-Varying Flows," *Water Resources Research*, 36(1), 335–348.
- Admiraal, D. and García, M. H. (2000). "Laboratory measurements of suspended sediment concentration using an acoustic concentration profiler (ACP)." *Experiments in Fluids*, 28, 116–227.
- Aguirre-Pe, J., Olivero, M. L., and Moncada, A. T. (2003). "Particle Densimetric Froude Number for Estimating Sediment Transport." *Journal of Hydraulic Engineering, ASCE*, 129(6), 428–437.
- Aguirre-Pe, J., and Fuentes, R. (1990). "Resistance to flow in steep rough streams." *Journal of Hydraulic Engineering, ASCE*, 116(11), 1374–1387.
- Aguirre-Pe, J., and Fuentes, R. (1995). "Stability and weak motion of riprap at a channel bed." *River, coastline and shore protection: erosion control using riprap and armourstone*, edited by C. R. Thorne, S. R. Abt, F.B.J. Barends, S. T. Maynard, K. W. Pilarczyk, John Wiley & Sons, New York, 77–92.
- Ahrens, J. P. (2000). "The fall-velocity equation." *Journal of Waterway, Port, Coastal, and Ocean Engineering, ASCE*, 126(2), 99–102.
- Ahrens, J. P. (2003). "Simple equations to calculate fall velocity and sediment scale parameter." *Journal of Waterway, Port, Coastal, and Ocean Engineering, ASCE*, 129(3), 146–150.
- Akiyama, J., and Fukushima, Y. (1986). "Entrainment of noncohesive bed sediment into suspension." *Third International Symposium on River Sedimentation*, S. Y. Wang, H. W. Shen, and L. Z. Ding, eds. The University of Mississippi, Mississippi, 804–813.
- Allen, J.R.L. (1978). "L. van Bendegom: a neglected innovator in meander studies." *Fluvial sedimentology*, A. D. Miall, ed., Memoir No. 5, Canadian Society of Petroleum Geologists, Calgary, 199–209.
- Allen, J.R.L. (1982). "Free meandering channels and lateral deposits." *Sedimentary structures: their character and physical basis*, Vol. 2, Elsevier, Amsterdam, 53–100.
- Almedeij, J. H., and Diplas, P. (2003). "Bedload transport in gravel-bed streams with unimodal sediment" *Journal of Hydraulic Engineering, ASCE*, 129(11), 896–904.
- Alonso, C. V. (1980). "Selecting a formula to estimate sediment transport capacity in nonvegetated channels." Chapter 5, *CREAMS—A field scale model for chemicals, runoff, and erosion from agriculture management system*, Conservation Research Report No. 26, W. G. Knisel, ed., U.S. Department of Agriculture, Washington D.C., pp. 426–439.
- Alonso, C. V., and Mendoza, C. (1992). "Near-bed sediment concentration in gravel-bedded streams." *Water Resources Research*, 28(9), 2459–2468.
- Amsler, M. A., and García, M. H. (1997). "Discussion of sand-dune geometry of large rivers during floods by P. Y. Julien and G. J. Klaasen," *Journal of Hydraulic Engineering, ASCE*, 123(6), 582–584.
- Amsler, M. L., and Schreider, M. I. (1999). "Dune height prediction at floods in the Paraná River, Argentina." *River Sedimentation: theory and applications*, A. W. Jayewardena, J.H.W. Lee and Z. Y. Wang, eds., A. A. Balkema. Rotterdam, pp. 615–620.
- Amsler, M. L., and Prendes, H. H. (2000). "Transporte de sedimentos y procesos fluviales asociados." Chapter 5, *El Río Paraná, en su tramo medio*, C. U. Paoli and M. I. Schreider, eds., Universidad Nacional de Litoral, Santa Fe, Argentina, pp.233–306.
- Amsler, M. L., Prendes, H. H., Montagnini, M. D., Szupiany, R. and García, M. H. (2003). "Prediction of dune height in sand-bed rivers: the case of the Paraná River, Argentina." *Proceedings 3rd Symposium on River, Coastal and Estuarine Morphodynamics*, Politechnic University of Catalunya, Barcelona, Spain.
- Anderson, A. G. (1953). "The characteristics of sediment waves formed by flow in open channels." *Proceedings Third Midwest Conference in Fluid Mechanics*, University of Minnesota, Minneapolis, 379–395.
- Anderson, R. S., and Haff, P. K. (1988). "Simulation of eolian saltation." *Science*, 241, 820–823.
- ASCE Task Committee (2000). "Hydraulic Modeling: concepts and practice." *Manuals and Reports on Engineering Practice No. 97, ASCE*, Reston, Virginia.
- ASCE Task Force (2002). "Flow and transport over dunes." *Journal of Hydraulic Engineering, ASCE*, 128(8), 726–728.
- Ashida, K., and Michiue, M. (1972). "Study on hydraulic resistance and bed-load transport rate in alluvial streams." *Transactions Japan Society of Civil Engineering*, 206, 59–69.
- Ashley, G. M. (1990). "Classification of large-scale subaqueous bedforms: a new look at an old problem." *Journal of Sedimentary Petrology*, 60(1), 160–172.
- Ashworth, P. J., Bennett, S. J., Best, J. L. and McLelland, S. J., Eds. (1996). *Coherent Flow Structures in Open Channels*, John Wiley and Sons, New York.
- Ayala, L., and Oyarce, O. (1993). "Energy loss in mountain streams conditioned by armoring and bedload transport." *Proceedings IX Chilean Hydraulics Congress*, Chilean Society of hydraulic Engineering, Concepcion, Chile (in Spanish).
- Baas, J. H. (1999). "An empirical model for the development and equilibrium morphology of current ripples in fine sand." *Sedimentology*, 46, 123–138.
- Bagnold, R. A. (1954). "Experiments on the gravity-free dispersion of large solid spheres in a Newtonian fluid under shear." *Proceedings of the Royal Society of London*, A225, 49–63.
- Bagnold, R. A. (1956). "The flow of cohesionless grains in fluids." *Philosophical Transactions of the Royal Society of London, Series A*, 249, 315–319.
- Bagnold, R. A. (1962). "Auto-suspension of transported sediment; turbidity currents." *Proceedings Royal Society of London, Series A*, 205, 473–504.
- Bagnold, R. A. (1966). "An Approach to the Sediment Transport Problem from General Physics," U.S. Geol. Survey, Prof. Paper 422-I.
- Bagnold, R. A. (1973). "The Nature of Saltation and of Bed Load Transport in Water." *Proceedings Royal Society of London, Series A*, 332, 473–504.
- Bathurst, J. C. (1985). "Flow resistance equation in mountain rivers." *Journal of Hydraulic Engineering, ASCE*, 111(4), 1103–1122.
- Bathurst, J. C., Graf, W. H., and Cao, H. H. (1987). "Bedload discharge equations for steep mountain rivers." *Sediment Transport in Gravel-Bed Rivers*, C. R. Thorne, J. C. Bathurst, and R. D. Hey, eds., John Wiley & Sons, 453–477.
- Bechteler, W., Vogel, G., and Vollmers, H. J. (1991). "Model investigations on the sediment transport of a lower alpine river." *Fluvial Hydraulics of Mountain Regions*, A. Armanini anf

- G. Di Silvio, Eds., Lecture Notes in Earth Sciences, Springer-Verlag, Berlin, 179–194.
- Bedford, K. W., Wai, O., Libicki, C. M., and Van Evra III, R. (1987). “Sediment entrainment and deposition measurements in Long Island Sound.” *Journal of Hydraulic Engineering, ASCE*, 113(10), 1325–1342.
- Bell, H. S. (1942). “Stratified flow in reservoirs and its use in preventing of silting.” *Misc. Publ. 491*, U.S. department of Agriculture, U.S. Government Printing Office, Washington, D.C.
- Bennett, J. P. (1995). “Algorithm for resistance to flow and transport in sand-bed channels,” *Journal of Hydraulic Engineering, ASCE*, 121(8), 578–590.
- Bennett, S. J., and Best, J. L. (1995a). “Mean flow and turbulence structure over fixed, two dimensional dunes: implications for sediment transport and dune stability.” *Sedimentology*, 42, 491–514.
- Bennett, S. J., and Best, J. L. (1995b). “Particle size and velocity discrimination in a sediment-laden turbulent flow using phase Doppler anemometry,” *Journal of Fluids Engineering*, 117, 505–511.
- Bennett, S. J., and Best, J. L. (1996). “Mean flow and turbulence structure over fixed ripples and the ripple-dune transition.” *Coherent flow structures in open channels*, P. J. Ashworth, S. J. Bennett, J. L. Best and S. J. McLellan, eds., John Wiley and Sons, Chichester, U.K., 281–304.
- Bennett, S. J., and Venditti, J. (1997). “Turbulent flow and suspended sediment transport over fixed dunes.” *Proceedings Conference on Management of Landscapes Disturbed by Channel Incision*, S.S.Y. Wang, E. J. Langendoen and F. D. Shields Jr., eds., Center for Computational Hydroscience and Engineering, University of Mississippi, Oxford, 949–954.
- Bennett, S. J., Bridge, J. S. and Best, J. L. (1998). “The fluid and sediment dynamics of upper-stage plane beds.” *Journal of Geophysical Research*, 103, 1239–1274.
- Berezowsky, M., and Lara, M. A. (1986). “Determination of the friction slope in non-uniform or unsteady flow in rivers considering bedforms.” *Third International Symposium on River Sedimentation*, S. Y. Wang, H. W. Shen, and L. Z. Ding, eds., The University of Mississippi, Mississippi, 834–841.
- Best, J. L. (1996). “The fluid dynamics of small-scale alluvial bedforms,” *Advances in Fluvial Dynamics and Stratigraphy*, P. A. Carling and M. R. Dawson, eds., John Wiley and Sons, Chichester, United Kingdom, 67–125.
- Best, J. (2005). “The fluid dynamics of river dunes: a review and some future research directions.” *Journal of Geophysical Research*, 110, F04S02, doi:10.1029/2004JF000218.
- Best, J. L. and Ashworth, P. J. (1994). “A high-resolution ultrasonic bed profiler for use in laboratory flumes.” *Journal of Sedimentary Research A*, 64, 674–675.
- Best, J. L., and Kostaschuk, R. A. (2002). “An experimental study of turbulent flow over a low-angle dune.” *Journal of Geophysical Research*, 107, 3135–3153.
- Best, J. L., Bennett, S. J., Bridge, J. B., and Leeder, M. R. (1997). “Turbulence modulation and particle velocities over flat sand beds at low transport rates,” *Journal of Hydraulic Engineering, ASCE*, 123, 1118–1129.
- Best, J. L., Kostaschuk, R. A., and Villard, P. V. (2001). “Quantitative visualization of flow fields associated with alluvial sand dunes: results from the laboratory and field using ultrasonic and acoustic Doppler anemometry.” *Journal of Visualization*, Vol. 4, 373–381.
- Best, J. L., Ashworth, P. J., Bristow, C. S., and Roden, J. E. (2003). “Three-dimensional sedimentary architecture of a large, mid-channel sand braid bar, Jamuna River, Bangladesh.” *Journal of Sedimentary Research*, Vol. 73, 516–530.
- Best, J., P. Ashworth, P. J., Sarker, M. H., and Roden, J. (2006). “The Brahmaputra-Jamuna River.” *Large Rivers: Geomorphology and Management*, A. Gupta, ed., John Wiley and Sons, Chichester, United Kingdom.
- Bettess, R. (1984). “Initiation of sediment transport in gravel streams.” *Proceedings Institute of Civil Engineers*, 77(2), 79–88.
- Bhowmik, N. G., Bonini, A. P., Bogner, W. C. and Byrne, R. P. (1980). “Hydraulics of Flow and Sediment Transport in the Kankakee River in Illinois.” *Report of Investigation 98*, Illinois State Water Survey, Champaign, Illinois.
- Blondeaux, P. (2001). “Mechanics of Coastal Forms.” *Annual Reviews of Fluid Mechanics*, 33, 339–370.
- Blondeaux, P., and Seminara, G. (1985). “A unified bar-bend theory of river meanders.” *Journal of Fluid Mechanics*, 157, 449–470.
- Boguchwal, L. A., and Southard, J. B. (1990). “Bed configurations in steady unidirectional water flows. Part 3. Effects of temperature and gravity.” *Journal of Sedimentary Petrology*, 60, 680–686.
- Bonnefille, R. (1963). “Essais de synthese des lois de debut d’entrainement des sediments sous l’action d’un courant en regime uniform.” Bulletin du Centre de Recherche et d’Essais de Chatou, 5, France (in French).
- Boudreau, B. B., Jorgensen, B. B., Eds., (2001). *The benthic boundary layer: transport processes and biogeochemistry*. Oxford University Press, Oxford. 2001.
- Bravo-Espinosa, M., Osterkamp, W. R., and Lopes, V. L. (2003). “Bedload transport in alluvial channels.” *Journal of Hydraulic Engineering, ASCE*, 129(10), 783–795.
- Bray, D. I. (1979). “Estimating average velocity in gravel-bed rivers.” *Journal of the Hydraulics Division, ASCE*, 105(9), 1103–1122.
- Bridge, J. S., and Bennett, S. J. (1992). “A model for the entrainment and transport of sediment grains of mixed sizes, shapes and densities.” *Water Resources Research*, 28, 337–363.
- Bridge, J. S. (1992). “A revised model for water flow, sediment transport, bed topography, and grain size sorting in natural river bends.” *Water Resources Research*, 28, 999–1013.
- Bridge, J. S., and Dominic, D. F. (1984). “Bed load grain velocities and sediment transport rates.” *Water Resources Research*, 20, 476–490.
- Bridge, J. S. (2003). *Rivers and floodplains: forms, processes, and sedimentary record*. Blackwell, Oxford, United Kingdom.
- Brooks, N. H. (1963). Discussion of “Boundary shear stress in curved trapezoidal channels,” by A. T. Ippen and P. A. Drinker, *Journal of the Hydraulics Division, ASCE*, 89(5), 327–323.
- Brownlie, W. R. (1981). “Re-examination of Nikuradse roughness data.” *Journal of the Hydraulics Division, ASCE*, 107(1), 115–119.
- Brownlie, W. R. (1981). “Prediction of flow depth and sediment discharge in open channels.” *Report No. KH-R-43A*, Keck Laboratory of Hydraulics and Water Resources, California Institute of Technology, Pasadena, California.
- Brownlie, W. R. (1983). “Flow depth in sand-bed channels.” *Journal of Hydraulic Engineering, ASCE*, 109(7), 959–990.

- Bruk, S., rapporteur (1985). "Methods of computing sedimentation in lakes and reservoirs." *International Hydrological Programme IHP-II, Project A.2.6.1*, UNESCO, Paris, France.
- Bruschin, J. (1985). Discussion on "Flow depth in sand-bed channels by W. R. Brownlie, *Journal of Hydraulic Engineering, ASCE*, 109(7), 959–990." *Journal of Hydraulic Engineering, ASCE*, 111(4), 736–739.
- Brush, L. M. (1989). "Wash load, autosuspensions and hyper-concentrations." *Taming the Yellow River: Silt and Floods.* *Proceedings of a Bilateral Seminar on problems in the Lower Reaches of the Yellow River*, L. M. Brush, M. G. Wolman, and H. Bing-Wei, eds., Kluwer Academic Publishers, Boston, Mass.
- Buffington, J. M. (1999). "The Legend of A. F. Shields." *Journal of Hydraulic Engineering, ASCE*, 125(4), 376–387.
- Buffington, J., Dietrich, W. E. and Kirchner, J. W. (1992). "Friction angle measurements on a naturally-formed gravel streambed: implications for critical boundary shear stress." *Water Resources Research*, 28, 411–425.
- Buffington, J. M., and Montgomery, D. R. (1997). "A systematic analysis of eight decades of incipient motion studies, with special reference to gravel-bedded rivers." *Water Resources Research*, 33, 1993–2029.
- Buffington, J. M., Montgomery, D. R., and Greenberg, H. M. (2004). "Basin-scale availability of salmonid spawning gravel as influenced by channel type and hydraulic roughness in mountain catchments." *Canadian Journal of Fisheries and Aquatic Sciences*, 61, 2085–2096.
- Calantoni, J. (2002). "Discrete particle model for bedload sediment transport in the surf zone." PhD Dissertation, Physics Department, North Carolina State University, Raleigh, N.C., 93 p.
- Calantoni, J., and Drake, T. G. (1999). EOS Trans. American Geophysical Union, 80 (17), Spring Meeting Suppl., S194.
- Calantoni, J., Holland, K. T., and Drake, T. G. (2004). "Modelling Sheet-Flow Sediment Transport in Wave-Bottom Boundary Layers Using Discrete-Element Modelling," *Philosophical Transactions Royal Society of London, Series A-Math. Phys. Eng. Sci.* 362(1822), 1987–2001.
- Camacho, R., and Yen, B. C. (1991). "Nonlinear resistance relationships for alluvial channels." *Channel flow resistance: centennial of Manning's formula*, B. C. Yen, ed., pp. 186–194, Water Resources Publications, Highlands Ranch, Colorado.
- Cao, Z. (1999). "Equilibrium near-bed concentration of suspended sediment." *Journal of Hydraulic Engineering, ASCE*, 125 (12), 1270–1278.
- Carling, P. A. (1999). "Subaqueous gravel dunes." *Journal of Sedimentary Research*, 69, 534–545.
- Carling, P. A., Kelsey, A., and Glaister, M. S. (1992). "Effect of bed roughness, particle shape, and orientation on initial motion criteria." In: *Dynamics of Gravel-Bed Rivers*, P. Billi, R. D. Hey, C. R. Thorne, and P. Tacconi, eds., John Wiley & Sons, Chichester, United Kingdom, 23–37.
- Carling, P. A., Götz, E., Orr, H. G., and Radecki-Pawlik, A. (2000a). "The morphodynamics of fluvial sand dunes in the River Rhine near Mainz, Germany, Part I: sedimentology and morphology." *Sedimentology*, 47, 227–252.
- Carling, P. A., Williams, J. J., Götz, E., and Kelsey, A. D. (2000b). "The morphodynamics of fluvial sand dunes in the River Rhine near Mainz, Germany, Part II: hydrodynamics and sediment transport." *Sedimentology*, 47, 253–278.
- Celik, I., and Rodi, W. (1988). "Modeling Suspended Sediment Transport in Nonequilibrium Situations." *Journal of Hydraulic Engineering, ASCE*, 114(10), 1157–1191.
- Celik, I., and Rodi, W. (1984). "A deposition-entrainment model for suspended sediment transport." Report SFB 210/T/6, University of Karlsruhe, Germany.
- Cellino, M., and Graf, W. H. (2000). "Experiments on suspension flow in open channels with bed forms." *Journal of Hydraulic Research, IAHR*, 38(4), 289–298.
- Chaubert, J., and Chauvin, J. L. (1963). "Formation des Dunes et des Rides dans les Modèles Fluviaux." *Bulletin du Centre de Recherches et d'Essais de Chaton*, 4.
- Chen, H. Y., and Nordin, Jr., C. F. (1976). "Missouri River: Temperature effects in the transition from dunes to plane bed." *Missouri River Sediment Series Rep. 14*, U. S. Army Corps of Engineers, Omaha, Nebraska.
- Chen, C. L. (1991). "Unified theory on power laws for flow resistance." *Journal of Hydraulic Engineering, ASCE*, 117(3), 371–389.
- Cheng, N. S. (1997). "A simplified settling velocity formula for sediment particle." *Journal of Hydraulic Engineering, ASCE*, 123(2), 149–152.
- Cheng, N. S., and Chiew, Y. (1998). "Pickup probability for sediment entrainment." *Journal of Hydraulic Engineering, ASCE*, 124(2), 232–235.
- Cheng, N. S., and Chiew, Y. (1999). "Incipient sediment motion with upward seepage." *Journal of Hydraulic Research, IAHR*, 37(5), 665–681.
- Cheng, N. S. (2002). "Exponential formula for bedload transport." *Journal of Hydraulic Engineering, ASCE*, 128 (102), 942–946.
- Chien, N., and Wan, Z. (1999). *Mechanics of Sediment Transport*, ASCE Press, Reston, Virginia.
- Chiew, Y., and Parker, G. (1994). "Incipient sediment motion on nonhorizontal slopes." *Journal of Hydraulic Research, IAHR*, 32(5), 649–660.
- Choi, S. U., and García, M. H. (1995). "Modeling of One-Dimensional Turbidity Currents with a Dissipative-Galerkin Finite Element Method." *Journal of Hydraulic Research, IAHR*, 33:5: 623–648.
- Choi, S-U., and Garcia, M. H. (2001). "Spreading of gravity plumes on an incline." *Coastal Engineering*, 43, 221–237.
- Chollet, J. P., and Cunge, J. A. (1979). "New interpretation of some head loss-flow velocity relationships for deformable movable beds." *Journal of Hydraulic Research, IAHR*, 17(1), 1–13.
- Chollet, J. P., and Cunge, J. A. (1980). "Simulation of unsteady flow in alluvial streams." *Applied Mathematical Modeling*, 4(8).
- Chow, V. T. (1959). *Open Channel Hydraulics*, McGraw-Hill, New York.
- Christensen, B. A. (1972). "Incipient motion on cohesionless channel banks." *Sedimentation, Chapter 4*, H. W. Shen, ed., Water Resources Publications, Littleton, Colorado.
- Christofferson, J. B., and Jonsson, I. G., (1985). "Bed friction and dissipation in a combined current and wave motion." *Ocean Engineering*, 12, 387–423.
- Colby, B. R. (1957). "Relationship of unmeasured sediment discharge to mean velocity." *Transactions American Geophysical Union*, 38(5), 708–717.

- Coleman, N. L. (1967). "A theoretical and experimental study of drag and lift forces acting on a sphere resting on a hypothetical stream bed." *Proceedings of the Twelfth Congress, International Association for Hydraulic Research*, Fort Collins Colorado, 185–192.
- Coleman, N. L. (1969). "A new examination of sediment suspension in open channels." *Journal of Hydraulic Research, IAHR*, 7(1), 67–82.
- Coleman, N. L. (1970). "Flume studies of the sediment transfer coefficient," *Water Resources Research*, AGU, 6, 801–809.
- Coleman, N. L. (1981). "Velocity profiles with suspended sediment." *Journal of Hydraulic Research, IAHR*, 19, 211–229.
- Coleman, N. L. (1986). "Effects of suspended sediment on the open-channel velocity distribution." *Water Resources Research*, 22, 1377–1384.
- Coleman, N. L., and Alonso, C. V. (1983). "Two-dimensional channel flows over rough surfaces." *Journal of Hydraulic Engineering, ASCE*, 109(?), 175–188.
- Coleman, S. E., and Melville, B. W. (1994). "Bed-form development." *Journal of Hydraulic Engineering, ASCE*, 120(4), 544–560.
- Coleman, S. E., and Melville, B. W. (1996). "Initiation of bed forms on a flat bed." *Journal of Hydraulic Engineering, ASCE*, 122(6), 301–310.
- Coleman, S. E., Fedele, J. J., and García, M. H. (2003). "Closed-conduit bed-form initiation and development." *Journal of Hydraulic Engineering, ASCE*, 129(12), 956–965.
- Coleman, S. E., and Eling, B. (2000). "Sand wavelets in laminar open-channel flows." *Journal of Hydraulic Research, IAHR*, 38(?), 331–338.
- Coleman, S. E., and Fenton, J. D. (2000). "Potential flow instability theory and alluvial stream bed forms." *Journal of Fluid Mechanics*, 418, 101–117.
- Coles, D. F. (1956). "The law of the wake in turbulent boundary layer." *Journal of Fluid Mechanics*, 1, 191–226.
- Colombini, M., Seminara, G., and Tubino, M. (1987). "Finite amplitude alternate bars." *Journal of Fluid Mechanics*, 181, 213–232.
- Colombini, M., Tubino, M. and Whiting, P. (1992). Topographic expression of bars in meandering channels. In *Dynamics of gravel-bed rivers*, P. Billi, R. D. Hey, C. R. Thorne, and P. Tacconi (eds). John Wiley & Sons Ltd.
- Colosimo, C., Copertino, V. A., and Veltri, M. (1986). "Average velocity estimation in gravel-bed rivers." *Procs. 5th IAHR-APD Congress*, Seoul, South Korea, Vol. 2, 1–15.
- Cruickshank, C., and Maza, J. A. (1973). "Flow resistance in sand bed channels." *International Symposium on River Mechanics, IAHR*, Bangkok, Thailand, A30:1–9.
- Dade, W. B., Nowell, A.R.M., and Jumars, P. A. (1992). "Predicting erosion resistance of muds." *Marine Geology*, 105, 285–297.
- Dade, W. B., Hogg, A. J., and Boudreau, B. P. (2001). "Physics of flow above the sediment-water interface." In *The benthic boundary layer: transport processes and biogeochemistry*, B. P. Boudreau and B. B. Jørgensen, eds., Oxford University Press, Oxford.
- Damgaard, J. S., Whitehouse, R.J.S., and Soulsby, R. L. (1997). "Bed-load sediment transport on steep longitudinal slopes, *Journal of Hydraulic Engineering, ASCE*, 123(12), 1130–1138.
- Damgaard, J. S., Soulsby, R. L., Peet, A., and Wright, S. (2003). "Sand transport on steeply sloping plane and rippled beds." *Journal of Hydraulic Engineering, ASCE*, 129(9), 706–719.
- Dancey, C. L., Diplas, P., Papanicolau, A., and Bala, M. (2002). "Probability of individual grain movement and threshold condition." *Journal of Hydraulic Engineering, ASCE*, 128(12), 1069–1075.
- De Cesare, G., Schleiss, A., and Hermann, F. (2001). "Impact of turbidity currents on reservoir sedimentation." *Journal of Hydraulic Engineering, ASCE*, 127(1), 6–16.
- De Vries, M. (1993). "Use of models for river problems." *Studies and reports in hydrology 51*, International Hydrological Programme (IHP-IV), UNESCO Publishing, Paris.
- Dey S. (1999). "Sediment threshold." *Applied Mathematical Modelling*, 23(5), 399–417.
- Dey S. (2003). "Threshold of sediment motion on combined transverse and longitudinal sloping beds." *Journal of Hydraulic Research, IAHR*, 41(4), 405–415.
- Dey S., Sarker, H. K., and Debnath, K. (1999). "Sediment threshold under stream flow on horizontal and sloping beds." *Journal of Engineering Mechanics, ASCE*, 125(5), 545–553
- Dey S., and Debnath, K. (2000). "Influence of stream-wise bed slope on sediment threshold under stream flow." *Journal of Irrigation and Drainage Engineering, ASCE*, 126(4), 255–263.
- Dey S., and Zanke U.C.E. (2004). "Sediment threshold with upward seepage." *Journal of Engineering Mechanics, ASCE*, 130(9), 1118–1123.
- Dietrich, W. E. (1982). "Settling Velocities of Natural Particles." *Water Resources Research*, 18(6), 1615–1626.
- Dietrich, W. E., and Whiting, P. J. (1989). "Boundary shear stress and sediment transport in river meanders of sand and gravel." *River Meandering*, S. Ikeda, and G. Parker, eds., pp. 1–50, American Geophysical Union Water Resources Monograph 12, Washington D.C.
- Dietrich, W. E. and Gallinatti, J. (1991). "Fluvial geomorphology." *Field Experiments and Measurement Programs in Geomorphology*. O. Slaymaker, ed., A. A. Balkema, Rotterdam, 169–229.
- Dinehart, R. L. (1989). "Dune migration in a steep, coarse-bedded stream." *Water Resources Research*, 25(5), 911–923.
- Dinehart, R. L. (1992). "Evolution of coarse gravel bed forms: field measurements at flood stage." *Water Resources Research*, 28, 2667–2689.
- Dinehart, R. L., Burau, J. R. (2005). "Repeated surveys by acoustic Doppler current profiler for flow and sediment dynamics in a tidal river." *Journal of Hydrology*, v. 314, iss. 1–4, 1–21.
- Diplas, P., and Vigilar, G. (1992). "Hydraulic geometry of threshold channels." *Journal of Hydraulic Engineering, ASCE*, 118(4), 597–614.
- Diplas, P., and Sutherland, A. J. (1988). "Sampling techniques for gravel sized sediments." *Journal of Hydraulic Engineering, ASCE*, 114(5), 484–501.
- Dooge, J.C.I. (1991). "The Manning formula in context." *Channel Flow Resistance: Centennial of Manning's Formula.*, B. C. Yen, ed., 136–185, Water Resource Publications, Highland Ranch, Colorado.
- Drake, T. G., and Calantoni, J. (2001). "Discrete particle model for sheet flow sediment transport in the nearshore." *Journal of Geophysical Research-Oceans*, 106(C9), 19859–19868.

- Drake, T. G., Shreve, R. L., Dietrich, W. E., Whiting, P. J., and Leopold, L. B. (1988). "Bedload transport of fine gravel observed by motion-picture photography." *Journal of Fluid Mechanics*, 192, 193–217.
- Duan, J. G., Wang, S.S.Y., and Jia, Y. (2001). "The applications of the enhanced CCHE2D model to study the alluvial channel migration processes." *Journal of Hydraulic Research, IAHR*, 39(5), 469–480.
- Duan, J. G., and Julien, P. Y. (2005). "Numerical simulation of the inception of channel meandering." *Earth Surface Processes and Landforms*, 30, 1093–1110.
- Dyer, K. R. (1986). *Coastal and estuarine sediment dynamics*. John Wiley and Sons Limited, London, UK.
- Egiazaroff, L. V. (1965). "Calculation of Non-Uniform Sediment Concentration." *Journal of the Hydraulics Division, ASCE*, 91(HY4), 225–248.
- Einstein, H. A. (1942). "Formulas for the transportation of bed load." *Transactions American Society of Civil Engineers*, 117, 561–597.
- Einstein, H. A. (1950). "The Bedload Function for Bedload Transportation in Open Channel Flows." *Technical Bulletin No. 1026*, U.S.D.A., Soil Conservation Service, 1–71.
- Einstein, H. A., and Barbarossa, N. L. (1952). "River Channel Roughness." *Transactions of the American Society of Civil Engineers*, 117, 1121–1146.
- Einstein, H. A., and Chien, N. 1953. "Can the rate of wash load be predicted from the bed-load function?" *Transactions American Geophysical Union*, 34(6), 876–882.
- Einstein, H. A., and Chien, N. (1955). "Effect of Heavy Sediment Concentration Near Bed Motion Velocity and Sediment Distribution." U.S. Army Corps of Engineers, Division Series 8.
- Ellison, T. H. and Turner, J. S. (1959). "Turbulent entrainment in stratified flows." *Journal of Fluid Mechanics*, 6, 423–448.
- Engel, P., and Lau, Y. L. (1980). "Computation of bed load using bathymetric data." *Journal of the Hydraulics Division, ASCE*, 106(3), 639–380.
- Engelund, F. (1966). "Hydraulic Resistance of Alluvial Streams." *Journal of the Hydraulics Division, ASCE*, 92(2), 315–326.
- Engelund, F. (1970). "Instability of Erodible Beds." *Journal of Fluid Mechanics*, 42(2), 225–244.
- Engelund, F. (1974). "Flow and bed topography in channel bends." *Journal of the Hydraulics Division, ASCE*, 100, 1631–1648.
- Engelund, F., and Hansen, E. (1967). "A Monograph on Sediment Transport in Alluvial Streams." Teknisk Vorlag, Copenhagen, Denmark, 1967.
- Engelund, F., and Fredsoe, J. (1976). "A Sediment Transport Model for Straight Alluvial Channels." *Nordic Hydrology*, 7, 293–306.
- Engelund, F., and Fredsøe, J. (1982). "Sediment Ripples and Dunes." *Annual Reviews in Fluid Mechanics*, 14, 13–37.
- Ettema, R. (2006). "Hunter Rouse—his work in retrospect." *Journal of Hydraulic Engineering, ASCE*, 132(12), 1248–1258.
- Exner, F. M. (1920). "Zur Physik der Dunen." *Sitzber. Akad. Wiss Wien*, Part IIa, Bd. 129 (in German).
- Exner, F. M. (1925). "Über die Wechselwirkung zwischen Wasser und Geschiebe in Flüssen." *Sitzber. Akad. Wiss Wien*, Part IIa, Bd. 134 (in German).
- Falcon, M. A., and Kennedy, J. F. (1983). "Flow in alluvial-river curves." *Journal of Fluid Mechanics*, 133, 1–16.
- Fan, J. (1986). "Turbid density currents in reservoirs" *Water International, IWRA*, 11:33, 107–116.
- Fan, J., and Morris, G. L. (1992). "Reservoir sedimentation I: delta and density current deposits." *Journal of Hydraulic Engineering, ASCE*, 118(3), 354–369.
- Fan, J., and Morris, G. L. (1992). "Reservoir sedimentation II: reservoir desiltation and long-term storage capacity." *Journal of Hydraulic Engineering, ASCE*, 118(3), 370–384.
- Fedele, J. J. (1995). "Dune velocity in sand bed rivers." *XXVI International Association for Hydraulic Research Congress (IAHR)*, John F. Kennedy Student Paper Competition, London, U.K., 37–42.
- Fedele, J. J., and García, M. H. (2001). "Hydraulic roughness in alluvial streams: a boundary layer approach." *Riverine, Coastal, and Estuarine Morphodynamics*, G. Seminara and P. Blondeaux, eds., Springer-Verlag, Berlin, 37–60.
- Fenton, J., and Abbot, J. E. (1977). "Initial Movement of Grains on a Stream Bed: The Effect of Relative Protrusions," *Proceeding of the Royal Society of London, Series A-352*, 523–537.
- Fernandez Luque, R., and van Beek, R. (1976). "Erosion and Transport of Bed Sediment." *Journal of Hydraulic Research, IAHR*, 14(2), 127–144.
- Fernandez, R. L., and Imberger, J. (2006). "Bed roughness induced entrainment in a high Richardson number underflow." *Journal of Hydraulic Research*, 44 (6), 725–738.
- Fernandez, R., Best, J., and Lopez, F. (2006). "Mean flow, turbulence structure, and bed form superimposition across the ripple-dune transition." *Water Recourses Research*, 42, W05406, doi:10.1029/2005WR004330.
- Fisher, J. S., Sill, B. L., and Clark, D. F. (1983). "Organic detritus particles: initiation of motion criteria in sand and gravel beds," *Water Research*, 19(6), 1627–1637.
- Flemming, B. W. (2000). "The role of grain size, water depth and flow velocity as scaling factors controlling the size of subaqueous dunes." *Proceedings of Marine Sandwave Dynamics*, A. Trentesaux and T. Garlan, eds., Lille, France, 23–24.
- Fredsøe, J. (1974). "On the development of dunes in erodible channels." *Journal of Fluid Mechanics*, 64, 1–16.
- Fredsøe, J. (1982). "Shape and dimensions of stationary dunes in rivers." *Journal of the Hydraulics Division, ASCE*, 108(8), 932–947.
- Fredsøe, J. (1989). "Computation of small scale river morphology and stage-discharge curves in alluvial streams." *Third International Symposium on alluvial River Problems*, University of Roorke, India, Balkema, Rotterdam, 83–94.
- Fredsøe, J. (1996). "The stability of a sandy river." *Issues and Directions in Hydraulics*, T. Nakato and R. Ettema, eds., Balkema, Rotterdam, 99–113.
- Fredsøe, J., and R. Deigaard (1992). *Mechanics of Coastal Sediment Transport*. World Scientific.
- French, R. H. (1987). *Hydraulic processes on alluvial fans*, Elsevier Science, Amsterdam.
- Fuentes, R. and Carrasquel, S. (1981). Discussion of "Re-examination of Nikuradse roughness data by W. R. Brownlie." *Journal of the Hydraulics Division, ASCE*, 107(11), 1573–1575.
- Fukushima, Y., Parker, G., and Pantin, H. M. (1985). "Prediction of ignitive turbidity currents in Scripps Submarine Canyon." *Marine Geology* 67, 55–81.
- Gabel, S. L. (1993). "Geometry and kinematics of dunes during steady and unsteady flows in the Calamos River, Nebraska, USA." *Sedimentology*, 40, 237–269.
- Garcia, M. H., and Parker, G. (1989). "Experiments on Hydraulic Jumps in Turbidity Currents Near a Canyon-Fan Transition." *Science*, 117(4), 393–396.

- García, M. H., and Parker, G. (1991). "Entrainment of Bed Sediment into Suspension." *Journal of Hydraulic Engineering, ASCE*, 117(4), 414–435.
- García, M. H. (1992). "Turbidity Currents." *Encyclopedia of Earth System Science*, Vol. 4, edited by W. A. Nieremberg, Academic Press Inc., 399–408.
- García, M. H. (1993). "Hydraulic Jumps in Sediment-laden Bottom Currents." *Journal of Hydraulic Engineering, ASCE*, 119(6), 1094–1117.
- García, M. H., and Parker, G. (1993). "Experiments on the Entrainment of Sediment into Suspension by a Dense Bottom Current", *Journal of Geophysical Research (oceans)*, AGU, 98(C3), 4793–4807.
- García, M. H. (1994). "Depositional Turbidity Currents Laden with Poorly-Sorted Sediment." *Journal of Hydraulic Engineering, ASCE*, 120(110), 1240–1263.
- García, M. H., and Y. Niño. (1993). "Dynamics of sediment bars in straight and meandering channels: experiments on the resonance phenomenon." *Journal of Hydraulic Research, IAHR*, 31(6), 739–761.
- García, M. H., Niño, Y., and Lopez, F. (1996). "Laboratory Observations of Particle Entrainment Into Suspension by Turbulent Bursting" *Coherent Flow Structures In Open Channels: Origins Scales, and Interaction with Sediment Transport and Bed Morphology*, Edited by Ashworth, P., Bennetts, S., Best, T., and McLellan, S., John Wiley & Sons, Ltd., Chapter 3, 63–86.
- García, M. H., Admiraal, D. M., and Rodriguez, J. F. (1999). "Laboratory Experiments on Navigation-Induced Bed Shear Stresses and Sediment Resuspension." *International Journal of Sediment Research*, 14(2), 303–317.
- García, M. H. (1999). "Sedimentation and Erosion Hydraulics." *Hydraulic Design Handbook*, Chapter 6, Larry Mays, ed., McGraw-Hill, Inc.
- García, M. H. (2000). Discussion of "The Legend of A. F. Shields," *Journal of Hydraulic Engineering, ASCE*, 126(9), 718–720.
- García, M. H. (2001). "Modeling Sediment Entrainment into Suspension, Transport, and Deposition in Rivers." *Model Validation in Hydrologic Science*, Paul Bates and Malcolm Anderson, eds., Wiley and Sons, Chichester, U.K.
- García-Flores, M., and Maza-Alvarez, J. A. (1997). "Inicio de movimiento y acorazamiento." Capítulo 8 del Manual de Ingeniería de Ríos, *Serie del Instituto de Ingeniería* 592, UNAM, Mexico (in Spanish).
- Gelfenbaum, G., and Smith, J. D. (1986). "Experimental evaluation of a generalized suspended-sediment transport theory." *Sedimentology of Shelf Sands and Sandstones*, R. J. Knight, and J. R. McLean, eds., Canadian Society of Petroleum Geologists, Memoir II, 133–144.
- Gessler, J. (1970). "Self-Stabilizing Tendencies of Sediment Mixtures with Large Range of Grain Sizes." *Journal of Waterway and Harbor Division, ASCE*, 96(2), 235–249.
- Gessler, J. (1971). "Beginning and Ceasing of Sediment Motion." Ch. 7 in *River Mechanics*, H. W. Shen, ed., Water Resources Publications, Littleton, CO.
- Gilbert, G. K. (1914). "The transportation of debris by running water." *U.S. Geological Survey Professional Paper 86*, 263 p.
- Giri, S., and Shimizu, Y. (2006). "Numerical computation of sand dune migration with free surface flow." *Water Resources Research*, 42, W10422, doi:10.1029/2005WR004588.
- Gladki, H. (1979). "Resistance to flow in alluvial channels with coarse bed materials." *Journal of Hydraulic Research, IAHR*, 17(2), 121–128.
- Glover, R. E., and Florey, Q. L. (1951). "Stable Channel Profiles." U.S. Bureau of Reclamation, Hydraulics, 325.
- Gomez, B. and Church, M. (1989). "An assessment of bed load sediment transport formulae for gravel bed rivers." *Water Resources Research*, 25, 1161–1186.
- Gradowczyk, M. H. (1968). "Wave propagation and boundary instability in erodible-bed channels." *Journal of Fluid Mechanics*, 33, 93–112.
- Graf, W. H., and Cellino, M. (2002). "Suspension flows in open channels: experimental study." *Journal of Hydraulic Research, IAHR*, 40(4), 435–447.
- Graf, W. H., and Pazis, G. C. (1977). "Les phenomenes de dépôt et d'érosion dans un canal alluvionnaire." *Journal of Hydraulic Research, IAHR*, 15, 151–165.
- Graf, W. H., and Suszka, L. (1987). "Sediment transport in steep channels." *Journal of Hydroscience and Hydraulic Engineering, JSCE*, 5(1), 11–26.
- Graf, W. H. (1984). *Hydraulics of Sediment Transport*, Water Resources Publications, Highlands Ranch, Colorado.
- Graf, W., Whitehouse, R.J.S., Soulsby, R. I., and Damgaard, J. S. (2000). "Inception of Sediment Transport on Steep Slopes." *Journal of Hydraulic Engineering, ASCE*, 126(7), 553–555.
- Grass, A. J. (1970). "The initial instability of fine sand." *Journal of the Hydraulics Division, ASCE*, 96(3), 619–632.
- Greimann, B. P., and Holly, F. M. (2001). "Two-phase flow analysis of concentration profiles." *Journal of Hydraulic engineering, ASCE*, 127(9), 753–762.
- Griffiths, G. A. (1981). "Flow resistance in coarse gravel-bed rivers." *Journal of the Hydraulics Division, ASCE*, 107(7), 899–918.
- Grover, N., and Howard, C. (1938). "The passage of turbid water through lake Mead." *Transactions of the ASCE*, 103, 720–790.
- Guo, J. and Wood, W. L. (1995). "Fine suspended sediment transport rates." *Journal of Hydraulic Engineering, ASCE*, 121(12), 919–922.
- Guo, J. (2002). "Logarithmic matching and its application in computational hydraulics and sediment transport." *Journal of Hydraulic Research, IAHR*, 40(5), 555–565.
- Guo, J., and Julien, P. Y. (2004). "Efficient algorithm for computing Einstein Integrals." *Journal of Hydraulic Engineering, ASCE*, 130(12) 1198–1201.
- Guy, H. P., Simons, D. B. and Richardson, E. V. (1966). "Summary of alluvial channel data from flume experiments." Professional Paper 462-I, 1956–1961, U.S. Geological Survey.
- Gyr, A. and Kinzelbach, W. (2004). "Bed forms in turbulent channel flow." *Applied Mechanics Reviews*, 57, 77–93.
- Hager, W., and Del Giudice, G. (2001). Discussion of "Movable Bed Roughness in Alluvial Rivers." *Journal of Hydraulic Engineering, ASCE*, 127(7), 627–629.
- Hammond, F.D.C., Heathershaw, A. D., and Langhorne, D. N. (1984). "A comparison between Shields' threshold criterion and the movement of loosely packed gravel in a tidal channel." *Sedimentology*, 31, 51–62.
- Hanes, D. M. (1986). "Grain flows and bed-load sediment transport—review and extension." *Acta Mechanica*, 63(1–4), 131–142.
- Hanes, D. M., and Bowen, A. J. (1985). "A granular-fluid model for steady intense bed-load transport." *Journal of Geophysical Research-Oceans*, 90(C5), 9149–9158.

- Hanes, D. M., and Inman, D. L. (1985). "Observations of Rapidly Flowing Granular Fluid Materials," *Journal of Fluid Mechanics*, 150, 357–380.
- Haque, M. I., and Mahmood, K. (1985). "Geometry of ripples and dunes." *Journal of the Hydraulic Engineering, ASCE*, 111, 48–63.
- Haque, M. I., and Mahmood, K. (1986). "Analytical study on steepness of ripples and dunes." *Journal of the Hydraulic Engineering, ASCE*, 112(3), 220–236.
- Hasegawa, K., 1981, "Research on an equation of bank erosion considering non-equilibrium conditions, *Proceedings Japan Society of Civil Engineering*, 316(12), 37–50.
- Hasegawa, K. (1989). "Universal bank erosion coefficient for meandering rivers." *Journal of Hydraulic Engineering, ASCE*, 115(6), 744–765.
- Havinga, H. (1983). "Discussion of 'Bed load discharge coefficient.'" *Journal of the Hydraulics Division, ASCE*, 109, 157–160.
- Hayashi, T. (1970). "Formation of dunes and antidunes in open channels." *Journal of the Hydraulic Division, ASCE*, 96, 357–366.
- Henderson, F. M. (1966). *Open Channel Flow*, Macmillan, New York.
- Hey, R. D. (1979). "Flow resistance in gravel-bed rivers." *Journal of the Hydraulics Division, ASCE*, 105, 365–379.
- Hill, P. S., and McCave, I. N. (2001). "Suspended particle transport in benthic boundary layers." *The benthic boundary layer: transport processes and biogeochemistry*, B. P. Boudreau and B. B. Jørgensen, eds., Oxford University Press, Oxford.
- Hirano, M. (1973). "River-bed variation with bank erosion." *Proceedings Japan Society of Civil Engineering*, 210, 13–20 (in Japanese).
- Holmes, Jr., R. R. (2003). "Vertical Velocity Distributions in Sand-Bed Alluvial Rivers." Ph.D. Dissertation, Department of Civil and Environmental Engineering, University of Illinois at Urbana-Champaign, Urbana, Illinois, 325 pp.
- Hotchkiss, R. H. and Parker, G. (1991). "Shock fitting of aggradational profiles due to backwater." *Journal of Hydraulic Engineering*, 117(9), 112–91144.
- Howard, A. D. (1977). "Effect of Slope on the Threshold of Motion and Its Application to Orientation of Wind Ripples", *Bull. Geol. Soc. Am.*, 88, 853–856.
- Huang, X., and García, M. H. (2000). "Pollution of gravel spawning grounds by deposition of suspended sediment." *Journal of Environmental Engineering, ASCE*, 126(10), 963–967.
- Hulscher, S.J.M.H., and Dohmen-Jansen, C. M. (2005). "Introduction to special section on marine sand wave and river dune dynamics." *Journal of Geophysical Research*, 110, F04S01, DOI 10.1029/2005JF000404.
- Ikeda, H. (1983). "Experiments on bedload transport, bedforms, and sedimentary structures using fine gravel in the 4-meter wide flume." *Paper No. 2* University of Tsukuba, Japan, Environmental Research Center.
- Ikeda, S. (1982). "Incipient Motion of Sand Particles on Side Slopes," *Journal of the Hydraulics Division, ASCE*, 108 (1), 95–114.
- Ikeda, S. (1984). "Prediction of alternate bar wavelength and height." *Journal of Hydraulic Engineering, ASCE*, 110, 317–386.
- Ikeda, S., and Asaeda, T. (1983). "Sediment suspension with rippled bed." *Journal of Hydraulic Engineering, ASCE*, 109, 409–423.
- Ikeda, S., and Nishimura, T. (1986). "Flow and bed profile in meandering sand-silt rivers." *Journal of the Hydraulics Division, ASCE*, 112, 562–579.
- Ikeda, S., and Parker, G. (1989). "River Meandering." *Water Resources Monograph 12*, American Geophysical Union, Washington D. C.
- Imran, J., Parker, G., and Katopodes, N. (1998). "A numerical model of channel inception on submarine fans." *Journal of Geophysical Research*, 103(C1), 1219–1238.
- Irmay, S. (1949). "On steady flow formulae in pipes and channels." *Proceedings 3rd Congress, International Association for Hydraulic Research*, Paper III-3, Grenoble, France.
- Itakura, T., and Kishi, T. (1980). "Open channel flow with suspended sediments." *Journal of the Hydraulics Division, ASCE*, 106(8), 1325–1343.
- Iversen, J. D., and Rasmussen, K. R. (1994). "The effect of surface slope on saltation threshold." *Sedimentology*, 41:721–728.
- Iwagaki, Y. (1956). Fundamental study on critical tractive force." *Proceedings, Japan Society of Civil Engineering*, 41, 1–21.
- Jackson, R. G. (1976). Sedimentological and fluid dynamics implications of the turbulent bursting phenomenon in geophysical flows." *Journal of Fluid Mechanics*, 77, 531–560.
- Jaeggi, M.N.R. (1984). "Formation and effects of alternate bars." *Journal of Hydraulic Engineering, ASCE*, 110, 142–156.
- Jain, S. C. and Kennedy, J. F. (1974). "The spectral evolution of sedimentary bed forms." *Journal of Fluid Mechanics*, 63, 301–314.
- James, C. S. (1990). "Prediction of entrainment conditions for nonuniform, noncohesive sediments." *Journal of Hydraulic Research*, 28, 25–41.
- Jang, C. L., and Shimizu, Y. (2005). "Numerical simulation of the behavior of alternate bars with different bank strengths." *Journal of Hydraulic Research, IAHR*, Vol. 43 (6),
- Jansen, P. Ph., van Bendegom, L., van den Berg, J., de Vries, M., and Zanen, A. (1979). "Principles of River Engineering: the non-tidal river." Pitman Publishing Inc.
- Jarrett, R. D. (1984). "Hydraulics of high-gradient streams." *Journal of Hydraulic Engineering, ASCE*, 110, 1519–1539.
- Jenkins, J. T., and Hanes, D. M. (1998). "Collisional sheet flows of sediment driven by a turbulent fluid." *Journal of Fluid Mechanics*, 370, 29–52.
- Jerolmack, D. J., Mohrig, D., and McElroy (2006). "A unified description of ripples and dunes in rivers." *River, Coastal, and Estuarine Morphodynamics*, G. Parker and M. H. Garcia, eds., Taylor & Francis Group, London, 843–851.
- Ji, Z. G., and Mendoza, C. (1997). "Weakly Nonlinear Stability Analysis for Dune Formation." *Journal of Hydraulic Engineering*, 123(11), 979–985.
- Jiang, Z., and Haff, P. K. (1993). "Multiparticle simulation methods applied to the micromechanics of bedload transport." *Water Resources Research*, 29(2), 399–412.
- Jimenez, J. A., and Madsen, O. S. (2003). "A Simple Formula to Estimate Settling Velocity of Natural Sediments." *Journal of Waterways, Port, Coastal, and Ocean Engineering, ASCE*, 129(2), 70–78.
- Johanesson, H. and Parker, G. (1989a). "Secondary flow in mildly sinuous channel." *Journal of Hydraulic Engineering, ASCE*, 115, 289–308.
- Johanesson, H. and Parker, G. (1989b). "Linear theory of river meanders." *River Meandering*, S. Ikeda and G. Parker, eds., *AGU Water Resources Monograph 12*, 181–213.
- Johanesson, H. and Parker, G. (1989c). "Velocity redistribution in meandering rivers." *Journal of Hydraulic Engineering, ASCE*, 115, 1010–1039.
- Julien, P. Y. and Klaassen, G. J. (1995). "Sand-dune geometry of large rivers during floods." *Journal of Hydraulic Engineering, ASCE*, 121, 657–663.

- Julien, P. Y. and Anthony, D. J. (2002). "Bedload motion by size fractions in meander bends." *Journal of Hydraulic Research*, IAHR, 40(2), 125–133.
- Julien, P.Y. (1992). "Study of bed form geometry in large rivers," report Q1386, delft Hydraulics, The Netherlands.
- Julien, P. Y. (1995). *Erosion and Sedimentation*, Cambridge University Press, Cambridge, U.K.
- Julien, P. Y. (2002). *River Mechanics*, Cambridge University Press, Cambridge, U.K.
- Julien, P. Y., Klaassen, G. J., ten Brinke, W.B.M., and Wilbers, A.W.E. (2002). "Case Study: bed resistance of Rhine River during 1988 flood." *Journal of Hydraulic Engineering*, ASCE, 128, 1042–1050.
- Kadota, A., and Nezu, I. (1999). "Three-dimensional structure of space-time correlation on coherent vortices generated behind dune crest." *Journal of Hydraulic Research*, IAHR, 37, 59–80.
- Kamphuis, J. W. (1974). "Determination of sand roughness for fixed beds." *Journal of Hydraulic Research*, 12(2), 193–203.
- Karim, F. (1995). "Bed configuration and flow resistance in alluvial-channel flows." *Journal of Hydraulic Engineering*, ASCE, 121(1), 15–25.
- Karim, F. (1998). "Bed material discharge prediction for nonuniform sediments," *Journal of Hydraulic Engineering*, ASCE, 124(6), 597–604.
- Karim, F. (1999). "Bed-form geometry in sand-bed flows." *Journal of Hydraulic Engineering*, ASCE, 125, 1253–1261.
- Karim, F. and Kennedy, J. F. (1981). "Computer-based predictors for sediment discharge and friction factor of alluvial streams." *Report 242*, Iowa Institute of Hydraulic Research, University of Iowa, Iowa City, Iowa.
- Karim, F., and Kennedy, J. F. (1990). "Menu of coupled velocity and sediment discharge relationships for rivers." *Journal of Hydraulic Engineering*, ASCE, 116(8), 978–996.
- Katul, G., Wiberg, P., Albertson, J., and Hornberger, G. (2002). "A Mixing Layer Theory for Flow Resistance in Shallow Streambeds." *Water Resources Research*, 38(11), 1250–1258.
- Kennedy, J. F. (1961). "Stationary Waves and Antidunes in Alluvial Channels." W. M. Keck Laboratory of Hydraulics and Water Research, California Institute of Technology, Report KH-R-2.
- Kennedy, J. F. (1963). "The mechanics of dunes and antidunes in erodible-bed channels." *Journal of Fluid Mechanics*, 16, 521–544.
- Kennedy, J. F. (1964). "The formation of sediment ripples in closed rectangular conduits and in the desert." *Journal of Geophysical Research*, 69(8), 1517–1524.
- Kennedy, J. F. (1969). "The formation of sediment ripples, dunes and antidunes." *Annual Review of Fluid Mechanics*, 1, 147–168.
- Kennedy, J. F. (1983). "Reflections on Rivers, Research, and Rouse," *Journal of Hydraulic Engineering*, ASCE, 109(10), 1254–1271.
- Kennedy, J. F. (1995). "The Albert Shields Story." *Journal of Hydraulic Engineering*, ASCE, 121, 766–772.
- Kennedy, J. F. and Odgaard, A. J. (1991). "Informal monograph on riverine sand dunes." *Contract Report CERC-91-2*, Coastal Engineering Research Center, US Army Waterways Experiment Station, Vicksburg, Mississippi.
- Kennedy, J. F., and Falcon, M. (1965). "Wave-generated sediment ripples." *Report No. 86*, Hydrodynamics Laboratory, Department of Civil Engineering, Massachusetts Institute of Technology, Cambridge, Mass.
- Kerssens, P.J.M., Prins, A. D., and van Rijn, L. C. (1979). "Model for suspended load transport." *Journal of the Hydraulics Division*, ASCE, 105(5), 461–476.
- Keulegan, G. H. (1978). "An estimate of channel roughness of inter-oceanic canals." Technical Report H-78-13, US Army Engineer Waterways Experiment Station, Vicksburg, Mississippi.
- Keulegan, G. H. (1938). "Laws of turbulent flow in open channels." *Journal National Bureau of Standards*, Research Paper 1151, 21, 707–741, Washington, D.C.
- Kikkawa, H., Ikeda, S., and Kitagawa, A. (1976). "Flow and bed topography in curved open channels." *Journal of the Hydraulic Division*, ASCE, 102(9), 1317–1342.
- Kikkawa, H., and Ishikawa, T. (1978). "Total load of bed materials in open channels." *Journal of the Hydraulic Division*, ASCE, 104(7), 1045–1059.
- Kikkawa, H., and Ishikawa, T. (1979). "Resistance of Flow over dunes and ripples." *Proceedings Japan Society of Civil Engineering*, 281, 53–63 (in Japanese).
- Kinoshita, R., Miwa, H. (1974). "River channel formation which prevents downstream translation of transverse bars." *ShinSabo*, (94), 12–17. (in Japanese)
- Kirchner, J. W., Dietrich, W. E., Iseya, F., and Ikeda, H. (1990). "The variability of critical shear stress, friction angle, and grain protrusion in water-worked sediments." *Sedimentology*, 37, 647–672.
- Kleinhans, M. G. (2001). "The key role of fluvial dunes in transport and deposition of sand-gravel mixtures, a preliminary note." *Sedimentary Geology*, 143, 7–13.
- Kleinhans, M.G. (2002). "Sorting out sand and gravel: sediment transport and deposition in sand-gravel bed rivers." *Netherlands Geogr. Stud.*, 293, 317.
- Kleinhans, M. G. (2004). "Sorting in grain flows at the lee side of dunes." *Earth Science Reviews*, 65, 75–102.
- Knapp, R. T. (1938). "Energy-balance in stream-flows carrying suspended load." *Transactions American Geophysical Union*, Reports and Papers in Hydrology, 501–505.
- Knaapen, M.A.F., Hulscher, S.J.M.H. (2002). "Regeneration of sand waves after dredging." *Coastal Engineering*, 46(4), 277–289.
- Knappen, M.A.F., Hulscher, S.J.M.H., De Vriend, H. J., and Stolk, (2001). "A new type of sea bed waves," *Geophysical Research Letters*, 28, 1323–1326.
- Kobayashi, N., and Seung, N. S. (1985). "Fluid and Sediment Interaction over a Plane Bed." *Journal of Hydraulic Engineering*, ASCE, 111(6), 903–921.
- Komarova, N. L., and Newell, A. C. (2000). "Nonlinear dynamics of sand banks and sand waves." *Journal of Fluid Mechanics*, 415, 285–312.
- Koch, F. G. and Flokstra, C. (1980). "Bed level computations for curved alluvial channels." Proceedings of the XIX Congress of the IAHR, 2, New Delhi, India, 357.
- Komar, P. D., and Li, Z. (1986). "Pivoting analyses of the selective entrainment of sediments by shape and size with application to gravel threshold." *Sedimentology*, 33(3), 425–436.
- Komar, P. D. and Li, Z. (1988). "Applications of grain-pivoting and sliding analyses to selective entrainment of gravel and to allow competence evaluations." *Sedimentology*, 35, 681–695.
- Komar, P. D. (1996). "Entrainment of sediments from deposits of mixed grain sizes and densities." *Advances in Fluvial Dynamics and Stratigraphy*, P. A. Carling, and M. R. Dawson, (eds), Wiley, Chichester, 127–181.
- Kondap, D. M., and Garde, R. J. (1973). "Velocity of bed forms in alluvial channels." *Proceedings of the 15th Congress of*

- International Association for Hydraulic Research*, vol. 5, Istanbul, Turkey.
- Kostaschuk, R. A. (2000). "A field study of turbulence and sediment dynamics over subaqueous dunes with flow separation." *Sedimentology*, 47, 519–531.
- Kostaschuk, R. (2006). "Sediment transport mechanics and subaqueous dune morphology," River, Coastal and Estuarine Morphodynamics: RCEM 2005, G. Parker and M.H. Garcia (eds.), Taylor & Francis Group, London, 795–801.
- Kostaschuk, R. A., Church, M. A. and Luternauer, J. L. (1989). "Bedforms, bed material and bedload transport in a salt-wedge estuary: Fraser River, British Columbia." *Canadian Journal of Earth Sciences*, 26, 1440–1452.
- Kostaschuk, R. A., and Church, M. A. (1993). "Macroturbulence generated by dunes: Fraser River, Canada." *Sedimentary Geology*, 85, 25–37.
- Kostaschuk, R. A., and Ilersich, S. A. (1995) Dune geometry and sediment transport, in *River Geomorphology*, edited by E. J. Hickin, John Wiley & Sons, 19–36.
- Kostaschuk, R. A., and Villard, P. (1996). "Turbulent sand suspension events: Fraser River, Canada." *Coherent Flow Structures in Open Channels*, P. J. Ashworth, S. J. Bennett, J. L. Best, and S. J. McLellan, eds., Wiley & Sons, Chichester, 305–319.
- Kostaschuk, R., Villard, P., and Best, J. L. (2004). "Measuring velocity and shear stress over dunes with acoustic doppler profiler." *Journal of Hydraulic Engineering*, ASCE, 130, 932–936.
- Kostic, S., Parker, G., and Marr, J. G. (2002). "Role of turbidity currents in setting the slope of clinoforms prograding into standing fresh water." *Journal of Sedimentary Research*, 72(3), 353–362.
- Kostic, S., and Parker, G. (2003a). "Progradational sand-mud deltas in lakes and reservoirs. Part 1. Theory and numerical modeling." *Journal of Hydraulic Research*, 41(2) 127–140.
- Kostic, S., and Parker, G. (2003b). "Progradational sand-mud deltas in lakes and reservoirs. Part 2. Experiment and numerical simulation." *Journal of Hydraulic Research*, 41(2), 141–152.
- Kovacs, A. and Parker, G. (1994). "A new vectorial bedload formulation and its application to the time evolution of straight river channels," *Journal of Fluid Mechanics*, 267, 153–183.
- Kuroki, M., and Kishi, T. (1985). "Regime criteria on bars and braids in alluvial straight channels." *Proceedings Japan Society of Civil Engineers*, 342 (in Japanese).
- Lamb, M. P., Hickson, T., Marr, J. G., Sheets, B., Paola, C. and Parker, G. (2004). Surging versus continuous turbidity currents: flow dynamics and deposits in an experimental intraslope minibasin." *Journal of Sedimentary Research*, 74(1), 146–155.
- Lamb, M., Toniolo, H., and Parker, G. (2006). "Trapping of sustained turbidity currents by intraslope minibasins." *Sedimentology*, 53, 147–160.
- Lane, E. W. (1955). "Design of stable channels." *Transactions of the ASCE*, 120, 1234–1260.
- Lane, E. W. (1955). "The Importance of Fluvial Morphology in Hydraulic Engineering," *Proceedings ASCE*, 81 (745).
- Lane, E. W., and Carlson, E. J. (1953). "Some factors affecting the stability of canals constructed in coarse granular materials." *Proceedings, IAHR 5th Congress*, 1–4, 37–48, University of Minnesota, Minneapolis.
- Lanzoni, S. and Tubino, M. (1999). "Grain sorting and bar instability." *Journal of Fluid Mechanics*, 393, 149–174.
- Lanzoni, S. (2000a). "Experiments on bar formation in straight flume. 1. Uniform sediment." *Water Resources Research*, 36, 3337–3349.
- Lanzoni, S. (2000b). "Experiments on bar formation in straight flume. 2. Graded sediment." *Water Resources Research*, 36, 3337–3349.
- Lapointe, M. (1992). "Burst-like sediment suspension events in a sand bed river." *Earth Surface Processes & Landforms*, 17, 253–270.
- Lapointe, M. (1996). "Frequency spectra and intermittency of the turbulent suspension process in a sand-bed river." *Sedimentology*, 43, 439–449.
- Lau, Y. L., and Engel, P. (1999). "Inception of Sediment Transport on Steep Slopes." *Journal of Hydraulic Engineering*, ASCE, 125(5), 544–547.
- Lavelle, J. W., and Mofjeld, H. O. (1987). "Do Critical Stresses for Incipient Motion and Erosion Really Exist?" *Journal of Hydraulic Engineering*, 113(3), 370–385.
- Lebediev, V. V. (1959). "Gidrologia i Gidraulika v Mostovom Doroshnom, Straitielvie," Leningrad (in Russian).
- Lee, H-Y. and Hsu, I-S. (1994). "Investigation of saltating particle motion." *Journal of Hydraulic Engineering*, ASCE, 120, 831–845.
- Lee, H-Y., Chen, Y-H., You, J-Y., and Lin, Y-T. (2000). "Investigations of continuous bed load saltating process." *Journal of Hydraulic Engineering*, ASCE, 126, 691–700.
- Lee, H-Y., Lin, Y-T., You, J-Y., and Wang, H-W. (2006). "On three-dimensional continuous saltation process of sediment particles near the channel bed." *Journal of Hydraulic Research*, IAHR, 44(3), 374–389.
- Leeder, M. R. (1979). "Bedload dynamics: grain impacts, momentum transfer and derivation of a grain Froude number." *Earth Surface Processes and Landforms*, 4, 291–295.
- Leeder, M. R. (1983). "On the interactions between turbulent flow, sediment transport and bedform mechanics in channelized flows." in *Modern and Ancient Fluvial Systems, International Association of Sedimentologists, Special Publication*, J. D. Collinson and J. Lewin, eds., 6, 5–18.
- Leliavsky, S. (1966). *An Introduction to Fluvial Hydraulics*, Dover, New York, 257 p.
- Lemmin, U. and Rolland, T. (1997). "Acoustic velocity profiler for laboratory and field studies." *Journal of Hydraulic Engineering*, ASCE, 123, 1089–1098.
- Leopold, L. B., Wolman, M. G., and Miller, J. P. (1964). "Fluvial processes in geomorphology." W. H. Freeman, San Francisco.
- Li, R. M., Simons, D. B., and Stevens, M. A. (1976). "Morphology of Small Streams in Cobble Watersheds." *Journal of the Hydraulic Division*, 102(8), 1101–1117.
- Limerinos J. T. (1970). "Determination of the Manning coefficient from measured bed roughness in natural channels." *Water Supply Paper 1898-B*, U.S. Geological Survey, Washington D.C.
- Liu, H. D. (1957). "Mechanics of Sediment Ripple Formation," *Proceedings American Society of Civil Engineers*, ASCE, 83 (HY2), 1197–1 to 1197–23.
- Long, C. E., Wiberg, P. L., and Novell, A.R.M. (1993). "Evaluation of Von Kármán's constant from integral flow parameters." *Journal of Hydraulic Engineering*, ASCE, 119, 1182–1190.
- López, F., and García, M. H. (1998). "Open-Channel Flow Through Simulated Vegetation: Suspended Sediment Transport Modeling," *Water Resources Research*, 34(9), 2341–2352.

- López, F. and García, M. H. (2001). "Risk of Sediment Erosion and Suspension in Turbulent Flows." *Journal of Hydraulic Engineering, ASCE*, 127(3), 231–235.
- Lukerchenko, N., Chara, Z., and Vlasak, P. (2006). "2D Numerical model of particle–bed collision in fluid-particle flows over bed." *Journal of Hydraulic Research, IAHR*, 44(1), 70–78.
- Lyn, D. A. (1991). "Resistance in flat-bed sediment-laden flows." *Journal of Hydraulic Engineering, ASCE*, 117, 94–114.
- Lyn, D. A. (1993). "Turbulence measurements in open-channel flows over artificial bedforms." *Journal of Hydraulic Engineering, ASCE*, 119, 306–326.
- Lysne, D. K. (1969). "Movement of sand in tunnels." *Journal of the Hydraulics Division, ASCE*, 95, 1835–1846.
- Maddux, T. B. (2002). "Turbulent open channel flow over fixed three-dimensional dune shapes." Ph.D. Thesis, Univiversity of California, Santa Barbara.
- Maddux, T. B., Nelson, J. M., and McLean, S. R. (2003a). "Turbulent flow over threedimensional dunes: 1. Free surface and flow response." *Journal of Geophysical Research*, 108(F1), 10, 1–10, 19.
- Maddux, T. B., Nelson, J. M., and McLean, S. R. (2003b). "Turbulent flow over three-dimensional dunes: 2. Fluid and bed stresses." *Journal of Geophysical Research*, 108(F1), 11, 1–11, 17.
- Madsen, O. S. (1991). "Mechanics of cohesionless sediment transport in coastal waters." *Coastal Sediments '91*, N. C. Kraus, K. J. Gingerich, and D. L. Kriebel, eds., pp. 15–27, ASCE, New York.
- Mahmood, K. (1971). "Flow in Sand-Bed Channels," *Water Management Technical Report 11*, Colorado State University, Fort Collins, CO.
- Mantz, P. A. (1980). "Semi-empirical correlations for fine and coarse cohesionless sediment transport." *Proceedings Institution of Civil Engineers*, 75(2), 1–33.
- Mantz, P. A. (1977). "Incipient transport of fine grains and flakes by fluids-extended Shields diagram." *Journal of Hydraulic Engineering, ASCE*, 103(6), 601–616.
- Mantz, P. A. (1992). "Cohesionless, fine-sediment bed forms in shallow flows." *Journal of Hydraulic Engineering, ASCE*, 118, 743–764.
- Marchand, J. P., Jarrett, R. D., and Jones, L. L. (1984). "Velocity profile, water-surface slope, and bed-material size for selected streams in Colorado." U.S. Geological Survey Open File Report, 84–733, 82 pp.
- Marsh, N. A., Western, A. W., and Grayson, R. B. (2004). "Comparison of methods for predicting incipient motion for sand beds." *Journal of Hydraulic Engineering, ASCE*, 130(7), 616–621.
- Maynard, S. T. (1991). "Flow resistance of riprap." *Journal of Hydraulic Engineering, ASCE*, 117(6), 687–696.
- Maza-Alvarez, J. A., and Garcia-Flores, M. (1996). "Transporte de Sedimentos." Capítulo 10 del Manual de Ingeniería de Ríos, Series del Instituto de Ingeniería 584, UNAM, Mexico (in Spanish).
- McEwan, I. K., Jefcoate, B. J., and Willetts, B. B. (1999). "The grain-fluid interaction as a self-stabilizing mechanics in fluvial bed load transport." *Sedimentology*, 46, 407–416.
- McLean, S. R. and J. D. Smith, A model for flow over two-dimensional bedforms, *Journal of Hydraulic Engineering, ASCE*, Vol. 112, 300–317, 1986.
- McLean, S. R. (1990). "The stability of ripples and dunes." *Earth-Sciences Review*, 29, 131–144.
- McLean, S. R. (1990). "Depth-integrated suspended-load calculations." *Journal of Hydraulic Engineering, ASCE*, 117(11), 1440–1458.
- McLean, S. R. (1992). "On the calculation of suspended load for non-cohesive sediments." *Journal of Geophysical Research*, 97, 5759–5770.
- McLean, S. R., Nelson, J. M., and Shreve, R. L. (1996). "Flow-sediment interactions in separating flows over bedforms." *Coherent flow structures in open channels*, P. J. Ashworth, S. J. Bennett, J. L. Best and S. J. McLellan, eds., pp. 203–226, John Wiley and Sons, Chichester.
- McLean, S. R., Wolfe, S. R., and Nelson, J. M. (1999). "Predicting boundary shear stress and sediment transport over bed forms." *Journal of Hydraulic Engineering, ASCE*, 125, 725–736.
- McLean, S. R., Nelson, J. M. and Wolfe, S. R. (1994). "Turbulence structure over two-dimensional bed forms: implications for sediment transport." *Journal of Geophysical Research*, 99, 12, 729–747.
- Mehta, A. J., Lee, J., and Christensen, B. A. (1980). "Fall velocity of shells as coastal sediment." *Journal of the Hydraulics Division, ASCE*, 106 (11), 1727–1744.
- Molinás, A. and Wu, B. (2001). "Transport of sediment in large sand-bed rivers." *Journal of Hydraulic Research, IAHR*, 39(2), 135–146.
- Mendoza, C., and Shen, H. W. (1990). "Investigation of turbulent flow over dunes." *Journal of Hydraulic Engineering, ASCE*, 116, 549–477.
- Menduni, G., and Paris, E. (1986). "On the prediction of geometric characteristics of dunes." *Third International Symposium on River Sedimentation*, S. Y. Wang, H. W. Shen, and L. Z. Ding, eds. The University of Mississippi, Mississippi, Mississippi, 665–674.
- Meyer-Peter, E., and Muller, R. (1948). "Formulas for Bedload Transport." *Proceedings of the 2nd Congress, IAHR*, Stockholm, 39–64.
- Milhous, R. T. (1973). "Sediment transport in a gravel-bottomed stream." Ph.D. thesis, Oregon State University, Corvallis.
- Miller, M. C., McCave, I. N., and Komar, P. D. (1977). "Threshold of sediment motion in unidirectional currents." *Sedimentology*, 24, 507–528.
- Miller, R. L., and Byrne, R. J. (1966). "The Angle of repose for a single grain on a fixed rough bed." *Sedimentology*, 6, 303–314.
- Mohrig, D., and Smith, J. D. (1996). "Predicting the migration rates of subaqueous dunes." *Water Resources Research*, 10, 3207–3217.
- Morris, G. L., and Fan, J. (1997). *Reservoir sedimentation handbook*. McGraw-Hill.
- Mostafa, M. G., and McDermid, R. M. (1971). Discussion of "Sediment transportation mechanics: F. hydraulic relations for alluvial streams." by the Task Committee for Preparation of Sedimentation Manual, J. Hydraul. Div., Am. Soc. Civ. Eng., 97(HY10), 1777–1780.
- Murphy, P. J., and Hooshiari, H. (1982). "Saltation in water dynamics." *Journal of the Hydraulics Division*, 108, 1251–1267.
- Muste, M. (2002). "Sources of Bias Errors in Flume Experiments on Suspended-Sediment Transport." *Journal of Hydraulic Research*, 40(6), 695–708.
- Muste, M., and Patel, V. C. (1997). "Velocity profiles for Particles and Liquid in open-channel flow with suspended sediment." *Journal of Hydraulic Engineering, ASCE*, 123 (9), 742–751.

- Nakagawa, H., and Tsujimoto, T. (1980). "Sand bed instability due to bed load motion." *Journal of the Hydraulic Division, ASCE*, 106(12), 2029–2051.
- Nakagawa, H., and Tsujimoto, T. (1984). "Spectral Analysis of Sand Bed Instability." *Journal of Hydraulic Engineering, ASCE*, 110(4), 467–483.
- Nakato, T. (1984). "Numerical integration of Einstein's integrals, I1 and I2." *Journal of Hydraulic Engineering*, 110(12), 1863–1868.
- National Research Council (NRC). (1996). *Alluvial fan flooding*, National Academy Press, Washington, D.C.
- NEDECO (1959). *River studies and recommendations on improvement of Niger and Benue*, North-Holland Publishing Company, Amsterdam, 1000p.
- Neill, C. R. (1968). "Note on Initial Movement of Coarse Uniform Material." *Journal of Hydraulic Research, IAHR*, 6(2), 157–184.
- Neill, C. R. and Yalin, M. S. (1969). "Qualitative definition of beginning of bed movement." *Journal of the Hydraulics Division, ASCE*, 95 (1), 585–587.
- Nelson, J. M., and Smith, J. D. (1989). "Flow in meandering channels with natural topography." *River meandering*, S. Ikeda and G. Parker, eds., Water Resources Monograph No. 12, American Geophysical Union, Washington, D.C., 69–102.
- Nelson, J. M., McLean, S. R., and Wolfe, S. R. (1993). "Mean flow and turbulence fields over two-dimensional bed forms." *Water Resources Research*, 29, 3935–3953.
- Nelson, J. M., Shreve, R. L., McLean, S. R., and Drake, T. G. (1995). "Role of near-bed turbulence structure in bed load transport and bed form mechanics." *Water Resources Research*, 31, 2071–2086.
- Nelson, J. M., Schmeeckle, M. W., Shreve, R. L., and McLean, S. R. (2001). "Sediment entrainment and transport in complex flows." *River, Coastal and Estuarine Morphodynamics*, G. Seminara and P. Blondeaux, eds., Springer, Berlin, 11–35.
- Nemeth, A. A., Hulscher, S.J.M.H. and de Vriend, H. J. (2002). "Modelling sand wave migration in shallow shelf seas," *Continental Shelf Research*, 22 (18-19), 2795–2806.
- Nezu, I., and Nakagawa, H. (1993). *Turbulence in Open-channel Flows*. International Association for Hydraulic Research, Monograph Series, Balkema, Rotterdam, The Netherlands.
- Nezu, I., and Rodi, W. (1986). "Open-channel flow measurements with a laser Doppler anemometer." *Journal of Hydraulic Engineering, ASCE*, 112, 335–355.
- Nielsen, P. (1992). "Coastal Bottom Boundary Layers and Sediment Transport." World Scientific, River Edge, N.J.
- Nikora, V. I., and Goring, D. G. (2000). "Flow turbulence over fixed and weakly mobile gravel beds." *Journal of Hydraulic Engineering, ASCE*, 126, 679–690.
- Nikora, V. I., and Hicks, D. M. (1997). "Scaling relationships for sand wave development in unidirectional flow." *Journal of Hydraulic Engineering, ASCE*, 123(12), 1152–1156.
- Nikora, V., Goring, D., McEwan, I., and Griffiths, G. (2001). "Spatially-averaged open-channel flow over a rough bed." *Journal of Hydraulic Engineering, ASCE*, 127(2), 123–133.
- Nikuradse, J. "Laws of flows in rough pipes." (translation of "Stromungsgesetze in rauhen Rohren." Forsch. Geb. Ingenieurwes., Ausg. Beill., 4, 361, 1933), *National Advisory Committee of Aeronautics Tech Memo 1292*, Washington, D.C., 1950, 62 pp.
- Niño, Y., García, M. H. and Ayala, L. (1994). "Gravel Saltation I: Experiments." *AGU Water Resources Research*, 30(6), 1907–1914.
- Niño, Y., and M. H. García. (1994). "Gravel Saltation II: Modeling." *Water Resources Research, AGU*, 30(6), 1915–1924.
- Niño, Y., and García, M. H. (1996). "Experiments on Particle-Turbulence Interactions in the Near Wall Region of an Open Channel Flow: Implications for Sediment Transport." *Journal of Fluid Mechanics*, 326, 285–319.
- Niño, Y. and García, M. H. (1998a). "On Engelund's Analysis of Turbulent Energy and Suspended Load." *Journal of Engineering Mechanics, ASCE*, 124(4), 480–483.
- Niño, Y. and García, M. H. (1998b). "Using Lagrangian Particle Saltation Observations for Bedload Sediment Transport Modeling." *Hydrological Processes*, 12, 1197–1218.
- Niño, Y. and García, M. H. (1998c). "Experiments on Saltation of Fine Sand." *Journal of Hydraulic Engineering, ASCE*, 124(10), 1014–1025.
- Niño, Y. (2002). "A simple model for the downstream variation of sediment median size in Chilean rivers." *Journal of Hydraulic Engineering, ASCE*, 128(10), 934–941.
- Niño, Y., Atala, A., Barahona, M., and Aracena, D. (2002). "Using a discrete particle model to analyze the development of bedforms." *Journal of Hydraulic Engineering, ASCE*, 128(4), 381–389.
- Niño, Y., Lopez, F., and Garcia, M. (2003). "Threshold for particle entrainment into suspension." *Sedimentology*, 50, 247–263.
- Nnadi, F. N., and Wilson, K. C. (1992). "Motion of contact-load particles at high shear stress." *Journal of Hydraulic Engineering, ASCE*, 118(12), 1670–1684.
- Nordin, C. F., Jr. (1985a). Discussion of "The principle and application of sediment effective power." *Journal of Hydraulic Engineering, ASCE*, 111(6), 1023–1024.
- Nordin, C. F., Jr. (1985b). "Sediment studies of the rio Orinoco." *Third US-Pakistan Binational Symposium on Mechanics of Alluvial Channels*, Lahore, Pakistan.
- Nordin, C. F., Jr., and Perez-Hernandez, D. (1985). "The waters and sediments of the Rio Orinoco and its major tributaries, Venezuela and Colombia." *U.S. Geological Survey Open File Report*, Washington, D.C.
- Novak P., and Cabelka J. (1981). "Models in Hydraulic Engineering," Pitman, London.
- Nowell, A.R.M., and Jumars, P. A. (1984). "Flow environments of aquatic benthos." *Annual Review Ecological Systems*, 15, 303–328.
- National Research Council (1996). *Alluvial fan flooding*, National Academy Press, Washington, D.C.
- O'Brien, M. P. (1933). "Review of the theory of turbulent flow and its relation to sediment transportation." *Transactions of the AGU*, 14, 487–491.
- O'Connor, D. J. (1995). "Inner region of smooth pipes and open channels." *Journal of Hydraulic Engineering, ASCE*, 121, 555–560.
- Ogink, H.J.M. (1988). "Hydraulic roughness of bedforms." *Delft Hydraulics Report M2017*, Delft, The Netherlands.
- Oldenziel, D. M., and Brink, W. E. (1974). "Influence of suction and blowing on entrainment of sand particles." *Journal of the Hydraulic Division, ASCE*, 100(7), 935–949.
- Olesen, K. W., (1987). "Bed topography in shallow river bends," Doctoral Thesis, University of Delft, The Netherlands, 265 p.
- Owen, P. R. (1964). "Saltation of uniform grains in air." *Journal of Fluid Mechanics*, 20(2), 225–242.

- Packman, A. I., and Brooks, N. H. (2001). "Hyporheic exchange of solutes and colloids with moving bed forms." *Water Resources Research*, 37, 2591–2605.
- Packman, A. I., and MacKay, J. S. (2003). "Interplay of stream subsurface exchange, clay particle deposition, and stream bed evolution." *Water Resources Research*, 39, 1097, 10.1029/2002WR001432.
- Packman, A. I., Salehin, M., and Zaramella, M. (2004). "Hyporheic exchange with gravel beds: basic hydrodynamic interactions and bedform-induced advective flows." *Journal of Hydraulic Engineering, ASCE*, 130, 647–656.
- Pacheco-Ceballos, R. (1989). "Transport of sediments: analytical solution." *Journal of Hydraulic Research, IAHR*, 27(4), 501–518.
- Pacheco-Ceballos, R. (1992). "Bed-load coefficients." *Journal of Hydraulic Engineering, ASCE*, 118(10), 1436–1442.
- Paintal, A. S. (1971). "Concept of critical shear stress in loose boundary open channels." *Journal of Hydraulic Research, IAHR*, 9, 91–113.
- Paola, C., and Southard, J. B. (1983). "Autosuspension and the energetics of two-phase flows: reply to comments on "Experimental test of autosuspension,"" *Earth Surface Processes and Landforms*, 8, 273–279.
- Papanicolaou, A. N., Diplas, P., Balakrishnan, M., and Dancey, C. L. (1999). "Computer vision technique for tracking bed load movement." *Journal of Computing in Civil Engineering, ASCE*, 13(2), 71–79.
- Papanicolaou, A., Diplas, P., Dancey, C. L., and Balakrishnan, M. (2001). "Surface roughness effects in near-bed turbulence: Implications to sediment entrainment." *Journal of Engineering Mechanics, ASCE*, 127(3), 211–218.
- Papanicolaou, A., Diplas, P., Evangelopoulos, N., and Fotopoulos, S. (2002). "Stochastic incipient motion criterion for spheres under various packing conditions." *Journal of Hydraulic Engineering, ASCE*, 128(4), 369–380.
- Parker, G. (1975). "Sediment inertia as a cause of river antidunes." *Journal of the Hydraulics Division, ASCE*, 101 (HY2), 211–221.
- Parker, G. (1979). "Hydraulic geometry of active gravel rivers," *Journal of Hydraulic Engineering, ASCE*, 105(9), 1185–1201.
- Parker, G. (1990). "Surface-based bedload transport relation for gravel rivers." *Journal of Hydraulic Research, IAHR*, 28(4), 417–436.
- Parker, G., and Anderson, A. G. (1977). "Basic principles of river hydraulics," *Journal of Hydraulic Engineering, ASCE*, 103 (HY9), 1077–1087.
- Parker, G. (1978). "Self-formed straight rivers with equilibrium banks and mobile bed, Part 2. The gravel river." *Journal of Fluid Mechanics*, 89(1), 127–146.
- Parker, G., and Peterson, A. W. (1980). "Bar resistance of gravel bed rivers." *Journal of the Hydraulic Division, ASCE*, 106, 1559–1575.
- Parker, G. (1982). "Conditions for the ignition of catastrophically erosive turbidity currents." *Marine Geology*, 46, 307–327.
- Parker, G., Klingeman, P. C., and McLean, D. G. (1982). "Bedload and size distribution in paved gravel-bed streams." *Journal of Hydraulic Engineering, ASCE*, 108(4), 544–571.
- Parker, G. (1984). "Discussion of 'Lateral bed load transport on side slopes,'" *Journal of Hydraulic Engineering, ASCE*, 110(2), 197–199.
- Parker, G., and Coleman, N. L. (1986). "Simple model of sediment-laden flows." *Journal of Hydraulic Engineering, ASCE*, 112, 356–375.
- Parker, G., Fukushima, Y., and Pantin, H. M. (1986). "Self-accelerating turbidity currents." *Journal of Fluid Mechanics*, 171, 145–181.
- Parker, G., García, M. H., Fukushima, Y., and Yu, W. (1987). "Experiments on turbidity currents over an erodible bed." *Journal of Hydraulic Research*, 25(1) 123–147.
- Parker, G., Solari, L., and Seminara, G. (2003) "Bedload at low Shields stress on arbitrarily sloping beds: alternative entrainment formulation." *Water Resources Research*, 39(7), 1183, doi:10.1029/2001WR001253.
- Parker, G. (2005). *ID morphodynamics of rivers and turbidity currents*. <[http://cee.uiuc.edu/people/parkerg/morphodynamics\\_e-book.htm](http://cee.uiuc.edu/people/parkerg/morphodynamics_e-book.htm)>.
- Parker, G., and García, M. H. (eds.) (2006). River, coastal and estuarine morphodynamics: RCEM 2005 (Vols. I & II), Taylor & Francis/Balkema, Leiden, The Netherlands.
- Parker, G., and Toniolo, H. (2007). "Note on the analysis of plunging of density flows." *Journal of Hydraulic Engineering, ASCE*, 133(6) 690–694.
- Parsons, D. R., Best, J. L., Hardy, R. J., Kostaschuk, R., Lane, S. N. and Orfeo, O. (2005). "Morphology and flow fields of three-dimensional dunes, Rio Paraná, Argentina: results from simultaneous multibeam echo sounding and acoustic Doppler current profiling." *Journal of Geophysical Research*, 110(F4), F04S04, DOI 10.1029/2004JF000231.
- Pedocchi, F., and García M. H. (2006). "Evaluation of the LISST-ST instrument for suspended particle size distribution and settling velocities." *Continental Shelf Research*, 26, 943–958.
- Posada-García, L. (1995). "Transport of sands in deep rivers." Ph.D. Dissertation, Department of Civil Engineering, Colorado State University, Fort Collins, Colorado.
- Pyle, R., and Novak, P. (1981). "Coefficient of friction in conduits with large roughness." *Journal of Hydraulic Research, IAHR*, 19(2), 119–140.
- Ramonell, C. G., Amsler, M. L., and Toniolo, H. (2002). "Shifting modes of the Paraná River thalweg in its middle/lower reach." *Zeitschrift für Geomorphologie, Supplementbände*, Band 129, 129–142, Berlin-Stuttgart.
- Ranga Raju, K. G. and Soni, J. P. (1976). "Geometry of ripples and dunes in alluvial channels." *Journal of Hydraulic Research, IAHR*, 14, 77–100.
- Ranga-Raju, K. G., Garde, R. J., and Bhardwaj, R. C. (1981). "Total-load transport in alluvial channels," *Journal of the Hydraulics Division, ASCE*, 107(2), 179–191.
- Raudkivi, A. J. (1990). *Loose Boundary Hydraulics*, 3rd ed., Pergamon Press, New York.
- Raudkivi, A. J. (1998). *Loose Boundary Hydraulics*. Balkema, The Netherlands.
- Raudkivi, A. J., and Witte, H-H. (1990). "Development of bed features." *Journal of Hydraulic Engineering, ASCE*, 116, 1063–1079.
- Raudkivi, A. J. (1997). "Ripples on stream bed." *Journal of Hydraulic Engineering, ASCE*, 116, 58–64.
- Reizes, J. A. (1978). "Numerical study of continuous saltation." *Journal of the Hydraulics Division, ASCE*, 104(9), 1303–1321.
- Reynolds, A. J. (1965). "Waves on the Bed of an Erodible Channel," *Journal of Fluid Mechanics*, 22(1), 113–133.

- Reynolds, A. J. (1976). "A decade's investigation of the stability of erodible stream beds." *Nordic Hydrology*, 7, 161–180.
- Rhoads, B. L. and Welford, M. R. (1991). "Initiation of River Meandering." *Progress in Physical Geography*, 15, 127–156.
- Richards, K. J. (1980). "The formation of ripples and dunes on an erodible bed." *Journal of Fluid Mechanics*, 99, 597–618.
- Rickenmann, D. (1991). "Hyperconcentrated flow and sediment transport at steep slopes." *Journal of Hydraulic Engineering, ASCE*, 117(11), 1419–1439.
- Rickenmann, D. (1991). "Bed load transport and hyperconcentrated flow at steep slopes." Bechteler, W., Vogel, G., and Vollmers, H. J. (1991). *Fluvial Hydraulics of Mountain Regions*, A. Armanini and G. Di Silvio, Eds., Lecture Notes in Earth Sciences, Springer-Verlag, Berlin, 429–441.
- Robert, A., and Uhlman, W. (2001). "An experimental study on the ripple-dune transition." *Earth Surface Processes and Landforms*, 26, 615–629.
- Roden, J. E. (1998). *The sedimentology and dynamics of megadunes, Jamuna River, Bangladesh*, Ph.D thesis, Department of Earth Sciences and School of Geography, University of Leeds, Leeds, United Kingdom, 310 pp.
- Rouse, H. (1937). "Modern Conceptions of the Mechanics of Turbulence," *Transactions of the American Society of Civil Engineers*, vol. 102, Paper No. 1965, 463–543.
- Rouse, H. (1938). "Experiments on the mechanics of sediment suspension." *Proceedings, 5th International Congress for Applied Mechanics*, vol. 55, 550–554, John Wiley & Sons, New York.
- Rouse, H. (1939). "An analysis of sediment transportation in the light of fluid turbulence," U.S. Department of Agriculture, Soil Conservation Service, SCS-TR 25, Washington D.C.
- Rubin, D. M., and Hunter, R. S. (1982). "Bedform climbing in theory and nature." *Sedimentology*, 29, 121–138.
- Rutherford, J. C. (1994). *River Mixing*, John Wiley & Sons, New York.
- Sambrook-Smith, G. H., Best, J. L., Bristow, C. S., and Petts, G. E., eds. (2006). Braided Rivers: process, deposits, ecology and management. Special Publication 36, International Association of Sedimentologists (IAS), Blackwell, Malden, MA.
- Sarma, K.V.N., Lakshminarayana, P., Rao, N.S.L. (1983). "Velocity distribution in smooth rectangular channels." *Journal of Hydraulic Engineering, ASCE*, 109, 270–289.
- Sarmiento, O. A., and Falcon, M. A. (2006). "Critical Bed Shear Stress for Unisize Sediment." *Journal of Hydraulic Engineering, ASCE*, 132(2), 172–179.
- Schindler, R. J., and Robert, A. (2004). "Suspended sediment concentration and the ripple-dune transition." *Hydrological Processes*, 18, 3215–3227.
- Schllichting, H. (1979). *Boundary Layer Theory*, 7th Edition, McGraw-Hill, New York.
- Schmeeckle, M. W. and Nelson, J. M. (2003). "Direct numerical simulation of bedload transport using a local, dynamic boundary condition." *Sedimentology*, 50, 279–301.
- Schmeeckle, M. W., Nelson, J. M., Pitlick, J., and Bennett, J. P. (2001). "Interparticle collision of natural sediment grains in water." *Water Resources Research*, 37, 2377–2391.
- Schreider, M. I., and Amsler, M. L. (1992). "Bedform steepness in alluvial streams." *Journal of Hydraulic Research, IAHR*, 30(6), 725–742.
- Schreider, M. I., Scacchi, G., Franco, F., Fuentes, R. y Moreno, C. (2001). "Aplicación del Método de Lischtvan y Levediev al Cálculo de la Erosión General." *Ingeniería Hidráulica en México*, XVI (1), 15–26.
- Schumm, S. A., and Winkley, B. R., eds. (1994). *The variability of large alluvial rivers*, ASCE Press, New York.
- Sechet, P., and Le Guennec, B. (1999). "Bursting phenomenon and incipient motion of solid particles in bed-load transport." *Journal of Hydraulic Research, IAHR*, 37(5), 683–696.
- Sekine, M., and Parker, G. (1992). "Bed-load transport on transverse slope. I." *Journal of Hydraulic Engineering, ASCE*, 118(4), 513–535.
- Sekine, M., and Kikkawa, H. (1992). "Mechanics of saltating grains. II." *Journal of Hydraulic Engineering, ASCE*, 118(4), 536–558.
- Seminara, G., and Tubino, M. (1989). "Alternate bars and meandering: free, forced and mixed interactions." *River meandering*, S. Ikeda and G. Parker, eds., *Water Resources Monograph No. 12*, American Geophysical Union, Washington, D.C., 267–320.
- Seminara, G. (1995). "Effect of grain sorting on the formation of bedforms." *Applied Mechanics Reviews*, 48, 549–563.
- Seminara, G., and Blondeaux, P., eds. (2001). *River, Coastal and Estuarine Morphodynamics*, Springer-Verlag, Berlin.
- Seminara, G., Solari, L., and Parker, G. (2002). "Bed load at low Shields stress on arbitrarily sloping beds: failure of the Bagnold hypothesis." *Water Resources Research*, 38 (11), 1249. doi:10.1029/2001WR000681.
- Serra, S. G., and Vionnet, C. A. (2006). "Migration of large dunes during extreme floods of the Parana River, Argentina." *River, coastal and estuarine morphodynamics: RCEM 2005*, G. Parker and M. H. García, eds., Taylor & Francis/Balkema, Leiden, The Netherlands, 897–901.
- Shen, H. W., and Cheong, H. F. (1977). "Statistical properties of sediment bed profiles." *Journal of the Hydraulics Division*, 103(11), 1303–1321.
- Shen, H. W., and Hung, C. S. (1972). "An engineering approach to total bed material load by regression analysis," *Proceedings of the Sedimentation Symposium to Honor Professor Hans Albert Einstein*, H. W. Shen (ed.), 14–1–14–17.
- Shen, H. W., Mellema, W. J., and Harrison, A. S. (1978). "Temperature and Missouri River stages near Omaha." *Journal of the Hydraulics Division, ASCE*, 104(1), 1–20.
- Shen, H. W., ed. (1972). *Sedimentation: Symposium to honor Prof. H. A. Einstein*. Colorado State University, Fort Collins, CO.
- Shen, H. W. (1990). Movable bed physical models. *NATO Advanced Science Institute Series C-312*, Kluwer Academic Publishers, Boston.
- Shen, H. W., Fehlman, H. M., and Mendoza, C. (1990). "Bed form resistance in open channel flows." *Journal of Hydraulic Engineering, ASCE*, 116(6), 799–815.
- Shields, A., (1936). "Anwendung der Aechichkeits-Mechanik und der Turbulenz Forschung auf die Geschiebewegung' Mitt Preussische," *Versuchsanstalt für Wasserbau und Schiffbau*, Berlin, Germany (translated to English by W. P. ott and J. C. van Uchelen, California Institute of Technology, Pasadena, California).
- Shirazi, M. A., and Seim, W. K. (1981). "Stream system evaluation with emphasis on spawning habitat from salmonids." *Water Resources Research*, 17(3), 592–594.
- Shvidchenko, A. B., and Pender, P. (2000). "Flume study of the effect of relative depth on the incipient motion of coarse uniform sediments." *Water Resources Research*, 36, 619–628.
- Shvidchenko, A. B. and Pender, G. (2001). "Macroturbulence structure of open-channel flow over gravel beds." *Water Resources Research*, 37, 709–719.

- Simons, D. B., and Richardson, E. V. (1961). "Forms of bed roughness in alluvial channels." *Journal of the Hydraulics Division, ASCE*, 87(3), 87–105.
- Simons, D. B., and Richardson, E. V. (1966). "Resistance to flow in alluvial channels." *Professional Paper 422J*, U.S. Geological Survey, Washington, D.C.
- Simons, D. B., and Albertson, M. L. (1963). "Uniform water conveyance channels in alluvial material." *Transactions American Society of Civil Engineers*, vol. 128, part 1.
- Simons, D. B., Richardson, E. V., and Nordin, C. F. (1965a). "Sedimentary structures generated by flow in alluvial channels." *Primary sedimentary structures and their hydrodynamic interpretation*, G. V. Middleton, ed., *SEPM Special Publication 12*:34–53.
- Simons, D. B., Richardson, E. V., and Nordin, C. F. (1965b). "Bedload equation for ripples and dunes." *Professional Paper 462H*, U.S. Geological Survey, Washington, D.C.
- Simons, D., and Senturk, F. (1992). "Sediment transport technology." *Water and sediment dynamics*, Water Resources Publications, Littleton, Colorado.
- Slingerland, R. L. (1977). "The effects of entrainment on the hydraulic equivalence relationships of light and heavy minerals in sand." *Journal of Sedimentary Petrology*, 54, 137–150.
- Sloff, C. J. (1994). "Modelling turbidity currents in reservoirs." *Communications on Hydraulic and Geotechnical Engineering, Report No. 94-5*, Faculty of Civil Engineering, Delft University of Technology, The Netherlands, 141p.
- Smart, G. M. (1984). "Sediment transport formula for steep channels." *Journal of Hydraulic Engineering, ASCE*, 110(3), 267–276.
- Smart, G. M. (1999). "Turbulent Velocity Profiles and Boundary Shear in Gravel Bed Rivers," *Journal of Hydraulic Engineering, ASCE*, 125(2), February 1999, 106–116.
- Smart, G. M., Duncan, M. J., and Walsh, J. M. (2002). "Relatively Rough Flow Resistance Equations". *Journal of Hydraulic Engineering, ASCE*, 128(6), 568–578.
- Smith, J. D. (1970). "Stability of a Sand Bed Subjected to a Shear Flow of Low Froude Number." *Journal of Geophysical Research*, 75(30), 5928–5940.
- Smith, J. D. (1977). "Modeling of sediment transport on continental shelves." *The Sea: ideas and observations on progress in the study of the seas*, E. D. Goldberg, ed., John Wiley and Sons, New York, 538–577.
- Smith, J. D., and McLean S. R. (1977a). "Spatially averaged flow over a wavy surface." *Journal of Geophysical Research*, 83, 1735–1746.
- Smith, J. D., and McLean, S. R. (1977b). "Boundary layer adjustments to bottom topography and suspended sediment." *Bottom Turbulence: Proceedings of the 8th International Liege Colloquium on Ocean Hydrodynamics*, J.C.J. Nihoul, ed., Elsevier Scientific Publishing Company, Liege, Belgium, 112, 123–151.
- Smith, W.O., Vetter, C.P., Cummings, G.B. (1954). "Comprehensive survey of Lake Mead: 1948–1949." *Professional Paper 295*, U.S. Geological Survey, Washington, D.C.
- Song, T. and Graf, W. H. (1994) "Velocity and turbulence distribution in unsteady open-channel," *Journal of Hydraulic Engineering, ASCE*, 120(12), 1385–1400.
- Soulsby, R. L., and Wainright, B. L. (1987). "A criterion for the effect of suspended sediment on near-bottom velocity profiles." *Journal of Hydraulic Research, IAHR*, 25, 341–356.
- Soulsby, R. L. (1997). *Dynamics of marine sands*, Thomas Telford, London, 249 pp.
- Soulsby, R. L. and Whitehouse, R.J.S.W. (1997). "Threshold of sediment motion in coastal environments." *Proceedings Pacific Coasts and Ports '97 Conference*, Christchurch, 1, 149–154, University of Canterbury, New Zealand.
- Southard, J. B., and Mackintosh, M. E. (1981). "Experimental test of autosuspension." *Earth Surface Processes and Landforms*, 6, 103–111.
- Southard, J. B. (1989). "Synthesis of data on bed configurations in alluvial channels, and the effect of water temperature and suspended-load concentration." *Taming the Yellow River: Silt and Floods.*" *Proceedings of a Bilateral Seminar on problems in the Lower Reaches of the Yellow River*, L. M. Brush, M. G. Wolman, and H. Bing-Wei, eds., Kluwer Academic Publishers, Boston, Mass.
- Southard, J. B., and Boguchwal, L. A. (1990). "Bed configurations in steady unidirectional flows. Part 2. Synthesis of flume data." *Journal of Sedimentary Petrology*, 60, 658–679.
- Southard, J. B. (1991). "Experimental determination of bed-form stability." *Annual Review of Earth Sciences*, 19, 423–455.
- Stevens, M. A., and Simons, D. B. (1973). "Flow resistance in the Padma River, Pakistan, IAHR Congress.
- Stevens, M. A., Simons, D. B., and Lewis, G. L. (1976). "Safety factors for riprap protection." *Journal of the Hydraulics Division, ASCE*, 102(5), 637–655.
- Strickler, A. (1923). "Beitrage zur Frage der Geschwindigkeitsformel und der Rauhigkeitszahlen fur Strome, Kanale und geschlossene Leitungen." *Mitteilungen des Eidgenossischen Amtes fur Wasserwirtschaft* 16, Bern, Switzerland (Translated as "Contributions to the question of a velocity formula and roughness data for streams, channels and closed pipelines." by T. Roesgan and W. R. Brownlie, Translation T-10, W. M. Keck Lab of Hydraulics and Water Resources, Calif. Inst. Tech., Pasadena, Calif. January 1981).
- Struiksma, N., Olsen, K. W., Flokstra, C., and De Vriend, H. J. (1985). "Bed deformation in curved alluvial channels." *Journal of Hydraulic Research, IAHR*, 23, 57–78.
- Sukegawa, N. (1973). "Condition for the formation of alternate bars in straight alluvial channels." *International Symposium of River Mechanics, IAHR*, Bangkok, Thailand, A58, 1–11.
- Sukhodolov, A., Fedele, J. J. and Rhoads, B. L. (2004). "Turbulent flow over mobile and molded bedforms: a comparative field study." *River Flow 2004, IAHR*, Napoli, Italy, 317–325.
- Sumer, B. M., and Bakoglu, M. (1984). "On the formation of ripples on an erodible bed." *Journal of Fluid Mechanics*, 144, 177–190.
- Sumer, B. M., and Deigaard, R. (1981). "Particle motions near the bottom in turbulent flow in an open channel. Part 2," *Journal of Fluid Mechanics*, 109, 311–337.
- Sumer, B. M., Kozakiewicz, A., Fredsøe, J., and Deigaard, R. (1996). "Velocity and concentration profiles in sheet-flow layer of movable bed." *Journal of Hydraulic Engineering, ASCE*, 122(10), 549–558.
- Sumer, B. M., Chua, L.H.C., Cheng, N. S., and Fredsøe, J. (2003). "Influence of turbulence on bed load sediment transport." *Journal of Hydraulic Engineering, ASCE*, 129(8), 585–596.
- Suszka, L., and Graf, W. H. (1987). "Sediment transport in steep channels." *Proceedings 23rd Congress of IAHR*, Ottawa, Canada.
- Swamee, P. K., and Ojha, C.S.P. (1991). "Drag coefficient and fall velocity of nonspherical particles." *Journal of Hydraulic Engineering, ASCE*, 117(5), 660–667.

- Swamee, P. K. (1993). "Generalized inner region velocity distribution equation." *Journal of Hydraulic Engineering, ASCE*, 119(5), 651–656.
- Swenson, J. B., Voller, V. R., Paola, C., Parker, G., and Marr, J. (2000). "Fluvio-deltaic sedimentation: a generalized Stefan problem." *European Journal of Applied Mathematics*, 11, 433–452.
- Takahashi, T. (1987). "High velocity flow in steep erodible channels." *Proceedings 22nd IAHR Congress*, Ecole Polytechnique Federale de Lausanne, Lausanne, Switzerland, Technical Session A: 42–53.
- Talmon, A. C., Struiksm, N., and Van Mierlo, M.C.L.M. (1995). "Laboratory measurements of the direction of sediment transport on transverse alluvial-bed slopes." *Journal of Hydraulic Research, IAHR*, 33(4), 495–518.
- Taylor, B. D., and Vanoni, V. A. (1972) "Temperature effects in flat-bed flows." *Journal of Hydraulics Division, ASCE*, 98(8), 1427–1445.
- Ten Brinke, W.B.M., Wilbers, A.W.E., and Wesseling, C. (1999). "Dune growth, decay and migration rates during a large-magnitude flood at a sand and mixed sand-gravel bed in the Dutch Rhine River system." *Special Publication of International Association of Sedimentologists*, 28, 15–32.
- Tjerry, S., and Fredsøe, J. (2005). "Calculation of dune morphology." *Journal of Geophysical Research*, 110, F04013, doi: 10.1029/2004JF000171.
- Thibodeax, L. J., and Boyle, J. D. (1987). "Bedform-generated convective transport in bottom sediment." *Nature*, 325, 341–343.
- Thompson, S. M., and Campbell, P. L. (1979). "Hydraulics of a large channel paved with boulders." *Journal of Hydraulic Research*, 17(4), 341–354.
- Thorne, C. R., MacArthur, R. C., and Bradley, J. B., eds. (1988). *The physics of sediment transport by wind and water*. A collection of hallmark papers by R. A. Bagnold, ASCE, New York.
- Thorne, C. R., and Osman, A. M. (1988). "Riverbank stability analysis. II: applications." *Journal of Hydraulic Engineering, ASCE*, 114(2), 151–172, 1988.
- Thorne, C. R., Bathurst, J. C., and Hey, R. D. eds. (1987). *Sediment transport in gravel-bed rivers*. Wiley, New York.
- Toffaleti, F. B. (1968). "A Procedure for computation of the total river sand discharge and detailed distribution, bed to surface." *Technical Report No. 5*, Committee on Channel Stabilization, U.S. Army Corps of Engineers Waterways Experiment Station, Vicksburg, Mississippi.
- Toffaleti, F. B. (1969). "Definite computations of sand discharges in rivers." *Journal of the Hydraulic Division, ASCE*, 95(1), 225–248.
- Toniolo, H. (2002). "Debris flow and turbidity current deposition in the deep sea and reservoirs." Ph.D Dissertation, University of Minnesota, Minneapolis, Minnesota.
- Toniolo, H., Parker, G., and Voller, V. (2007). "Role of ponded turbidity currents in reservoir trap efficiency." *Journal of Hydraulic Engineering, ASCE*, 133(6) 579–595.
- Toniolo, H., and Schultz, J. (2005). "Experiments on sediment trap efficiency in reservoirs." *Lakes and Reservoirs: Research & Management*, 10(1), 13–24.
- Tsujimoto, T., and Nakagawa, H. (1983). "Stochastic study on successive saltation by flowing water." *Proceedings 2nd International Symposium on River Sedimentation, Beijing, China*, pp. 187–201.
- Tsujimoto, T. (1989). "Longitudinal stripes of sorting due to cellular currents." *Journal of Hydroscience and Hydraulic Engineering*, 7, 23–34.
- Tsujimoto, T. (1991). "Mechanics of Sediment Transport of Graded Materials and Fluvial Sorting," *Report*, Project 01550401, Kanazawa University, Japan, 126 p.
- Tsujimoto, T. (1992). "Fractional transport rate and fluvial sorting." *Proceedings of International Grain Sorting Seminar (Monte Verita, Ascona)*, VAW Mitteilungen 117, ETH, Zurich, Switzerland, 227–249.
- Tubino, M. (1991). "Growth of alternate bars in unsteady flows." *Water Resources Research*, 27, 37–52.
- Tubino, M., and G. Seminara, G. (1990). "Free-forced interactions in developing meanders and suppression of free bars." *Journal of Fluid Mechanics*, 214, 131–159.
- van Bendegom, L. (1947). "Some considerations on river morphology and river improvement," *De Ingenieur*, 59(4), B1-B11 (in Dutch; English translation available as *Translation 1054*, National Research Council of Canada, 1963).
- Van den Berg, J. H., and Van Gelder, A. (1993). "A new bedform stability diagram, with emphasis on the transition of ripples to plane bed in flows over fine sand and silt." *Alluvial sedimentation*, M. Marzo and C. Pudefabregas, eds., International Association of Sedimentologists, Special Publication 17, 11–21.
- Van den Berg, J. H. (1987). "Bedform migration and bed-load transport in some rivers and tidal environments." *Sedimentology*, 34, 681–698.
- Van Mierlo, M.C.L.M., de Ruiter, and J.C.C. (1988). "Turbulence measurements above artificial dunes." *Technical Report TOW A55 Q789*, Delft Hydraulics., Delft, The Netherlands.
- Van Rijn, L. C. (1982). "Equivalent roughness of alluvial bed." *Journal of the Hydraulic Division, ASCE*, 108(10), 1215–1218.
- Van Rijn, L. C. (1984a). "Sediment transport, part I: bed load transport." *Journal of Hydraulic Engineering, ASCE*, 110(10), 1431–1456.
- Van Rijn, L. C. (1984b). "Sediment transport, part II: suspended load transport." *Journal of Hydraulic Engineering, ASCE*, 110(11), 1613–1641.
- Van Rijn, L. C. (1984c). "Sediment transport, part III: Bed forms and alluvial roughness." *Journal of Hydraulic Engineering, ASCE*, 110(12), 1733–1754.
- Van Rijn, L. C. (1986). "Application of sediment pick-up functions." *Journal of Hydraulic Engineering, ASCE*, 112(9).
- Van Rijn, L. C. (1993). *Principles of sediment transport in rivers, estuaries, and coastal areas*. Aqua Publications, Amsterdam, The Netherlands.
- Van Rijn, L. C. (1996). "Combining laboratory, field, and mathematical modeling research for bed forms, hydraulic roughness, and sediment transport during floods." *Issues and Directions in Hydraulics*, T. Nakato and R. Ettema, eds., Balkema, Rotterdam, 55–73.
- Vanoni, V. A. (1946). "Transportation of sediment by water." *Transactions of the AGU*, 3, 67–133.
- Vanoni, V. A., and Brooks, N. H. (1957). "Laboratory studies of the roughness and suspended load of alluvial streams." *Report No. E68, Sedimentation Laboratory*, California Institute of Technology, Pasadena, California.
- Vanoni, V. A. (1964). "Measurements of critical shear stress for entraining fine sediments in a boundary layer." *Report KH-R-7*, W. M. Keck Laboratory of Hydraulics and Water Resources, California Institute of Technology, Pasadena, California.

- Vanoni, V. A., and Brooks, N. H. (1957). "Laboratory studies of the roughness and suspended load of alluvial streams." *Report No. E68, Sedimentation Laboratory*, California Institute of Technology, Pasadena, California.
- Vanoni, V. A. (1974). "Factors determining bed form of alluvial streams." *Journal of Hydraulic Engineering, ASCE*, 100 (HY3), 363–378.
- Vanoni, V. A., ed., (1975). *Sedimentation Engineering*, ASCE Manual and Reports on Engineering-Practice, 54, New York.
- Vanoni, V. A. (1980). "Sediment studies in the Brazilian Amazon River basin." United Nations Development Program, *Report KH-P-168*, W.M. Keck Laboratory of Hydraulics and Water Resources, California Institute of Technology, Pasadena, California.
- Vanoni, V.A. (1984). "Fifty years of sedimentation," *Journal of Hydraulic Engineering, ASCE*, 110(8), August, 1021–1057.
- Vanoni, V. A., ed., (2006). *Sedimentation Engineering-Classic Edition*, ASCE Manual and Reports on Engineering Practice 54, ASCE/EWRI, Reston, Virginia.
- Venditti, J. G., and Bennett, S. J. (2000). "Spectral analysis of turbulent flow and suspended sediment transport over fixed dunes." *Journal of Geophysical Research*, 105(22), 035–47.
- Villard, P. V., and Kostaschuk, R. A. (1998). "The relation between shear velocity and suspended sediment concentration over dunes: Fraser Estuary, Canada." *Marine Geology*, 148, 71–81.
- Vionnet, C. A., Marti, C., Amsler, M. L., and Rodriguez, L. (1998). "The use of relative celerities of bedforms to compute sediment transport in the Paraná River" *Modelling Soil Erosion, Sediment Transport and Closely Related Hydrological Processes, International Association of Hydrological Sciences Special Publication* 249, 399–406.
- Vlugter, H. (1942). "Sediment transport by running water." *De Ingenieur van Nederlands Indie*, 8(3), 139–147. (in Dutch)
- Vlugter, H. (1962). "Sediment transport by running water and the design of stable channels in alluvial solis." *De Ingenieur*, 74(36), B 227–231.
- Vollmers, V. J., and Giese, E. (1970). "Instability of flat bed in alluvial channels." Discussion, *Journal of the Hydraulics Division, ASCE*, 96(6).
- Wan, Z. and Z. Wang (1994). *Hyperconcentrated Flow*, Balkema, Rotterdam 290 pp.
- Wang, S. (1984). "The principle and application of sediment effective power." *Journal of Hydraulic Engineering, ASCE*, 110(2), 97–107.
- Weber, K. J. (1986). "How heterogeneity affects oil recovery." in *Reservoir Characterization*, Academic Press, 487–541.
- White, W. R., Milli, H., and Crabbe, A. D. (1973). "Sediment transport: an appraisal of available methods." *Report INT 119*, Hydraulic Research Station, Wallingford, U.K.
- White, W. R., Paris, E., and Bettess, R. (1980). "The frictional characteristics of alluvial streams: a new approach." *Proceedings of the Institution of Civil Engineers*, Part 2, Vol. 69, 737–750.
- White, W. R., Bettess, R., and Paris, E. (1982). "Analytical approach to river regime." *Journal of the Hydraulics Division, ASCE*, 108(10), 1179–1193.
- Wheatcroft, R. A. (2002). "In situ measurements of near-surface porosity in shallow-water marine sands." *Ocean Engineering*, 27(3), 561–570.
- White, C. M. (1946). "The Equilibrium of Grains on the Bed of Stream." *Proceedings of the Royal Society of London*, Series A, Mathematical and Physical Sciences, 174 (958).
- Whitehouse, R.J.S., and Hardisty, J. (1988). "Experimental assessment of two theories for the effect of bedslope on the threshold of bedload transport." *Marine Geology*, 79, 135–139.
- Whitehouse, R.J.S., Soulsby, R. L., and Damgaard, J. S. (2000). "Discussion of Inception of sediment transport on steep slopes by Lau, Y. L and P. Engel, Journal of Hydraulic Engineering, 125(5), 1999." *Journal of Hydraulic Engineering, ASCE*, 126(7), 553–555.
- Whiting, P. J., and W. E. Dietrich. (1990). "Boundary shear stress and roughness over mobile alluvial beds." *Journal of Hydraulic Engineering, ASCE*, 116(12), 1495–1511.
- Wiberg, P. L. (1987). "Mechanics of bedload transport." Ph.D. Dissertation, School of Oceanography, University of Washington, Seattle, Washington, 132 p.
- Wiberg, P. L., and Smith, J. D. (1985). "A theoretical model for saltating grains." *Journal of Geophysical Research*, 90 (C4), 7341–7354.
- Wiberg, P. L., and Smith, J. D. (1987). "Calculations of the critical shear stress for motion of uniform and heterogeneous sediments." *Water Resources Research*, 23(8), 1471–1480.
- Wiberg, P. L., and Smith, J. D. (1989). "Model for calculating bedload transport of sediment." *Journal of Hydraulic Engineering, ASCE*, 115(1), 101–123.
- Wiberg, P. L., and Rubin, D. M. (1989). "Bed roughness produced by saltating sediment." *Journal of Geophysical Research*, 94(C4), 5011–5016.
- Wiberg, P. L., and Smith, D. (1991). "Velocity distribution and bed roughness in high gradient streams." *Water Resources Research*, 27, 825–838.
- Wiberg, P. L., Drake, D. E., and Cacchione, D. A. (1994). "Sediment resuspension and bed armoring during high bottom stress events on the northern California inner continental shelf: measurements and predictions." *Continental Shelf Research*, 14(10/11), 1191–1219.
- Wilbers, A.W.E., and ten Brinke, W.B.M. (2003). "The response of subaqueous dunes to floods in sand and gravel bed reaches of the Dutch Rhine." *Sedimentology*, doi: 10.1046/j.1365–3091.2003.000585.x.
- Williams, D. T., and Julien, P. Y. (1989). "Applicability index for sand transport equations." *Journal of Hydr. Eng.*, 115(11), 1578–1581.
- Williams, J. J., Bell, P. S., and Thorne, P. D. (2003). "Field measurements of flow fields and sediment transport above mobile bed forms." *Journal of Geophysical Research*, Vol. 108, doi: 10.1029/2002JC001336.
- Wilson, K. C. (1966). "Bedload Transport at High Shear Stresses." *Journal of the Hydraulics Division, ASCE*, 92 (HY6), 49–59.
- Wilson, K. C. (1987). "Analysis of bed-load motion at high shear stress." *Journal of Hydraulic Engineering, ASCE*, 113(1), 97–103.
- Wilson, K. C. (1989). "Mobile bed friction at high shear stress." *Journal of Hydraulic Engineering, ASCE*, 115(6), 825–830.
- Wilson, K. C. (2005). "Rapid increase in suspended load at high bed shear." *Journal of Hydraulic Engineering, ASCE*, 131(1), 46–51.
- Wong, M., and Parker, G. (2006a). "Flume experiments with tracer stones under bedload transport." *River, Coastal, and Estuarine Morphodynamics*, G. Parker and M. H. Garcia, eds., Taylor & Francis Group, London, 131–139.
- Wong, M., and Parker, G. (2006b) "Re-analysis and correction of bedload relation of Meyer-Peter and Muller using their own

- database." *Journal of Hydraulic Engineering*, ASCE, 132(11), 1159–1168.
- Wright, S., and Parker, P. (2004a). "Density stratification effects in sand-bed rivers." *Journal of Hydraulic Engineering*, 130(8), 783–795.
- Wright, S., and Parker, P. (2004b). "Flow Resistance and Suspended Load in Sand-Bed Rivers: Simplified Stratification ModelDensity." *Journal of Hydraulic Engineering*, 130(8), 796–805.
- Wright, S., and Parker, P. (2005a). "Modeling downstream fining in sand-bed rivers, I: Formulation." *Journal of Hydraulic Research*, 43, 6, 612–619.
- Wright, S., and Parker, G. (2005b). "Modeling downstream fining in sand-bed rivers, II: Application." *Journal of Hydraulic Research*, 43, 6, 620–630.
- Wu, W. and Wang, Sam S. Y. (1999), "Movable Bed Roughness in Alluvial Rivers." *Journal of Hydraulic Engineering*, ASCE, Vol. 125, No. 12, pp. 1309–1312. See also closure to discussion, *Journal of Hydraulic Engineering*, ASCE, Vol. 127(7), 628–629, 2001.
- Wu, W., and Wang S.S.Y. (2006). "Formulas for sediment porosity and settling velocity." *Journal of Hydraulic Engineering*, ASCE, 132(8), 858–862.
- Wu, F. C., and Chou, Y. J. (2003). "Rolling and lifting probability for sediment entrainment." *Journal of Hydraulic Engineering*, ASCE, 129(2), 102–112.
- Yalin, M. S. (1963). "An Expression for Bedload Transportation." *Journal of the Hydraulic Division*, ASCE, 89 (HY3), 221–250.
- Yalin, M. S. (1964). "Geometrical properties of sand waves," *Journal of the Hydraulics Division*, ASCE, 90, 105–119.
- Yalin, M. S. (1977). *Mechanics of sediment transport*. Pergamon Press, 2nd Ed, New York.
- Yalin, M. S., and Karahan, E. (1979). "Inception of sediment transport." *Journal of Hydraulic Engineering*, ASCE, 105 (HY11), 1433–1443.
- Yalin, M. S. (1985). "On the determination of ripple geometry." *Journal of Hydraulic Engineering*, ASCE, 111, 1148–1155.
- Yalin, M. S. (1992). *River mechanics*, Pergamon Press, New York.
- Yalin, M. S., and da Silva, A. M. (2001). *Fluvial Processes*, IAHR Monograph, International Association of Hydraulic Engineering and Research, Delft, The Netherlands.
- Yang, C. T. (1973). "Incipient motion and sediment transport." *Journal of Hydraulic Engineering*, ASCE, 99(10), 1679–1704.
- Yang, C. T. (1979). "Unit stream power equations for total load." *Journal of Hydrology*, 40, 123–138.
- Yang, C. T. and Molinas, A. (1982). "Sediment transport and unit stream power function." *Journal of the Hydraulic Division*, ASCE, 108 (HY. 6), 774–793.
- Yang, C. T., and Wan, S. (1991). "Comparisons of selected bed-material load formulas." *Journal of Hydraulic Engineering*, ASCE, 117(8), 973–989.
- Yang, C. T. (1996). *Sediment transport: theory and practice*, McGraw-Hill, New York.
- Yang, C. T., Molinas, A., and Wu, B. (1996). "Sediment transport in the Yellow River." *Journal of Hydraulic Engineering*, ASCE, 122(5), 237–244.
- Yang, C. T., and Simoes, F.J.M. (2005). "Wash load and bed-material load transport in the Yellow River." *Journal of Hydraulic Engineering*, ASCE, 131(5), 413–418.
- Yang, S. Q. (2005). "Sediment transport capacity." *Journal of Hydraulic Research*, 42(3), 131–138.
- Yen, B. C. (1991). "Hydraulic resistance in open channels." in *Channel Flow Resistance: Centennial of Manning's Formula*, B. C. Yen, ed., Water Resource Publications, Highlands Ranch, Colo., 1–135.
- Yen, B. C., ed. (1991). *Channel Flow Resistance: Centennial of Manning's Formula*, Water Resource Publications, Highlands Ranch, Colorado, 453 p.
- Yen, B. C. (1992). "Dimensionally homogeneous Manning's formula." *J. Hydraul. Eng.*, 118(9), 1326–1332; Closure: *ibid.* (1993), 119(12), 1443–1445.
- Yen, B. C. (1993). Closure to Discussion by B. A. Christensen of "Dimensionally Homogeneous Manning's Formula," *Journal of Hydraulic Engineering*, ASCE, 119(12), 1442–1443.
- Yen, B. C. (2002). "Open channel flow resistance." *Journal of Hydraulic Engineering*, ASCE, 128, 20–39.
- Yoon, J. Y., and Patel, V. C. (1996). "Numerical model of turbulent flow over sand dune." *Journal of Hydraulic Engineering*, ASCE, 122, 10–18.
- Yu G, and Lim S., (2003). "Modified Manning formula for flow in alluvial channels with sand-beds." *Journal of Hydraulic Research*, IAHR, 41, 597–608.
- Zanke, U. (1977). "Berechnung der Sinkgeschwindigkeiten von Sedimenten." *Mitteilungen des Franzius-Institutes*, 46, 231–245.
- Zanke, U.C.E. (2003). "On the influence of turbulence on the initiation of sediment motion." *International Journal of Sediment Research*, 18(1), 17–31.
- Zedler, E. A., and Street, R. L. (2001). "Large-eddy simulation of sediment transport: currents over ripples." *Journal of Hydraulic Engineering*, ASCE, 127, 444–452.
- Zegzhda, A. P. (1938). *Theoriia podobiiaei metodika rascheta gidrotekhnicheskikh modelei*. (Theory of similarity and methods of design of models for hydraulic engineering.), Gosstroizdat, Leningrad.
- Zeng, J., Constantinescu, S. G. and Weber, L. (2005), "Validation of a computational model to predict suspended and bed load sediment transport and equilibrium bed morphology in open channels," *River, Coastal and Estuarine Morphodynamics: RCEM 2005*, G. Parker and M.H. Garcia (eds.), Taylor & Francis Group, London, 259–270.
- Zhou, D., and Mendoza, C. (2005). "Growth model for sand wavelets." *Journal of Hydraulic Engineering*, ASCE, 131(10), 866–876.
- Zwamborn, J. A. (1966). "Reproducibility in hydraulic models of prototype river morphology." *La Houille Blanche*, 3, 291–297.
- Zwamborn, J. A. (1981). "Umfolzi road bridge hydraulic model investigation." *Journal of the Hydraulics Division*, ASCE, 107(11), 1317–1333.
- Zyberman, J., and Fredsoe, J. (1994). "Data analysis of bed concentration of suspended sediment." *Journal of Hydraulic Engineering*, ASCE, 120, 1021–1042.

*This page intentionally left blank*